Flow and Bed-Features Dynamics in Seepage Affected Alluvial Channels

Thesis submitted in partial fulfilment of the requirements for the award of the degree of

Doctor of Philosophy

in

Civil Engineering

by

Mahesh Patel

Department of Civil Engineering

Indian Institute of Technology Guwahati

Guwahati - 781039, India

MARCH, 2017

Dedicated to

***Parents, Lt. Ghanshyam** Mama Ji*

and friends !

For their unconditional love, patience, sacrifices and continued support during my successful journey

There's a harsh river that's flowing outside,
I can hear it from inside the house;
While I'm still slumbering after my rouse -
It is tugging the sand and eroding the riverside.
It is uprooting tragically the trees from within;
Yes it's quite ugly in its flow -I don't tease,
It's true because it is breaking its new lease;
I surmise, its turbulent flow breaks a fish a fin.
And to add, the rain is pouring heavily with hail still,
Intensifying its flow at riptide; I hear a ripple in fine
And fast rough water that breaks the riverine -
And the sound of shivering and swaying water lily.
And as sweet with these admixture of sounds I fall asleep;
As solely does the sleep in sound mine is just too deep.

Choene Alley Semenya (2015)

Declaration

I certify that

- The work contained in this thesis is original and has been done by myself and under the general supervision of my supervisor(s).
- The work reported herein has not been submitted to any other Institute for any degree or diploma.
- Whenever I have used materials (concepts, ideas, text, expressions, data, graphs, diagrams, theoretical analysis, results, etc.) from other sources, I have given due credit by citing them in the text of the thesis and giving their details in the references. Elaborate sentences used verbatim from published work have been clearly identified and quoted.
- I also affirm that no part of this thesis can be considered plagiarism to the best of my knowledge and understanding and take complete responsibility if any complaint arises.
- I am fully aware that my thesis supervisor(s) are not in a position to check for any possible instance of plagiarism within this submitted work.

March 27, 2017 Mahesh Patel

Department of Civil Engineering
Indian Institute of Technology Guwahati
Guwahati - 781039, India

Dr. Bimlesh Kumar
Associate Professor
Email : bimk@iitg.ernet.in
Phone : +91-361-258-2420

Certificate

This is to certify that this thesis entitled "**Flow and Bed-Features Dynamics in Seepage Affected Alluvial Channels**" submitted by **Mahesh Patel**, in partial fulfilment of the requirements for the award of the degree of Doctor of Philosophy, to the Indian Institute of Technology Guwahati, Assam, India, is a record of the bonafide research work carried out by him under my guidance and supervision at the Department of Civil Engineering, Indian Institute of Technology Guwahati, Assam, India. To the best of my knowledge, no part of the work reported in this thesis has been presented for the award of any degree at any other institution.

Date: March 27, 2017
Place: IIT Guwahati

(Dr. Bimlesh Kumar)

Publications

Book Chapters

1. **Mahesh Patel**, Vishal Deshpande, and Bimlesh Kumar. "Effect of seepage on the friction factor in an alluvial channel." 4^{th} *IAHR Europe Congress*, Liege Belgium 27–29 July 2016- *Sustainable Hydraulics in the Era of Global Change* – Erpicum et al. (Eds.), 473–477, 2016 Taylor & Francis Group, CRC Press London, ISBN 978-1-138-02977-4.

2. **Mahesh Patel**, Sainath Panigrahi, and Bimlesh Kumar. "Flow over fluvial bedforms with suction." *Fluid Mechanics and Fluid Power Contemporary Research Lecture Notes in Mechanical Engineering* – Saha et al. (Eds.), 12–14 Dec. 2014, IIT Kanpur, Springer, 1069-1077, 2016. (doi:10.1007/978-81-322-2743-4_101)

Journals

1. **Mahesh Patel** and Bimlesh Kumar. "Flow and bedform dynamics in an alluvial channel with downward seepage." *CATENA*, Elsevier, 158, 219-234, 2017.

2. **Mahesh Patel**, Shantanaba Majumder and Bimlesh Kumar. "Effect of seepage on flow and bedforms dynamics." *Earth Surface Processes and Landforms*, Wiley, 2017. (Available online: http://dx.doi.org/10.1002/esp.4134)

3. **Mahesh Patel**, Vishal Deshpande, and Bimlesh Kumar. "Turbulent characteristics and evolution of sheet flow in an alluvial channel with downward seepage." *Geomorphology*, Elsevier, 248(1), 161–171, 2015.

4. Anurag Sharma, **Mahesh Patel** and Bimlesh Kumar. "Turbulent parameters and corresponding sediment transport in curved cross-section channel." *ISH Journal of Hydraulic Engineering*, Taylor & Francis, 21(3), 333–342, 2015.

Communicated

- Vishal Deshpande, **Mahesh Patel** and Bimlesh Kumar. "Seepage in threshold alluvial channels: an insight into the changing flow hydrodynamics". Submitted to *Royal Society Open Science*, 2016. (minor revision submitted)

- **Mahesh Patel**, Shantanaba Majumder and Bimlesh Kumar. "Statistical description of morphological characteristics of bedforms in seepage affected alluvial channels." Submitted to *Canadian Journal of Civil Engineering*, NRC Research Press, 2017. (under review)

Conferences

---

1. **Mahesh Patel**, Vishal Deshpande, and Bimlesh Kumar. "Resistance to flow in an alluvial channel subjected to seepage." 20^{th} *Congress of the Asia Pacific Division of the International Association for Hydro Environment Engineering and Research* held at Colombo, Sri Lanka, 28 – 31 August, 2016.

2. Anurag Sharma, Dengkhw Brahma, **Mahesh Patel**, and Bimlesh Kumar. "Turbulent Scale Measurement in Mobile Bed channel." *National Conference on Water Resources and Hydropower*, 17th – 18th June, 2016, University of Petroleum and Energy Studies, Dehradun, India.

3. Anurag Sharma, **Mahesh Patel**, and Bimlesh Kumar. "Turbulence in curvilinear bed streams." 36^{th} *IAHR World Congress* 2015 held at The Hague, Netherlands, 28 June–3 July, 2015.

4. Jaideep Sehrawat, **Mahesh Patel**, and Bimlesh Kumar. "Gaussian process regression to predict incipient motion of alluvial channel." *International Confer-ence on Soft Computing for Problem Solving*, 27–29 Dec. 2014, NIT Silchar, India, Springer, 336, 431–437, 2015. (DOI:10.1007/978-81-322-2220-0_35)

5. **Mahesh Patel**, Sainath Panigrahi, and Bimlesh Kumar. "Dam break analysis: case studies of Bettakumbri and Hongadhalla dam." *National conference on Water and its Sustainability in Mining and Other Environment*: *VISION* 2050, ISM Dhanbad, India, 28–29 March, 2014.

6. **Mahesh Patel** and Bimlesh Kumar. "Resistance predictor with bedforms in alluvial channel." *International Conference on Sustainable Innovative Techniques in Civil and Environmental Engineering*, JNU Delhi, India, 5–6 June, 2013.

7. Vishal Deshpande, **Mahesh Patel**, and Bimlesh Kumar. "Spatio-temporal variation of critical parameters in threshold channel." *International Conference on Climate Change, Water Resources and Disasters in Mountainous Regions: Building Resilience to Changing Climate*, SOHAM, Kathmandu, Nepal, 27–29 Nov., 2013.

8. **Mahesh Patel**, Sumit Talukdar, Vishal Deshpande, and Bimlesh Kumar. “Use of large tilting flume to characterize the sediment movement in alluvial stream.” *International Conference on Environmentally Sustainable Urban Ecosystems*, IIT Guwahati, India, 24–26 Feb., 2012.

Other Publication

- Anurag Sharma, **Mahesh Patel** and Bimlesh Kumar. “Performance appraisal of velocity predictors in channel flow." *Journal of Indian Water Works Association*, 47 (1), 2015.

Acknowledgements

The PhD Journey is not only about engaging in the research. In fact, it is a life itself that we live it and learn a lot by several challenges, ups, and downs in this entire period. This work would not have been possible without the help and support I received from many people during this wonderful journey of PhD.

First and foremost, I would like to express cordial thanks to my supervisor **Dr. Bimlesh Kumar** for his endless intellectual support and help. His boundless enthusiasm and encouragement were integral, which would help throughout my life. One of the most important qualities about him is that he provides a free hand to his student to work in your own way. He was very calm and always available to help me at various stages of my work. I really admire him because of his great passion about research including publishing articles that would always go in my favour. He will always be my inspiration because of his friendly and supportive nature. I feel lucky to have him as a mentor of my Thesis.

I take utmost pleasure to thank Chairman of my Doctoral Committee **Professor Rajib Kumar Bhattacharya** and other members **Dr. Manish Kumar Goyal** and **Dr. Vinayak Kulkarni** for their valuable suggestions and inputs. I am also very grateful to **Dr. Sreeja P.** for her constructive comments and encouragement at every stage of my research work.

I would like to thank to **Prof. Gautam Biswas** Director of IITG for creating wonderful atmosphere for doing research in the institute. I owe sincere thanks to the Ministry of Human Resources and Development, Govt. of India for providing fellowship in the duration of my PhD. I am equally grateful to Central Workshop, Central Library and state of art facilities provided by IITG to carry out advance level of research.

I gratefully acknowledge for financial support provided by the Department of Science and Technology (DST), Govt. of India to carry out research work presented in the Thesis. I am also thankful to Science and Engineering Research Board - DST for funding me to present a paper in the 4^{th} IAHR International Conference in Liege, Belgium.

I express my sincere gratitude to **Prof. Subashisa Dutta**, Head of Department of Civil Engineering, IITG for providing an excellent environment to conduct research work without any difficulty. He has brought a significant change in the work culture to encourage students to work with more passion and interests.

I would like to give my earnest gratitude to **Dr. Praveen Kumar** and **Prof. Harshal B. Nemade** from the Department of Electronics and Electrical Engineering for their precious time and technical support when Ultrasonic Ranging System had stopped working. I am also thankful to **Prof. A.K. Singh**, **Prof. A. K. Sarma**, **Prof. Gautam Baru**a, **Dr. Suresh Kartha**, and **Dr. Arindam Dey** for their invaluable advice and suggestions. A special thanks to **Dr. Ajay Kalamdhad** for his great support and recommendations whenever I required at it. He always helped me apart from his busy schedule in academic duties.

I also thankful for the great support received from Staff of Civil Engineering Department. I would

like to thank **Mr. Rajib**, **Mr. Dipak**, and **Mrs. Juri**. They were always cordial and supportive. I am very thankful to **Jonali Ma'am** for her assistance provided during my work. I would like to express my special thanks to **Dr. Kumar Pallav** for his kind support whenever I required assistance and moral support.

A very special gratitude goes out to my senior cum best friend **Dr. Vishal Deshpande**. The endless discussion with him on various topics including research and life always helped me from the day I registered in M Tech program. His presence always felt me of my elder brother and I discussed all small and big problems with him. He provided me the most useful advice to take various decisions related to research and future whenever I used to be confused. I would like to say "Thank you My Brother".

The person, I came to know about helping people without any expectation, would be known as **Mr. Mayank Agarwal**. I learnt a lot from his technical knowledge related to computer and his ability to do work quickly. His etiquettes are always adorable that helped me to improve my personality and behaviour. I would like to say thank you Mayank for everything you did in this fantastic journey. The discussion with Mayank and Dr. Vishal over mess table (like small assembly) was so entertaining and funny.

I am also very grateful to have friends like **Smrati**, **Isha** and **Jayshree** in this awesome journey. The unconditional care received from Smrati is commendable. I owe her for her support at several stages whenever I needed. I would like to say thank you Isha for a long chat and discussion on various issues those moments would be memorable forever. I learnt a lot from her extensive knowledge and way to see the world. There are many qualities and skills in Jayshree that anyone can learn from her. A big thanks to Jayshree for teaching me how to be calm and cool in any situation. I would like to say many thanks to all of you for a wonderful company and to make my journey entertaining.

I am indebted to **Bazal Da** for his assistance and guidance to conduct the experiments. He was always available whenever I required, without him these experiments were not possible to perform smoothly. I also owe to his wife (Shakina Bhabhi) and son Imran for their love and care as a family.

I would like to thank my friend Ankit Dalal, brother Amit, Kashyap and Neeraj from EEE Department for a helping hand to repair and fix the Ultrasonic Ranging System (URS). I am equally thankful to Dr. Christopher Jette for his consistent response to rectify the URS. I would also like to cordially thank to Tushar, Neelkant, and Hema from the CSE Dept for their technical assistance whenever I asked to them.

I would like to thank to Mr. Upain Gohain and Mr. Kshetri for manufacturing various support systems and trolley that made my work very simple. I am equally thankful to Mr. Subhash Barman (carpenter) for fabricating wooden shape and bedforms.

I thank my fellow fluvial group members Anurag, Bandita, Rutuja, Pankaj, Sumit, Rakesh and Dr. Bebina for their backing when I was doing my experiments. I am very thankful to Shantanaba Majumder and Dengkhw Brahma for extreme help provided by them in my experimental work. I owe to my friend cum younger brother Jaideep for his enormous help. He was always available whenever I called him to prepare the channel. I would also like to thank my labmates Shivam, Uttam, Vishal Singh, Manas, Ashutosh, Needhi and Sagarika for all the fun we had in the lab. Special thanks to

Saumya for her kindness and all cherish moment with her.

I wish to acknowledge Amit Bhaiya and Arpit Bhiaya for all the help they provided and for funny moments and humours in this journey. I am thankful to my friends Kamlesh, Harinder, Subhadeep, Vinay, Rituraj, Swati, Swapnali, Rakhee, and Tampha for fun and enjoyment we had during my M Tech period.

The journey to reach at this stage was not possible without the astonishing company of Rahul Rajput and Mayank Tiwari. We had very long chat and discussions about everything in life and we supported each other whenever needed. Thank you guys for all the fun and fight we had. I am equally thankful to my friend Neelam for standing always my side during my ups and downs. I am also thankful to my friend Khushboo for pushing me to work hard and fulfil the dreams.

I would like to express my sincere gratitude to **Prof. K K Panjabi** for his great advice and intellectual help. His fathomless knowledge always provided a right direction to everyone.

I would like to gratefully acknowledge to **Lt. Ghanshyam Mama Ji** for his innumerable love and encouragement. I gained a lot from him from a long chat and conversations related to society and life. You are not alive but your memories always would be in my heart. I am also thankful to my brother in laws Raghvendra, Ashish and cousins Sulekha, Sunita, Ravikant, Meena, Ravindra, Piyush, Prince, Charan and Arjun Bhai for all the lovely moments at home.

Last but not the least, I would like to thank my family: my **Mata Shree** and **Papa Ji** and to my awesome brothers Ajay, sister Swarthi, sister in law Sonam, and niece Saanvi (Popli) for supporting and believing me throughout my study. The sacrificed you people did for me cannot be repaid ever. Thank you my lovely Maa and Papa Ji because whatever I am today only because of both of you. A special to thanks to my elder brother **Ajay** for his believe and love he showed to me.

March 27, 2017 Mahesh Patel

Abstract

This study, using an experimental approach, focuses on the effect of downward seepage on a threshold alluvial channel morphology and corresponding turbulent flow characteristics. Experiments have been carried out in a curvilinear cross-sectional shaped channel with two different sediment beds i.e., fine (median diameter = 0.41 mm) and coarse (median diameter = 0.41 mm) sands under no seepage and with seepage conditions. It has been observed that an alluvial channel, which remained at threshold condition of sediment movement during the no seepage experiment, started transporting sediments after the application of seepage in a vertically downward direction. In experimental methodology, Acoustic Doppler Velocimeter developed by Nortek was used to measure instantaneous flow velocities in streamwise, transverse and vertical directions in both the conditions. Bed elevation variations were recorded by using Ultrasonic Ranging System at different time intervals in the presence of seepage.

In case of a fine sand bed channel, results show that Shields stress of the threshold channel is significantly increased from its critical value after the application of downward seepage, leading to the deformation of the cross-sectional shape and subsequent development of bedforms. The role of turbulence in the development of bedforms has also been investigated. Measures of turbulent statistics show that the time-mean velocities and Reynolds stresses are increased significantly with the application of downward seepage. Under the action of seepage conditions, increase in the flux of streamwise turbulent kinetic energy in the streamwise direction is observed in the region close to the channel boundary. Also, quadrant analysis exhibits the increase in the contributions from all the bursting events and the thickness of the sweep-dominated zone in near-bed region after the application of downward seepage. A bedform tracking tool has been used to evaluate the physical characteristics of bedforms. These developing bedforms are classified as current and linguoid ripples according to their evolution with time. It has been further observed that the variations in Shields stress and corresponding bedform geometry reached an equilibrium state in the presence of downward seepage when the experiments were run over a longer period of time (24-31 h).

This work is extended to analyse the flow and statistics of bedform dynamics in terms of multi-scalar bedforms with different percentages of seepage. These multi-scalar ubiquitous bedforms cast a potential impact on flow turbulence as well as stream bed morphology in

sand bed channels. Wavelet has been used to analyse temporally lagged spatial bed elevation profiles that were obtained from a set of laboratory experiments and synchronized the wavelet coefficients according to bed elevation fluctuations at different length scales. A spatial cross-correlation analysis based on the wavelet coefficients is performed on these bed elevation datasets to observe the effect of downward seepage on the dynamic behaviour of bedforms at different length scales. Bedform celerity is best approximated by a probability density function such as Rayleigh distribution under varying downward seepage. Statistical analysis of physical parameters of bedforms ascertains that the bedform celerity is reduced as a result of increased bedform size. In addition, wavelet coefficients have been used to perform structure function analysis of bed elevation profiles and to plot exceedence probability. This suggests that bed elevation fluctuations become higher under the influence of increased seepage. Also, the slope of the power spectral density increases significantly with the increment in seepage percentage, which indicates more inhomogeneous and rapid arrangement of bedforms because of increased seepage discharge. In order to get an insight of flow, integral scales of flow are evaluated and it is found that scales of eddy length and eddy turnover time increase significantly with the application of downward seepage, leading to increased sediment transport and initiation of bedforms along the channel length. As the amount of seepage discharge increases, eddy length(s) and turnover time are further increased, causing the development of larger bedforms. It has been established that the geometry of bedforms is linked with the size of eddies.

An experimental investigation of the flow hydrodynamics and temporal changes in the cross-sectional profile with coarse sand bed shows that the stream power and the value of Shields parameter are increased under the action of downward seepage, causing bed particles to move in the form of a sheet layer. Sheet layer development causes reduction in flow depth and rapid channel widening. Cross-sectional parabolic shape of the threshold channel transforms into a trapezoidal shape in the presence of a sheet layer. With the passage of time (11 h), the channel attains a different equilibrium geometrical state with the value of Shields stress around 0.074 (greater than its corresponding value from the no seepage scenario i.e., 0.0399). Measures of turbulent characteristics such as near-bed time-mean velocities and Reynolds stresses have been found increased with the application of downward seepage. Integral scales of flow suggest that the size of eddies increases with the application of downward seepage, which is linked to the evolution of the sheet layer. Also, the hydraulics of sheet flow is defined by formulating an empirical equation for the sheet flow rate with the consideration of downward seepage.

Keywords: Bedforms, Sheet layers, Shields stress, downward seepage, turbulent flow, wavelet, integral scales.

Contents

List of Figures

List of Tables

List of Symbols

Symbols	Description
ϕ	Angle of repose (dry)
M_{21} and M_{12}	Advection of RNS in the streamwise and vertical direction
Ap	Area of the pipe in flow meter
U	Average flow velocity
u_s	Average velocity of flow for with seepage case
u_0	Average velocity of flow for no seepage case
Q_s	Average discharge for with seepage case
$R_x(\tau)$	Auto-correlation function
τ	Bed shear stress
S_0	Bed slope of the channel
Δ	Bedform height
Λ	Bedform length
C_d	Coefficient of discharge
C_s	Celerity of the ultrasounding waves
A	Cross-sectional area of channel
$Sk(u_i)$	Coefficient of skewness of a velocity time series
T_c	Crest elevation
C_v	Coefficient of variation
z	Distance of measurement point from the channel bed
d	Distance from the prob to the reflecting surface
X	Distance from the tail gate
ρ_s	Dry density of the sediments

ρ	Density of the fluid
$\eta_{i,H}$	Detection function
D_u and C_u	Empirical parameters suggested by Nezu and Nakagawa (1993)
E_T	Eulerian integral time scale
E_L	Eulerian integral length scale
f	Frequency of the signal
S_f	Friction slope
F_0 and F_s	Froude number for no seepage and with seepage case
F_{ku} and F_{kw}	Flux of turbulent kinetic energy in the streamwise and vertical direction
$S_{i,H}$	Fractional contribution of RSS
M_{30} and M_{03}	Flux of the Reynolds normal stress in the streamwise and vertical direction
R_e	Flow Reynolds number
σ_g	Geometric standard deviation
H_b	Height of water above the rectangular notch
R_{h0} and R_{hs}	Hydraulic radius for no seepage and with seepage case
u_i, v_i, and w_i	Instantaneous velocities in the streamwise, lateral and vertical directions
H	Hyperbolic hole region
ν	Kinematic viscosity of water
L_n	Length of the rectangular notch
D	Length of the conductor
S_l	Lee face slope
b	Location parameter
γ	Lower bound in probability density function
Δ_{max}	Maximum height of ripple
h	Maximum depth of flow of the channel
D_{50}	Median particle diameter
Q	Main channel discharge
N	Number of data points of the bed elevation series
$h^+ = z/h$	Normalized depth of flow

σ_u and σ_w	Normalized turbulent intensity in streamwise and vertical directions
T_P and E_D	Non dimensional turbulence production and energy dissipation
P_0 and P_s	Perimeter for no seepage and with seepage case
$S_x(f)$	Power spectral density function
τ_{uw}	Reynolds shear stresses
c_1 and c_2	Roughness of the wave series and intermittency parameter
B_s	Strength of the magnetic field
V_s	Seepage velocity through the sand bed of length L
u^*_{0b} and u^*_{sb}	Shear velocity under no seepage and with seepage condition
G	Specific gravity
γ_s and γ	Specific weight of sediment particles and fluid
Ω	Stream power of the channel
q_s	Seepage discharge
θ_c	Shields stress
R_*	Shear Reynolds number
$F_{uu}(f)$	Streamwise velocity power spectra
S_u	Standard deviation
S_d	Standard uncertainity
u_{*t}	Shear velocity evaluated by the linear projection of the RSS profile
$1/\sqrt{a}$	Scaling factor of mother wavelet
R	Set of real number
a	Scaling parameter
$M(q,q)$	Structure function or statistical moment
$\tau(q)$	Scaling exponent function
q_b	Sheet flow rate
R_{es}	Seepage flow Reynolds number
α	Tail index
u, v and w	Time-mean velocities in the streamwise, lateral, and vertical directions, respectively
B	Top width of the channel

τ_{turb} and τ_{visc}	Turbulent and viscous shear stresses
TI	Turbulent intensity
T	Total sampling time of velocity pulse
t_p and e_D	Turbulence production and turbulent diffusion
T_t	Trough elevation
ν	Truncation parameter in probability density function
E	Voltage generated in a conductor
u_c	Velocity of the conductor
S_w	Water surface slope
S_{ws}	Water surface slope for with seepage case

List of Abbreviations

Terms	Abbreviations
ADV	Acoustic Doppler Velocimeter
BEPs	Bed Elevation Profiles
BTT	Bedform Tracking Tool
BES	Bed Elevation Series
CDF	Cumulative Distribution Function
PDF	Probability Density Function
PSD	Power Spectral Density
pdf	Probability Distribution Function
RSS	Reynolds Shear Stress
TI	Turbulent Intensities
TKE	Turbulent Kinetic Energy

"This riparian stuff is not rocket science . . . it's much more complex than that"

Steve Nelle

Retired NRCS Wildlife Biologist San Angelo, Texas

1

Introduction

1.1 Background

The intrinsic behavior of mobile beds in natural environments is complex if one attempts to understand their innate creation. Mobile beds transform themselves and evolve into different patterns such as sediment waves, which alter the flow and sediment transport. Understanding of these intriguing patterns is significantly important for river management, bed load transport, and structures in fluvial system. Earlier, the studies on fluvial bedforms are widely carried out to get an insight into physics behind the initiation of bedforms over rough beds in natural environments. In addition, various research institutions and founding societies in Mesopotamia, China, India, Egypt, and the Roman Empire have studied and observed the sediment transport and associated bedforms for utilizing natural and man-made channels.

In ancient times, the historical progression of irrigation and rivers is encapsulated in Indian religious scripture, which shows details of control of erosion and deposition in alluvial channels (Garde, 1995). Italian hydraulician Guglielmini (Gulieminus) (1710) was the first person who laid down the cornerstone in the area of loose boundary hydraulics. Graf (1984) reported basics statements about behaviour of deformable boundaries in terms of bedform dynamics, migration of bedforms including "furrow" shapes and size, which are given in the experimental and theoretical studies of Italian hydraulician Guglielmini (Gulieminus) (1710) and French hydraulician DuBuat (1779).

In the progression of observations and measurements of bed-features morphology, re-

searchers infer their details of evolutions of historical currents. Development of small size of bedforms such as ripple, including their geometry, patterns, variation, and sediment transport are discussed by De La Beche (1851) and Sorby (1859). Partiot (1871) suggested an expression for propagation speed based on the measurement in River Loire. Further, detailed studies of bedform initiation and dynamics were progressed at a rapid pace in late 1800s using controlled experimental measurements. Deacon (1894) performed experiments in order to define the orientation, shape, patterns, celerity, and bed load transport in the form of current ripples with the variation in flow strengths. Cornish (1901) pointed out the large wavy structure of bedforms including their shape, orientation, and variation with the flow. Gilbert and Murphy (1914) reported that the characteristics of flow and river sedimentation are significantly affected by the development and resistance offered by bedforms in alluvial channels. Hence, this phenomenon has been used widely in the river management and the study of sand-bed morphology.

Bucher (1919) worked extensively on the origin of ripple formation mechanics and related sand-bed patterns. These patterns were in terms of rhomboid, linguoid, meta ripples, sand waves and transitions amongst them. In his study, initiation of bedforms, bedform migration, changes in shape and size according to velocity, flow strength and controlling factors (flow depth, dynamic viscosity, and different sand size), by considering an influence of Helmholtz instability for dunes and corresponding sediment transport were investigated. In the early work of Velikanov in 1923, an investigation of bedform development using advance technologies such as photography, high speed motion pictures, and special emulsion drop over the period of 1936-1946 was performed and the role of turbulent flow on bedform initiation was also studied.

Inglis (1949) carried out an extensive review on alluvial ripples and dunes in Indian alluvial channels using ranges of sediment sizes from 0.2 mm to 19.4 mm. It was noted different type of bedforms patterns on the rough boundary such as principally ripplets, ripples, dunes, and sheet layer. The linkage and mechanics between flow and bedforms development in terms of controlling factors (flow depth, velocity discharge, and bed load) and interactions with turbulent structures was discussed.

Thus, significant efforts have been made over the period of 20^{th} and 21^{st} centuries to solve this complex phenomena regarding initiation, sizes, shape, variation, and statistical nature of fluvial bedforms. However, the assured answer still need to be discovered.

1.2 Development of Bedforms

Alluvial bedforms developed by unidirectional flow of water over rough beds in sedimentary environments. The cause of development of bedforms can be one of the following reasons: (a) flow turbulence motions (b) instability of water-sediment flow system (c) sediment transport mechanics. In addition to this, sand bed channel exhibits a variety of bedforms, whenever the bed shear stress exceeds from its critical value. Geometrical features of these bedforms are governed by the amount of increase in the bed shear stress.

Simons (1961) found that small increment in bed shear stress from its critical value created series of sand waves in mobile bed channels, which were defined as ripples, dunes, antidunes, and so forth. He observed those bedforms in triangular shape with gentle upstream slope and lee side. It was also observed that when flow passed through dunes than sediment moved from upstream of dune to the lee side along the flow of the channel. Consequently, flow separated at the lee side of the dune that caused development of larger eddies and boils, resulting in increased turbulence in the flows. Thus, it was hypothesized that the physical characteristics of bedforms depend on the flow variations and properties of bed materials.

van Rijn (1982) observed bedforms, while increasing the bed shear stress from its threshold value. In his study, the transport parameters in terms of excess shear stress was used to predict the bedform shape and size. A relationship was established amongst flow-sediment conditions and bedform geometry (length and height). Further, he extended his work and developed a pioneering relation to calculate friction factor formula considering roughness due to development of bedforms.

Flow in natural channels is ubiquitous in the turbulent nature that has the potential to influence the bed morphology and develop the fluvial bedforms (Velikanov, 1955; Kondrat'ev et al., 1959; Jackson, 1976; Yalin, 1992). Several studies have been conducted to understand the linkage between the flow turbulence and bedform characteristics in plane bed channels (Coleman and Melville, 1996; Best, 1992; Yalin, 1992; Raudkivi, 1997; Robert and Uhlman, 2001; Schindler and Robert, 2005; Venditti et al., 2005).

Best (1992) carried out a series of visualization experiments to understand the structure of boundary layers over mobile sand beds. A model was proposed using graphical presentation to explain the process of sediment entrainment and formation of bed-defects as shown in Figure 1.1. In this model, initially hairpin vortex developed because of interac-

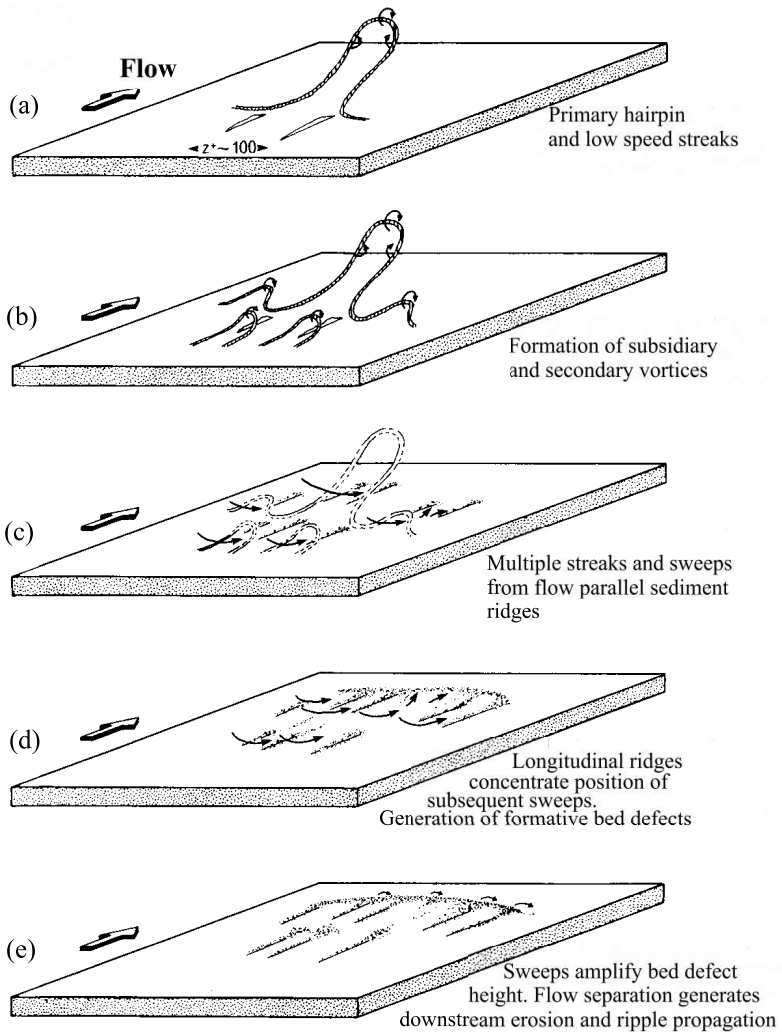

Figure 1.1: A model to describe the structure of the boundary layers and development of bed defects over rough bed in natural environment (Best, 1992)

tions between flow and boundary (Figure 1.1a) and when it moved away from the wall and interacted with the fluid it was followed by secondary hairpin vortices (Figure 1.1b). Those hairpin vortices postulated the formation of multiple sweeps events which ascribed to keep sediments in incipient motion condition (Figure 1.1c). Further, impact of those grouped sweep events continued till the lineation over mobile boundary or generation of formative bed defect (Figure 1.1d). Flow parallel ridges were developed because of amplification of grouped sweeps events caused erosion and deposition of sediment particles along the flow in the form of ripples (Figure 1.1e).

Nelson et al. (1995) investigated the turbulent events and sediment movements during bed load transport using laser-Doppler velocimetry and high speed cinematography over

rough boundary channel. They found that the sweep events contribute positively to local bed shear stress, causing majority of sediment motions. They signified that the increase in bed shear stress is related to increased sediment flux, which plays a significant role in the bedform mechanism. Also, sweep events can move far more sediment than bursts i.e. equally contributed by bed shear stress. Further, they suggested that the variations in bed shear stress and corresponding magnitude and duration of the sweeps, bursts, inward, and outward interactions can produce significant peaks in sediment transport and thus supporting the hypothesis that flow separation plays an important role in the bedform development.

Coleman and Melville (1996) carried out series of experiments to know the process of bedform development on a flat sand bed. The development of initial sand waves, defined as sand-wavelets, on the flat sand bed was observed and they were instigated by the occurrence of a random pileup of sediment, which caused trapping of bed sediment in different shapes. This process of pileup kept on that ascribed to increase in height of bedform and corresponding roughness on the bed.

Furthermore, it has been hypothesized that the bedform development is a function of turbulent flow characteristics, where sweeps (bursting events) govern the initiation of bed features in the near-bed region (Williams and Kemp, 1971; Raudkivi and Witte, 1990; Raudkivi, 1997). Raudkivi (1997) revealed that turbulence bursting processes can be a probable reason behind the development of variety of ripples on the flat surface.

Robert and Uhlman (2001) conducted the flume experiments to define different stages of ripple-dune transition. Bedforms were observed on flat bed surface (uniform sand bed) by increasing the flow velocity, where bed transformed into a two dimensional rippled bed. They observed that on increasing the flow velocity, those bedforms turned into irregular linguoid ripples and then transformed into dunes. Flow measurement was taken on fixed bed surface and found that turbulent intensity and Reynolds stresses gradually increased through the transition period.

Gyr and Kinzelbach (2004) investigated the mechanism of bedform development due to interaction between sediment transport, flow turbulence, and gravitational settling. The mechanism can be characterized by the length scales of the sediment, bedforms, and flow structure. They signified that the size and shape of bedforms are the function of scale of flow turbulence.

Schindler and Robert (2005) worked extensively to define the transformation process of ripple to dune transformation by performing experiments in the laboratory. They used seven

distinct stages of the transitions from ripples to dunes. Turbulent flow structure over mobile bedforms at several stages of transitions were presented and the results of fixed ripples and dunes were compared with each other. They also proposed an upgraded model to define the ripple-dune transition.

Venditti et al. (2005) examined the bedform initiation on a flat sand bed channel in unidirectional flows. They observed two kinds of bed structure i.e. defect on the channel bed and instantaneous initiation of bedforms. Initially defects occurred at lower flow stages, where sediment movement was sporadic and patchy in nature and they characterized by defect migration related to flow separation. Instantaneous initiation of bed movement was observed at larger flow strength. They investigated that turbulent flow structure did not always influence the bedform initiation. They suggested that the initiation of bed defects and their length are linked to the integral scales of flow.

Langlois and Valance (2007) investigated the development and migration of sand ripples in turbulent flow environment using open flume with spherical glass beads. They suggested that the turbulent instability is responsible for the formation of bedforms and found that initially wavelength of bedform is related to grain size and the friction velocity. The effect of grain size on bedform geometry was discussed, for example, on fine grained bed the logarithmic increase of the wavelength and amplitude was observed, while on coarse sand bed this process was enhanced at a faster rate. A large eddy simulation model has been used by Frias and Abad (2013) to define the characteristics of turbulent flow before and after the development of bedforms.

These studies are based on turbulence descriptions, which have not satisfactorily explained the scaling of sand waves because sediment size also plays a significant role in the characteristics of bedforms rather than turbulent flow characteristics.

1.3 Classification of Bedforms

Earlier, extensive studies have been performed in past 50 years in flume and rivers to describe the sequence of fluvial bedforms, which were developed due to increase in flow strength. Simons et al. (1965) classified those bedforms in three regimes i.e. lower, transitional, and upper regime as described in Figure 1.2. In lower flow regime, bedforms developed under tranquil flow ($F_r < 1$) were classified as ripples and dunes. When the inflow discharge was gradually increased, transition stage appeared where bedforms in lower

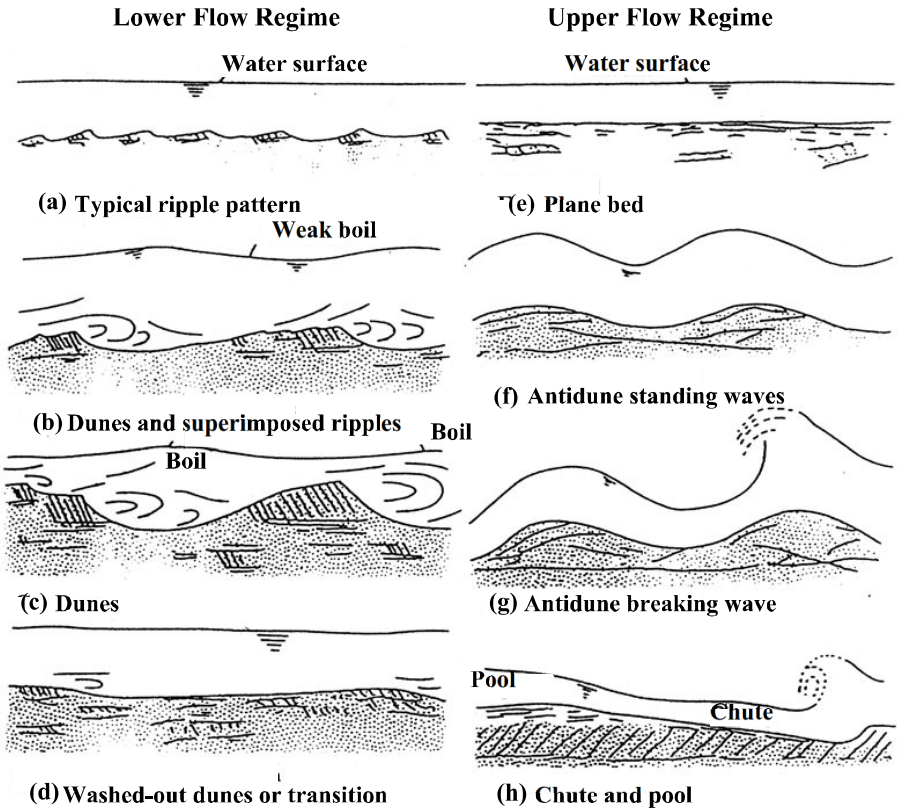

Figure 1.2: Initiation process of bedforms in sand bed channels. Descriptions of bed morphologies (a-h) with increasing flow discharge (Simons et al., 1965)

regime started to wash out bedforms caused plane bed. In the upper flow regime, inflow discharge was further increased, resulting development of antidunes, standing dunes, and pools with greater sediment transport in the channel. They found that the most common features of bed forms are ripples and dunes; and they are formed in the subcritical flow ($F_r < 1$), where small geometry of bedforms (wavelength varied from 0.12 to 0.6 m and height varied from 0.006 to 0.06 m) are defined as ripples and large size of bedforms are represented as dunes. Apart from ripples, dunes contain large geometrical features that occurred at higher inflow discharge and sediment size (greater than 0.6 mm), and they play a significant role to influence the characteristics of flow and bed roughness. Further, dimension of dunes was given for natural channel by Ashley et al. (1990) i.e. 1 m to 1000 m of wavelength.

Best (1992) observed that ripples are developed in the study on the sand size less than 0.7 mm, when the flow condition was hydraulically smooth throughout the experimental run (i.e., $R_* < 10$, where R_* is the shear Reynolds number). In the experimental study on fine and very fine grained sands, current ripples and non-equilibrium linguoid ripples

were observed by Baas (1994, 1999). Current ripples have small geometrical feature (i.e. average height and length are generally less than 10 mm and 0.6 m, respectively) and their development can be characterized with sediment size and shear Reynolds number (Yang, 1976; Baas, 1994; Carling, 1999). Robert and Uhlman (2001) also estimated average height of 12 mm and length of 0.13 m for current ripples and average height of 25 mm and length of 0.25 m for linguoid ripples in their experimental study.

1.4 Prediction of Bedforms

Prediction of bedforms has been widely discussed in existing literature. Here, a brief introduction about the prediction of small scale geometrical features of bedforms such as currents ripples and lingouid ripples is discussed i.e.

Yalin (1964) suggested an equation in terms of sediment size to predict the current ripple (Λ) length i.e.

$$\Lambda = 1000 D_{50} \tag{1.1}$$

Later, Yalin (1985) modified the equation to predict the current ripple length as:

$$600 D_{50} \leq \Lambda \leq 2000 D_{50} \tag{1.2}$$

In recent study of Soulsby et al. (2012) proposed the relations to predict the dimensions of current ripple (height and length) using dimensionless grain size (D_*) i.e.

Maximum height of current ripple,

$$\Delta_{\max} = 202 D_{50} D_*^{-0.554} \tag{1.3}$$

Maximum length of current ripple,

$$\Lambda_{\max} = \left(500 + 1881 D_*^{-3/2}\right) D_{50} \tag{1.4}$$

Where D_* can be calculated as:

$$D_* = \left[\frac{g\,(G-1)}{\nu^2}\right]^{1/3} D_{50} \tag{1.5}$$

Further, Nelson et al. (2013) also developed a model by using data from field and flume experiments to predict the dimensions of ripples. The developed model is mostly applicable to regular ripples. The following equations were suggested for evaluating bedform's physical characteristics

Length of ripples

$$\Lambda = 6.76 A_b^{0.68} D_{50}^{0.32} \tag{1.6}$$

where A_b is the orbital amplitude and it can be calculated as:

$$A_b = \frac{2\pi u_o}{T} \tag{1.7}$$

Here T is defined as wave period.

Height of ripple can be obtained as:

$$\Delta = 0.115 \Lambda^{0.89} \tag{1.8}$$

They also suggested a relation to evaluate steepness of ripple i.e.

$$\frac{\Delta}{\Lambda} = 0.12 \Lambda^{-0.056} \tag{1.9}$$

1.5 Statistical Description of Bedforms

Migration of developing bedforms cast a potential impact on the hydraulics, sediment transport, and habitant in the river environment. Dynamics of these bedforms are exceedingly complex because they vary in shape and size within a single flow system depending on the variation of bed shear stress and sediment grain size. This complex system is subjected to exert a substantial effect on the ecological system of the river and its flow dynamics (Yarnell et al., 2006). Coleman and Melville (1994) carried out experiments and recorded several wave series profiles to investigate the celerity of bedforms in terms of bedform dimensions. They observed that the larger bedforms generally form under subcritical flow regime and achieve a dynamic quasi-equilibrium state under steady state flow conditions, where the changes in average bedform height, length, and celerity become negligible. Celerity of bedforms was decreased, while increasing the height of bedforms with imposed flow.

However, exhaustive observations and rigorous experimental evidences indicate that the equilibrium condition is characterized by uninterrupted splitting and merging of bedforms at different spatial scales (ASCE, 2002; Wilbers, 2004). Defina (2003) carried out a numerical study on bed-features such as bars, and suggested that geometry of bars and celerity are the function of each other. In addition, Jerolmack and Mohrig (2005) investigated the morphodynamic evolution of bedforms to understand the process of splitting and merging of bedforms in different size over loose boundary channel. The time-lapse photography was used to visualize the evolution of bedforms for the characterization of their size, shape, and spacing, according to the imposed flow. They suggested that the variation in bedform geometry strongly influences the hydrodynamics of channel. Also, the variability in bedforms is dependent on the interaction among bedform development and unidirectional flows.

Spectral analysis of spatial and temporal bed elevation series at multiple scales has been performed to characterize the bedforms statistically (Nordin and Algert, 1966; Nikora et al., 1997; Nikora and Goring, 2001). These studies have shown the presence of multi-scale dynamic properties in migrating alluvial bedforms. Analysis of bed elevation series helps to get an insight into the multi-scale dynamic changes in bedforms and bed morphology in natural system (Nikora and Goring, 2001). In this regard, Singh et al. (2010) discussed the wide ranges of velocity power spectra and corresponding bedforms dynamics over a gravel bed using different grain sizes on a large flume. They recorded a set of bed elevation series and instantaneous streamwise velocities on a large scale experimental channel under two inflow discharges. They defined the scaling regimes of streamwise velocity power spectra and identified the temporal scales of bedform dynamics at different imposed flows. In the extension of their previous work, Singh et al. (2011) demonstrated the statistical description of developing bedforms using wavelet decomposition. They characterized the spatial and temporal scales of bed elevation series recorded in a 84 m long and 2.75 wide recirculating flume. Celerity of the bedforms was found to be decreased as a result of the increase in bedform dimensions and inflow discharge.

Furthermore, previous studies suggested that the prediction of variability in the bedform geometry plays an important role in the morphology of alluvial channels (Wang and Shen, 1980; Gabel, 1993; Van der Mark et al., 2008), which is stochastic in nature. Knowledge of the geometric variability of bedforms is important in the field applications such as dredging (a process necessary to keep a navigational channel sufficiently deep), which requires information on the highest crest elevations.

The mode of sediment transport is not always in the form of bedforms, it can also be in the form of sheet flow depending upon hydraulic conditions, shape, and size of sediment in the sedimentary environments.

1.6 Evolution of Sheet Flow

In an alluvial channel, sheet flow contributes significantly to sediment transport. Sheet flow occurs when tractive force is greater than resistive force, causing large amount of sediment transport under sheet flow (Gotoh and Sakai, 1997). Sheet flow is a thin layer of high sediment concentration that occurs above plane and noncohesive sediment beds. Available literature on laboratory and field observations of the sheet flow of bed material suggests that under sheet flow conditions the bed remains fairly plane where ripples and other bed topography features are absent and the bed material movement is restricted to a layer with few centimeters in thickness and comprised of moving sediment particles (Dingler and Inman, 1976; Wilson, 1987; King Jr, 1991; Conley and Inman, 1992; Ribberink and Al-Salem, 1994; Sumer et al., 1996).

The sheet flow layer thickness is closely related to erosion depth. Many researchers (Wilson, 1989; Asano, 1992; Sumer et al., 1996) have observed an approximately linear relation between the nondimensional sheet flow layer thickness and the Shields parameter. Inman et al. (1986) performed measurements in the field and observed a significant increase in the thickness of the sheet flow layer because of turbulent bursting that occurred near the moment of maximum velocity. Field measurements of sand concentration in the sheet flow layer have been carried out in the swash zone on a beach on the island of Norderney by Bakker et al. (1989) and Yu et al. (1991). Li and Sawamoto (1995) found that the sheet flow layer thickness also depends on the unsteadiness of the flow. They measured maximal intrusion depth of sheet flow about 2 to 5 mm and the maximal moving layer about 8 mm. Flores and Sleath (1998) carried out an experimental study and proposed relations for the sheet flow layer thickness with Shields parameter and median particle diameter. Dohmen-Janssen et al. (2001) observed that turbulence damping and roughness height were increased in presence of a sheet layer. Ahmed and Sato (2003) proposed a model to predict sheet layer movement through representative grain diameter of heterogeneous sediments.

Dohmen-Janssen et al. (2002) developed a model and also performed several experiments in a large oscillating water tunnel to study the sheet flow phenomenon. Sheet develops on

a high velocity regime when bed-features such as ripples and dunes are washed out and sediment transport consists in a thin layer close to the bed. They showed that the behavior of sheet flow is dependent on the near bed orbital velocity. In their experiments, a phase lag parameter (between sediment concentration and near bed velocity) is defined in terms of high velocities and short wave periods. Findings were compared with quasi-steady model and new semi-unsteady model, and found that for a large data set semi-unsteady model yields better agreement with respect to quasi-steady model.

O'Donoghue and Wright (2004) presented the detailed time and height-varying concentration measurement of oscillatory sheet flow in Aberdeen Oscillatory Flow Tunnel. They utilized conductivity concentration meter probes to measure the sheet flow layer thickness. An empirical equation was developed to characterize the time dependent concentration profile in the sheet flow layer, which involved erosion depth and reference concentration.

Myrhaug and Holmedal (2007) defined the characteristics of oscillatory sheet flow transport in terms of erosion depth and sheet flow layer thickness. Analytical relations were evaluated for characteristic statistical values of sheet flow layer thickness considering a stationary Gaussian narrow-band random process.

Dong and Sato (2011) conducted experiments to investigate the sediment transport in the form of sheet flow using uniform sand under asymmetric oscillatory flows in combination with relatively strong opposite currents. They used image analysis to predict maximum sheet layer thickness in the given scenarios. Also, the validity of the developed model was examined under wide range of experimental conditions.

Revil-Baudard and Chauchat (2013) proposed an analytical model by using the dense granular rheology and dilatancy law coupled with a mixing length approach and found the nondimensional relation for sheet flow layer thickness with Shields parameter, static friction coefficient, mean sheet flow layer concentration, and median particle diameter.

Pitlick et al. (2013) carried out experiments to explain the flood effect on bank erosion. Sheet flow was observed because of increased value of Shields stress from its critical value under the condition of overbank flow. Lanckriet et al. (2014) used the conductivity concentration profiler in their field study for quantifying the swash-zone hydrodynamics and sediment transport. They evaluated the relationships for sheet layer thickness and sheet load as a function of mobility number.

In the aforementioned studies, it has been revealed that bed-features such as bedforms and sheet layers were observed by increasing the main channel discharge, thus providing

excess shear stress. These studies were performed on the plane bed channels, where influence of seepage was neglected on the development and characteristic of bed-features.

1.7 Problem Descriptions

Granular boundaries of sand bed channels are permeable in nature, which allow water to penetrate through them in the lateral directions. The difference among the groundwater table and flow level in an alluvial channel causes lateral flow (seepage) through the granular boundary. Exchange of water can take place either way, i.e., flow from the channel (downward seepage) or flow into the channel (upward seepage), depending upon the difference of levels between the water in the channel and the surrounding groundwater table (see Figure 1.3). The exchange of water between main channel discharge and seepage flow is of significant importance because of its role in the sediment transport and morphodynamics of alluvial channels. Consequently, seepage has the potential to influence the flow characteristics such as velocity profiles and bed shear stresses in the vicinity of the channel bed. Seepage velocity through the channel boundaries may also affect the bed structure over rough boundary. This is an important parameter in the hydraulics of alluvial channels, which may lead to bed deformation and bank erosion.

In the current scenario, the ground water table is lowering because of maximum use of tube-wells in the surrounding area of natural channels. Therefore, the difference in the ground water table and flow level is increasing day by day in the flood plains of alluvial channels, causing downward seepage. Downward seepage plays an exceedingly important role in order to the design hydraulics structures such as dams and canals, particularly, it influences the stability of bed particles and canal slopes. Previous literatures suggest that unlined irrigation canals in permeable soils allow considerable loss of water through the bed and sides of the canals, resulting to reduce the conveyance efficiency of the canal (Krishnamurthy and Rao, 1969; Sharma and Chawla, 1975; Raja et al., 1983; Berenbrock, 1999; Carlson and Petrich, 1999; Fipps, 2005; Martin and Gates, 2014).

In the study of Krishnamurthy and Rao (1969), they investigated the seepage losses on Ganga canal using radioisotopes and reported the seepage losses as 2.2 m^3/day/m. Seepage loss in unlined channel was estimated by Raja et al. (1983) using nuclear technique and they found that the seepage losses vary from 1.3 to 4.3 m^2/106 m^2 of the wetted surface area. The field study was carried out by Dukker (1994) in order to measure the seepage losses using inflow-outflow technique on Lower Gugera Branch Canal and they observed a

significant variation in seepage rate ranges from 3.54 to 62.04 cm per day because of errors and uncertainties during measurements.

Regarding volumetric losses due to seepage in an alluvial channel, Berenbrock (1999) and Carlson and Petrich (1999) carried out studies on New York Canal and estimated cumulative seepage losses of around 12% and 20% of the inflow discharge. Yussuff et al. (1994) and Tanji and Kielen (2002) estimated 20-50% of water loss by volume of total flow in earthen canals of semi-arid regions. The study of Carr et al. (1990) reported that an irrigation canal in United States lost the water around 17% caused by evaporation or seepage, which was released for irrigation in the year 1985. An analysis of conveyance efficiency of the canal at the diversion of canal to the field in the Lower Rio Grande Valley in Texas was obtained as 69.7%, indicating loss of water in the form of seepage (Fipps, 2005). Kinzli et al. (2010) estimated more than 40% of water loss because of downward seepage using acoustic Doppler instrument to measure flow discharge in the earthen canal of New Mexico. In recent study, Martin and Gates (2014) carried out water balance analysis on earthen irrigation canals and estimated a loss of about 15% of the upstream flow because of seepage.

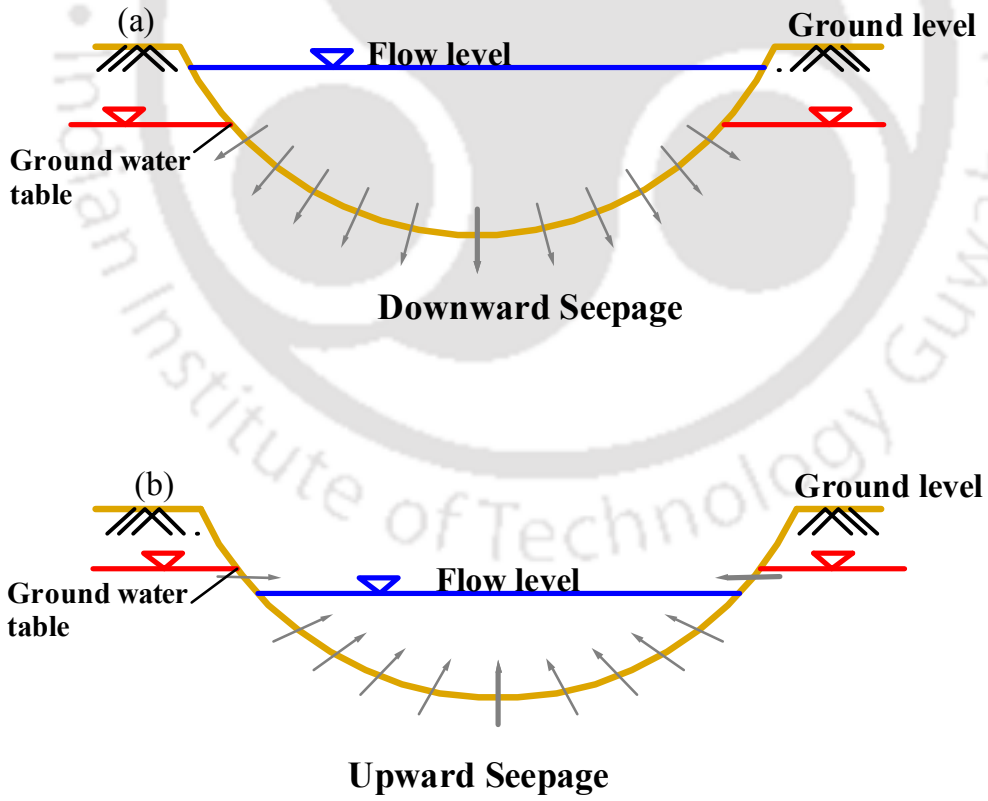

Figure 1.3: Seepage through boundary of an alluvial channel (a) downward seepage (flow from the channel) (b) upward seepage (flow into the channel)

Consideration of these losses is particularly important when building dams on small rivers, where the seepage losses may vary from 30% to 30-50% of the total discharge. The problem of seepage losses is very important for reservoirs on medium and large rivers, where the ground water inflow within the boundary of the reservoir forms a substantial part of the average river discharge.

Interaction amongst ground water and main stream flow is of significant importance due to its role in maintaining the river system and contaminates transport (Brunke and Gonser, 1997; Jones and Mulholland, 2000). This interaction of flows influences the hydrodynamics process of river system, which may lead to modification of the flow resistance, sediment movement characteristics, and bed morphology. The study of Willetts and Drossos (1975) noted that a water intake, when water was extracted from the channel caused a high speed flow towards the channel bed, can increase the local bed shear stress, which led to bed erosion in the vicinity of intake structure. In the costal environment, interaction of flows is more complex because of temporal and spatial variations of seepage in swash zone (Turner, 1995; Karambas, 2003).

Watters and Rao (1971) carried out an experimental study to observe the effect of seepage on the stability of bed particles. They evaluated the drag and lift forces on bed particle in the injection and suction scenarios and observed that injection inhibits the particle motion, causing increase the stability, whereas, suction increases the sediment movement. Regarding lift force, injection hinders the bed particle movement and suction holds opposite result.

Oldenziel and Brink (1974) reported that an increase in shear stress causes appreciably increases the bed particle movement on plane bed channel. They suggested that the rate of sediment transport decreases (increases) in case of upward (downward) seepage.

Willetts and Drossos (1975) conducted experiments on a narrow flume providing a small seepage zone and found that downward seepage causes localized scour hole around the seepage affected zone. Also, faster grains movement was observed over the length of seepage zone rather than elsewhere in the flume.

Maclean and Willetts (1986) investigated the changes of bed shear stress in with and without seepage conditions by visualizing the initiation of motion of the indicator grains. It was found that bed shear stress increases with the application of downward seepage.

Maclean (1991a) performed two sets of experiments in an open channel and a wind tunnel to measure the velocity by providing high rates of downward seepage. He observed that velocity decreases toward water surface and increases close to the channel bed under

the condition of downward seepage in the open channel.

Maclean (1991b) observed that the increase in bed shear stress in the presence of downward seepage, leading to local scour around the seepage zone. He found that an increase of downward seepage velocity by 10% causes around two times increase in bed shear stress as compared to uniform shear stress.

Prinos (1995) explained the Reynolds-average Navier-Stokes equation in order to study the influence of downward seepage on the boundary shear stress. In the seepage zone, it was found that the bed shear stress increases, while increasing downward seepage rate. The quantitative analysis signified that the increase in seepage velocity by 9% causes increase in the bed shear stress by eight times as compared to the without seepage case.

Cheng and Chiew (1999) carried out analytical and experimental studies considering additional force because of seepage on a sediment particle in threshold condition. They showed that the critical shear velocity decreases with the application of upward seepage.

Rao and Sitaram (1999) studied the seepage effect on the stability of bed particle by performing several experiments on experimental flume in the laboratory. They observed that downward seepage reduces the stability of bed particle and can initiate the movement of particle, whereas, upward seepage increases stability and it hinders the movement of sediment. Also, they found that bed erosion increases with increasing the downward seepage rate, while, upward seepage holds opposite result. They emphasized that the presence of seepage disturbs the stability of bed particles and it needs to be considered during the design of the stable alluvial channel.

Krogstad and Kourakine (2000) showed the effect of localized upward seepage on turbulent flow structure close to the channel bed in their experimental study. They found that bed shear stress significantly reduced when water entered through the channel boundary in the form upward seepage.

Chen and Chiew (2004) investigated the influence of downward seepage on the flow hydrodynamics on the plane bed channel using experimental approach. They observed that near the channel bed (towards water surface) velocities increases (decreases) with application of downward seepage. It was observed that the vertical distribution of streamwise velocities does not follow universal law of the wall in the presence of seepage. In addition to this, origin displacement, slip velocity, and shear velocity increases with increase in relative downward seepage, indicating distortion of boundary layer.

Lu et al. (2008) carried out an extensive review on the effects of seepage on the movement of sediment particles and they showed that the effective weight of a sediment particle increases with the application of downward seepage. The graphical representation of effective weight of particles and bed shear stress variations in accordance with the downward and upward seepages is shown in Figure 1.4. In the Figure 1.4, the positive and negative

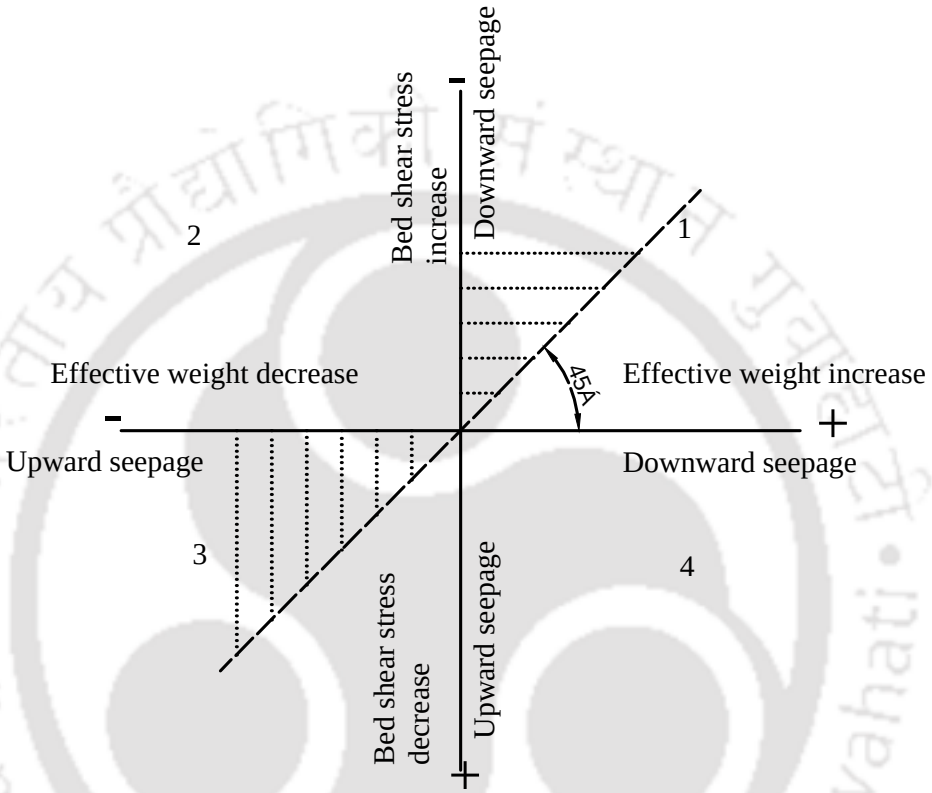

Figure 1.4: Description of bed particle stability under the influence of seepage using quadrant analysis of various forces acting on a particle (Lu et al., 2008)

signs signify the increase and decrease the movement of bed particles, respectively. As discussed earlier that downward and upward seepage cause increase and decrease of bed shear stress, respectively. It can be observed from Quadrant 2 that stability of bed particle reduced because of increase in bed shear stress and decrease in the effective weight of bed particles. However, stability of bed particle enhanced because of decrease in bed shear stress and rise of effective of weight as shown in Quadrant 4. Hence these both phenomenon can not be happened together. Apart from this, it can be observed from Quadrant 1 that downward seepage increases the effective weight of particles, resulting increasing the stability. In contrast, downward seepage has the propensity to increase bed shear stress, causing reduction the stability of bed particles. From these scenarios, it is signified that the movement of bed

particle depends on the relative magnitude of these opposing effects. Thus, stability of a sediment particle can be defined in terms of the equilibrium of forces, for example, if the effective weight of a sediment particle is less (more) than the force acting on it caused by flow then greater (no) movement occurs.

Rao and Sreenivasulu (2009) pointed out the significance of seepage in the canal design. They showed that downward seepage in any direction, either upward or downward, influences the resistance to flow as well as mobility of sediment particle on a stable channel bed. They observed that suction reduces the stability of the sediment particles and can initiate the bed particle movement, whereas, injection does the opposite. Thereby, it was concluded that effect of seepage should be examined before designing the earthen canals.

Kavcar and Wright (2009) modified the Shields parameters by considering the influence of vertical pore water flux (downward seepage) on the movement of sediment particles. Required bed shear stress for incipient motion of bed sediment was increased as the amount of downward seepage was increased. They also found that the bed hydraulic slope plays a significant role in order to characterize the initiation of sediment motion.

Sreenivasulu et al. (2011) presented the variation of stream power in the presence of downward in seepage affected channels and observed higher stream power at upstream end of channel and it decreases towards downstream direction because of changes in seepage quantity. It was observed that the higher stream power caused erosion at upstream end, consequently, eroded material deposited at downstream end due to reduction in stream power.

Rao et al. (2011) considered the effect of downward seepage on the geometry of sand bed channels. They found that the presence of seepage alters the stability of the regime channel as well as flow characteristics. They defined that the regime channels are free to adjust section, pattern, geometry, and shape in response to hydraulic changes. The bivariate and trivariate regression relationships were developed for an alluvial channel under the influence of downward seepage.

Liu and Chiew (2012, 2014) performed both theoretical and experimental investigations in order to understand the seepage effects on the initiation of cohesionless sediment particles. In their theoretical analysis, external force exerted because of downward seepage was examined. They conducted five experiments on uniform sand bed to quantitatively show downward seepage effects on sediment entrainment. These analytical and experimental works provide an overall understanding regarding seepage effects on the sediment move-

Table 1.1: Literature to show the effect of seepage on channel flow and bed dynamics

Authors	Flume and seepage dimensions			Seepage effects			
	Length (m)	Width (m)	Seepage zone (m)	Bed shear stress		Sediment transport rate	
				US	DS	US	DS
Watters and Rao (1971)	4.6	0.7	1.5	NA	NA	-	+
Oldenziel and Brink (1974)	15	0.5	4	NA	NA	+	-
Willetts and Drossos (1975)	3.6	0.076	0.125	NA	NA	NA	+
Maclean and Willetts (1986)	5	0.076	5	NA	+	NA	NA
Maclean (1991a)	12	0.3	0.28	NA	+	NA	NA
Maclean (1991b)	5	0.075	0.13	No	+	No	+
Cheng and Chiew (1998)	30	0.7	2	-	NA	NA	NA
Chen and Chiew (2004)	30	0.7	2	NA	+	NA	NA
Cheng and Chiew (1999)	7.6	0.21	0.5	-	NA	+	NA
Rao and Sitaram (1999)	3.6	0.158	2.4	+/-	+/-	-	+
Krogstad and Kourakine (2000)	3.5	0.46	0.12	-	NA	NA	NA
Chen and Chiew (2004)	30	0.7	2	NA	+	NA	NA
Lu and Chiew (2007a)	30	0.7	2	NA	NA	-	+
Kavcar and Wright (2009)	7.5	0.6	2	-	+	NA	NA
Dey and Nath (2010)	12	0.6	2	-	+	NA	NA
Sreenivasulu et al. (2010)	25	1.8	20	NA	+	NA	NA
Dey et al. (2011)	15	0.6	2.1	-	+	NA	NA
Rao et al. (2011)	25	1.8	16	NA	NA	NA	+
Liu and Chiew (2012)	30	0.7	2	-	+	NA	NA
Sreenivasulu et al. (2011)	25	1.8	20	NA	NA	NA	+
Cao and Chiew (2014)	9	0.3	0.5	NA	NA	NA	+
Deshpande and Kumar (2016b)	20	1	15.2	NA	+	NA	+

ment. In their study, results indicate that downward (upward) seepage increase (decreases) shear velocity.

Cao and Chiew (2014) carried out laboratory experiments and theoretical analysis to investigate the influence of downward seepage on sediment transport in closed-conduit flows. Small seepage rate did not influence the overall sediment transport and movement of bed particles remained unchanged. Theoretical analysis shown that bed particle experiences additional force because of downward seepage, which caused external vertical drag, induced by suction, on the bed particle. In the flow analysis, they found that suction causes increase in horizontal and vertical near bed velocities ascribed to driving force on the bed particle, indicating sediment transport in the presence of downward seepage.

Deshpande and Kumar (2016a) observed that downward seepage alters the channel morphology and increases the bed shear stress. They developed an empirical relationship for the thickness of sheet flow layer by considering downward seepage as an independent parameter. Lu and Chiew (2007a), Dey and Nath (2010), Dey et al. (2012), and Deshpande and Kumar (2016b) investigated the effect of seepage on turbulent characteristics of flow in open channels. They observed that near-bed velocities increases after the application of downward seepage. Important findings and among others in terms of influence of seepage on bed shear stress and sediment transport are summarized in Table 1.1.

1.8 Hydrodynamics Perspective Cross-sectional Shape of the Channel

Dynamics of sediment transport can be introduced as a part of the field of two face flows, i.e. flows of a water that contains within it discrete particles of some solid such as sediment. In sediment transporting flows, turbulent characteristics are far more important than laminar flows properties. In this regard, turbulent sediment-transporting flows show one of the most complex problems in all of fluid mechanics and hydraulics for two important reasons (1) the presence of the included phase can alter the turbulent structure and (2) in many cases the flow boundary consists of the sediment particles, and then the flow can develop its own boundary but in turn it may get affected by that developed boundary.

Changes in the essential nature of the flows, starting with turbulent flow in a closed conduit and sediment transporting over a loose sediment bed in the last have presented in the Figure 1.5. The step from a circular pipe to a rectangular duct brings the presence of a weak but non-negligible secondary circulation, but there is no big difference in the structure of the shear flow turbulence. In the next step from rectangular duct to an open rectangular channel, the turbulence structure is again only slightly different, as are the secondary circulations. But the presence of deformable free surface here in open rectangular channel

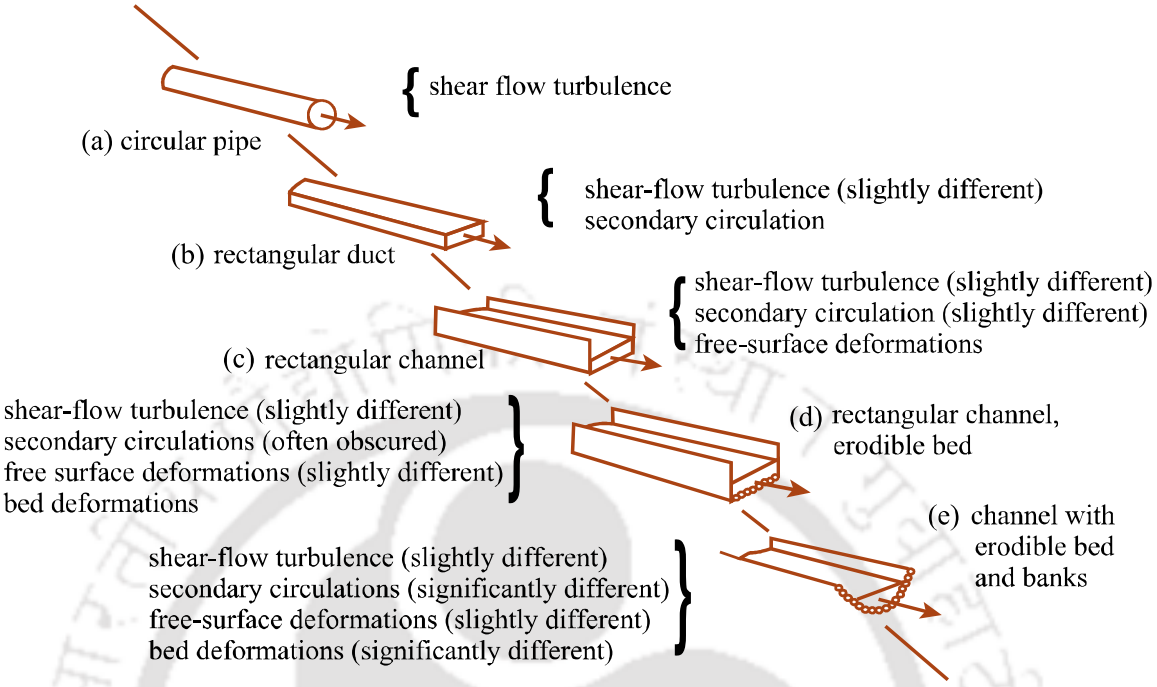

Figure 1.5: Complexity in sediment-transporting flows (Image source: MIT OpenCourseWare)

makes for rather different effects in unsteady flows. In the next step to an open rectangular channel with a loose sediment bed, is the big one: because the flow here can mold the bed now, and the bed too has a strong effect on the flow, the turbulence structure and the free-surface geometry are significantly different in certain ranges of flow. The last step, to an open channel with erodible boundaries, makes for greatly different bed geometry, at least in certain ranges of the flow.

1.9 Research Gap

In spite of the highlighted studies and progress regarding bed-features dynamics till date are not significant to give answer to the general questions such as 'how to explain initiation of bed-features, including shapes and sizes, variability, and statistical natures?' A wide range of aspects of the alluvial channels with deformable boundaries are still active areas of research, where the variability in bedform geometry is influenced by the material transport from the channel banks. As discussed earlier, there is a significant scope for exploring the

effects of the downward seepage in alluvial channels, having a curvilinear cross-sectional profile.

Very few studies with flow variations over the bedforms subjected to seepage have been reported. For example, Harrison (1968) carried out experiments on the artificial bedforms with downward seepage and observed that the angle of the lee face of bedform increased by 10 degrees. Lu and Chiew (2004) and Lu (2006) found that the downward seepage affects the height of the dunes. Lu and Chiew (2007b) carried out measurements on fixed bedforms with downward seepage and found reduction in the separation length. Thus, seepage being an integral part of alluvial flow is needed to understand the morphology and hydrodynamics of fluvial bedforms. In the Section 1.7, studies suggested that alluvial channels can have a wide range of seepage (approximately 12-50% of main channel discharge) depending upon the field specific conditions.

From the all previous research and discussion, it can be stated that alluvial channels experience a significant loss of water through their bed and banks in the form of downward seepage. Apart from depleting the conveyance capacity of the alluvial channel, hydrodynamic behavior and hydraulics alter in the presence of downward seepage. Therefore, it is needed to consider the influence of downward seepage with an appropriate precision in order to design the earthen canals for the hydraulic engineers. Because of practical complications in measuring data in actual field condition, it is intended to gain insight into the physics behind the development of bed-features in the presence of downward seepage by using instruments and experimental method.

1.10 Objectives of the Study

Alluvial channels are designed on the basis of the incipient motion condition of the particles resting on the bed and banks of the channel, which are intended to have stable boundaries that do not exhibit an appreciable erosion or deposition along the channel length. Majority of the experimental studies are performed to analyze the turbulent flow characteristics and bed morphology on the plane and fixed beds. Therefore, the aim of this study is to observe the influence of downward seepage on a threshold curvilinear cross-sectional shape alluvial channel using fine and coarse sand beds. The present study examines the role of turbulent flow in the development of bed-features with the application of downward seepage to an otherwise threshold channel. Based on this, following are the objectives of the present study:

1. Investigation of the turbulent flow structure for no seepage and with seepage conditions in threshold alluvial channels. Analysis of the temporal variations in the Shields stress and corresponding development of bed-features such as bedforms and sheet layer under the influence of downward seepage.

2. Temporal quantification and classification of the evolving bedforms in the presence of seepage.

3. Statistical analysis of the developing bedforms at different percentages of seepage and time intervals.

4. Observation of the hydraulics of sheet flow and its propagation over time and space on a threshold channel with downward seepage.

A flow chart of the objectives outlines in the present research work is shown below

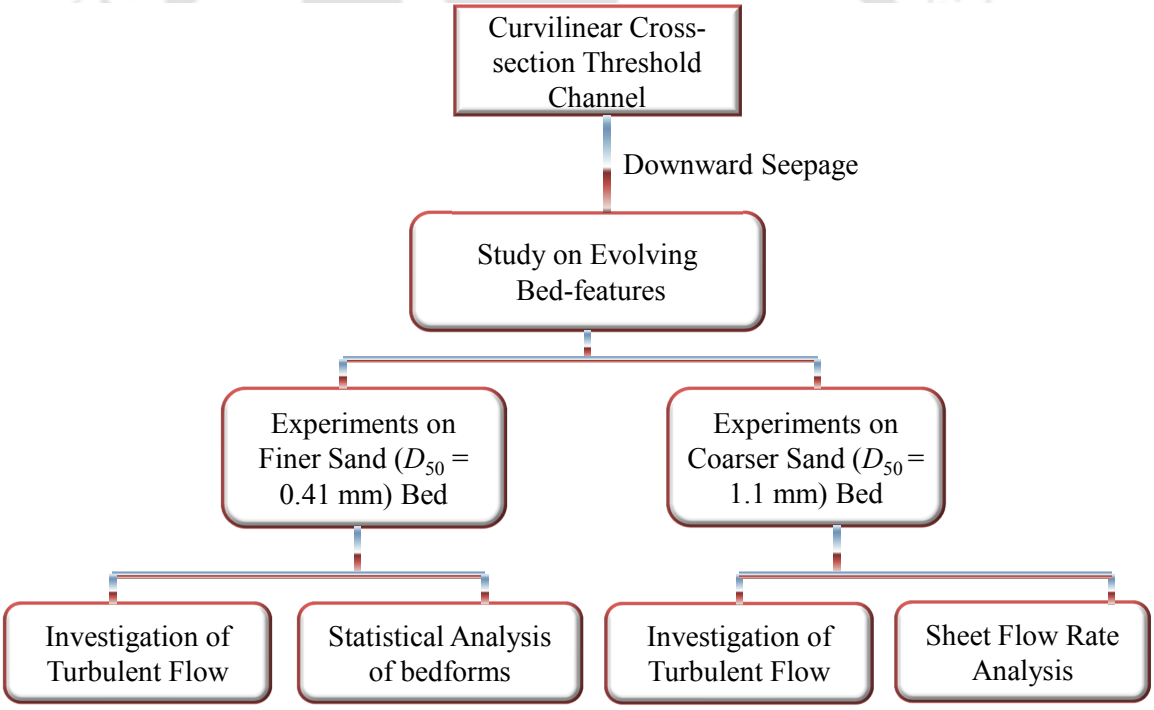

Figure 1.6: Experimental flow chart of the present research work

1.11 Scope of Thesis

To achieve the above mentioned objectives, laboratory experiments were performed on a large tilting flume. Experimental framework was designed for investigating the impact of seepage on the morphological and hydro-dynamical behaviours of stable channel in the sedimentary environment. In the first step, stability of curvilinear cross-sectional shape channel was checked without providing or extracting external flow discharge of channel. After successful completion of first step, this was followed by extracting the water from channel in the downward direction without stopping the experiment. In this scenario, turbulent flow dynamics and corresponding bed morphological changes in alluvial channels were analyzed. In addition, two different bed materials i.e. fine and coarse sands were used in the present study.

Organization of Thesis

The present study has been documented in the following six chapters:

Chapter 1 presents history of sand bed channels in the natural environment. Previous pioneering studies regarding bed-features development, classifications, and their characteristics in fluvial system were discussed. It shows the process of bed-features development (bedforms and sheet flow) and corresponding changes in turbulent flow structure. A detailed review regarding effect of downward seepage on sediment transport and the stability of alluvial channel is documented. After an extensive review, research gap, objectives of the study are outlined in this chapter.

Chapter 2 provides the detailed description of the experimental flume and methodology including channel design, selection of test section, and measurements. Bed sediment and state of art instruments used in the proposed experimental study are presented. By following this, experimental framework and program were discussed in this chapter. Detailed procedure of the data collection and its post-processing with temporal variations is given.

Chapter 3 gives the knowledge about the development of bedforms on fine sand bed channel when downward seepage applied on a stable alluvial channel. Also, the changes in turbulent of flow structure with the application of downward seepage are discussed to get an insight into physics behind the initiation of bedforms. Temporal and spatial descriptions of migrating bedforms and variation in channel cross section including equilibrium state

of the channel are shown. Further, variability and classifications of these bedforms in the presence of seepage are discussed.

Chapter 4 presents the statistical analysis of migrating bedforms with varying downward seepage percentages. Analysis of celerity of these bedforms including probability density function, and tail behaviour is presented. Dynamic behaviour of developing bedforms is characterized at different time intervals and seepages using probability distribution function, scale dependent statistical analysis, power spectral density function. In addition, influence of different seepage discharges on turbulent flow characteristics is discussed.

Chapter 5 deals with the effect of downward seepage on stable coarse sand bed channel. It shows the changes in bed morphology and flow process when seepage was applied in downward seepage on this channel. Variations of Shields stress and stream power with channel cross section are presented. Hydraulic characteristics of sheet layers at different time intervals are discussed. Linkage between flow and sheet layer development is described by analysing the turbulent flow. Also, an empirical equation to calculate sheet flow rate is documented by taking seepage into consideration.

Chapter 6 includes the conclusions and future recommendations of the study.

"The river dragged both of them out and,
current took them down the stream..."

Robert Whalen

2

Experimental Set–up and Methodology

2.1 Overview

Study on the experimental flume is most important and interesting way to solve the problem related to sediment transport and bed morphology because of a greater control on the hydraulic conditions in the flume. Therefore, hydraulic engineers depend on the empirical relations, developed based on the experimental measurements and intuitions, to design of the hydraulic structures. Sound physical basis for an empirical formulation is important in a way that it may have a far greater significance in solving complex problems. Various hydraulic flow conditions can be simulated by performing experiments in laboratory through suitable dimensional analysis in the light of basic principles of mechanism. In the previous studies, experimental investigations have been done for the chronological development in several fields of sediment transport such as incipient motion and bed morphology in sedimentary environment.

As discussed in Chapter 1, the aim of this study is to analyze the role of downward seepage behind the development of different bed-features of sand bed channels such as bedforms and sheet layers and corresponding turbulent characteristics of flow. An experimental approach can be used to simulate the behavior of the channel morphology in different given scenarios. To observe the overall fundamental effect, various hydraulic conditions can be provided by changing bed material, bed slope, flow rate, and seepage velocity. In the present work, experimental framework was designed in such a way that the maximum

use of the available equipments and facilities in the lab. In this beginning of this chapter, detailed description of experimental set-up and equipment and measurements procedure are discussed. At the end of chapter, details of experimental methodology and techniques are presented in order to achieve the objectives of the present study.

2.2 Bed Sediments

Two types of sands were used as the bed material in all the experimental runs. Sieve analysis was carried out to determine the particle size of the sand (see Figure 2.1). Grain size distribution for given sand can be considered as uniform sand if the value of the geometric standard deviation (σ_g) is less than 1.4 (Marsh et al., 2004). Geometric standard deviation is calculated as:

$$\sigma_g = D_{84}/D_{16} \tag{2.1}$$

where D_{84} (D_{16}) is defined as the size of grain for which 84% (16%) of the sample is finer by weight. Median diameter (D_{50}), geometric standard deviation, and dry angle of repose were obtained as given in Table 2.1 for the sand used in this study. In this study, both the sands are considered uniform.

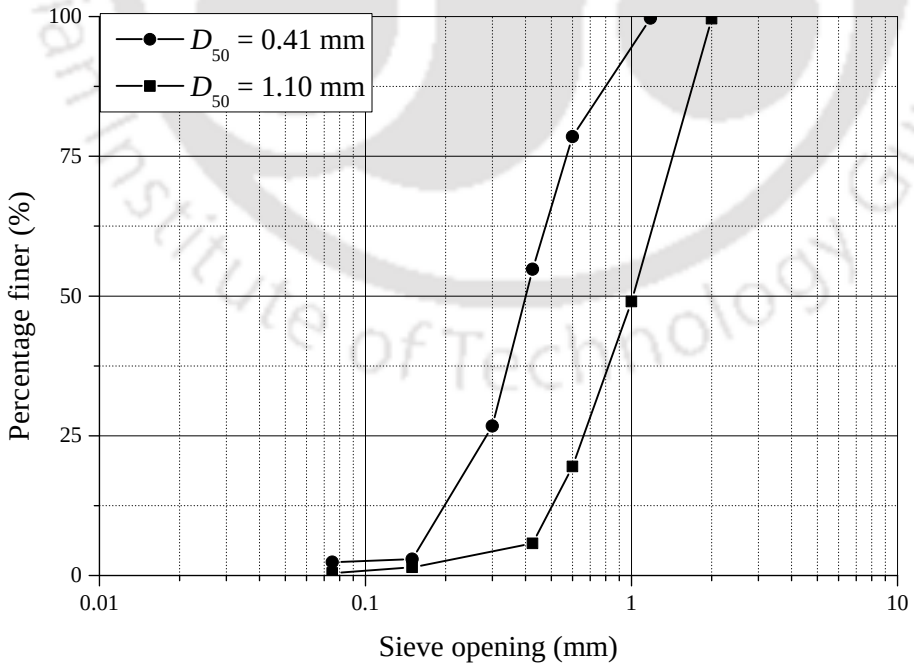

Figure 2.1: Grain size distributions of bed sediments

Table 2.1: Characteristics of bed sediment used in the present study

S.No.	Bed sediment	D_{50} mm	Standard deviation (σ_g)	Dry angle of repose, ϕ degree	Specific gravity, G
1	Fine Sand	0.41	1.17	32.55	2.65
2	Coarse Sand	1.1	1.03	31.15	2.65

2.3 Tilting Flume

The experiments were performed in a 20 m long, 1 m wide, and 0.72 m deep recirculating transparent plexi-glassed tilting flume as depicted in Figure 2.2. The schematic diagram of experimental flume is shown in Figure with detailed description.

The seepage facility was provided beneath the main channel as shown in Figure 2.3. Length, width, and depth of seepage chamber were (measured from the downstream end of the flume) 15.2 m, 1 m, and 0.22 m, respectively. Two meters of the upstream length of the main channel bed was made non-porous and the remaining length of the channel was made porous by covering with a fine mesh (0.1 mm x 0.1 mm aperture), which was supported with the help of a steel tube structure placed on the bottom of the channel (0.22 m high). The void space between bottom of the channel and the mesh formed a seepage chamber. This mesh hindered the sediment particles from entering into the chamber. The seepage chamber was used to extract water through the sand bed (uniformly) in the form of downward seepage. A tailgate was provided at the downstream end of the main channel to maintain flow depth in the channel. Three pumping units (10 HP each) were deployed to supply water into the overhead tank. A regulating valve was used to supply a controlled amount of water in the main channel connected with the overhead tank. Main channel discharge was measured using a rectangular notch provided at the downstream collection tank. Two baffle walls were installed in the upstream tank in order to ensure smooth entry of flow in the flume. A photograph of the side view of the experimental tilting flume is shown in Figure 2.4.

2.4 Test Section

In the flume, flow is significantly affected because of entry and exit conditions of the channel. Strong fluctuations develop in the flow if it supplies to the flume directly such as through pipes. According to Nowell and Jumars (1987), “the problem can be viewed as

Figure 2.2: Photograph of the experimental flume erected at the Water Resources Laboratory, Indian Institute of Technology Guwahati, India

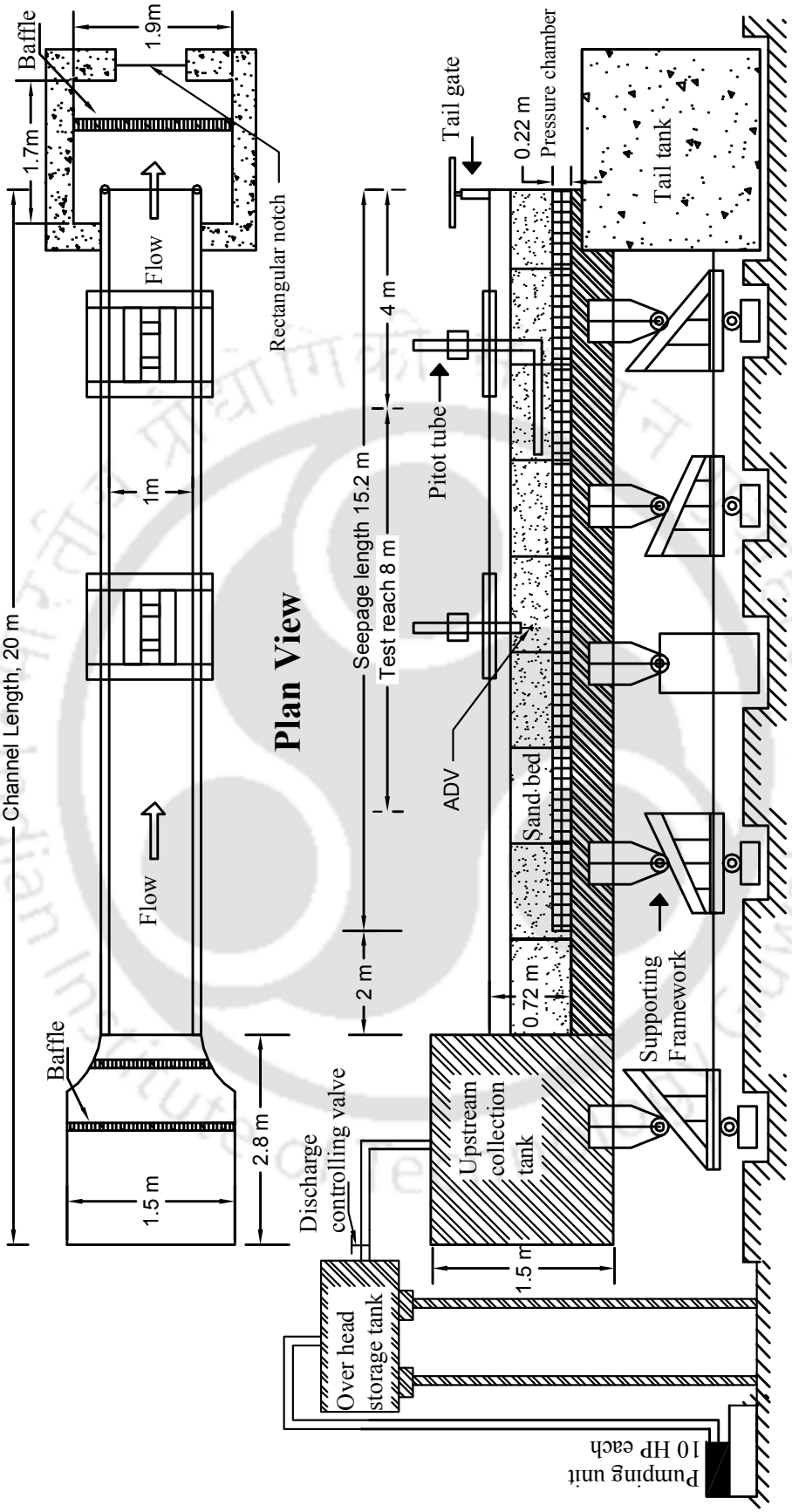

Figure 2.3: Schematic diagram of the experimental flume and facilities. Flow direction is from left to right

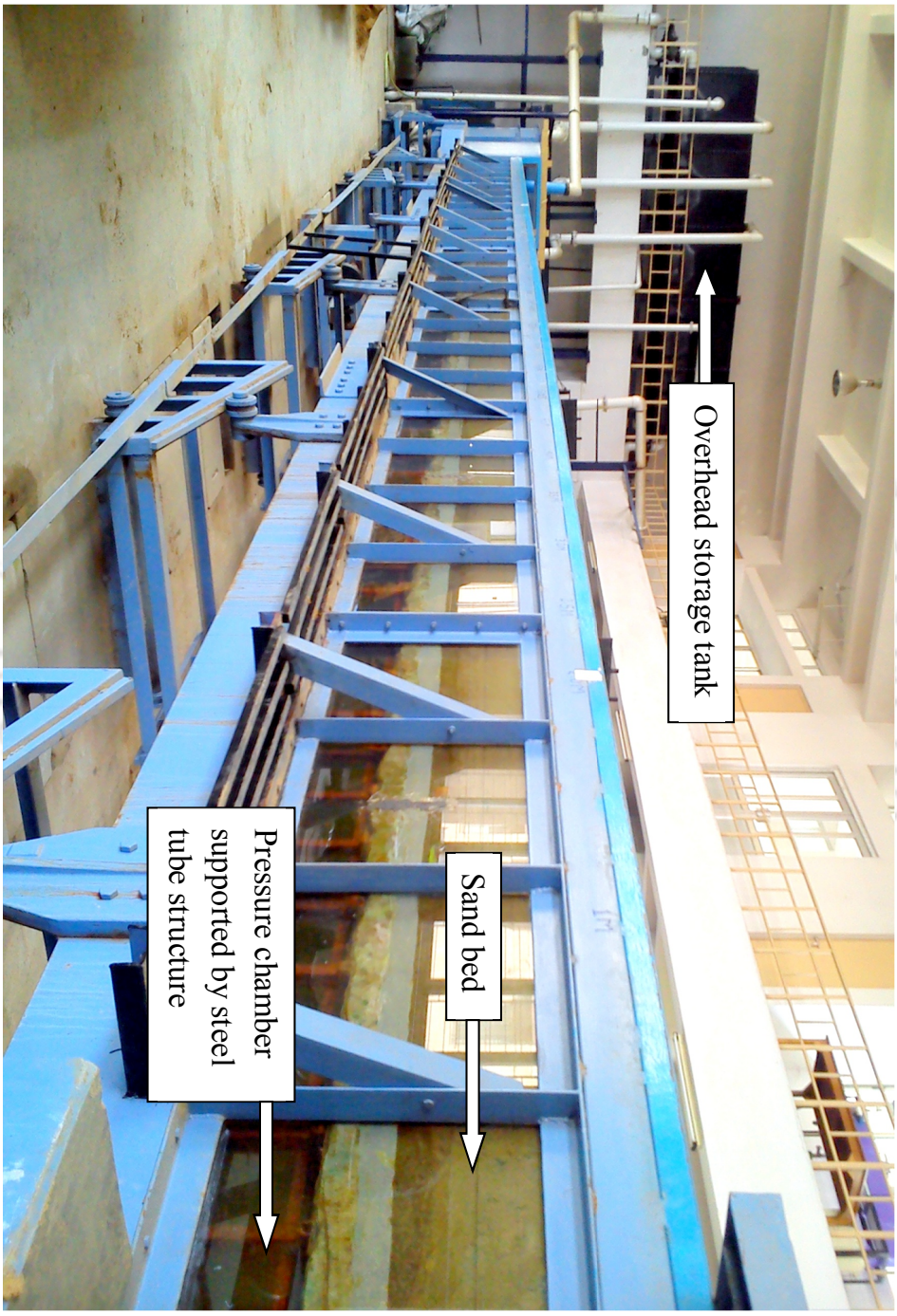

Figure 2.4: Photograph of side view of the experimental flume

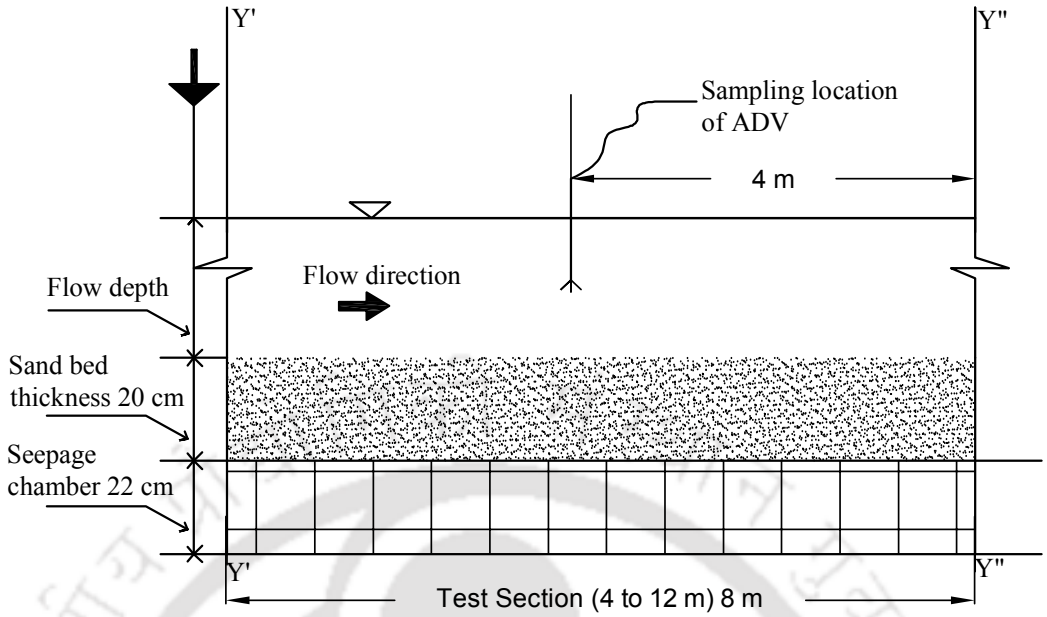

Figure 2.5: Test section considered in the flume between 4 to 12 m from the downstream end

getting the flow to 'forget' its recent history". In the present experiments, the arrangement was made in such a way to avoid the strong fluctuations present in the flow because of pipes. First water was collected in the upstream collection tank of the flume. After that water was released slowly and level of water increased gradually in the upstream tank prior to its introduction into the main channel. Couple of baffle walls was installed in the upstream tank of the channel entrance in order to ensure smooth entry of flow in the flume. Nowell and Jumars (1987) further pointed out that the exit problem can be viewed as not letting the flow know what is coming, i.e. of making a smooth exit without breaking cadence." Free overfall of the flow from the tailgate causes acceleration of flow in the near-bed region just upstream of the tailgate. Figure 2.5 shows the length of test section considered between two sections ($Y' - Y'$ and $Y'' - Y''$) of the flume. The test section of 8 m long was selected (4-12 m from the upstream end) in the center of the channel to minimize the effects of entry and exit of the flow. Measurement of geometry and flow were taken in this proposed test section only.

2.5 Main Channel Discharge

A regulating valve was used to supply a controlled amount of water in the main channel connected with the overhead tank. Main channel discharge (Q) was measured using a

Figure 2.6: Measurement of main channel discharge over rectangular notch located at downstream end of the flume

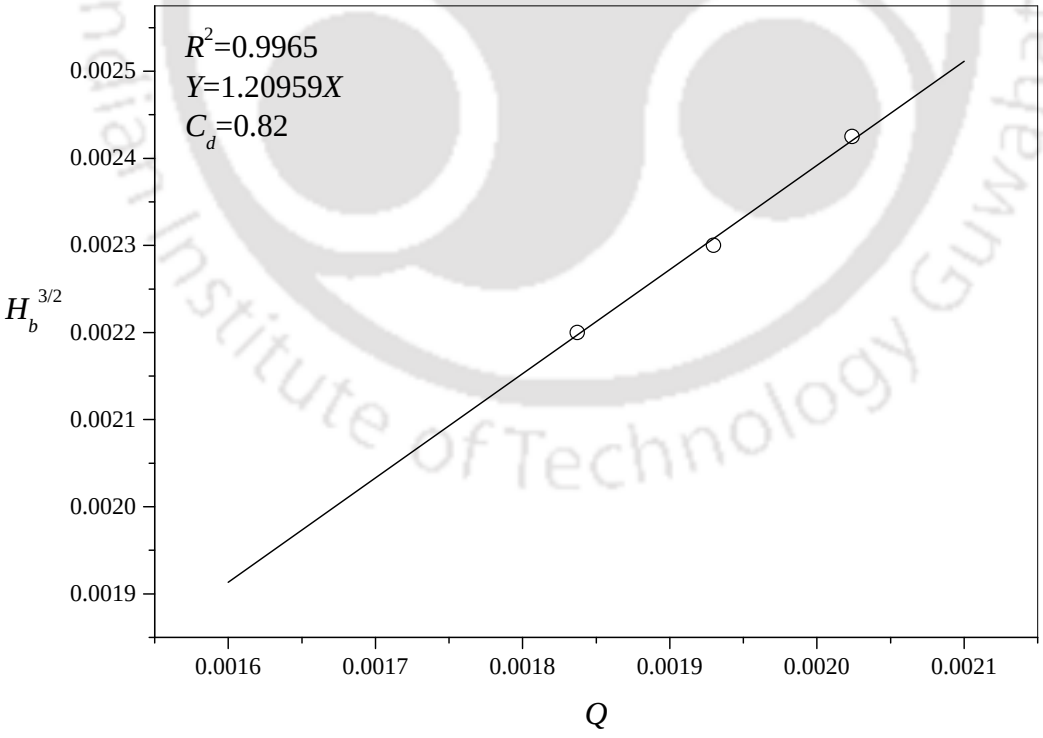

Figure 2.7: Calculation of coefficient of discharge for rectangular notch

rectangular notch provided at the downstream collection tank (Figure 2.6). Weir and baffle walls were installed in the downstream collection tank to get smooth flow over rectangular notch. Main channel discharge can be calculated as:

$$Q = \frac{2}{3} C_d L_n \sqrt{2g} (H_b)^{1.5} \tag{2.2}$$

where L_n is length of the notch (L_n = 0.5 m), g is the gravitational acceleration and H_b is the height of flow above the notch. And C_d is the coefficient of discharge for the rectangular notch and it was obtained to be 0.82 as presented in Figure 2.7.

2.6 Measurement of Downward Seepage

Couple of electromagnetic flow meters were installed at the downstream end of the chamber to measure and control of the downward seepage discharge (q_s). These flow meters were connected through the pipes to the seepage chamber as per the standards suggested in the manual. The electromagnetic flow meters are presented in Figure 2.8. The working principle of the electro-magnetic flow meter is based on the Faraday's Law. According to the Faraday's Law the voltage induced across any conductor when it moves at right angles

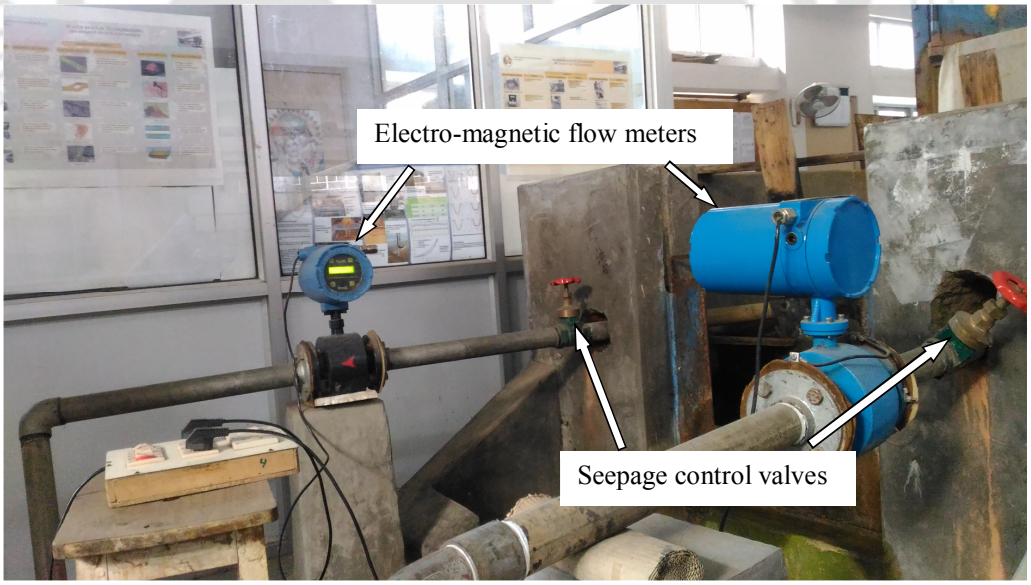

Figure 2.8: Electro-magnetic flow meters connected to the seepage chamber at downstream end of the flume

through a magnetic field is proportional to the velocity of that conductor

$$E = f\left(u_c, B_s, D\right) \tag{2.3}$$

where E is the voltage generated in a conductor, u_c is the velocity of the conductor, B_s is the strength of the magnetic field, D is the length of the conductor. The basic condition is that the fluid should be electrically conductive for the application of Faraday's Law. For measuring the flow discharge, an electro-magnetic field is generated in the whole cross section of the flow pipe. If this magnetic field is considered as the measuring element exposed to the hydraulic conditions in the entire cross section area of the pipe. Hence, the downward seepage discharge can be evaluated by using following formula:

$$q_s = A_p u_c \tag{2.4}$$

where q_s is the downward seepage discharge (m^3/s), A_p represents the cross section of the pipe (m^2), and u_c defines the fluid velocity passing through the flow meter (m/s)

2.7 Flow Depth

Flow depth of water in the channel was measured using a digital point gauge assembled on a moving trolley as depicted in Figure 2.9. This arrangement can move transverse and longitudinal directions to cover whole cross-sectional area along the test section. This is a direct indicating gauge, which eliminates observation errors caused by vernier and scale reading. It can be used in different ways as it can set to zero at any place in the operating range in order to get relative measurements. The liquid crystal digital display shows the reading of flow depth in different units and it has a resolution of $\pm$0.01 mm. A quick release mechanism allows smooth changes of positions. Where depth of flow is defined as the difference between the water surface level and the bed level.

2.8 Water Surface Elevation

The water surface slope in the experiments was obtained by using pitot tube and a digital display manometer (Rao, 2005). The outer tube consisting of static pressure holes and it was coupled with manometer that shows the piezometric height. This whole system was assembled on a moving trolley. This trolley moved along the flow and at the same time

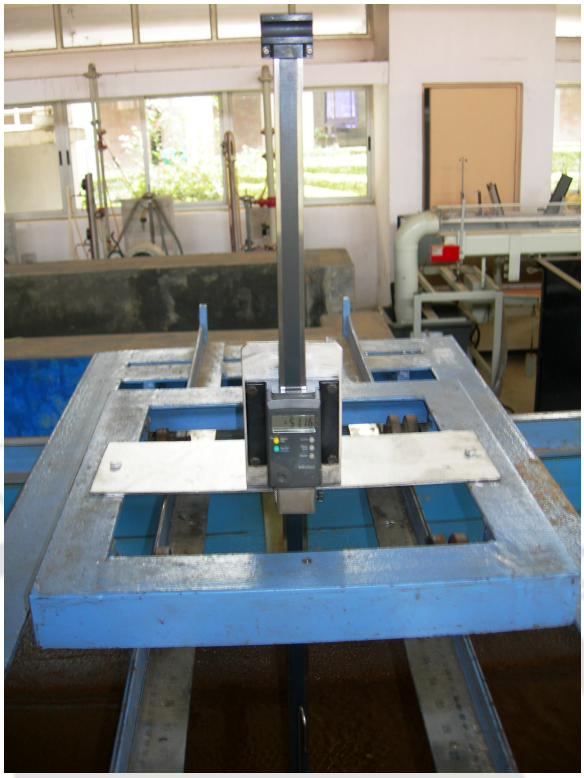

Figure 2.9: Digital point gauge assembled on a moving trolley

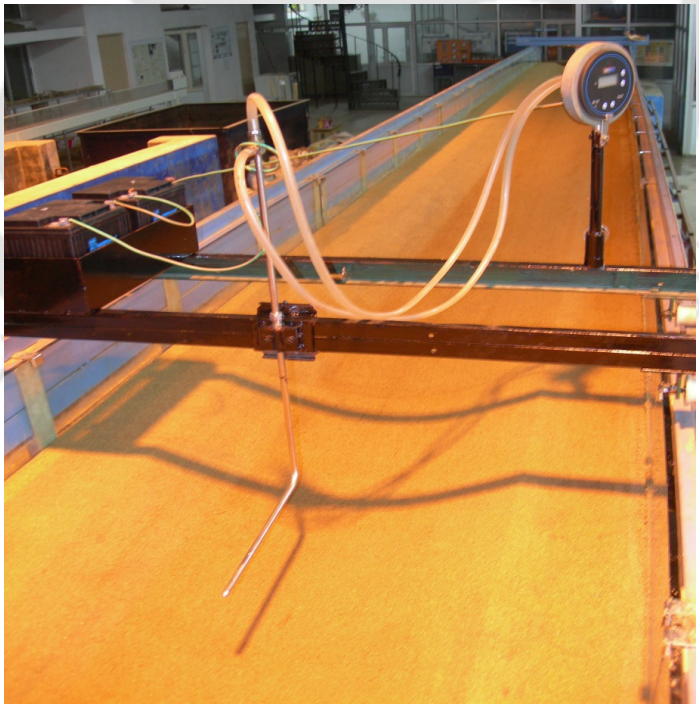

Figure 2.10: Assembly of Pitot tube and digital manometer for measuring the water surface slope

static pressure was recorded at different locations as presented in Figure 2.10.

2.9 Bed Slope

Bed slope of the channel was measured with the help of Total station as shown in Figure 2.11. A Total Station is a modern electronic device having the ability to simultaneously record a position horizontally and vertically. It has two components, a machine mounted on a static tripod, and a 'target' prism on a metal staff, which is moved around the site. The machine part of the Total Station has a lens somewhat like a telescopic rifle-sight with cross-hairs which are focused on the prism. The whole instrument revolves horizontally and the lens swivels vertically too. The Total Station is partly based on a principle used in traditional theodolites, where angles are calculated from vertical and horizontal 360-degree scales. It combines with a device known as an Electronic Distance Measurer or EDM.

Figure 2.11: Snapshot of the total station to measure the slope of channel bed

2.10 Geometric Measurements

Changes in the bed topography were monitored using 5 MHz Ultrasonic Ranging System manufactured by SeaTek. It contains eight transducers (depth sounding probes) attached to an automated moving trolley (Figure 2.12). The distance between each transducer was 25 mm center to center in transverse direction. The automated trolley can move in the longitudinal transect at a constant speed. The trolley was designed using four high torque DC geared motor connected to the wheels and speed was controlled with the help of Pulse width modulated DC motor speed controller switch in order match the sampling rate of the transducers. This instrument can record the samples at a maximum 5 MHz sound frequency to obtain the distance to a target. A transmit pulse of 10 microsecond duration is first sent from the transducer. The pulse travels through the water and is reflected off of a target. The reflected signal then travels back to the transducer. The transducer acts as both a transmitter and receiver. This return signal is then detected by the electronics. Since the speed of sound in water is known, and the time it took for the pulse to travel from the transducer to the target and back is known, the distance to the target can be calculated.

Figure 2.12: Transducers of SeaTek Ultrasonic Ranging System with automated moving trolley

Ultrasonic pulses transmitted by each probe were reflected off the sediment bed or water surface and received again by the probe. The distance d from the probe to the reflecting surface can be obtained as:

$$d = \frac{1}{2} C_s \partial t \tag{2.5}$$

where C_s is the celerity of the ultrasonic waves and dt is the measured time of the transmitted and received signal. The wavelength of 5 MHz sound waves in water is 0.3 mm. The resolution of the system is 0.1 mm, the accuracy (if several pings are processed per return) is +/- 0.2 mm. The limitation of the Ranging System is that it cannot measure the depth less than 3 cm and more than 100 cm.

2.11 Uncertainty Analysis

To obtain the accuracy in the measurements and data collection, uncertainty associated with the measured data has been carried out before performing the experiments. Uncertainty for the measurements of main channel discharge using rectangular notch (Q), seepage discharge from the electro-magnetic flow meter (q_s) and geometry measured from the SeaTek Ultrasonic Ranging System were analyses by using several repeated readings from each of these instruments. Transducers for distance measurement were kept over the water surface ensured to touch the water surface and the results are obtained shown in Table 2.2.

Table 2.2: Uncertainty analysis of the data collection

Statistical parameters	Q	q_s	h
Standard deviation	0.00068	0.00036	0.00092
Standard uncertainity	0.03478	0.03768	0.0184

2.12 Instantaneous Flow Measurement

For understanding the turbulent flow structure in the threshold channel under no seepage and downward seepage scenarios, instantaneous velocities were recorded with the help of a four beam down looking Vectrino+ acoustic Doppler velocimeter (ADV) developed by Nortek (Figure 2.13). The instrument allowed data collection at a higher sampling rate up

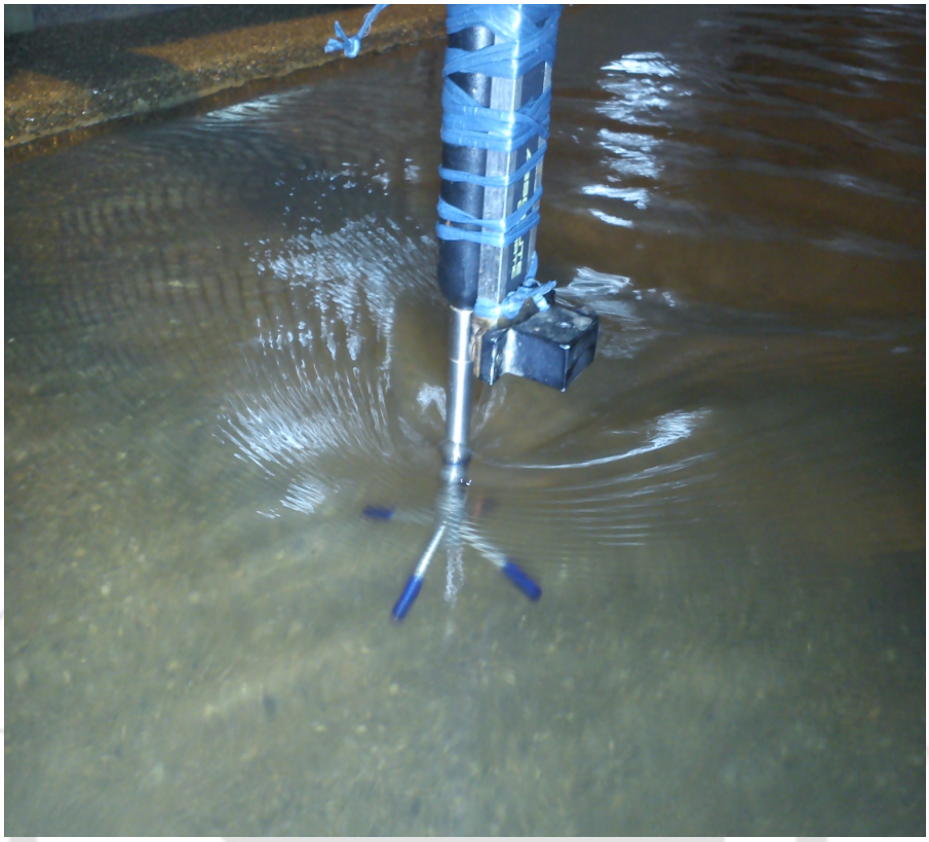

Figure 2.13: Vectrino+ Acoustic Doppler Velocimeter for measuring the instantaneous flow velocities

to 20 MHz. The Vectrino uses the Doppler effect to measure instantaneous velocity as shown in Figure. The Doppler effect is the change in pitch that is heard when either the source of a sound or the listener is in the motion. For example, when the listener hears the sound of a train horn, the pitch of the horn is higher when the train is approaching towards the listener, and the pitch is lower when the train is moving away from the listener. This variation in pitch tells us how the movement of train in terms of changes in the pitch of sound. Vectrino transmits short pairs of acoustic pulses, listens to their echoes and ultimately measures the change in pitch or frequency of the returned sound.

The ADV uses a pulse-to-pulse coherent Doppler methodology to record the sample the flow velocities (Brumley et al., 1991). This sound is not actually reflected from fluid particles. Velocity of water was considered as the sediment particles flow along the flow. It is rather reflected from the small particles or the seeding particles contaminated in water, which move with same average speed as of water. Consequently, the measured velocity is the velocity of the water. In a separate echo sounder mode, the ADV also allowed the

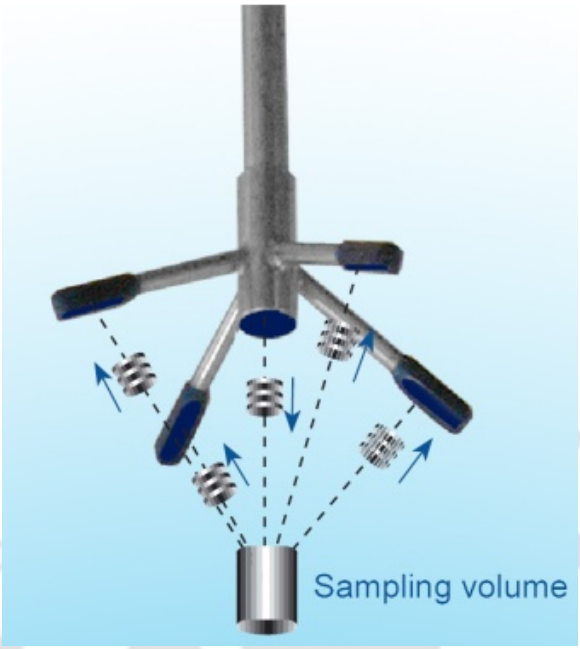

Figure 2.14: Graphical description of transmitter and four receiving probes with remote sampling volume in Vectrino+ ADV (Image source: Vectrino user guide)

measurement of the distance of the central transmitter from the boundary. The instrument collects data in a cylindrical remote sampling volume of user adjustable height located 5 cm below the central transmitter, thereby, the data could not be collected in the top 5 cm zone from the water surface (Figure 2.14).

The velocity data is collected in the computer system using the software Vectrino^{+} developed by Nortek as depicted in Figure 2.15. In the present experiments, the height of the sampling volume was set at 1 mm when very near to the bed ensure that the sampling volume did not touch the particles on the bed surface, and at 4 mm when away from the bed. Velocity measurements were carried out in a vertical profile and at each location instantaneous velocity samples were collected for the duration of 5 minutes at a sampling rate of 10 MHz. Velocity data was collected in the test section at the center line of the channel cross section at a distance of 8 m from the downstream end of the flume. To analyze uncertainty associated with the ADV measurements, 10 pulses were collected very near to the channel bed ($z \sim 10$ mm) each pulse had the duration of 5 minutes, where z is the distance of measurement point from the channel bed (positive in the vertically upward direction). Table 2.3 shows the values obtained from uncertainty analysis, where u, v, and w are the time-mean velocities in the streamwise, transverse, and vertical directions, respectively. Here, the term standard uncertainty of the mean describes the standard deviation of the mean for a set of

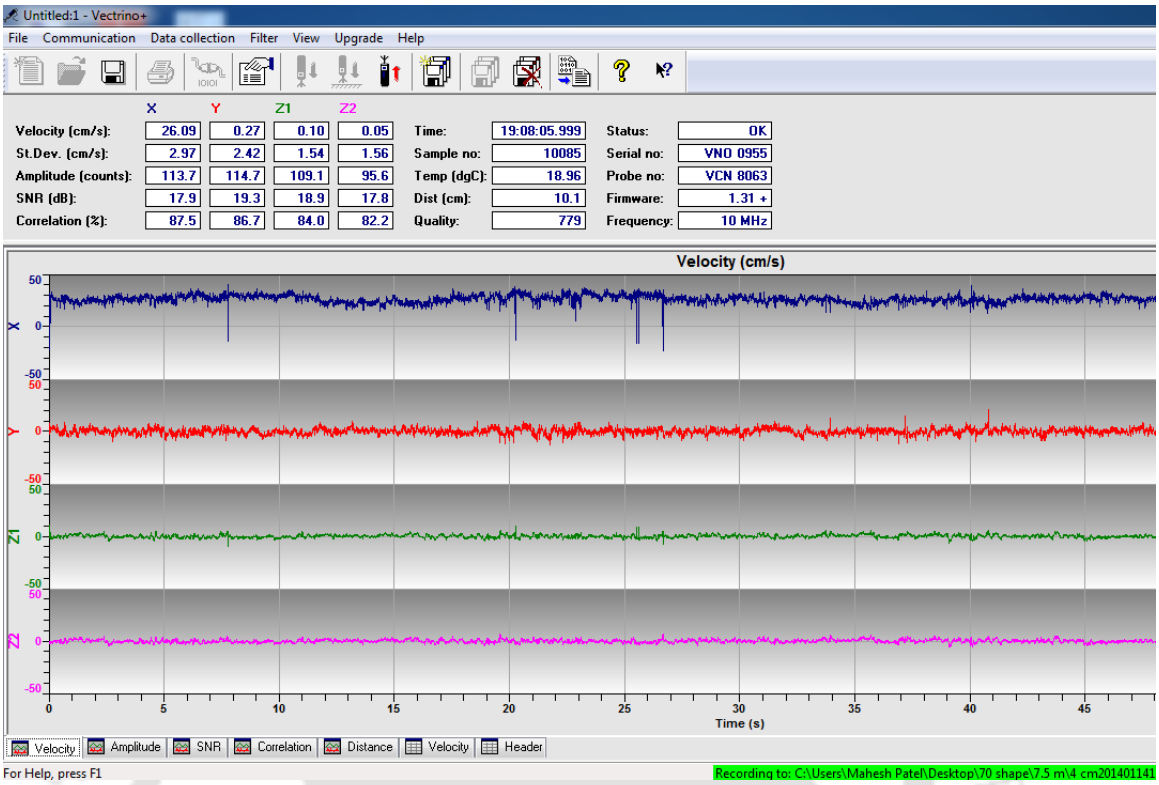

Figure 2.15: Vectrino+ software for data collection

several repeated pulses of instantaneous velocities. Standard uncertainty is calculated as:

$$S_u = \frac{S_d}{\sqrt{n}} \tag{2.6}$$

where S_d is the standard deviation and n is the number of measurements in the set. It can be said that the error present in the measured velocity was less than $\pm$5.4 mm/s for streamwise, transverse, and vertical directions and the uncertainty associated with the data was less than 1.7×10^{-3}

Table 2.3: Uncertainty associated with the ADV data

	u	v	w	$\left(\overline{u'u'}\right)^{0.5}$	$\left(\overline{v'v'}\right)^{0.5}$	$\left(\overline{w'w'}\right)^{0.5}$
Standard deviation, S_d	5.40×10^{-3}	8.08×10^{-4}	3.41×10^{-4}	1.59×10^{-3}	6.41×10^{-4}	2.5×10^{-4}
Standard uncertainty, S_u	1.7×10^{-3}	2.56×10^{-4}	1.08×10^{-4}	0.5×10^{-3}	2.03×10^{-4}	0.8×10^{-4}

In all the experiments, signal to noise ratio (>15) and correlation amongst transmitted and received signals (>70) were recommended as a cutoff value. In the region very close to

the channel bed, correlation of the samples were reduced approximately by ±5% (Dey et al., 2012). The measured pulses of instantaneous velocities contained some spikes because of interference between transmitted and received signals. These data were needed to be post processed or filtered. The spike removal technique (Goring and Nikora, 2002) was used in such a way that the Kolmogorov's -5/3 scaling-law was satisfied in the inertial subrange with acceleration threshold values ranging from 1 to 1.5 (Dey et al., 2012). Velocity power spectra for the no seepage and seepage runs are depicted in Figure (at $z \sim 10$ mm), where F_{uu} is power spectra for the streamwise component of the velocity, f is frequency in Hz, and h is maximum depth of flow. Power spectra for unfiltered velocity pulses are presented in Figures 2.16(a) and 2.16(c) for the no seepage and with seepage experiments, respectively. Figures 2.16(b) and 2.16(d) show the spectral density function for filtered pulses of no seepage and with seepage experiments, respectively. In these Figures, applicability of the Kolmogorov's -5/3 scaling-law is presented in the inertial subrange of streamwise velocity power spectra.

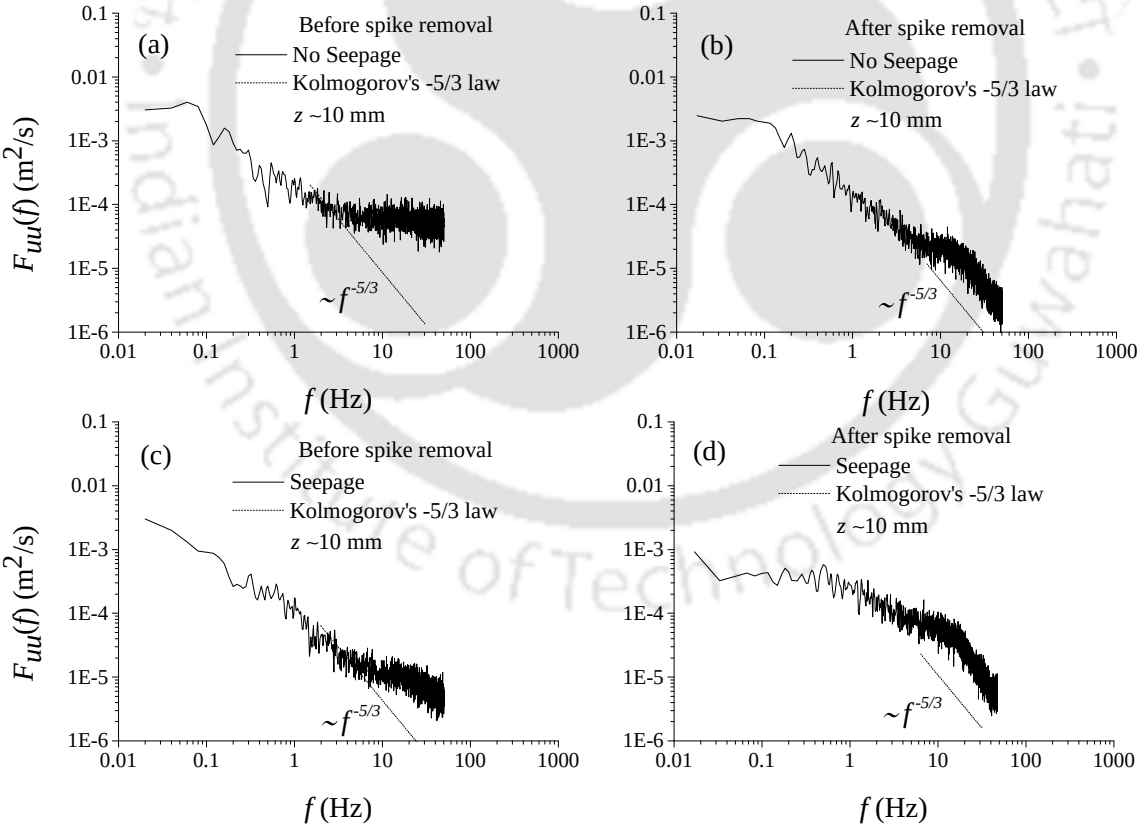

Figure 2.16: Streamwise velocity power spectra before and after spike removal with Kolmogorov's -5/3 law (at $z \sim 10$) mm) for the no seepage and seepage runs

2.13 Temperature and Kinematic Viscosity

Average temperature of water during an experiment is recorded by Vectrino+ ADV which has a temperature sensor (thermistor), located inside the probe head. The corresponding value of kinematic viscosity (m^2/s) is determined from standard tables.

2.14 Preparation of the Cross-Sectional Bed Profile

Shapes (plane and curvilinear bed in cross-sectional view) of threshold alluvial channels have been the subject to many investigations, as reported by the Thorne (1998). Hydrodynamics perspective of different types of shape in natural environment has been discussed in Section 1.8. Further, the cross-sectional shape of an alluvial river is governed by the interrelationship among water discharge, channel width, flow depth, velocity, channel slope, channel alignment, bed roughness, and sediment gradation of the alluvial soil. Stability of a channel is defined as the ability of a stream, over time, to transport the flows and sediments of the watershed while neither aggrading nor degrading and while maintaining a consistent dimension, pattern and profile (Rosgen, 2006). In natural rivers, cross-sectional shape controls the bed morphodynamics in terms of sediment transport from upstream that eroded from its bed and banks (Wobus et al., 2008). In this regard, Wolfert et al. (2006) discussed the deformation of cross-sectional shape and failure of banks during peak flows that cause widening of the river width and formation of depositional bedforms in natural streams. Many researchers have suggested that the natural stable streams are curved in their cross-sectional profile (Hey and Thorne, 1986; Millar and Quick, 1993). Existing literature seems to neglect the cross-sectional profile of the experimental channel bed before the development of bed-features. The theoretical regime equation developed by Lane (1953) fulfills the criteria contrary to the other empirical predictors. Mahmood et al. (1988) also stated that Lane's (1953) formulation of alluvial channel response is useful for trend analysis.

Lane (1953) proposed the curvilinear shape of a stable channel, which is derived on the basis that the tendency to motion of a particle in the direction transverse to the flow is proportional to the slope of the stream bed, as measured by the tangent of the angle with the horizontal, and the direction of flow is proportional to the depth of the stream. In Lane's (1953) geometric profile, at and above the water surface, the maximum angle of the side slope approaches the angle of repose of the material where the tractive stress provided by the flow vanishes. At points between the center and edge of the channel, the particles are

in a state of incipient motion under the action of the resultant of the gravity component of the particle's submerged weight acting down the side slope and the tractive force exerted by the flowing water. Thus, as the shear stress increases toward the center of the channel, the inclination of the side slope declines.

Relations between the centre line depth (h), lateral bank zone depth (y), area (A), average velocity (U), angle of repose of dry sand (ϕ), and top width (B) for a stable channel cross section have been given by Lane (1953) as:

$$A = \frac{2h^2}{\tan\phi} \tag{2.7}$$

$$U = \frac{1}{n}\left[\frac{h\cos\phi}{E\left(\sin\phi\right)}\right]^{2/3} S_0^{1/2} \tag{2.8}$$

$$B = \frac{h\pi}{\tan\phi} \tag{2.9}$$

$$E\left(\sin\phi\right) \approx \left(\pi/2\right)\left(1 - 1/4\sin^2\phi\right) \tag{2.10}$$

$$y = h\cos\left\{\left(\frac{\tan\phi}{h}\right)x\right\} \tag{2.11}$$

Shape of the main channel has been given using Equation (2.11). For top width 0.7 m, maximum depth of flow can be calculated as 0.135 m for coarse sands by rearranging Equation (2.9). Similar profile was obtained for the fine grained sand (0.41 mm), where top width is 0.7 m and maximum depth of flow is 0.14 m. A curvilinear cross-sectional profile was used in the main channel based on Lane's (1953) theory with a 0.70 m top width for finer sentiment is shown in X-X section of Figure 2.17.

2.15 Experimental Methodology

The experimental framework was designed for two types of experiments: no seepage and with seepage experiments. In no seepage experiment, i.e. particles were on the threshold of sediment movement without providing or extracting water through the channel bed and

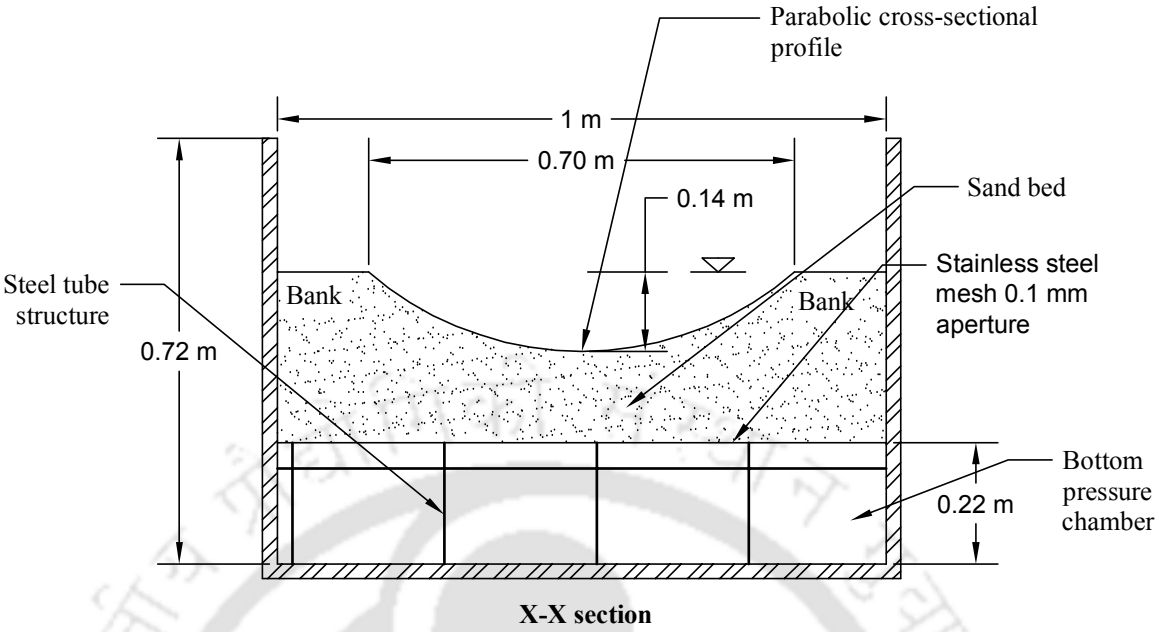

Figure 2.17: Curvilinear cross section of the channel according to Lane's (1953) geometric profile with top width 0.7 m and maximum depth 0.14 m for the finer sentiment

banks. In these experiments, the stability of Lane's (1953) geometric profiles on threshold condition was checked. At this stage, measurement of inflow discharge, water surface slope, and geometry of the cross section were recorded. After running no seepage experiment, when channel remained in stable condition after running several hours (10-12 h), some percentage of downward seepage (some percentage of no seepage inflow discharge) was applied and it was called as with seepage experiment. In the with seepage experiments, i.e. water was extracted in the downward direction from the threshold channel through the channel boundary, without any increment of inflow discharge. Detailed description of both types of experiments is given below.

2.15.1 No Seepage Experiments

The curvilinear cross-sectional Lane's (1953) shape of the main channel was prepared with the help of a wooden shaper (Figure 2.18). Special care was taken to prepare the channel to ensure the uniform geometry of channel cross section along the length of the channel (Figure 2.19). In the no seepage experiment, discharge was slowly introduced to the channel so that the average value of the shear stress increased gradually until the hydrodynamic forces of the flow were nearly identical with the resistive forces of the bed particles (on the bed surface). At this state, the sediment particles were at the threshold of motion

Figure 2.18: Wooden shaper for preparing the Lane's (1953) geometric profile in the flume

i.e. the bed shear stress was nearly equal to the critical bed shear stress. Yalin's (1976) criterion was used for the observation of incipient motion of the bed particles with the value of ϵ chosen as 10^{-6} for practical purposes. No seepage experiment was continued for the 10-12 h with sediment particles remaining in the state of incipient motion throughout the channel test reach as depicted in Figure 2.20. Sediment transport was sporadic along the test reach without developing any notable bed-features. In this conditions, stability of the channel was achieved with no deformation in the cross-sectional geometry of the channel.

In order to validate the threshold condition of the bed particles, Shields curve (Rao and Sreenivasulu, 2009) was used (see Figure 2.21) that gives a relationship between Shields stress (θ_c) and shear Reynolds number (R_*). Shields stress and shear Reynolds number can be calculated as:

$$\theta_c = \frac{\gamma R_h S_f}{(\gamma_s - \gamma)\, D_{50}} \tag{2.12}$$

$$R_* = \frac{u_{*b} D_{50}}{\nu} \tag{2.13}$$

Figure 2.19: Snapshot of the channel before performing the no seepage experiments

Figure 2.20: Channel after successful completion of no seepage experiment

where D_{50} is median particle diameter, u_{*b} is average shear velocity, ν is kinematic viscosity of water, and γ_s and γ are specific weights of sediment particles and water, respectively.

The average value of the shear velocity is evaluated as:

$$u_{*b} = \sqrt{gR_hS_f} \tag{2.14}$$

where g is gravitational acceleration, R_h is hydraulic radius, and S_f is friction slope and it can be calculated as:

$$S_f = S_w(1 - F^2) + S_0F^2 \tag{2.15}$$

where F is Froude number and S_w is water surface slope.

Figure 2.21 depicts the data plots between Shields stress and shear Reynolds number, in this plot the band indicates $\pm$10% variation from the Shields curve. Careful observation from Figure 2.21, it can be observed that the values of Shields parameters are overlapped within the band of Shields curve. This suggests that the bed particles were in the threshold state during no seepage experiments for both the sediment beds. Measurements of cross-sectional geometry, water surface slope, inflow discharge (Q_0), and flow depth (h) were taken during the experiment. The cross-sectional geometry along the length of the main channel was measured using Ultrasonic Ranging System.

2.15.2 With Seepage Experiments

Further, for investigating the influence of downward seepage on a threshold channel, water was extracted through the channel bed and banks in the form of downward seepage without stopping the no seepage experiment. It was observed that the sediment bed maintained in the threshold condition reached in the transporting condition. Particles were eroded from the bed and banks and deposited in the adjacent sections in the form of bed-features such as bedforms and sheet layers till the whole cross section was deformed. These experiments were continued for several hours until the channel geometry and physical characteristics of bed-features reached in the equilibrium condition depending upon sediments property such as fine and coarse sands. With seepage experiments were performed on fine and coarse sand beds in order to observe the effect of downward seepage on different type of bed sediment characteristics.

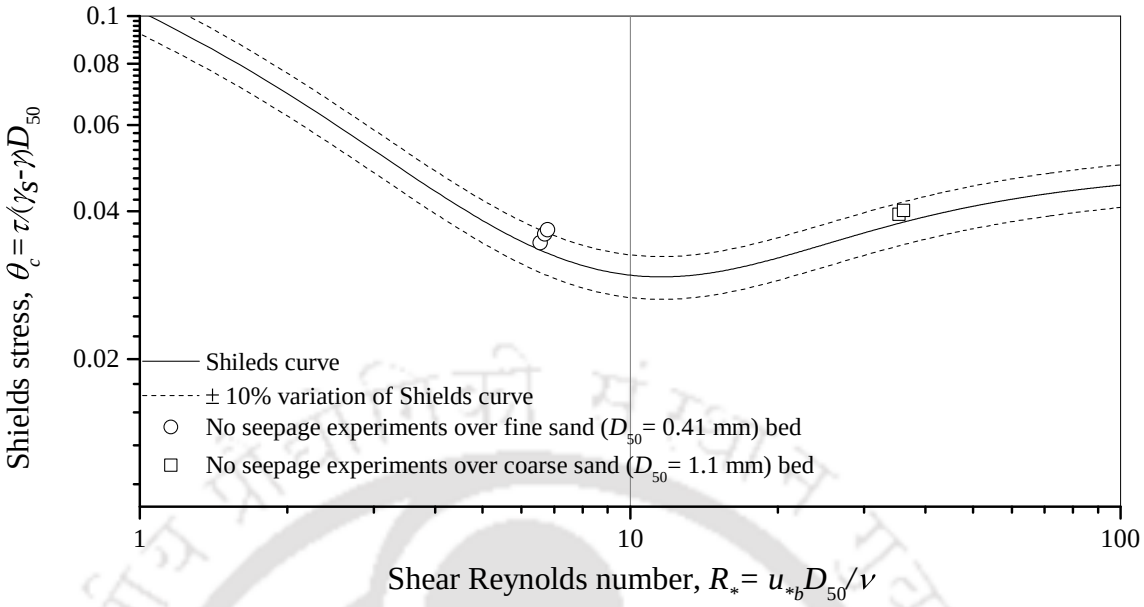

Figure 2.21: Investigations of Shields stress and shear Reynolds number for the incipient motion condition during no seepage experiments

2.15.2.1 Criteria to Consider the Seepage Velocity

In the Section 1.7, studies suggested that alluvial channels can have a wide range of seepage (approximately 12-50% of main channel discharge) depending upon the field specific conditions. These studies are performed on a field i.e. on a large scale, thereby, exact scaled model cannot be used in the experimental study. Therefore, the aim is to give the appropriate amount of the seepage in the present experimental study. Dey et al. (2011) suggested the criteria to consider the seepage velocity laboratory on the basis of natural system. They defined that the magnitude of seepage velocity can be taken as 1% or less of the average stream flow velocity. Furthermore, many experimental studies were performed on different seepage flow rates in terms of seepage velocities to investigate the influence of seepage in alluvial channels. For example, seepage velocities were considered as 0.0 to 0.88 mm/s by Richardson et al. (1985), 0.55 mm/s to 1.5 mm/s by Faruque and Balachandar (2011), and 0.4 mm/s to 7.3 mm/s by Cao and Chiew (2014) in their laboratory studies. In accordance with the ranges suggested for volumetric losses of water due to seepage and corresponding seepage velocities, the downward seepage was maintained at 15% and 20% of the main channel discharge for fine sand bed. The corresponding seepage velocities were provided as 0.2 mm/s and 0.26 mm/s, which are in accordance with the literature. In case of coarse sediment, the average flow velocity was greater for coarse sand bed than the fine sand,

thereby, higher seepage velocity was provided. Thus, the percentage of downward seepage was considered as 30% of the main channel discharge and corresponding seepage velocity 0.48 mm/s was provided.

2.15.2.2 Experiments on fine sand bed (median diameter = 0.41 mm)

Experiments were performed using fine sand (D_{50} = 0.41 mm) bed to observe the influence of downward seepage on turbulent flow characteristics and bed morphology. It was observed that stable shape of channel started to deform with the application of downward seepage as it was stable during no seepage experiment. Material transported from bed and banks was deposited at the adjacent section in the form of bedforms after running 3 h of seepage run as shown in Figure 2.22. In the beginning, small geometric features of bedforms were developed along the test reach. In the continuation of this process, cross-sectional shape of channel was deformed completely with a longer period of run (after 31 h), consequently, larger size of bedforms were seen at the end of seepage experiments (Figure 2.23)

Figure 2.22: Snapshot of the channel during run after 3 h run with the application of downward seepage on the sand of D_{50} = 0.41 mm

Figure 2.23: At the end of seepage experiment after 31 h of run

In these experiments, geometric measurements in the channel were made using Ultrasonic Ranging System that contains eight transducers. The transducers were assembled on an automated trolley in the transverse transect (distance between each transducer was 25 mm), which move on a rail at a constant speed. In order to understand the changes in channel morphology, measurements of the channel geometry in the test section, and water surface slope were recorded for the with seepage run and after 5 h, 10 h, 15 h, 24 h, and 31 h of the commencement of the seepage run for bed slopes 0.00176 and 0.00249. Similar measurements were taken after 9 h, 16 h, and 21 h during seepage experiments on slope 0.00116.

The phenomenon of erosion and deposition alters the channel geometry and flow dynamics everywhere along the length of the channel. Flow measurements provide the information about the changes in the hydrodynamics of the channel in the presence of seepage. For understanding the role of downward seepage behind the development of bedforms turbulent flow structure was investigated in no seepage and seepage scenarios. Instantaneous flow velocities were measured in three phases during no seepage and with seepage experiments.

1. **Phase-I measurement**: In this phase, when channel cross section was remained in stable condition after running several hours (10-12 h) during no seepage experiments, around 20-25 velocity samples were collected at center line of the cross section (8 m from the downstream reach end).

2. **Phase-II measurement**: Immediately after the application of downward seepage, when measuring location of the channel was not distorted until 3 h of seepage run, velocity measurements were taken during this period for determining the influence on the flow structure purely caused by the presence of downward seepage at the same location.

3. **Phase-III measurement**: Once the deformation starts after 2-3 h of downward seepage, this would have an effect of the flow structure. Measurement of flow was not possible at his duration because of abrupt deformation of channel boundaries. Therefore, with the passage of time (24-31 h) when cross section of channel attained an equilibrium state, velocity samples were collected at the same location after 24 h run.

2.15.2.3 Experiments on coarse sand bed (median diameter = 1.1 mm)

Similar experiments were carried out on the coarse sand bed to get the knowledge of the influence of downward seepage on higher grain size as bedforms were observed on fine sediment bed. In these experiments also, bed particles were eroded from the banks and deposited on the channel bed in the form of sheet layers with the application of seepage. It was observed that the cross section shape of channel was deformed and with the passage of time (11 h) channel attained different equilibrium cross-sectional shape (Figure 2.24). Finally, when the channel reached in an equilibrium state the experiment was stopped.

During with seepage experiment, measurements of the cross-sectional geometry, water surface slope, and variation in the bed profile of the main channel were recorded at 3 h, 4 h, 8 h, and 11 h after the commencement of seepage in the test section of the channel. Variations in turbulent flow are also evaluated using instantaneous flow measurement to understand the hydrodynamics of the channel in the presence of seepage. Instantaneous velocities were measured for no seepage and with seepage conditions. Phase-I and Phase-II measurements are taken at the same location and time as explained for fine sand bed. Also, for understanding the flow behaviour in the presence of sheet flow, velocity samples were collected over the sheet layer when cross-sectional geometry and progradation of sheet

Figure 2.24: Channel cross section at the end of seepage experiment on coarse sand of median diameter = 1.1 mm

Table 2.4: Descriptions of instantaneous flow velocity measurements

Sand type	Experimental condition	Flow measurement	Detail and time of measurement
Fine sand	No seepage experiment	Phase-I	During no seepage experiment
	With seepage experiment	Phase-II	Immediately after the application of seepage
		Phase-III	After 24 h run of the commencement of seepage
Coarse sand	No seepage experiment	Phase-I	During no seepage experiment
	With seepage experiment	Phase-II	Immediately after the application of seepage
		Phase-IV	After 8 h run of the commencement of seepage

flow reached in an equilibrium state after running several hours (between 8 and 11 h) of seepage run. Here, velocity measurement over sheet layer is defined as **Phase-IV measurement**. Table 2.4 shows the details regarding instantaneous flow velocity measurement in

different phases of experiment using fine and coarse sediment beds under no seepage and with seepage conditions.

2.15.3 Experimental Program

The experimental program consisted a set of experiments on a curvilinear cross section channel based on Lane's theory of stable channel. Top width of the channel was fixed to 0.70 m for all the experiments. Two types of sediment beds were used in order to distinguish the effect of downward seepage on physical characteristics of sediment. Seepage discharge and velocities were provided in accordance with the literature. Details of the experimental program are listed in Table 2.5.

Table 2.5: Summary of the experimental program for the present study

Bed sediment	Experimental run	Top width, B m	Maximum flow depth, h m	Bed slope, S	Inflow discharge, Q_0 m^3/s	Froude no., F_r	Seepage discharge, q_s ($\%Q_0$)	Seepage velocity, V_s mm/s
Fine sand	Set 1	0.70	0.140	0.00116	0.0175	0.30-0.40	15% and 20%	0.2 and 0.26
	Set 2		0.140	0.00176	0.0169			
	Set 3		0.140	0.00249	0.0161			
Coarse sand	Set 1		0.135	0.00116	0.0203	0.44-0.51	30%	0.48
	Set 2		0.135	0.00176	0.0209			

Experimental data for no seepage and with seepage experiments at different time intervals on fine and coarse sands is given in Table 2.6 to Table 2.16. Results were found to be consistent for all the slopes on both types of sands. Therefore, in order to avoid the duplicity and congestion, experimental data of single slope at different time intervals is given in the present work. Stream power (Ω) of the channel can be calculated as:

$$\Omega = \gamma Q S_f \tag{2.16}$$

where γ is specific weight of water and Q is main channel discharge.

[1]

In case of seepage experiment, friction slope for spatial varied flow can be calculated as

[1]Where one set defines the no seepage and with seepage experiments

suggested by Rao et al. (2011)

$$S_f = S_w(1 - F^2) + S_0F^2 + 2\rho u_s V_s/(h\gamma_s) \tag{2.17}$$

where F is Froude number, S_w is water surface slope, and S_0 is bed slope. Subscript '0' represents the parameter for no seepage experiments and subscript 's' represents the same parameter for with seepage experiments. Seepage velocity is V_s, u_s is average velocity in with seepage experiment, h is depth of flow, ρ_w is density of water. Average velocity of the flow (U) can be calculated as:

$$U = Q/A \tag{2.18}$$

where A is the cross-sectional area, Q is the main channel discharge:

$$Q_s = Q_0 - q_s\left(1 - {}^{X}/_{L}\right) \tag{2.19}$$

where Q_s is the discharge for the with seepage experiment, Q_0 is the discharge for the no seepage experiment, q_s is the seepage discharge over the seepage length (L) of the channel, and X is the distance from the tail gate. Seepage velocity (V_s) through the sand bed of the seepage length L can be evaluated as:

$$V_s = q_s/(PL) \tag{2.20}$$

where P is the perimeter.

Bed shear stress (τ) can be calculated as:

$$\tau = \gamma R_h S_f \tag{2.21}$$

where R_h is the hydraulic radius i.e. $R_h = A/P$

[2]

[2]Subscript '0' is used for no seepage experiment hydraulic parameters and similarly, subscript 's' is used for with seepage experiment hydraulic parameters

Table 2.6: Category: no seepage run (D_{50} = 0.41 mm, S_0 = 0.00176, Q_0 = 0.0169 m^3/s)

Cross Section	h_0 (m)	R_{h0}	Q_s (m^3/s)	u_0 (m/s)	F_0	S_{f0}	τ_0 (N/m^2)	u^*_{0b}	θ^*_0	R_*	Ω_0 (N/s)
12.00	0.138	0.076	0.0	0.280	0.324	0.00032	0.239	0.015	0.035	6.585	0.053
11.50	0.139	0.075	0.0	0.282	0.329	0.00032	0.238	0.015	0.035	6.579	0.054
11.00	0.140	0.074	0.0	0.284	0.333	0.00033	0.239	0.015	0.035	6.592	0.054
10.50	0.141	0.073	0.0	0.291	0.345	0.00034	0.243	0.016	0.035	6.644	0.057
10.00	0.142	0.073	0.0	0.294	0.348	0.00034	0.246	0.016	0.036	6.686	0.057
9.50	0.140	0.075	0.0	0.290	0.339	0.00034	0.246	0.016	0.036	6.678	0.056
9.00	0.140	0.075	0.0	0.290	0.339	0.00034	0.246	0.016	0.036	6.678	0.056
8.50	0.140	0.077	0.0	0.282	0.324	0.00032	0.241	0.016	0.035	6.614	0.053
8.00	0.139	0.074	0.0	0.297	0.349	0.00035	0.251	0.016	0.037	6.748	0.057
7.50	0.138	0.073	0.0	0.298	0.353	0.00035	0.250	0.016	0.036	6.738	0.058
7.00	0.141	0.072	0.0	0.292	0.347	0.00034	0.244	0.016	0.036	6.656	0.057
6.50	0.139	0.074	0.0	0.298	0.350	0.00035	0.251	0.016	0.037	6.752	0.058
6.00	0.140	0.075	0.0	0.286	0.335	0.00033	0.242	0.016	0.035	6.629	0.055
5.50	0.139	0.074	0.0	0.287	0.338	0.00033	0.241	0.016	0.035	6.614	0.055
5.00	0.138	0.075	0.0	0.289	0.337	0.00033	0.245	0.016	0.036	6.666	0.055
4.50	0.141	0.074	0.0	0.293	0.344	0.00034	0.247	0.016	0.036	6.697	0.056
4.00	0.138	0.077	0.0	0.285	0.329	0.00032	0.244	0.016	0.036	6.661	0.054

Table 2.7: Category: After 5 h with seepage run (D_{50} = 0.41 mm, S_0 = 0.00176, Q_0 = 0.0169 m^3/s), V_s = ∼0.20 mm/s (15% seepage)

Cross Section	h_s (m)	R_{hs}	Q_s (m^3/s)	u_s (m/s)	F_s	S_{fs}	τ_s (N/m^2)	u^*_{bs}	θ^*_s	R*	Ω_s (N/s)
12.00	0.119	0.070	0.016	0.297	0.358	0.00051	0.354	0.019	0.052	8.016	0.082
11.50	0.128	0.071	0.016	0.294	0.353	0.00050	0.346	0.019	0.051	7.931	0.079
11.00	0.129	0.071	0.016	0.292	0.350	0.00049	0.343	0.019	0.050	7.893	0.078
10.50	0.127	0.070	0.016	0.292	0.351	0.00050	0.343	0.019	0.050	7.891	0.078
10.00	0.130	0.071	0.016	0.288	0.344	0.00049	0.339	0.018	0.050	7.850	0.076
9.50	0.130	0.070	0.016	0.291	0.351	0.00049	0.339	0.018	0.049	7.846	0.077
9.00	0.129	0.070	0.016	0.288	0.347	0.00049	0.336	0.018	0.049	7.816	0.076
8.50	0.130	0.069	0.016	0.293	0.355	0.00050	0.339	0.018	0.049	7.844	0.077
8.00	0.132	0.070	0.016	0.285	0.344	0.00048	0.332	0.018	0.048	7.764	0.074
7.50	0.130	0.070	0.016	0.284	0.343	0.00048	0.332	0.018	0.048	7.766	0.074
7.00	0.132	0.069	0.015	0.285	0.346	0.00048	0.328	0.018	0.048	7.722	0.074
6.50	0.132	0.069	0.015	0.282	0.343	0.00048	0.326	0.018	0.048	7.690	0.073
6.00	0.132	0.068	0.015	0.287	0.350	0.00049	0.329	0.018	0.048	7.724	0.074
5.50	0.132	0.069	0.015	0.280	0.339	0.00048	0.324	0.018	0.047	7.669	0.071
5.00	0.132	0.071	0.015	0.272	0.326	0.00046	0.319	0.018	0.047	7.612	0.068
4.50	0.132	0.070	0.015	0.275	0.332	0.00047	0.321	0.018	0.047	7.631	0.069
4.00	0.132	0.070	0.015	0.272	0.327	0.00046	0.318	0.018	0.046	7.605	0.068

Table 2.8: Category: After 10 h with seepage run (D_{50} = 0.41 mm, S_0 = 0.00176, Q_0 = 0.0169 m^3/s), V_s = ∼0.20 mm/s (15% seepage)

Cross Section	h_s (m)	R_{hs}	Q_s (m^3/s)	u_s (m/s)	F_s	S_{fs}	τ_s (N/m^2)	u^*_{bs}	θ^*_s	R*	Ω_s (N/s)
12.00	0.115	0.065	0.016	0.316	0.396	0.00065	0.412	0.020	0.060	8.650	0.103
11.50	0.121	0.064	0.016	0.321	0.405	0.00065	0.408	0.020	0.060	8.608	0.103
11.00	0.116	0.065	0.016	0.312	0.389	0.00063	0.407	0.020	0.059	8.594	0.100
10.50	0.120	0.064	0.016	0.314	0.394	0.00064	0.403	0.020	0.059	8.556	0.100
10.00	0.123	0.065	0.016	0.311	0.389	0.00063	0.402	0.020	0.059	8.540	0.098
9.50	0.121	0.063	0.016	0.317	0.402	0.00065	0.402	0.020	0.059	8.540	0.101
9.00	0.122	0.065	0.016	0.309	0.387	0.00063	0.399	0.020	0.058	8.509	0.097
8.50	0.123	0.063	0.016	0.314	0.399	0.00064	0.397	0.020	0.058	8.492	0.099
8.00	0.124	0.063	0.016	0.315	0.401	0.00064	0.395	0.020	0.058	8.472	0.098
7.50	0.120	0.061	0.016	0.320	0.413	0.00066	0.397	0.020	0.058	8.495	0.101
7.00	0.124	0.064	0.015	0.308	0.390	0.00063	0.392	0.020	0.057	8.435	0.095
6.50	0.123	0.064	0.015	0.304	0.385	0.00062	0.387	0.020	0.057	8.384	0.094
6.00	0.123	0.063	0.015	0.307	0.389	0.00063	0.390	0.020	0.057	8.416	0.094
5.50	0.124	0.064	0.015	0.302	0.381	0.00062	0.387	0.020	0.056	8.378	0.092
5.00	0.125	0.066	0.015	0.291	0.361	0.00059	0.382	0.020	0.056	8.333	0.088
4.50	0.127	0.063	0.015	0.303	0.386	0.00062	0.383	0.020	0.056	8.335	0.092
4.00	0.127	0.063	0.015	0.302	0.385	0.00062	0.381	0.020	0.056	8.314	0.091

Table 2.9: Category: After 15 h with seepage run (D_{50} = 0.41 mm, S_0 = 0.00176, Q_0 = 0.0169 m^3/s), V_s = ∼0.20 mm/s (15% seepage)

Cross Section	h_s (m)	R_{hs}	Q_s (m^3/s)	u_s (m/s)	F_s	S_{fs}	τ_s (N/m^2)	u^*_{bs}	θ^*_s	R*	Ω_s (N/s)
12.00	0.099	0.062	0.016	0.326	0.417	0.00078	0.474	0.022	0.069	9.274	0.124
11.50	0.098	0.065	0.016	0.307	0.384	0.00073	0.470	0.022	0.069	9.234	0.116
11.00	0.101	0.064	0.016	0.315	0.398	0.00075	0.466	0.022	0.068	9.203	0.118
10.50	0.111	0.064	0.016	0.309	0.389	0.00072	0.457	0.021	0.067	9.107	0.114
10.00	0.124	0.065	0.016	0.302	0.377	0.00070	0.447	0.021	0.065	9.014	0.109
9.50	0.125	0.065	0.016	0.301	0.376	0.00069	0.445	0.021	0.065	8.989	0.108
9.00	0.127	0.066	0.016	0.298	0.372	0.00069	0.443	0.021	0.065	8.966	0.107
8.50	0.120	0.065	0.016	0.298	0.372	0.00069	0.446	0.021	0.065	8.996	0.107
8.00	0.120	0.064	0.016	0.302	0.381	0.00071	0.444	0.021	0.065	8.984	0.108
7.50	0.122	0.065	0.016	0.297	0.372	0.00069	0.442	0.021	0.064	8.954	0.106
7.00	0.123	0.064	0.015	0.298	0.374	0.00069	0.439	0.021	0.064	8.924	0.105
6.50	0.121	0.064	0.015	0.296	0.372	0.00069	0.438	0.021	0.064	8.915	0.105
6.00	0.124	0.065	0.015	0.289	0.361	0.00068	0.433	0.021	0.063	8.867	0.102
5.50	0.127	0.064	0.015	0.294	0.371	0.00069	0.432	0.021	0.063	8.852	0.103
5.00	0.129	0.067	0.015	0.281	0.348	0.00066	0.429	0.021	0.063	8.826	0.098
4.50	0.133	0.064	0.015	0.290	0.365	0.00068	0.425	0.021	0.062	8.787	0.100
4.00	0.134	0.064	0.015	0.289	0.365	0.00067	0.422	0.021	0.062	8.754	0.099

Table 2.10: Category: After 24 h with seepage run (D_{50} = 0.41 mm, S_0 = 0.00176, Q_0 = 0.0169 m^3/s), V_s = ∼0.20 mm/s (15% seepage)

Cross Section	h_s (m)	R_{hs}	Q_s (m^3/s)	u_s (m/s)	F_s	S_{fs}	τ_s (N/m^2)	u^*_{bs}	θ^*_s	R*	Ω_s (N/s)
12.00	0.118	0.059	0.016	0.326	0.427	0.00087	0.506	0.022	0.074	9.585	0.139
11.50	0.094	0.060	0.016	0.317	0.413	0.00088	0.519	0.023	0.076	9.712	0.139
11.00	0.088	0.059	0.016	0.328	0.433	0.00091	0.525	0.023	0.077	9.762	0.144
10.50	0.087	0.057	0.016	0.334	0.446	0.00093	0.522	0.023	0.076	9.739	0.146
10.00	0.102	0.057	0.016	0.334	0.446	0.00091	0.510	0.023	0.074	9.620	0.142
9.50	0.111	0.058	0.016	0.328	0.436	0.00089	0.501	0.022	0.073	9.540	0.138
9.00	0.116	0.060	0.016	0.311	0.405	0.00084	0.500	0.022	0.073	9.528	0.131
8.50	0.110	0.060	0.016	0.314	0.411	0.00086	0.502	0.022	0.073	9.549	0.132
8.00	0.107	0.056	0.016	0.333	0.448	0.00091	0.500	0.022	0.073	9.525	0.139
7.50	0.104	0.056	0.016	0.332	0.446	0.00091	0.501	0.022	0.073	9.535	0.138
7.00	0.099	0.061	0.015	0.300	0.388	0.00084	0.505	0.022	0.074	9.577	0.128
6.50	0.103	0.055	0.015	0.335	0.456	0.00092	0.498	0.022	0.073	9.508	0.139
6.00	0.104	0.059	0.015	0.313	0.412	0.00086	0.496	0.022	0.072	9.491	0.130
5.50	0.106	0.055	0.015	0.333	0.453	0.00091	0.492	0.022	0.072	9.452	0.137
5.00	0.113	0.058	0.015	0.310	0.410	0.00085	0.486	0.022	0.071	9.397	0.127
4.50	0.119	0.059	0.015	0.303	0.397	0.00083	0.483	0.022	0.070	9.363	0.123
4.00	0.114	0.057	0.015	0.311	0.415	0.00086	0.481	0.022	0.070	9.347	0.126

Table 2.11: Category: After 31 h with seepage run (D_{50} = 0.41 mm, S_0 = 0.00176, Q_0 = 0.0169 m^3/s), V_s = ∼0.20 mm/s (15% seepage)

Cross Section	h_s (m)	R_{hs}	Q_s (m^3/s)	u_s (m/s)	F_s	S_{fs}	τ_s (N/m^2)	u^*_{bs}	θ^*_s	R*	Ω_s (N/s)
12.00	0.124	0.059	0.016	0.328	0.433	0.00088	0.507	0.023	0.074	9.599	0.141
11.50	0.099	0.060	0.016	0.318	0.414	0.00089	0.523	0.023	0.076	9.742	0.141
11.00	0.092	0.060	0.016	0.319	0.415	0.00090	0.530	0.023	0.077	9.807	0.142
10.50	0.092	0.058	0.016	0.328	0.434	0.00092	0.526	0.023	0.077	9.777	0.145
10.00	0.107	0.058	0.016	0.326	0.431	0.00090	0.514	0.023	0.075	9.661	0.141
9.50	0.117	0.059	0.016	0.320	0.421	0.00088	0.506	0.022	0.074	9.585	0.136
9.00	0.122	0.062	0.016	0.304	0.390	0.00084	0.506	0.023	0.074	9.589	0.130
8.50	0.116	0.061	0.016	0.308	0.399	0.00085	0.508	0.023	0.074	9.603	0.131
8.00	0.112	0.057	0.016	0.326	0.435	0.00090	0.503	0.022	0.073	9.560	0.138
7.50	0.110	0.057	0.016	0.325	0.433	0.00090	0.504	0.022	0.074	9.570	0.137
7.00	0.105	0.063	0.015	0.291	0.370	0.00083	0.512	0.023	0.075	9.644	0.126
6.50	0.108	0.056	0.015	0.330	0.447	0.00092	0.501	0.022	0.073	9.539	0.138
6.00	0.110	0.059	0.015	0.308	0.403	0.00086	0.501	0.022	0.073	9.535	0.129
5.50	0.111	0.056	0.015	0.323	0.435	0.00090	0.496	0.022	0.072	9.492	0.134
5.00	0.119	0.059	0.015	0.304	0.399	0.00085	0.492	0.022	0.072	9.450	0.126
4.50	0.125	0.059	0.015	0.298	0.390	0.00083	0.485	0.022	0.071	9.385	0.123
4.00	0.120	0.061	0.015	0.291	0.377	0.00082	0.491	0.022	0.072	9.441	0.121

Table 2.12: Category: no seepage run (D_{50} = 1.1 mm, S_0 = 0.00176, Q_0 = 0.0209 m^3/s)

Cross Section	h_0 (m)	R_{h0}	Q_s (m^3/s)	u_0 (m/s)	F_0	S_{f0}	τ_0 (N/m^2)	u^*_{0b}	θ^*_0	R_*	Ω_0 (N/s)
12.00	0.122	0.072	0.0	0.385	0.456	0.00100	0.711	0.027	0.040	35.702	0.205
11.75	0.122	0.072	0.0	0.387	0.460	0.00100	0.709	0.027	0.040	35.665	0.206
11.50	0.123	0.072	0.0	0.387	0.460	0.00100	0.709	0.027	0.040	35.668	0.206
11.25	0.123	0.072	0.0	0.385	0.457	0.00100	0.710	0.027	0.040	35.686	0.205
11.00	0.124	0.073	0.0	0.384	0.455	0.00100	0.711	0.027	0.040	35.707	0.205
10.75	0.125	0.073	0.0	0.381	0.450	0.00099	0.712	0.027	0.040	35.744	0.204
10.50	0.125	0.073	0.0	0.382	0.452	0.00100	0.712	0.027	0.040	35.734	0.204
10.25	0.125	0.072	0.0	0.384	0.456	0.00100	0.710	0.027	0.040	35.693	0.205
10.00	0.125	0.073	0.0	0.383	0.454	0.00100	0.711	0.027	0.040	35.719	0.205
9.75	0.125	0.072	0.0	0.385	0.458	0.00100	0.710	0.027	0.040	35.679	0.205
9.50	0.126	0.073	0.0	0.384	0.455	0.00100	0.711	0.027	0.040	35.698	0.205
9.25	0.126	0.072	0.0	0.385	0.456	0.00100	0.710	0.027	0.040	35.689	0.205
9.00	0.126	0.073	0.0	0.383	0.454	0.00100	0.711	0.027	0.040	35.710	0.205
8.75	0.127	0.073	0.0	0.384	0.455	0.00100	0.711	0.027	0.040	35.695	0.205
8.50	0.128	0.073	0.0	0.380	0.449	0.00099	0.712	0.027	0.040	35.743	0.204
8.25	0.128	0.073	0.0	0.383	0.454	0.00100	0.710	0.027	0.040	35.694	0.205
8.00	0.130	0.073	0.0	0.383	0.454	0.00100	0.710	0.027	0.040	35.694	0.205
7.75	0.130	0.073	0.0	0.383	0.454	0.00100	0.710	0.027	0.040	35.695	0.205
7.50	0.131	0.073	0.0	0.380	0.449	0.00099	0.712	0.027	0.040	35.741	0.204
7.25	0.133	0.073	0.0	0.380	0.449	0.00099	0.712	0.027	0.040	35.734	0.204
7.00	0.134	0.073	0.0	0.380	0.448	0.00099	0.712	0.027	0.040	35.727	0.204
6.75	0.135	0.074	0.0	0.376	0.442	0.00099	0.714	0.027	0.040	35.791	0.202
6.50	0.133	0.073	0.0	0.381	0.450	0.00099	0.712	0.027	0.040	35.724	0.204
6.25	0.132	0.073	0.0	0.382	0.452	0.00100	0.711	0.027	0.040	35.706	0.204
6.00	0.132	0.073	0.0	0.381	0.450	0.00099	0.712	0.027	0.040	35.733	0.204
5.75	0.132	0.073	0.0	0.381	0.451	0.00100	0.711	0.027	0.040	35.716	0.204
5.50	0.131	0.072	0.0	0.384	0.455	0.00100	0.710	0.027	0.040	35.682	0.205
5.25	0.134	0.073	0.0	0.382	0.452	0.00100	0.711	0.027	0.040	35.704	0.204
5.00	0.132	0.072	0.0	0.384	0.457	0.00100	0.709	0.027	0.040	35.664	0.205
4.75	0.132	0.073	0.0	0.381	0.450	0.00099	0.712	0.027	0.040	35.733	0.204
4.50	0.132	0.073	0.0	0.381	0.451	0.00100	0.711	0.027	0.040	35.716	0.204
4.25	0.131	0.072	0.0	0.384	0.455	0.00100	0.710	0.027	0.040	35.682	0.205
4.00	0.134	0.073	0.0	0.382	0.452	0.00100	0.711	0.027	0.040	35.704	0.204

Table 2.13: Category: After 3 h with seepage run (D_{50} = 1.1 mm, S_0 = 0.00176, Q_0 = 0.0209 m^3/s), V_s = ∼0.48 mm/s (30% seepage)

Cross Section	h_s (m)	R_{hs}	Q_s (m^3/s)	u_s (m/s)	F_s	S_{fs}	τ_s (N/m^2)	u^*_{bs}	θ^*_s	R*	Ω_s (N/s)
12.00	0.090	0.067	0.019	0.355	0.437	0.00154	1.014	0.032	0.057	42.645	0.291
11.75	0.089	0.067	0.019	0.354	0.436	0.00154	1.013	0.032	0.057	42.615	0.290
11.50	0.090	0.066	0.019	0.358	0.443	0.00155	1.007	0.032	0.057	42.485	0.290
11.25	0.088	0.066	0.019	0.359	0.447	0.00156	1.005	0.032	0.056	42.447	0.291
11.00	0.086	0.065	0.019	0.360	0.450	0.00157	1.004	0.032	0.056	42.434	0.292
10.75	0.086	0.065	0.019	0.359	0.450	0.00157	1.000	0.032	0.056	42.340	0.290
10.50	0.085	0.065	0.019	0.359	0.451	0.00157	1.000	0.032	0.056	42.349	0.290
10.25	0.089	0.065	0.019	0.357	0.447	0.00155	0.987	0.031	0.055	42.080	0.284
10.00	0.088	0.064	0.019	0.360	0.454	0.00157	0.984	0.031	0.055	42.002	0.285
9.75	0.087	0.064	0.018	0.357	0.449	0.00156	0.986	0.031	0.055	42.057	0.283
9.50	0.089	0.064	0.018	0.355	0.446	0.00155	0.976	0.031	0.055	41.839	0.278
9.25	0.087	0.063	0.018	0.360	0.457	0.00157	0.972	0.031	0.055	41.756	0.281
9.00	0.089	0.064	0.018	0.356	0.451	0.00155	0.968	0.031	0.054	41.674	0.277
8.75	0.095	0.065	0.018	0.346	0.434	0.00151	0.960	0.031	0.054	41.495	0.267
8.50	0.100	0.066	0.018	0.338	0.420	0.00147	0.955	0.031	0.054	41.387	0.259
8.25	0.111	0.071	0.018	0.315	0.379	0.00139	0.965	0.031	0.054	41.609	0.244
8.00	0.107	0.071	0.018	0.313	0.376	0.00140	0.969	0.031	0.054	41.696	0.244
7.75	0.113	0.071	0.018	0.312	0.374	0.00138	0.957	0.031	0.054	41.423	0.239
7.50	0.116	0.071	0.018	0.308	0.369	0.00137	0.955	0.031	0.054	41.390	0.236
7.25	0.111	0.071	0.017	0.308	0.370	0.00138	0.958	0.031	0.054	41.454	0.237
7.00	0.107	0.071	0.017	0.306	0.368	0.00139	0.962	0.031	0.054	41.538	0.236
6.75	0.113	0.071	0.017	0.305	0.366	0.00137	0.950	0.031	0.053	41.270	0.232
6.50	0.116	0.071	0.017	0.301	0.360	0.00136	0.948	0.031	0.053	41.240	0.229
6.25	0.111	0.071	0.017	0.301	0.362	0.00137	0.951	0.031	0.053	41.302	0.230
6.00	0.107	0.071	0.017	0.300	0.360	0.00138	0.955	0.031	0.054	41.384	0.229
5.75	0.113	0.071	0.017	0.298	0.358	0.00136	0.943	0.031	0.053	41.118	0.225
5.50	0.116	0.070	0.017	0.294	0.354	0.00135	0.930	0.030	0.052	40.841	0.222
5.25	0.111	0.071	0.017	0.294	0.353	0.00136	0.944	0.031	0.053	41.146	0.223
5.00	0.107	0.071	0.017	0.293	0.351	0.00137	0.948	0.031	0.053	41.227	0.222
4.75	0.113	0.071	0.016	0.291	0.348	0.00135	0.944	0.031	0.053	41.136	0.218
4.50	0.116	0.072	0.016	0.287	0.342	0.00134	0.948	0.031	0.053	41.239	0.215
4.25	0.111	0.072	0.016	0.288	0.343	0.00135	0.951	0.031	0.053	41.291	0.216
4.00	0.107	0.072	0.016	0.286	0.341	0.00136	0.954	0.031	0.054	41.368	0.216

Table 2.14: Category: After 4 h with seepage run (D_{50} = 1.1 mm, S_0 = 0.00176, Q_0 = 0.0209 m^3/s), V_s = ∼0.48 mm/s (30% seepage)

Cross Section	h_s (m)	R_{hs}	Q_s (m^3/s)	u_s (m/s)	F_s	S_{fs}	τ_s (N/m^2)	u^*_{bs}	θ^*_s	R*	Ω_s (N/s)
12.00	0.086	0.064	0.019	0.369	0.467	0.00182	1.141	0.034	0.064	45.225	0.345
11.75	0.085	0.064	0.019	0.368	0.466	0.00182	1.140	0.034	0.064	45.214	0.344
11.50	0.086	0.063	0.019	0.373	0.476	0.00183	1.126	0.034	0.063	44.933	0.343
11.25	0.084	0.062	0.019	0.375	0.479	0.00184	1.126	0.034	0.063	44.931	0.344
11.00	0.083	0.062	0.019	0.374	0.480	0.00185	1.124	0.034	0.063	44.892	0.343
10.75	0.084	0.062	0.019	0.370	0.474	0.00184	1.121	0.033	0.063	44.838	0.339
10.50	0.086	0.062	0.019	0.372	0.477	0.00183	1.108	0.033	0.062	44.572	0.336
10.25	0.085	0.062	0.019	0.367	0.470	0.00182	1.112	0.033	0.062	44.664	0.334
10.00	0.086	0.062	0.019	0.365	0.467	0.00181	1.108	0.033	0.062	44.567	0.330
9.75	0.084	0.062	0.018	0.364	0.467	0.00183	1.111	0.033	0.062	44.638	0.331
9.50	0.083	0.061	0.018	0.368	0.475	0.00184	1.104	0.033	0.062	44.494	0.331
9.25	0.084	0.060	0.018	0.372	0.485	0.00184	1.088	0.033	0.061	44.162	0.330
9.00	0.080	0.060	0.018	0.370	0.482	0.00186	1.099	0.033	0.062	44.388	0.331
8.75	0.082	0.060	0.018	0.368	0.478	0.00185	1.092	0.033	0.061	44.255	0.327
8.50	0.084	0.061	0.018	0.364	0.473	0.00183	1.088	0.033	0.061	44.178	0.323
8.25	0.083	0.060	0.018	0.366	0.477	0.00184	1.083	0.033	0.061	44.072	0.322
8.00	0.084	0.060	0.018	0.367	0.480	0.00183	1.073	0.033	0.060	43.861	0.320
7.75	0.084	0.059	0.018	0.367	0.480	0.00183	1.068	0.033	0.060	43.769	0.318
7.50	0.089	0.060	0.018	0.358	0.465	0.00180	1.065	0.033	0.060	43.708	0.310
7.25	0.095	0.060	0.017	0.357	0.464	0.00177	1.047	0.032	0.059	43.337	0.304
7.00	0.119	0.067	0.017	0.315	0.389	0.00162	1.065	0.033	0.060	43.712	0.277
6.75	0.117	0.068	0.017	0.307	0.374	0.00162	1.085	0.033	0.061	44.119	0.274
6.50	0.115	0.068	0.017	0.308	0.377	0.00163	1.082	0.033	0.061	44.056	0.274
6.25	0.119	0.067	0.017	0.310	0.382	0.00162	1.061	0.033	0.060	43.622	0.271
6.00	0.117	0.068	0.017	0.301	0.368	0.00161	1.081	0.033	0.061	44.030	0.268
5.75	0.115	0.068	0.017	0.302	0.370	0.00162	1.078	0.033	0.061	43.965	0.268
5.50	0.119	0.067	0.017	0.304	0.376	0.00161	1.057	0.033	0.059	43.533	0.265
5.25	0.117	0.068	0.017	0.296	0.362	0.00161	1.077	0.033	0.060	43.942	0.263
5.00	0.115	0.068	0.017	0.297	0.364	0.00161	1.073	0.033	0.060	43.875	0.262
4.75	0.119	0.067	0.016	0.299	0.369	0.00161	1.052	0.032	0.059	43.444	0.260
4.50	0.117	0.068	0.016	0.291	0.355	0.00160	1.072	0.033	0.060	43.854	0.257
4.25	0.115	0.068	0.016	0.292	0.358	0.00161	1.069	0.033	0.060	43.785	0.257
4.00	0.119	0.067	0.016	0.294	0.363	0.00160	1.048	0.032	0.059	43.355	0.254

Table 2.15: Category: After 8 h with seepage run (D_{50} = 1.1 mm, S_0 = 0.00176, Q_0 = 0.0209 m^3/s), V_s = ∼0.48 mm/s (30% seepage)

Cross Section	h_s (m)	R_{hs}	Q_s (m^3/s)	u_s (m/s)	F_s	S_{fs}	τ_s (N/m^2)	u^*_{bs}	θ^*_s	R*	Ω_s (N/s)
12.00	0.087	0.064	0.019	0.357	0.449	0.00215	1.355	0.037	0.076	49.299	0.407
11.75	0.087	0.064	0.019	0.356	0.448	0.00214	1.353	0.037	0.076	49.264	0.405
11.50	0.086	0.064	0.019	0.357	0.451	0.00215	1.347	0.037	0.076	49.152	0.404
11.25	0.086	0.063	0.019	0.360	0.459	0.00215	1.331	0.036	0.075	48.855	0.402
11.00	0.087	0.063	0.019	0.357	0.453	0.00215	1.330	0.036	0.075	48.844	0.399
10.75	0.084	0.063	0.019	0.357	0.454	0.00216	1.333	0.037	0.075	48.885	0.399
10.50	0.084	0.063	0.019	0.355	0.453	0.00216	1.330	0.036	0.075	48.836	0.397
10.25	0.084	0.063	0.019	0.355	0.454	0.00216	1.324	0.036	0.074	48.729	0.395
10.00	0.082	0.062	0.019	0.355	0.455	0.00217	1.322	0.036	0.074	48.690	0.394
9.75	0.081	0.062	0.018	0.353	0.452	0.00217	1.324	0.036	0.074	48.734	0.393
9.50	0.082	0.062	0.018	0.355	0.456	0.00217	1.309	0.036	0.074	48.454	0.390
9.25	0.080	0.061	0.018	0.359	0.464	0.00218	1.303	0.036	0.073	48.342	0.391
9.00	0.080	0.060	0.018	0.359	0.467	0.00218	1.292	0.036	0.073	48.142	0.389
8.75	0.078	0.060	0.018	0.358	0.466	0.00219	1.295	0.036	0.073	48.200	0.388
8.50	0.078	0.059	0.018	0.361	0.473	0.00220	1.282	0.036	0.072	47.943	0.387
8.25	0.078	0.059	0.018	0.359	0.470	0.00220	1.282	0.036	0.072	47.951	0.385
8.00	0.078	0.059	0.018	0.359	0.472	0.00220	1.275	0.036	0.072	47.820	0.383
7.75	0.079	0.059	0.018	0.360	0.474	0.00219	1.265	0.036	0.071	47.623	0.380
7.50	0.080	0.059	0.018	0.356	0.467	0.00218	1.267	0.036	0.071	47.664	0.376
7.25	0.080	0.060	0.017	0.351	0.460	0.00218	1.272	0.036	0.071	47.761	0.373
7.00	0.079	0.059	0.017	0.354	0.466	0.00218	1.261	0.036	0.071	47.556	0.372
6.75	0.081	0.059	0.017	0.353	0.465	0.00217	1.251	0.035	0.070	47.367	0.368
6.50	0.081	0.059	0.017	0.348	0.457	0.00217	1.258	0.035	0.071	47.494	0.365
6.25	0.082	0.059	0.017	0.345	0.451	0.00216	1.257	0.035	0.071	47.485	0.361
6.00	0.085	0.059	0.017	0.347	0.458	0.00215	1.237	0.035	0.069	47.090	0.358
5.75	0.090	0.060	0.017	0.338	0.441	0.00212	1.244	0.035	0.070	47.238	0.350
5.50	0.122	0.068	0.017	0.290	0.355	0.00198	1.326	0.036	0.074	48.760	0.326
5.25	0.122	0.068	0.017	0.289	0.353	0.00198	1.325	0.036	0.074	48.744	0.324
5.00	0.122	0.068	0.017	0.287	0.351	0.00198	1.324	0.036	0.074	48.727	0.322
4.75	0.122	0.068	0.016	0.285	0.349	0.00197	1.323	0.036	0.074	48.711	0.319
4.50	0.122	0.068	0.016	0.284	0.346	0.00197	1.322	0.036	0.074	48.695	0.317
4.25	0.122	0.068	0.016	0.282	0.344	0.00197	1.321	0.036	0.074	48.679	0.315
4.00	0.122	0.068	0.016	0.280	0.342	0.00197	1.320	0.036	0.074	48.663	0.313

Table 2.16: Category: After 11 h with seepage run (D_{50} = 1.1 mm, S_0 = 0.00176, Q_0 = 0.0209 m^3/s), V_s = ∼0.48 mm/s (30% seepage)

Cross Section	h_s (m)	R_{hs}	Q_s (m^3/s)	u_s (m/s)	F_s	S_{fs}	τ_s (N/m^2)	u^*_{bs}	θ^*_s	R*	Ω_s (N/s)
12.00	0.083	0.061	0.019	0.370	0.478	0.00225	1.350	0.037	0.076	49.208	0.426
11.75	0.084	0.061	0.019	0.371	0.480	0.00225	1.341	0.037	0.075	49.038	0.424
11.50	0.083	0.060	0.019	0.373	0.485	0.00225	1.332	0.037	0.075	48.879	0.423
11.25	0.083	0.060	0.019	0.373	0.486	0.00225	1.326	0.036	0.075	48.768	0.421
11.00	0.082	0.060	0.019	0.370	0.482	0.00225	1.329	0.036	0.075	48.825	0.419
10.75	0.083	0.060	0.019	0.366	0.475	0.00224	1.329	0.036	0.075	48.825	0.414
10.50	0.082	0.060	0.019	0.364	0.473	0.00225	1.334	0.037	0.075	48.911	0.413
10.25	0.083	0.060	0.019	0.362	0.470	0.00224	1.329	0.036	0.075	48.827	0.410
10.00	0.080	0.061	0.019	0.359	0.465	0.00225	1.338	0.037	0.075	48.993	0.409
9.75	0.081	0.060	0.018	0.360	0.468	0.00225	1.327	0.036	0.075	48.778	0.407
9.50	0.080	0.060	0.018	0.362	0.473	0.00225	1.318	0.036	0.074	48.626	0.406
9.25	0.080	0.059	0.018	0.361	0.472	0.00225	1.315	0.036	0.074	48.563	0.404
9.00	0.078	0.059	0.018	0.363	0.478	0.00227	1.307	0.036	0.073	48.418	0.403
8.75	0.078	0.058	0.018	0.367	0.486	0.00227	1.290	0.036	0.072	48.102	0.402
8.50	0.076	0.058	0.018	0.366	0.486	0.00228	1.293	0.036	0.073	48.154	0.402
8.25	0.077	0.058	0.018	0.364	0.484	0.00228	1.289	0.036	0.072	48.070	0.399
8.00	0.077	0.057	0.018	0.367	0.491	0.00228	1.274	0.036	0.072	47.803	0.397
7.75	0.076	0.057	0.018	0.368	0.493	0.00228	1.270	0.036	0.071	47.718	0.396
7.50	0.076	0.057	0.018	0.364	0.488	0.00228	1.272	0.036	0.071	47.765	0.393
7.25	0.076	0.056	0.017	0.365	0.490	0.00228	1.265	0.036	0.071	47.620	0.391
7.00	0.078	0.056	0.017	0.365	0.491	0.00227	1.253	0.035	0.070	47.403	0.387
6.75	0.076	0.056	0.017	0.367	0.496	0.00228	1.248	0.035	0.070	47.308	0.387
6.50	0.076	0.056	0.017	0.364	0.493	0.00228	1.247	0.035	0.070	47.294	0.384
6.25	0.076	0.056	0.017	0.363	0.491	0.00228	1.244	0.035	0.070	47.229	0.382
6.00	0.078	0.056	0.017	0.360	0.487	0.00227	1.239	0.035	0.070	47.134	0.378
5.75	0.078	0.056	0.017	0.359	0.486	0.00227	1.236	0.035	0.069	47.081	0.375
5.50	0.078	0.056	0.017	0.355	0.479	0.00226	1.240	0.035	0.070	47.153	0.372
5.25	0.078	0.055	0.017	0.362	0.495	0.00227	1.213	0.035	0.068	46.644	0.371
5.00	0.082	0.055	0.017	0.357	0.487	0.00224	1.208	0.035	0.068	46.544	0.365
4.75	0.110	0.060	0.016	0.322	0.419	0.00211	1.245	0.035	0.070	47.251	0.341
4.50	0.117	0.065	0.016	0.296	0.372	0.00207	1.313	0.036	0.074	48.524	0.333
4.25	0.117	0.064	0.016	0.295	0.371	0.00207	1.309	0.036	0.074	48.449	0.331

"Big whorls have little whorls;
Which feed on their velocity,
And little whorls have lesser whorls,
And so on to viscosity
(in the molecular sense)"

Richardson (1922)

3

Flow Dynamics and Development of Bedforms with Downward Seepage

3.1 Overview

Fluvial processes in the natural environment comprise with aggradation or degradation of the channel bed and banks. Sediment movement can be characterized by the resistance offered by the sediment particles due to specific weight of particles. In this regard, for each sediment size, there is specific bed shear stress to start the movement of bed particle that is called the threshold (critical) shear stress. In alluvial channels, bedforms are developed, whenever the bed shear stress caused by flow exceeds from its critical value. These bedforms, such as ripples, dunes, and antidunes, occur at the bottom of natural channels and their impact on flow is complex and dynamic. Flow in natural channels experiences a greater resistance due to development of bedforms. In this regard, turbulent flow plays a major role in fluvial processes and bedform phenomenon.

Earlier studies suggested that the bedform development is a function of the coherent turbulent flow structures in sedimentary environments, where sweeps (bursting events) govern the initiation of bed features in the near-bed region (Williams and Kemp, 1971; Raudkivi and Witte, 1990; Best, 1992; Nelson et al., 1995; Raudkivi, 1997). In particular, development of hairpin vortices near the channel bed results in the generation of multiple bursting events such as ejections and sweeps. Moreover, impact of microturbulent sweeps

ascribe to create flow parallel ridge or defects over the rough boundary (Best, 1992). Gyr and Kinzelbach (2004) and Langlois and Valance (2007) suggested that the turbulent instability is responsible for the formation of bedforms. Venditti et al. (2005) observed that the initiation of bed defects and their length are linked to the integral scales of flow.

In this chapter, a brief introduction of turbulent flow characteristics and its importance in fluvial system are discussed. In particular, the experimental investigation of the temporal variation of Shields stress is performed on a stable alluvial channel in no seepage and with seepage scenarios. The stable shape of channel is distorted with the application of downward seepage, resulting in development of bedforms on the periphery of the channel bed. The role of downward seepage behind the development of bedforms and corresponding turbulent flow characteristics are analyzed on the threshold channel. Further, temporal quantification and classification of evolving bedforms are carried out in the presence of bedforms.

3.2 Turbulent Fluvial Flows

State of fluid flows in natural environment is characterized into two categories namely, laminar flow and turbulent flow. Laminar state is rarely observed in environment and occurs in low flow velocity that is envisaged as layered flow in which fluid layers smoothly slide over each other, thus maintaining a differential flow velocity in between the layers. Flow in natural channels is always turbulent in nature in which turbulence in the fluid flow is defined by irregular, diffusive, dissipative, and chaotic motion of fluid particles. Velocities of fluid particles vary rapidly in space and time. Further, turbulence in most of the geophysical flows is exceedingly complex because of intrinsic instability in such flows. Instability in such flows causes formation of eddies at different scales depending upon boundary condition. These eddies 'cascade', splitting into smaller and smaller eddies until their energy is dissipated through viscosity (Tennekes and Lumley, 1972).

Indeed, turbulence is an intricate natural phenomenon, which can not be defined straightforwardly. However, one can show its characteristic structures from the measurement of instantaneous velocity data. The most important characteristic of turbulence is its randomness and intermittency, which makes a deterministic approach potentially difficult. Thus, one has to describe the turbulence through statistical analysis of temporal velocity data. Important parameters of turbulent flow characteristics are included such as first order analysis is magnitude of mean of velocity fluctuations, second order is the variance of a sampled in-

stantaneous velocity series, third order analysis is higher-order moments such as skewness and kurtosis (which describes the temporal distribution of this variance), cross-correlations of velocity fluctuations which describe fluid momentum transfer, and parameters (integral scales of flow) describing the scales or sizes of eddies present. In this regard, statistical analysis of instantaneous velocities are used to describe turbulent flows in different scenarios.

3.2.1 Velocity Decomposition

At a point the time-mean streamwise and vertical velocities were obtained from the decomposition of instantaneous velocity (u_i) samples into the time-mean velocity and fluctuating component of the velocity (Figure 3.1). This process is known as Reynolds decomposition (Tennekes and Lumley, 1972) and it requires a steady state or quasi-steady flow.

$$u_i = u + u_i^{'} \tag{3.1}$$

where streamwise time-mean velocity is u and its fluctuating component is $u_i^{'}$. Similarly, vertical time-mean velocity can be defined as w and its fluctuating component can be represented as $w_i^{'}$.

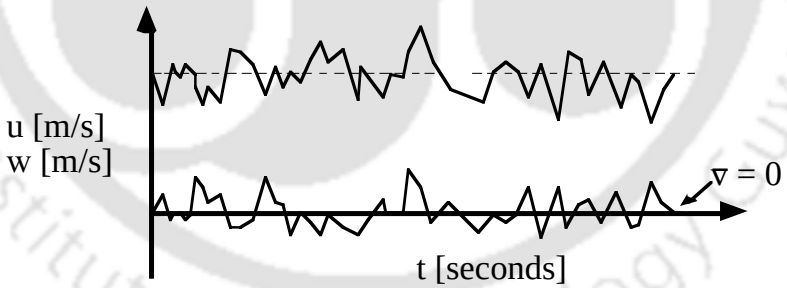

Figure 3.1: At a point velocity recorded signal

Time-mean velocity in the direction of flow 'u' and vertical direction 'w' can be calculated as:

$$\left.\begin{aligned} u &= \frac{1}{n}\sum_{i=1}^{n} u_i \\ w &= \frac{1}{n}\sum_{i=1}^{n} w_i \end{aligned}\right\} \tag{3.2}$$

Time-mean velocity can be similar for different fluctuating velocities and also it cannot

define the scale of fluctuations in the flows. Therefore, standard deviation of the set of 'random' or fluctuating velocities can be used to define the level or strength of turbulence in flow. Turbulence strength is the root mean square (RMS) velocity in streamwise (vertical) direction $u_{rms}(w_{rms})$ and it can be evaluated as:

$$u_{rms} = \left[\frac{1}{n}\sum_{i=1}^{n}(u_i - u)^2\right]^{0.5} \tag{3.3}$$

$$w_{rms} = \left[\frac{1}{n}\sum_{i=1}^{n}(w_i - w)^2\right]^{0.5} \tag{3.4}$$

When flow passes through irregular boundaries, such that mobile or deformation bed in different bed characteristics, time-mean velocity would vary in spatially and temporally. Turbulent fluctuations at a point are given by the deviations from the local time averaged velocity:

$$u_i\,(x, y, z, t) = u\,(x, y, z, t) + u_i{}'\,(x, y, z, t) \tag{3.5}$$

Variations in streamwise velocities near the channel bed lead to the formation of a shear mixing layer. In this regard, fluid layers or molecules move in unpredictable way in turbulent flow, causing an exchange of momentum from one portion of fluid layer to the other, and hence, the turbulent shear stresses (τ_{turb}) are generated also known as the Reynolds shear stresses (τ_{uw}). The Reynolds stresses can be presented by time-mean of the Navier-Stokes equation:

$$\left.\begin{aligned}\tau_{turb} = \tau_{uw} &= -\rho_w\overline{u'w'}\\ \overline{u'w'} &= \frac{1}{n}\sum_{i=1}^{n}(u_i - u)\,(w_i - w)\end{aligned}\right\} \tag{3.6}$$

In turbulent flow both viscosity and turbulence contribute to shear stress. The total shear stress (τ_{total}): where:

ρ_w : is the density of water.

$$\tau_{total} = \tau_{visc} + \tau_{turb} = \rho\nu\frac{dU}{dz} + \left(-\rho\overline{u'w'}\right) \tag{3.7}$$

where:

τ_{visc} : is the shear stress due to viscosity.

ν : is the kinematic viscosity.

3.2.2 Turbulence in 3-Dimensional Flow Field

The level of turbulence in a sampled velocity traditionally been described by the average magnitude of velocity fluctuations, commonly the RMS $\sqrt{\overline{u_i'^2}}$, or standard deviation of the velocity sample (Equation 3.3). This is commonly expressed as the non-dimensional turbulence intensity (TI) of velocity components, and the turbulent kinetic energy (TKE). Semi-empirical universal functions for (TI) and non-dimensional TKE in open-channel flow are proposed by Nezu and Nakagawa (1993), based on the $k-\epsilon$ turbulence model:

$$\left.\begin{aligned} TI &= \left(\frac{\sqrt{\overline{u'u'}}}{u_{*t}}\right) = D_u e^{(-C_u h^+)} \\ TKE &= \frac{1}{2}\left(\overline{u'^2} + \overline{v'^2} + \overline{w'^2}\right) \end{aligned}\right\} \tag{3.8}$$

where:

h^+ : is the non-dimensional depth.

D_u and C_u : are the empirical parameters set to 2.3 and 1, respectively, as suggested by Nezu and Nakagawa (1993).

These values of empirical parameters are suitable for the flat and smooth bed throughout the flow depth except very near to the boundary, where viscous effects are dominant and side currents are absent. These empirical parameters are not universal constant and are dependent on the bed roughness. Turbulence intensities in the near-bed region are reduced by the effect of increasing roughness height. With increasing relative roughness Bayazit (1976) observed significant reduction in turbulence intensities. These empirical parameters are not universal constant and are dependent on the bed roughness. Sukhodolov et al. (1998) have calculated new sets of constants for flows over rough bed.

The distribution of turbulence is further reflected by the higher moments of velocity fluctuations which aid in the identification of infrequent velocity fluctuations of large magnitude associated with sweep and ejection events (Grass, 1971). The third moment of turbulent velocity fluctuations or the coefficient of skewness $Sk(u_i)$ of a velocity time series describes the asymmetry in the probability density function of turbulent fluctuations. The coefficient of skewness is an important factor to describe infrequent velocity fluctuations of

large magnitude such as bursting events (Nezu and Nakagawa, 1993) can be defined as:

$$Sk\left(u_i\right) = \frac{\overline{u_i'^3}}{\left(\overline{u_i'^2}\right)^{3/2}} \tag{3.9}$$

Grinvald and Nikora (1988) reported from investigations in flumes and rivers at moderate velocity that the skewness coefficient for velocity in the streamwise direction is usually positive near the bed, becomes negative in the intermediate region, and again positive near the water surface, with absolute values generally less than 1. Measurements of Nikora and Smart (1997) in a gravel-bed river similarly show negative skewness coefficient for velocity in the streamwise direction over the majority of the flow depth. These negative values of skewness coefficient reflect the transport of turbulent energy from the bottom region to the upward direction (Nikora and Smart, 1997).

Experiments were performed on both the seepage discharges (i.e., 15% and 20%). Results from both the experiments were found to be consistent. Therefore, in the results section, in order to avoid the duplicity and congestion, findings from the experiment on 15% of the seepage on a bed slope 0.00176 are discussed in this chapter.

3.3 Assessment of Shields Stress

In order to confirm the incipient motion condition during the no seepage run, results were plotted on a Shields curve as shown in Figure 3.2. Mean line in Figure 3.2 represents the Shields curve, which has been plotted by using the empirical formulation of (Rao and Sreenivasulu, 2009). Shields stress (θ_c) and shear Reynolds number (R_*) have been calculated by using the following expressions

$$\theta_c = \frac{R_h S_f}{(G-1)\, D_{50}} \tag{3.10}$$

$$R_* = \frac{u_{*b} D_{50}}{\nu} \tag{3.11}$$

where R_h is hydraulic radius, S_f is friction slope, G is specific gravity, D_{50} is median particle diameter, u_{*b} is average shear velocity, and ν is kinematic viscosity of water. Figure 3.2 shows that for channel in the incipient motion condition during no seepage run, the value of Shields parameters falls within the band of Shields curve. The value of Shields stress for the

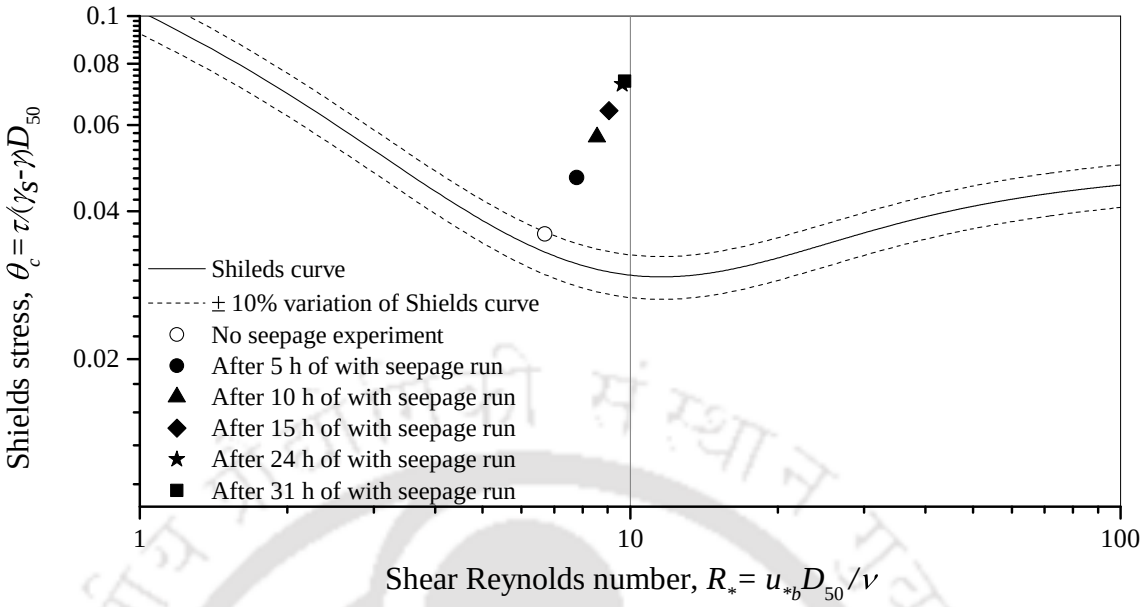

Figure 3.2: Shields curve (where dotted lines show ±10% variation from the mean curve) for the no seepage, 5 h, 10 h, 15 h, 24 h, and 31 h of the seepage run

no seepage run was obtained as 0.037. Few researchers (Liu, 1957; Bogardi, 1959; Southard and Dingler, 1971) reported stable beds with little sediment transport and no signatures of bedforms were seen. In addition, Venditti et al. (2005) observed that the flat sand bed ($d_{50} < 0.7$ mm) appear to be stable, for the condition of incipient motion for a longer period of run. In the present experimental study, the parabolic cross-sectional shape remained stable i.e. in the threshold of sediment movement for several hours (10-12 h) during the no seepage run, although sediment movement was sporadic along the channel as shown in Figure 3.3(a). Measurements of geometry are taken by using an ultrasonic ranging system and have been processed by using Surfer® as shown in Figure 3.3(b). When downward seepage was applied to the channel, bed shear stress exceeded significantly from its critical value. Quantitative observation of Shields curve suggests that after 5 h, 10 h, 15 h, 24 h, and 31 h of the initiation of the seepage run, values of Shields stress were increased by ∼27%, ∼53%, ∼73%, ∼96%, and ∼98%, respectively, from its critical value. The increase in Shields stress caused a surge in sediment transport and consequent deformation of cross-sectional shape of the channel. It was observed that sediment particles were eroded from the channel banks and deposited in the adjacent section in the form of bedforms. These bedforms were prograded from the upstream to the downstream end of the channel and resulted in the complete distortion of the cross-sectional shape of the channel. Detailed discussion on the temporal evolution of bedforms and their geometrical quantification can

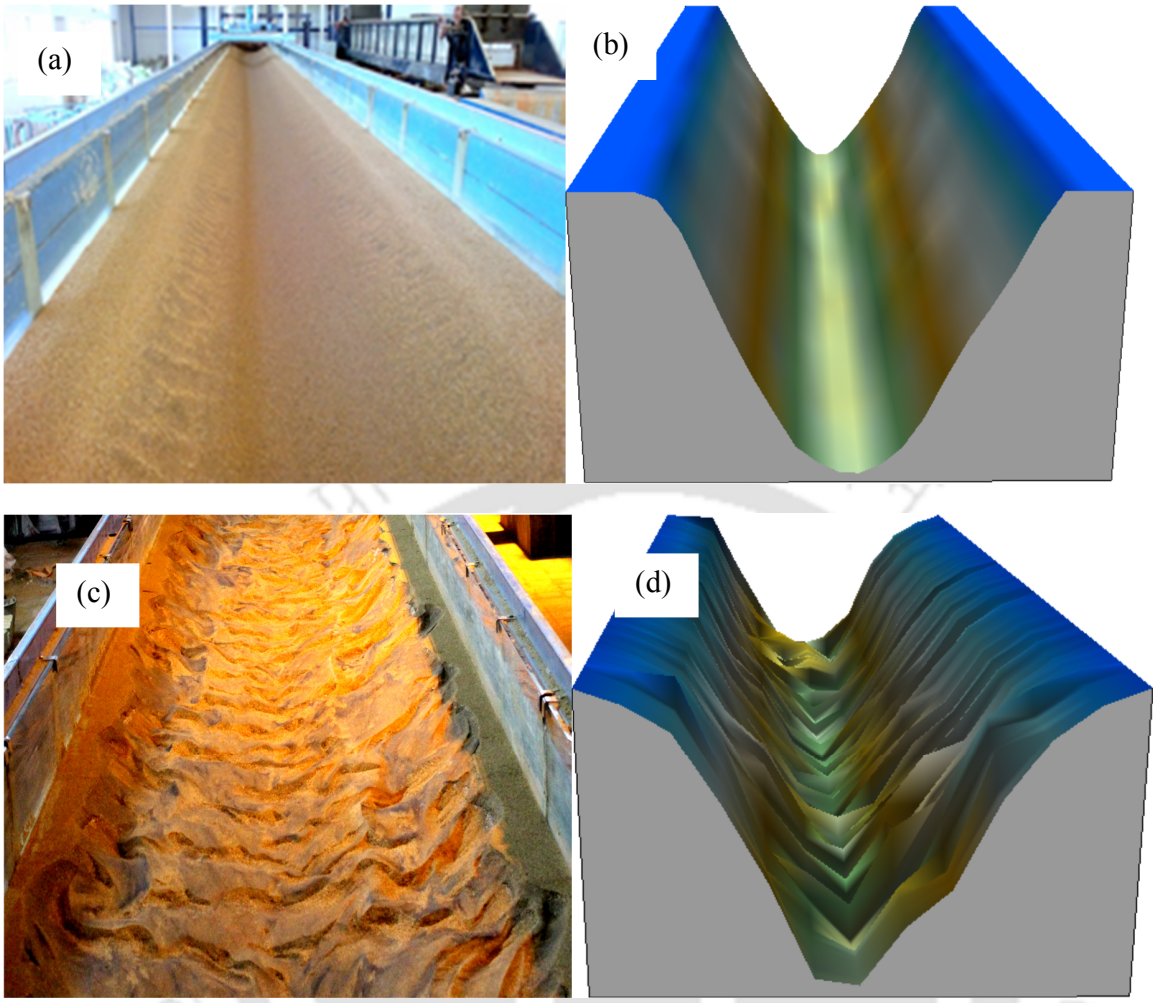

Figure 3.3: Profiles of the channel: (a) snapshot of the channel after successful completion of no seepage run, (b) processed curvilinear three-dimensional profile of channel cross section after several hours (10-12 h) of no seepage run, (c) snapshot of the channel after 31 h of seepage run, and (d) processed three-dimensional profile of channel cross section after 31 h of seepage run

be found out in Section 3.6.

Existing studies suggest that sediment transport increases when Shields stress reach towards ∼20% higher than its threshold value (Diplas, 1990; Ikeda et al., 1988). Bed features on the channel bed were observed when shear stress was increased from its threshold value (Kapdasli and Dyer, 1986; Best, 1992; Venditti et al., 2005; Langlois and Valance, 2007). In general, time required for the channel to reach in equilibrium state is higher for fine sand (Baas, 1999). In recent experimental study, Pitlick et al. (2013) observed that the overbank flow caused the bank distortion because of the high Shields stress associated with it and the channel attained equilibrium after longer period (10-12 h) of experimental run.

In addition, Patel et al. (2015) observed that Shields stress increased by ∼30% after the application of downward seepage, which caused the development of sheet flow of sediment particles. In the present study, cross-sectional shape of the channel was in stable condition during the no seepage run, while after the application of downward seepage, cross-sectional shape of the channel began to distort because of increased Shields stress (Figures 3.3 a-d). However, with the passage of time (during 24-31 h of the seepage run), the increment in Shields stress was very less (∼2% in 7 h duration). Channel attained a different stable cross-sectional shape at the end of the seepage run and Shields stress at this time was 0.073. Snapshot of the channel cross section obtained after 31 h of seepage run is shown in Figure 3.3(c) and it is processed in three-dimensional profile (Figure 3.3d).

3.4 Turbulent Flow Statistics

Understanding of the influence of downward seepage on the turbulent flow structure is necessary for the assessment of changes in the morphodynamics of the channel. As discussed in Table 2.4, for all the experiments i.e. no seepage (Phase-I measurement), with seepage (Phase-II measurement), and 24 h of seepage (Phase-III measurement) the following turbulent flow parameters are analyzed: (1) time-mean velocities, (2) Reynolds shear stresses, (3) turbulent intensities, (4) distributions of third-order correlations, (5) turbulent kinetic energy (TKE) flux components, (6) conditional statistics of RSS (7) Turbulent production and dissipation to get the better understanding cause of development of bedforms.

3.4.1 Time-mean Streamwise Velocity

At a point the time-mean streamwise velocity was obtained from the decomposition of instantaneous velocity samples into the time-mean velocity and fluctuating component of the velocity. Figure 3.4 shows the vertical distributions of time-mean velocities in the streamwise direction for all the runs, plotted against the normalized flow depth ($h^+ = z/h$). Careful observation of Figure 3.4 ascertains that after the application of downward seepage, streamwise velocities increased by ∼1-4% in the near-bed region of the channel. Flow depth was reduced because of the deformation of cross-sectional shape, which in turn resulted in further increase in the time-mean velocities after 24 h of the seepage run.

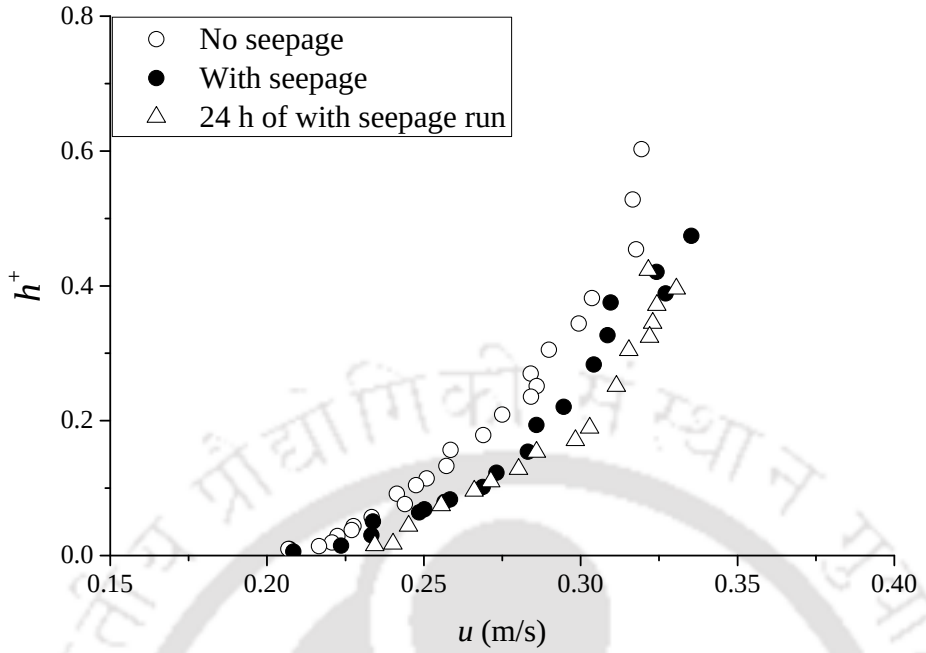

Figure 3.4: Profiles of time-mean velocities for the no seepage (Phase-I measurement), with seepage (Phase-II measurement), and after 24 h of the seepage run (Phase-III measurement)

3.4.2 Reynolds Shear Stress (RSS)

RSS defines the real time momentum flux of the streamwise velocity in the vertical direction caused by the fluctuating velocity field. RSS has been obtained for all the runs including vertical distributions are shown in Figure 3.5 and Figure 3.6. Shear velocity (u_{*t}) is obtained by the linear projection of the RSS profile to the channel bed ($u_{*t} = (u'w')^{0.5}{}_{at\ z=0}$) for all the runs as has been suggested by Dey et al. (2012). It has been assumed here that the shear stress caused by viscosity is negligible when compare to the shear stress due to RSS (Nezu, 1977). On careful examination of Figure 3.5 it can be observed that RSS increases towards the bed and obtains maximum value somewhere near the bed and then declines further. It is an indication of the presence of a roughness sublayer in the near-bed region. The distance of the maximum value of RSS from the channel bed increased under the action of downward seepage indicating an increase in the thickness of sublayer. Figure 3.5 suggests that after the application of downward seepage and 24 h of the seepage run, Reynolds stresses were increased ∼25-40% and ∼60-70%, respectively, from their values of the no seepage run, indicating the higher momentum transfer in the near-bed region under the condition of downward seepage. In addition to this, shear velocity was also increased in the presence of

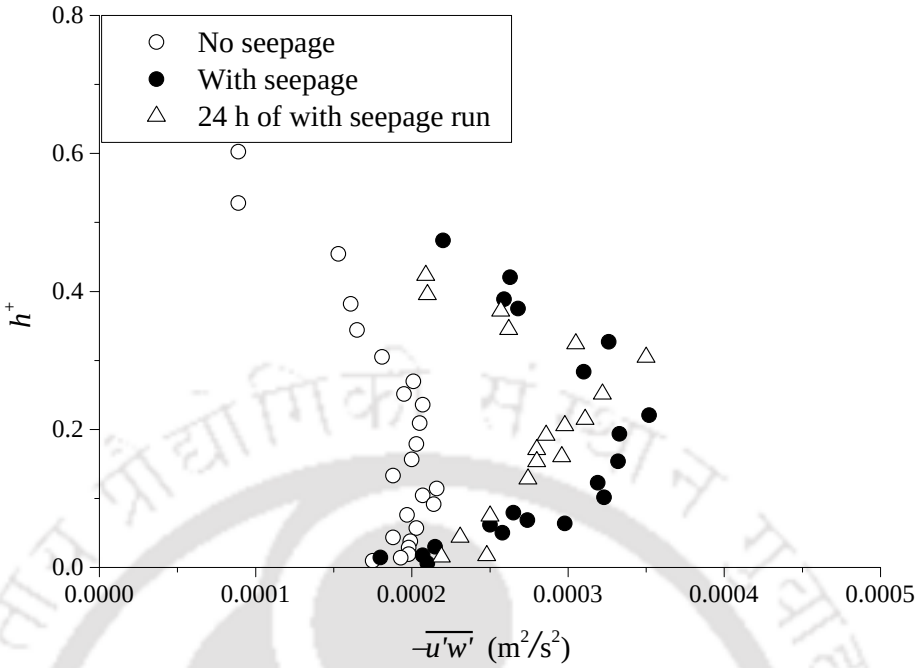

Figure 3.5: Profiles of Reynolds shear stresses for the no seepage (Phase-I measurement), with seepage (Phase-II measurement), and after 24 h of the seepage run (Phase-III measurement)

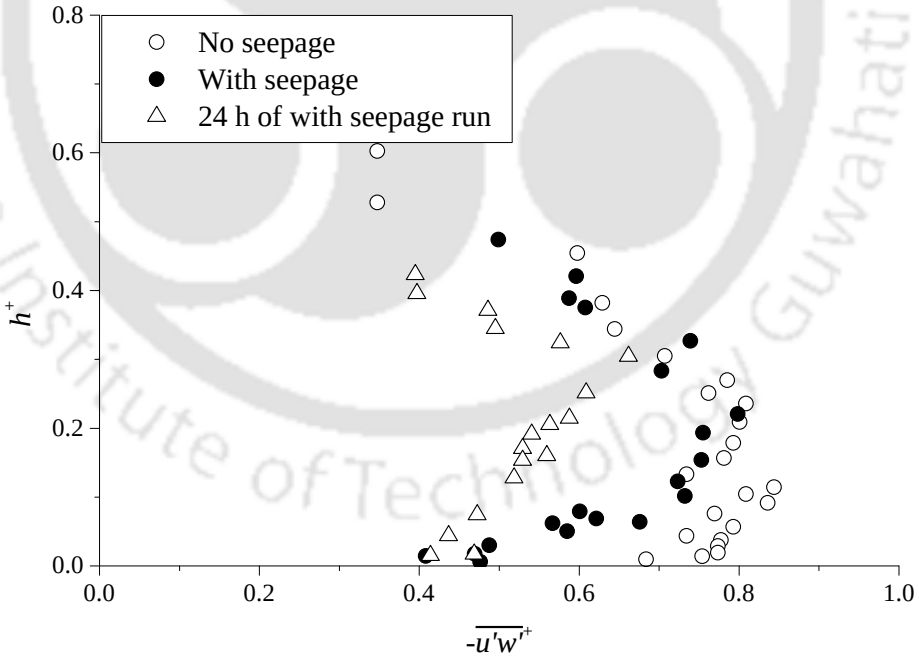

Figure 3.6: Profiles of nondimensional Reynolds shear stresses for the no seepage (Phase-I measurement), with seepage (Phase-II measurement), and after 24 h of the seepage run (Phase-III measurement)

seepage, which indicates an increase in the scale of the fluctuating components of velocity in the near-bed zone. Further, it can be observed that the position of maximum point of the RSS shifts towards the upward direction over the crest of the bedform after 24 h of seepage run during equilibrium condition.

In Figure 3.6 vertical distributions of nondimensional RSS ($\overline{u'w'}^{+} = -\overline{u'w'}/u_{*t}^2$) are plotted against normalized depth for all the runs. It can be observed that magnitude of the normalized RSS is reduced in the presence of downward seepage, which can be attributed to the increase in shear velocity.

3.4.3 Turbulent Intensities

Strength of turbulence in the flow is defined by the turbulent intensity, which can be calculated by the square root of the second moment of velocity. Figure 3.7 and Figure 3.8 show vertical distributions of the turbulent intensities in the streamwise ($\sqrt{\overline{u'u'}}$) and vertical ($\sqrt{\overline{w'w'}}$) directions, respectively, for all the experimental runs. From Figures 3.7 and 3.8, it can be observed that the streamwise and vertical turbulent intensities are increased by ∼10-30% and ∼20-30%, respectively, in the near-bed region ($h^+ < 0.2$) after the application of downward seepage and after 24 h of the seepage run. It is found that the strength of turbulence increases under the action of downward seepage. Vertical distributions of the normalized turbulent intensities in the streamwise ($\sigma_u^+ = -\sqrt{\overline{u'u'}}/u_{*t}$) and vertical ($\sigma_w^+ = -\sqrt{\overline{w'w'}}/u_{*t}$) directions are presented in Figure 3.9 and 3.10, respectively. Normalized turbulent intensities were reduced after the application of downward seepage and 24 h of the seepage run from that of the no seepage run, which is caused by an increase in the shear velocity.

Nezu and Nakagawa (1993) developed semiempirical equation to define normalized turbulent intensities (TI) for smooth bed by $TI = \left(\frac{\sqrt{\overline{u'u'}}}{u_{*t}}\right) = D_u e^{(-C_u h^+)}$, where D_u and C_u are empirical parameters. Values suggested for these parameters were 2.3 (D_u) and 1 (C_u). These values are suitable for the flat and smooth bed throughout the flow depth except very near to the boundary, where viscous effects are dominant and side currents are absent. These empirical parameters are not universal constant and are dependent on the bed roughness. Sukhodolov et al. (1998) have calculated new sets of constants for flows over rough bed. In the present observations, analysis has been carried out in the similar manner and they are presented in Figures 3.11, 3.12, and 3.13.

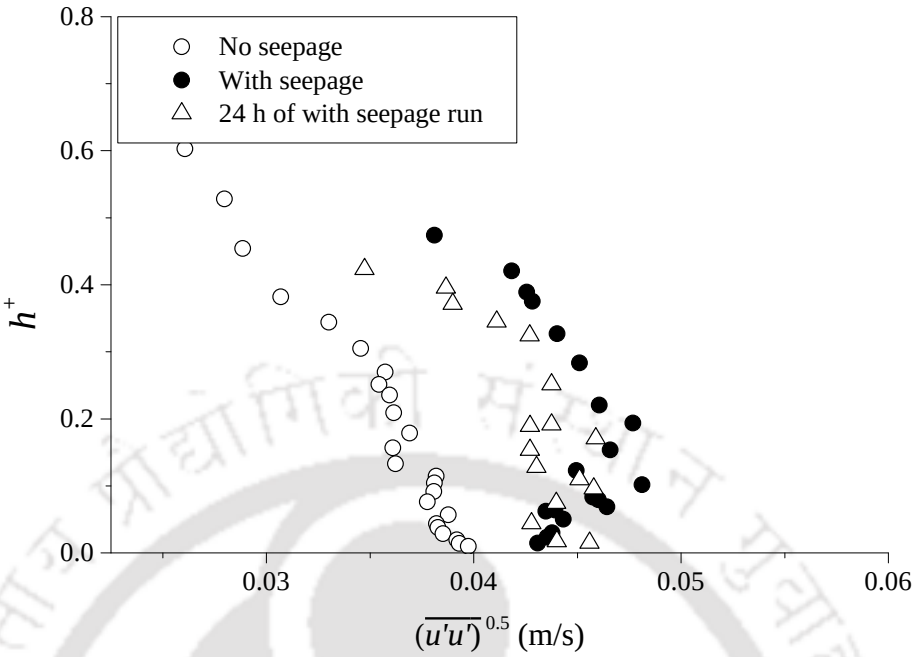

Figure 3.7: Profiles of (a) streamwise turbulent intensity ($\sqrt{\overline{u'u'}}$) for the no seepage (Phase-I measurement), with seepage (Phase-II measurement), and after 24 h of the seepage run (Phase-III measurement)

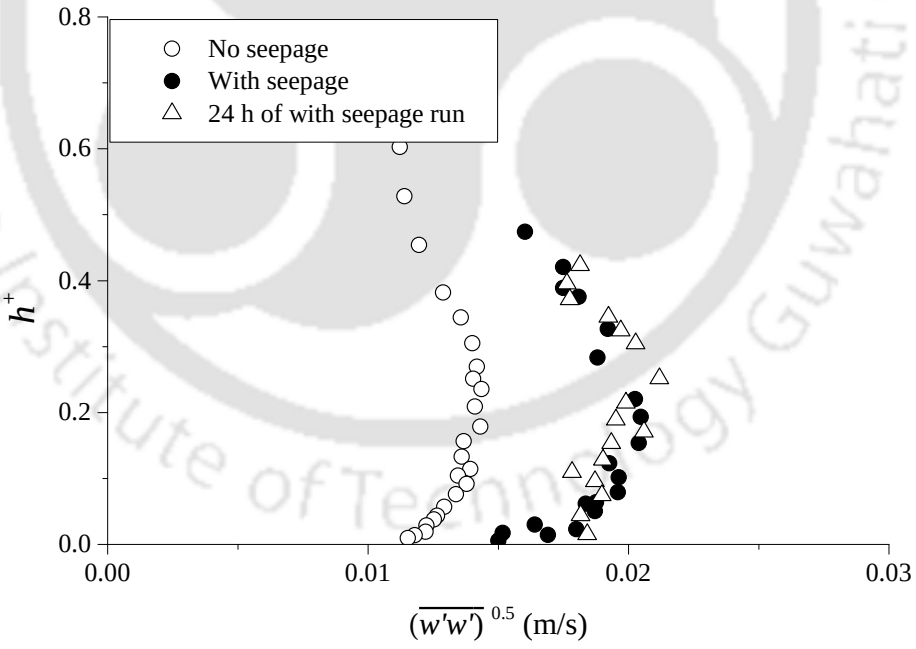

Figure 3.8: Profiles of (a) vertical turbulent intensity ($\sqrt{\overline{w'w'}}$) for the no seepage (Phase-I measurement), with seepage (Phase-II measurement), and after 24 h of the seepage run (Phase-III measurement)

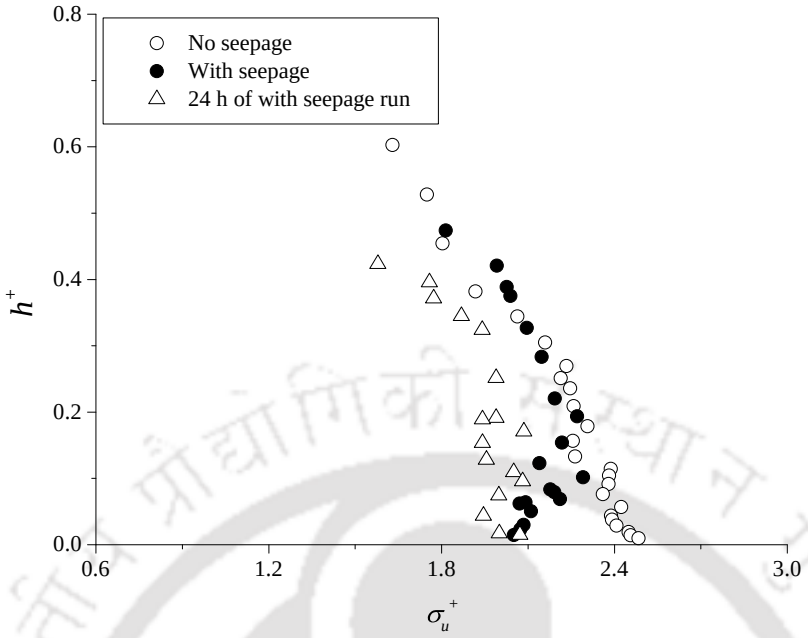

Figure 3.9: Profiles of (a) nondimensional streamwise turbulent intensity (σ_u^+) for the no seepage (Phase-I measurement), with seepage (Phase-II measurement), and after 24 h of the seepage run (Phase-III measurement)

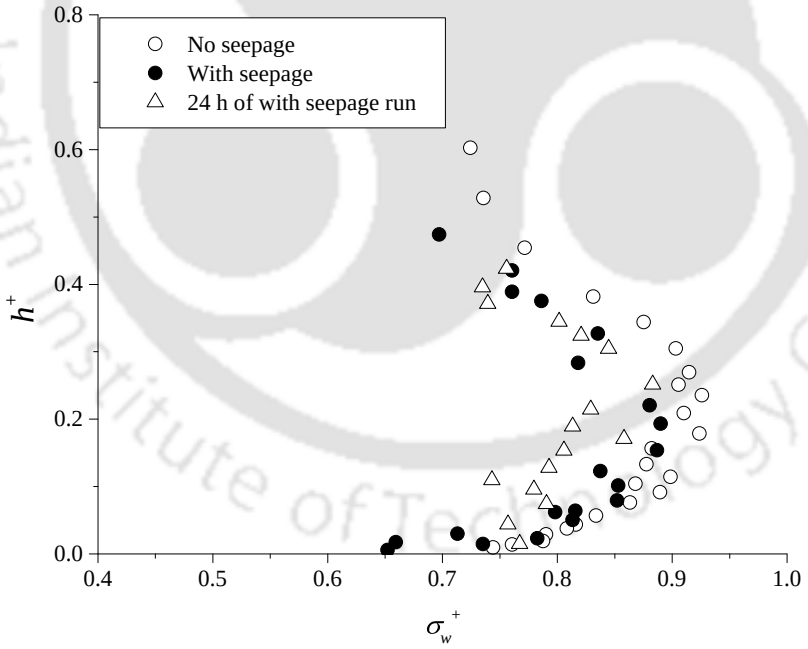

Figure 3.10: Profiles of (a) nondimensional vertical turbulent intensity (σ_w^+) for the no seepage (Phase-I measurement), with seepage (Phase-II measurement), and after 24 h of the seepage run (Phase-III measurement)

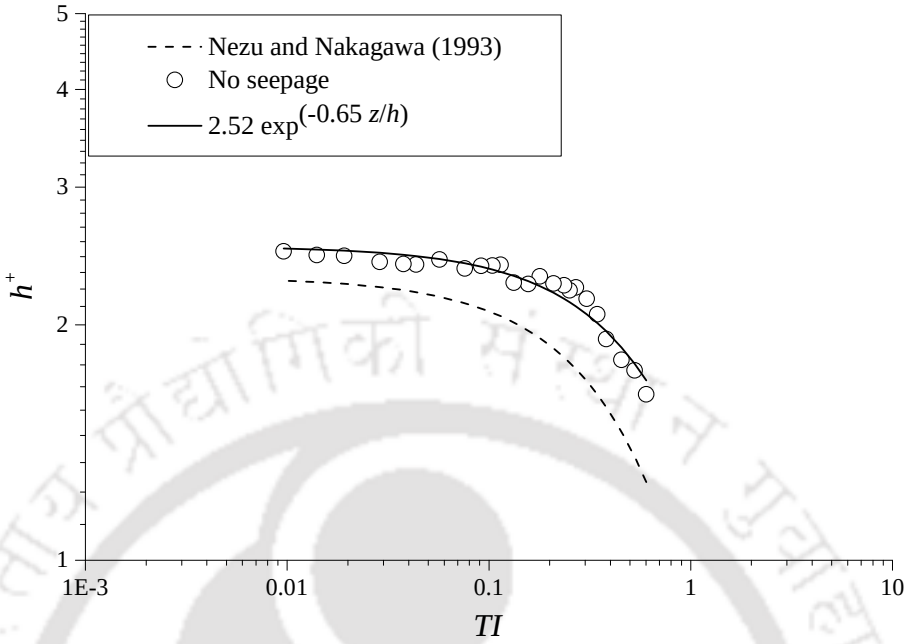

Figure 3.11: Comparison of streamwise turbulent intensities (TI) with Nezu and Nakagawa (1993) for the no seepage experiment (Phase-I measurement)

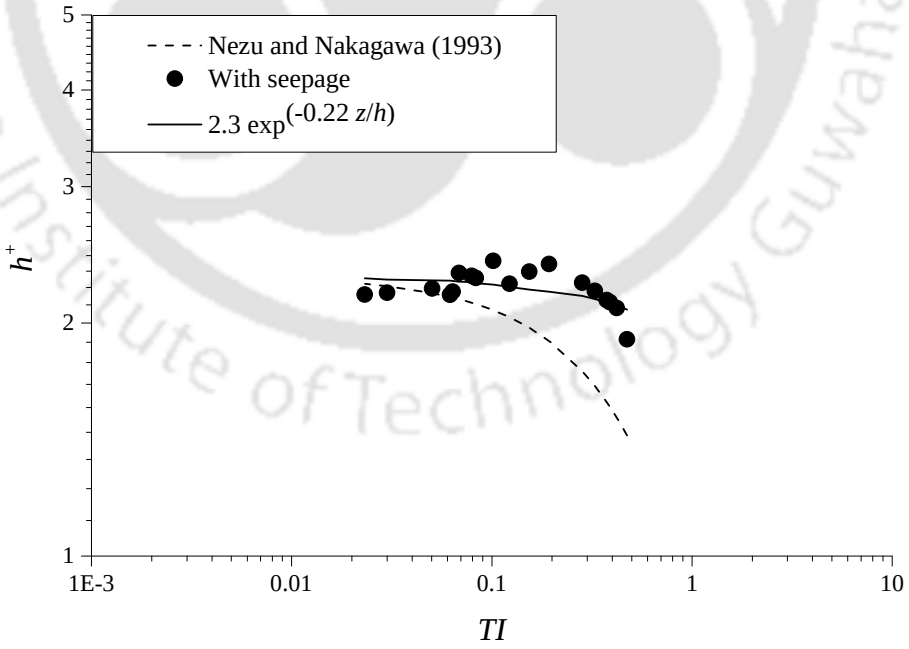

Figure 3.12: Comparison of streamwise turbulent intensities (TI) with Nezu and Nakagawa (1993) for with seepage experiment (Phase-II measurement)

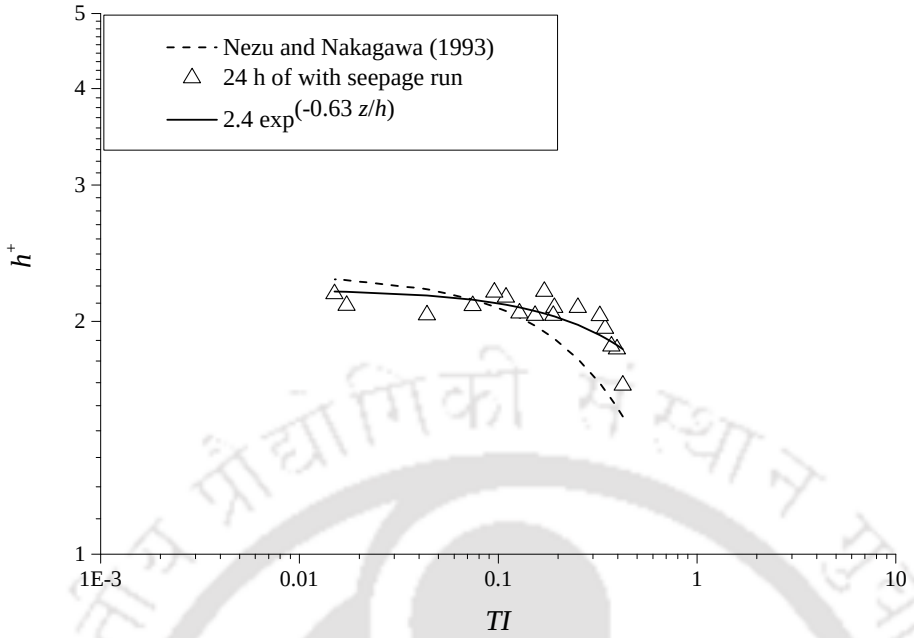

Figure 3.13: Comparison of streamwise turbulent intensities (TI) with Nezu and Nakagawa (1993) for after 24 h with seepage experiment (Phase-III measurement)

3.4.4 Distributions of Higher-order Correlations

Third-order correlations define the characteristics of Reynolds normal stresses produced by the turbulence. A set of third-order correlations (M_{jk}) of velocity fluctuations can be obtained by $M_{jk} = \overline{\widehat{u}^j \widehat{w}^k}$, where $j + k = 3$, $\widehat{u} = u'/\left(\overline{u'u'}\right)^{0.5}$, and $\widehat{w} = w'/\left(\overline{w'w'}\right)^{0.5}$ Raupach (1981). The third-order correlations can be classified as $M_{30} = \overline{u'^3}/\left(\overline{u'u'}\right)^{1.5}$, $M_{03} = \overline{w'^3}/\left(\overline{w'w'}\right)^{1.5}$, $M_{12} = \overline{u'w'^2}/\left(\overline{u'u'}\right)^{0.5}\left(\overline{w'w'}\right)$, and $M_{21} = \overline{u'^2w'}/\left(\overline{u'u'}\right)\left(\overline{w'w'}\right)^{0.5}$, where M_{30} defines the flux of streamwise Reynolds normal stress (RNS) in the streamwise direction or the skewness of u', M_{03} defines the vertical flux of RNS in the vertical direction or skewness of w', M_{12} defines the advection of vertical RNS in stream wise direction, and M_{21} defines the advection of streamwise RNS in the vertical direction. Distributions of the third-order correlations for all the experimental runs are shown in Figures 3.14, 3.15, 3.16, 3.17, 3.18, and 3.19. Figures 3.14 and 3.15 show the distributions of third-order correlations for the no seepage run, where M_{30} and M_{12} have small positive values, and M_{03} and M_{21} have small negative values in the near-bed region ($h^+ \leq 0.10$). Away from the boundary, M_{30} and M_{12} are negative, and M_{03} and M_{21} are positive in the rest of the measured depth.

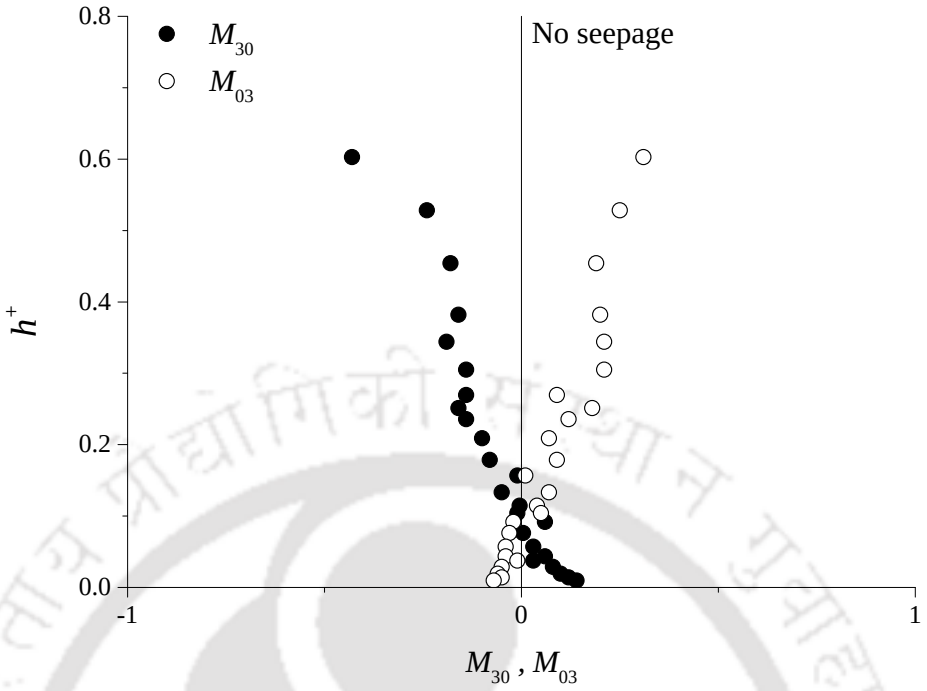

Figure 3.14: Profiles of the fluxes of RNS (M_{30} and M_{03}) for no seepage experiment (Phase-I measurement)

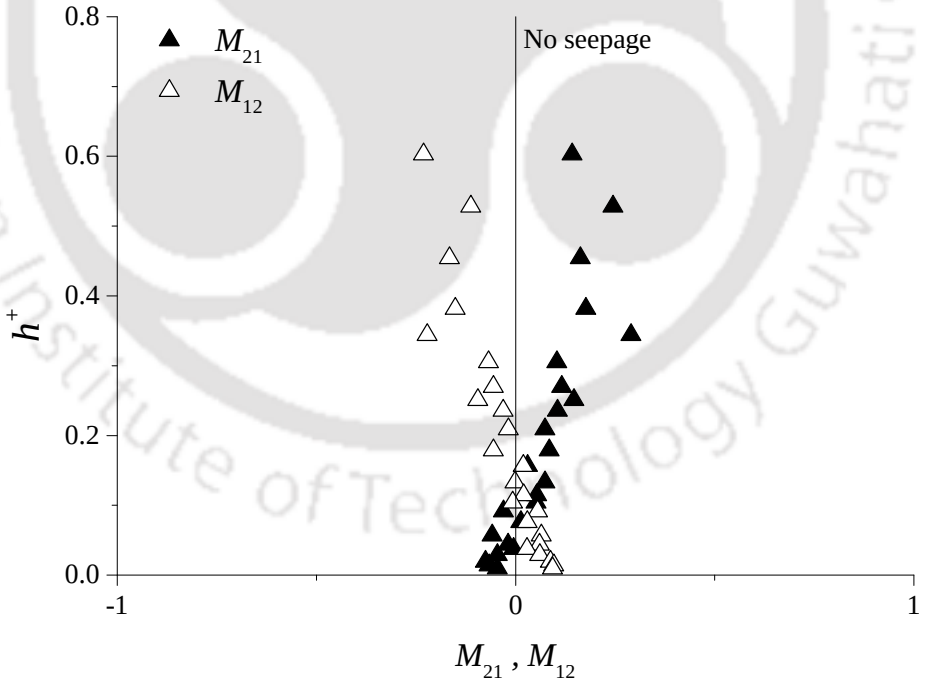

Figure 3.15: Profiles of the fluxes of RNS (M_{21} and M_{12}) for no seepage experiment (Phase-I measurement)

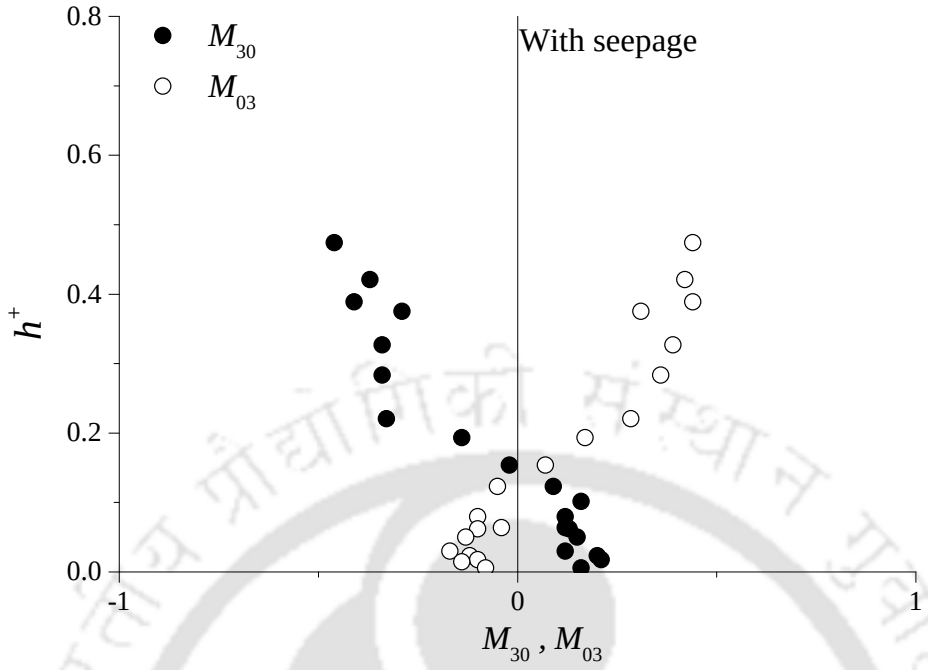

Figure 3.16: Profiles of the fluxes of RNS (M_{30} and M_{03}) for with seepage experiment (Phase-II measurement)

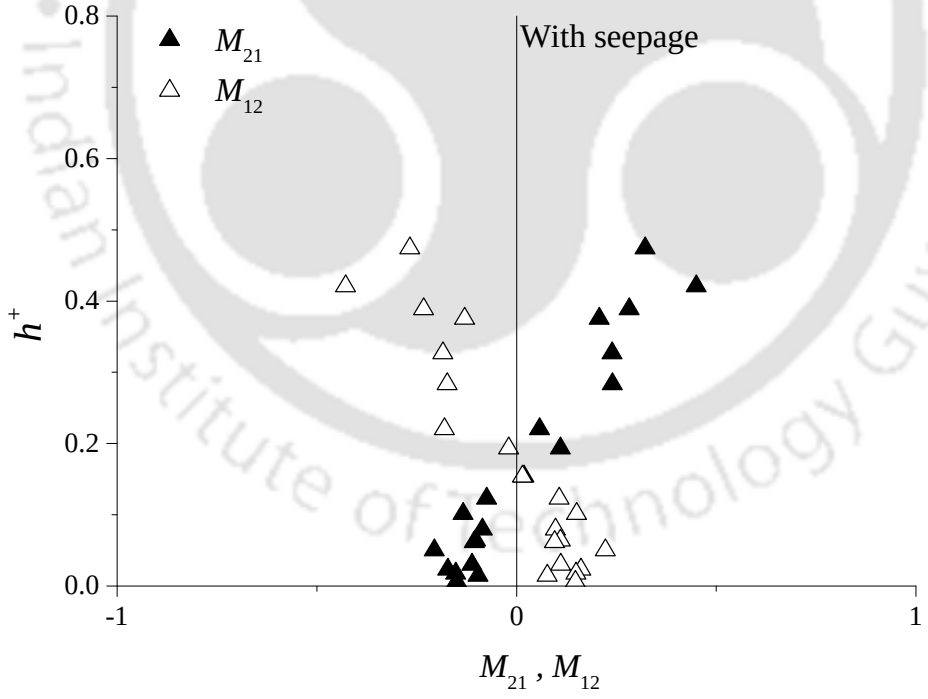

Figure 3.17: Profiles of the fluxes of RNS (M_{21} and M_{12}) for with seepage experiment (Phase-II measurement)

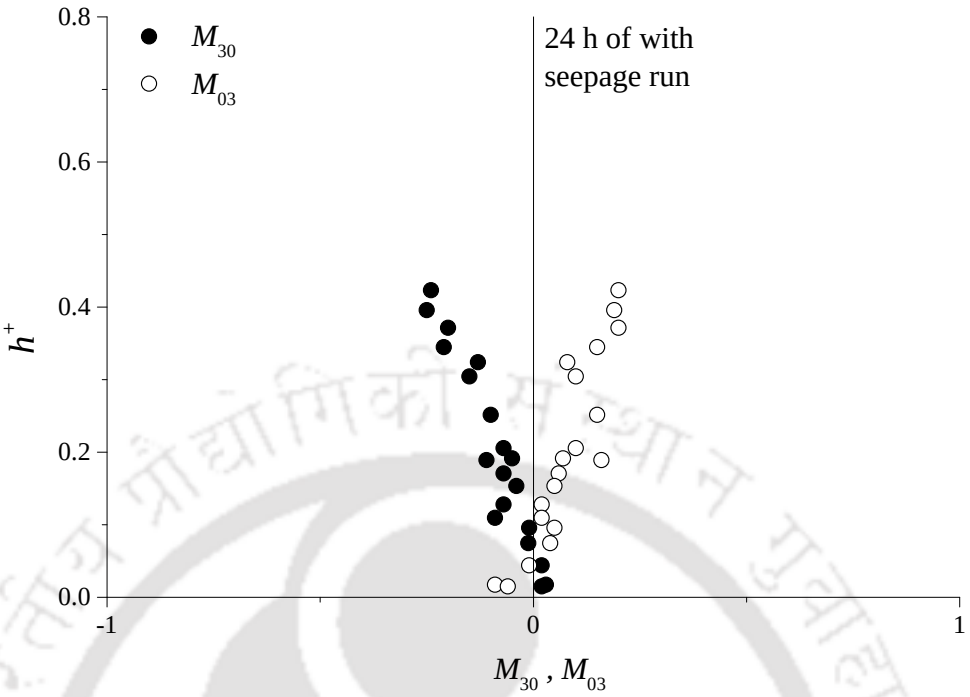

Figure 3.18: Profiles of the fluxes of RNS (M_{30} and M_{03}) for after 24 h of seepage run (Phase-III measurement))

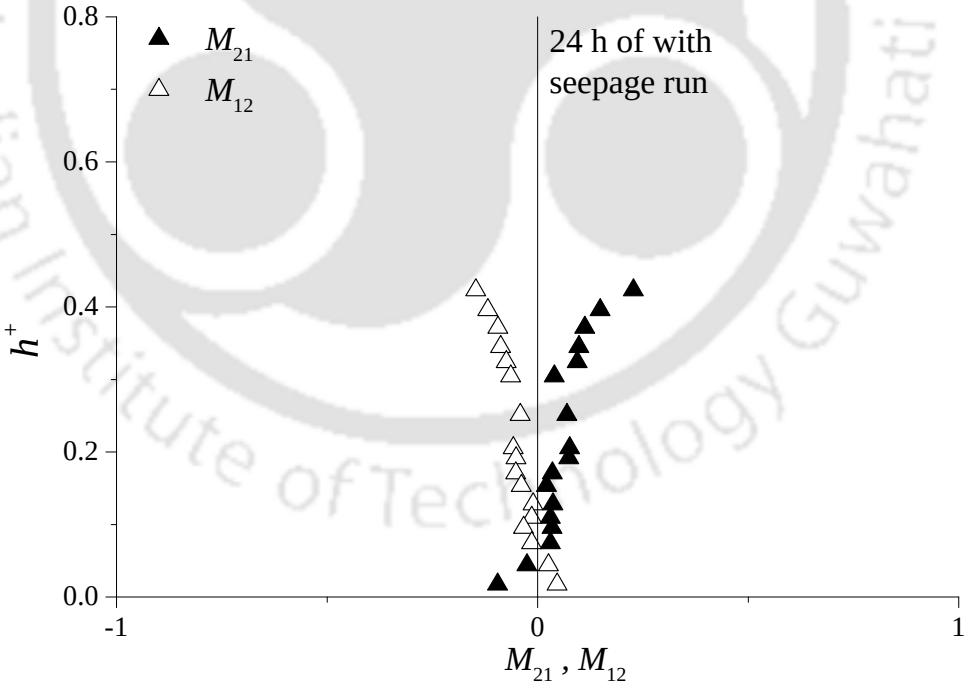

Figure 3.19: Profiles of the fluxes of RNS (M_{21} and M_{12}) for after 24 h of seepage run (Phase-III measurement)

Similar profiles of the third-order correlations are observed after the application of downward seepage (see Figures 3.16 and 3.17), but the magnitudes of M_{30} and M_{12} values are increased (greater positive) in the near-bed region ($h^+ \geq 0.17$). Increased positive values of M_{30} and M_{12} indicate a greater flux of streamwise RNS in the streamwise direction and an increase in the advection of vertical RNS in the streamwise direction under the action of downward seepage. It can also be observed that magnitudes for M_{03} and M_{21} are increased (greater negative) in the region close to the boundary, suggesting a greater vertical flux of RNS and an increase in the advection of streamwise RNS in the downward direction when downward seepage was applied to the channel. Analysis of the third-order correlations suggests that after the application of downward seepage movement of bed particles increases. Small magnitudes of the third-order correlations in the near-bed region during the no seepage run indicate the condition of incipient motion of bed particles. After the application of downward seepage, greater magnitudes of these correlations in the near-bed region are associated with the increased sediment transport in the channel.

However, after 24 h of the seepage run, magnitude of the positive values of M_{30} and M_{12}, and magnitude of the negative values of M_{03} and M_{21} are decreased in the region very close to the channel bed ($h^+ \leq 0.07$), when compared with the corresponding values of these correlations immediately after the application of seepage (see Figures 3.18 and 3.19).

3.4.5 TKE-Flux Components

TKE-flux is an important indicator of sediment movement in an alluvial channel. Streamwise and vertical flux of the TKE are evaluated as follows (Krogstadt and Antonia, 1999):

$$\left.\begin{aligned} f_{ku} &= 0.75\left(\overline{u'u'u'} + \overline{u'w'w'}\right) \\ f_{kw} &= 0.75\left(\overline{w'w'w'} + \overline{w'w'u'}\right) \end{aligned}\right\} \tag{3.12}$$

Flux of the TKE in the streamwise (f_{ku}) and vertical (f_{kw}) directions are nondimensionalized by the shear velocity (u_{*t})

$$\left.\begin{aligned} F_{ku} &= f_{ku}/u_{*t}^3 \\ F_{kw} &= f_{kw}/u_{*t}^3 \end{aligned}\right\} \tag{3.13}$$

where F_{ku} and F_{kw} are the nondimensional forms of f_{ku} and f_{kw}, respectively.

Figures 3.20, 3.21, and 3.22 show the vertical distributions F_{ku} and F_{kw} for all the runs. It can be observed from Figure 3.20 that values of F_{ku} are positive and F_{kw} are negative

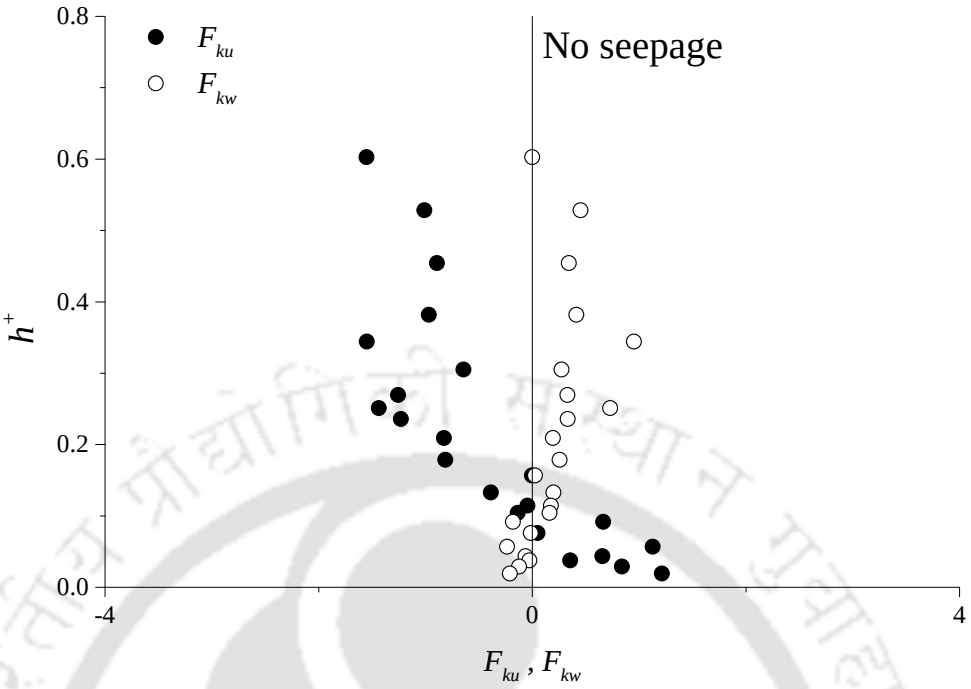

Figure 3.20: Profiles of TKE-Flux components in streamwise (F_{ku}) and vertical (F_{kw}) directions for no seepage experiment (Phase-I measurement)

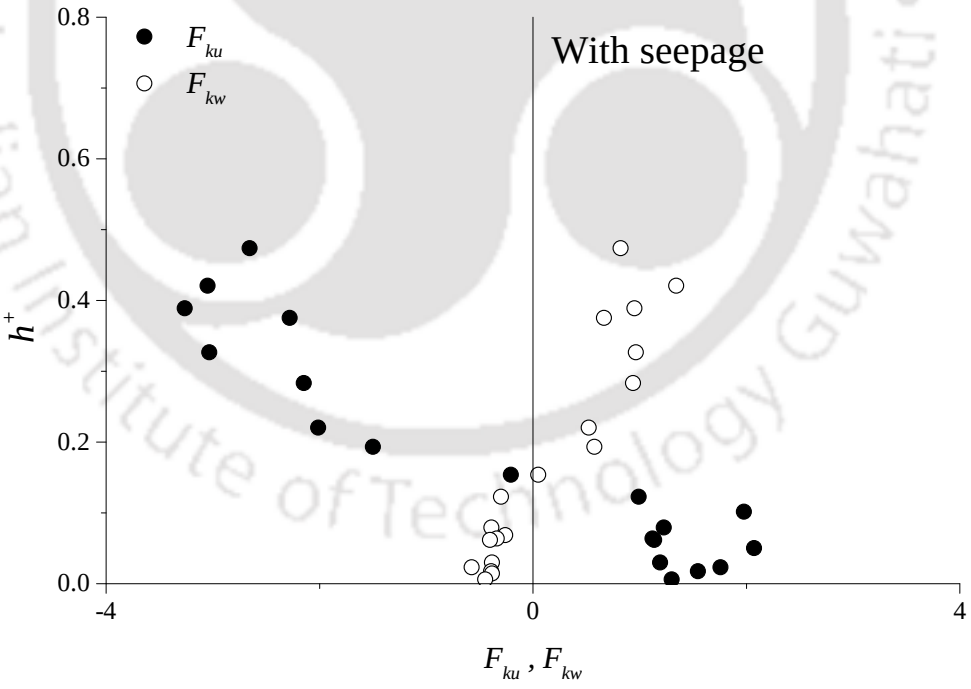

Figure 3.21: Profiles of TKE-Flux components in streamwise (F_{ku}) and vertical (F_{kw}) directions for with seepage experiment (Phase-II measurement)

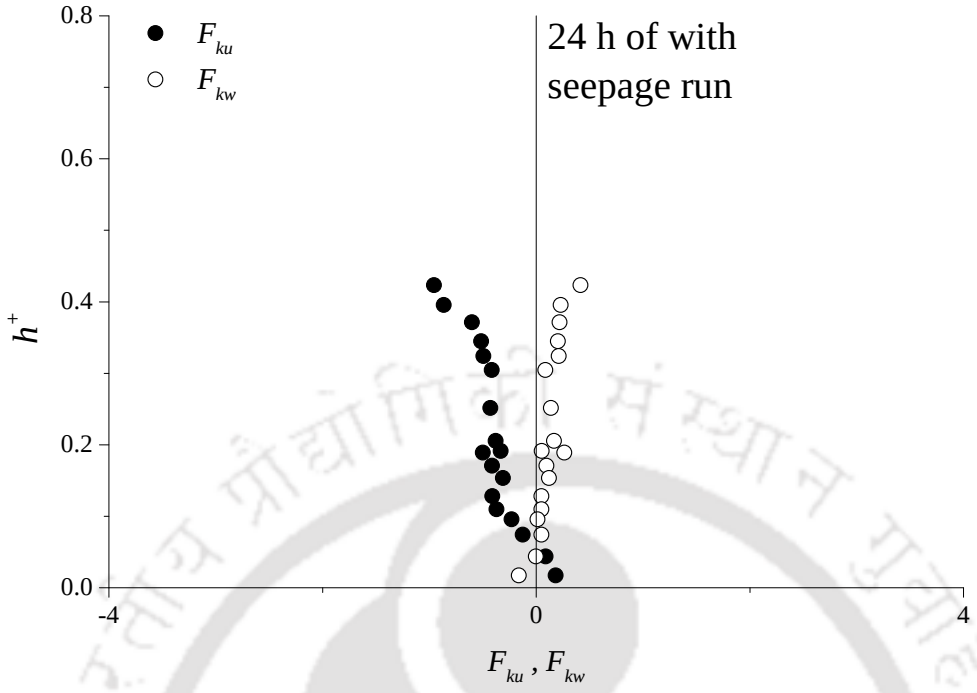

Figure 3.22: Profiles of TKE-Flux components in streamwise (F_{ku}) and vertical (F_{kw}) directions for 24 h of seepage run (Phase-III measurement)

with small magnitude in the near-bed region ($h^+ \leq 0.1$) for no seepage run, where bed particles are in the incipient motion condition. It can be seen from Figure 3.21 that after the application of downward seepage, magnitude of F_{ku} becomes greater positive and magnitude of F_{kw} becomes greater negative in the region close to the channel boundary ($h^+ \leq 0.16$). This suggests that in the presence of downward seepage, increased flux of streamwise TKE is travelling in the streamwise direction and increased flux of vertical TKE is traveling in the downward direction. The combination of the TKE fluxes in the near-bed region corresponds to the increased sediment transport in the channel when the downward seepage is applied to it. Further, Figure 3.22 shows that magnitudes of F_{ku} and F_{kw} for 24 h for the seepage run are decreased in the near-bed zone ($h^+ \leq 0.06$) as compared to their values with immediate application of seepage run, suggesting the reduction of sediment movement after 24 h of the seepage run.

3.4.6 Conditional RSS Distributions

Distributions of the velocity fluctuations u' and w' in the u', w' plane are used to characterize different bursting events at any point of measurement in the flow. In this study, the

technique of Lu and Willmarth (1973) is used for the quantification of u' and w' according to their respective signs in all the quadrants $Q_i (i = 1, 2, 3, 4)$. Q_1 (first quadrant) defines outward interactions (where $u' > 0$ and $w' > 0$), Q_2 (second quadrant) defines ejections (where $u' < 0$ and $w' > 0$), Q_3 (third quadrant) is inward interactions (where $u' < 0$ and $w' < 0$) and Q_4 (fourth quadrant) defines sweeps (where $u' > 0$ and $w' < 0$). Contributions toward RSS production from all four quadrants, i.e. Q_1, Q_2, Q_3, and Q_4 describe the bursting events. These events are composed with a sequence of cyclic flow patterns referred to as outward interactions, ejections, inward interactions, and sweeps, respectively.

In order to obtain the larger contributions towards the RSS production from various quadrants, a hole-size parameter (H) is introduced as suggested by Nezu and Nakagawa (1993). Where H is evaluated by $H = \sqrt{\overline{(u'u')}}\sqrt{\overline{(w'w')}}/|u'w'|$, which defines the hyperbolic hole-region for a given hole-size value (see Figure 3.23). At any point, contributions from different quadrants towards RSS ($-\overline{u'w'}$) production outside the hole-size H is evaluated by:

$$\left\langle u^{'} w^{'} \right\rangle_{i,H} = \lim_{T\to\infty} \frac{1}{T} \int_0^T u^{'}(t) w^{'}(t)\, \eta_{i,H}(t)\, dt \tag{3.14}$$

where angle brackets define the conditional averaging, T is the sampling period, t is the

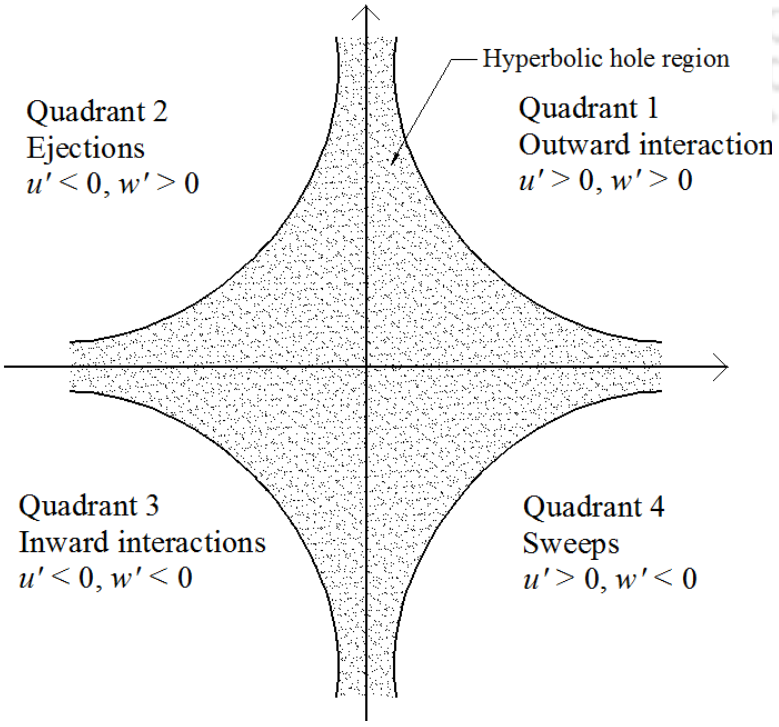

Figure 3.23: Graphical representation of quadrants and hole region

time, and $\eta_{i,H}$ is the detection function. The detection function is evaluated as:

$$\eta_{i,H}(t) = \begin{cases} 1 \text{ if } (u^{'}, w^{'}) \text{ are in Quadrant } i \text{ and if } \left|u^{'}w^{'}\right| \geq H\sqrt{\overline{(u'u')}}\sqrt{\overline{(w'w')}} \\ 0 \text{ otherwise} \end{cases} \tag{3.15}$$

The fractional contribution ($S_{i,H}$) from any quadrant in total RSS production can be obtained by

$$S_{i.H} = \langle u'w' \rangle_{i,H} / \overline{u'w'} \tag{3.16}$$

Where $S_{i,H}$ is positive for quadrants Q_2 and Q_4, and negative for quadrants Q_1 and Q_3. At any particular point, the sum of $S_{i,H}$ from all the quadrants is always unity for $H = 0$. Distributions of fractional contributions towards RSS production from different bursting events for all the runs are plotted in Figures 3.24, 3.25, 3.26, 3.27, 3.28, and 3.29.

Analysis of the fractional contributions ($S_{i,H}$) towards RSS production provide an insight into the coherent structure of the flow. In general, the major contribution towards RSS production comes from the ejection and sweep events, while the outward and inward events contribute very less. Figure 3.24 presents the distributions of $S_{i,H}$ for $H = 0$ for no seep-

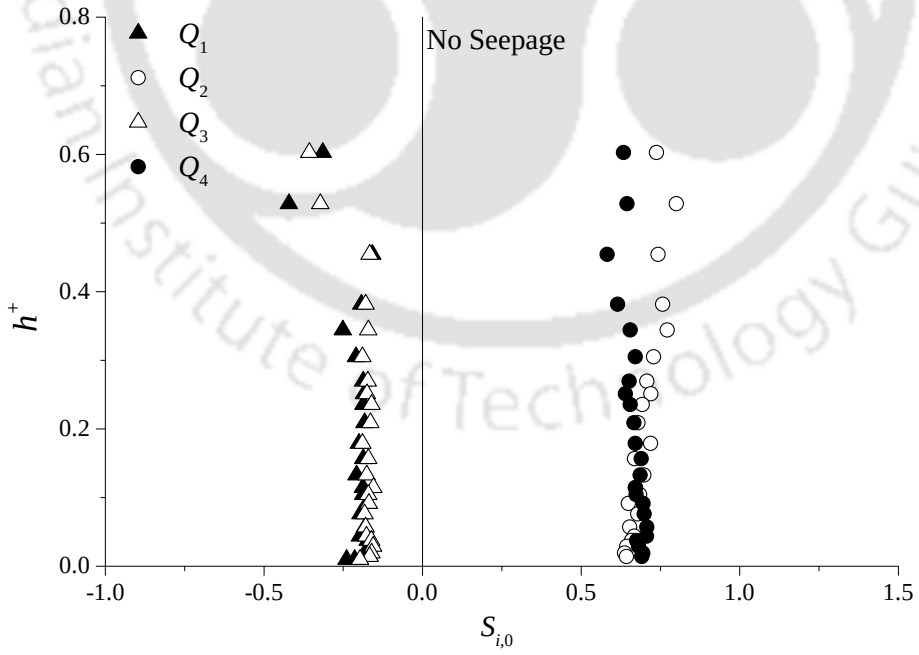

Figure 3.24: Profiles of the conditional RSS distributions of $S_{i,0}$ for no seepage experiment (Phase-I measurement)

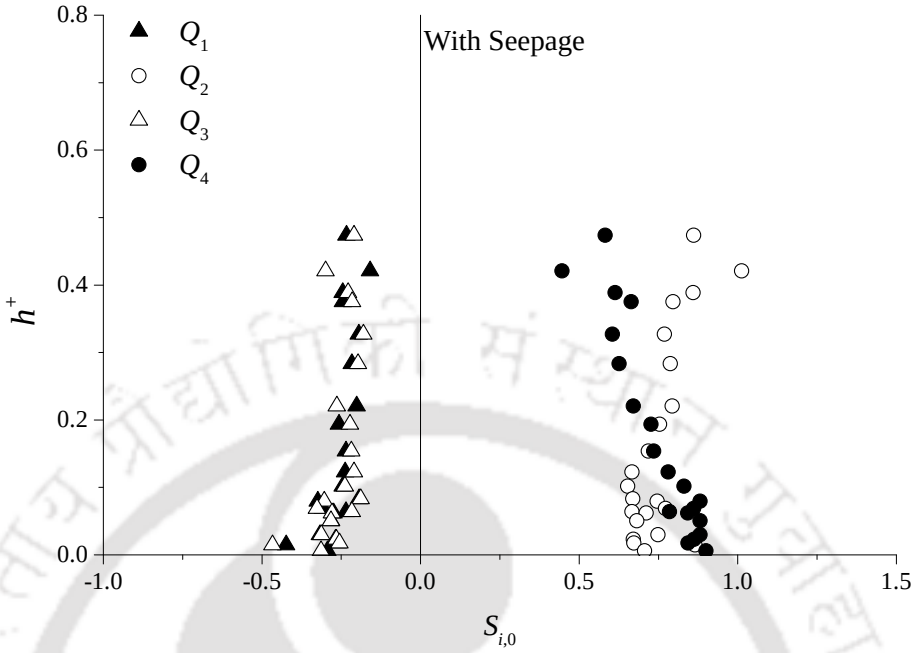

Figure 3.25: Profiles of the conditional RSS distributions of $S_{i,0}$ for with seepage experiment (Phase-II measurement)

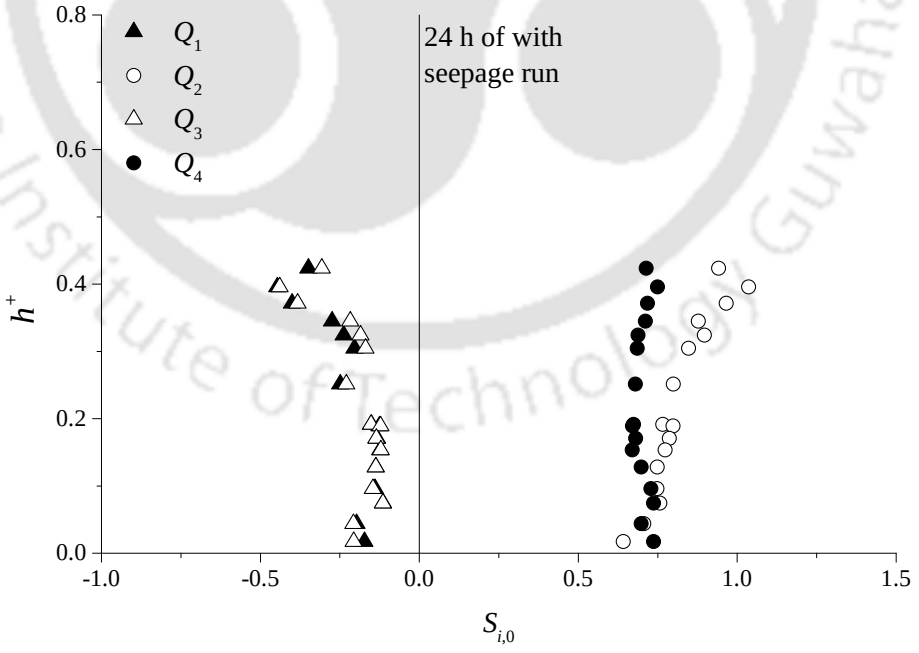

Figure 3.26: Profiles of the conditional RSS distributions of $S_{i,0}$ for 24 h of seepage run (Phase-III measurement)

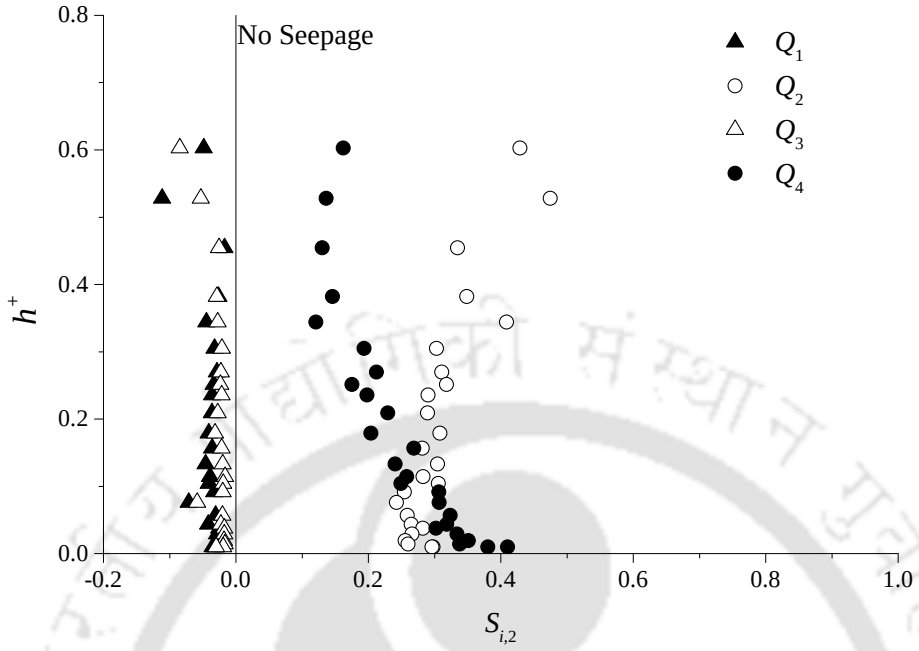

Figure 3.27: Profiles of the conditional RSS distributions of $S_{i,2}$ for no seepage experiment (Phase-I measurement)

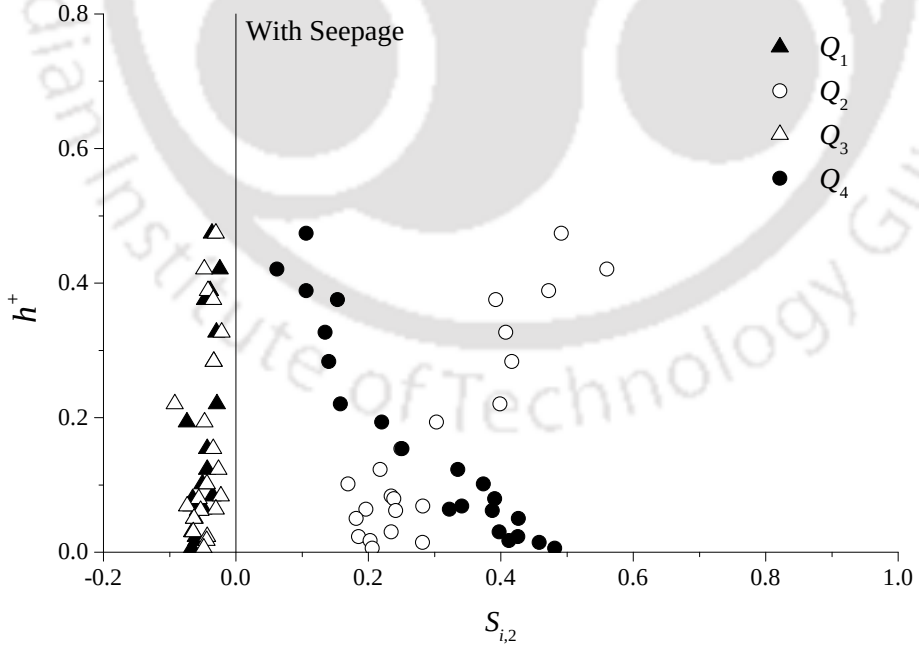

Figure 3.28: Profiles of the conditional RSS distributions of $S_{i,2}$ for with seepage experiment (Phase-II measurement)

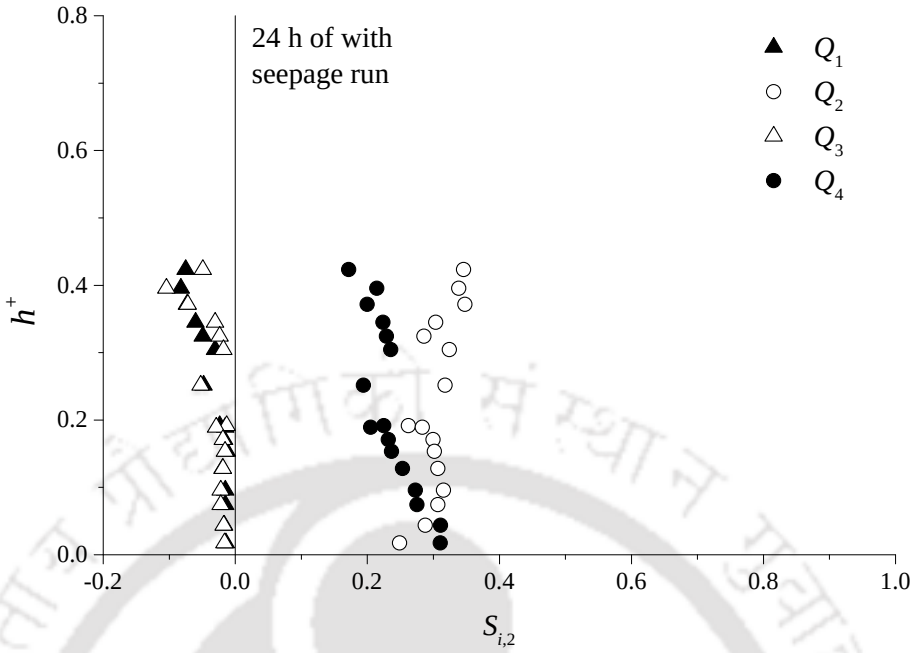

Figure 3.29: Profiles of the conditional RSS distributions of $S_{i,2}$ for 24 h of seepage run (Phase-III measurement)

age run. It can be observed that the contributions come from Q_2 and Q_4 events towards the RSS production are nearly equal to 69% in the near-bed region. In the same region, contributions from Q_1 events are 21% and from Q_3 events are 19%.

It can be observed from Figure 3.25 that after application of downward seepage, contributions from all the bursting events are increased significantly as compared with the no seepage case. Sweep events become the largest contributor ($\sim$89%) in the region close to the boundary, while the contribution from ejections is nearly equal to 70%. Contribution from interactions (outward and inward) is still very less (31% from Q_1 and 29% from Q_3). Corresponding, thickness of the sweep-dominated region is increased from that of the no seepage case. Significant increase in the contribution from the sweep events corresponds to the increased sediment transport in the channel after the application of downward seepage. In contrast, contributions from all bursting events in RSS production are decreased (see Figure 3.26) after 24 h of the seepage as compared with the immediate application of seepage. Contributions from Q_1, Q_2, Q_3, and Q_4, events are observed as 17%, 64%, 20%, and 73%, respectively, in the region close to the channel bed. A decrease in the contribution towards the RSS production from these events indicates the reduction in the mobility of bed material.

Furthermore, hole-size $H = 2$ is used to analyze the contributions from stronger events for

all the runs. Figures 3.24 to 3.29 shows that the contributions from Q_2 and Q_4 are notable, while contributions from Q_1, and Q_3 are insignificant. The thickness of sweep-dominated region is extended from $h^+ \sim 0.09$ to $h^+ \sim 0.12$ after the application of downward seepage, suggesting the development larger eddies in the near-bed zone (see Figure 3.28). However, with the passage of time (24 h of the seepage run), the thickness of sweep-dominated region shrinks to $h^+ \sim 0.04$ (Figure 3.29).

3.4.7 Turbulence Production and Dissipation

Figures 3.30 and 3.31 depict the vertical distributions of turbulent production and turbulent kinetic energy dissipation for all the runs, which were evaluated as Krogstadt and Antonia (1999):

$$t_p = -\overline{u'w'}\frac{\partial u}{\partial z} \tag{3.17}$$

$$e_d = \frac{15\upsilon}{u^2}\left(\frac{\partial u'}{\partial t}\right)^2 \tag{3.18}$$

where υ is the kinematic viscosity. Quantities t_p and e_d are non-dimensionalized by mul-

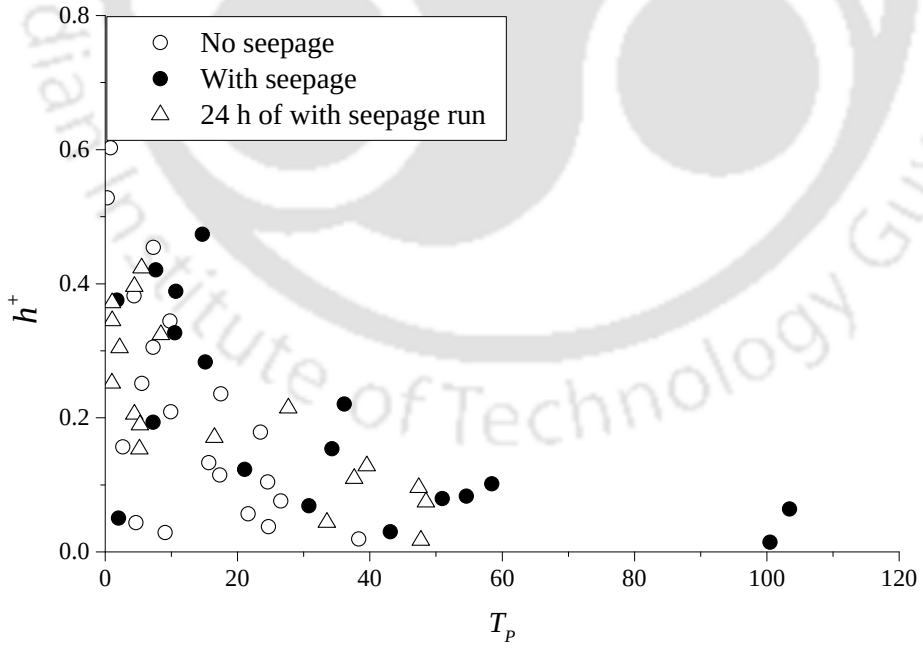

Figure 3.30: Vertical distributions of turbulent production (T_P) for for the no seepage (Phase-I measurement), with seepage (Phase-II measurement), and after 24 h of the seepage run (Phase-III measurement)

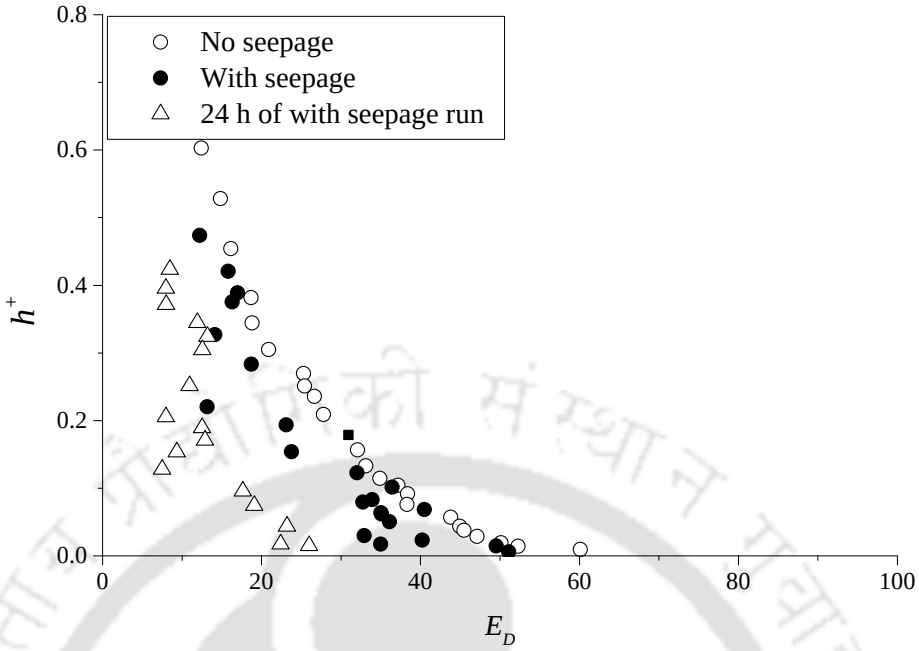

Figure 3.31: Vertical distributions of turbulent kinetic energy dissipation (E_D) for for the no seepage (Phase-I measurement), with seepage (Phase-II measurement), and after 24 h of the seepage run (Phase-III measurement)

tiplying with h/u_{*t}^3, and are expressed as T_P and E_D, respectively. Turbulent production comes from the interchange of mean flow energy to fluctuations. It can be observed from Figure 3.30 that the turbulent production is increased when the downward seepage is applied to the channel. This increased T_P is in agreement with the higher momentum transfer under the seepage condition. Also, it can be implied that larger roughness over the boundary of the channel with the application of seepage, causes more turbulent production in the flow. Further, it can be observed that the turbulent dissipation (E_D) is reduced when water is extracted in the downward direction from the sand bed as shown in Figure 3.31. Under the action of downward seepage, more energy is converted to turbulent fluctuations in the flow, resulting in the reduced dissipation of the turbulent kinetic energy.

3.5 Key Findings and Discussion

The experiments were carried out on a threshold channel with parabolic cross-sectional shape to observe the variation in the flow structure and effects on the channel morphology, when downward seepage was applied to the channel. Previous researchers have observed that the time-mean velocities in the near-bed region and tractive stress were increased when

downward seepage was applied in a small test section of the flat bed channels (Maclean, 1991b; Chen and Chiew, 2004). However, in their study stability of a threshold channel with seepage was not considered. Further, Sumer et al. (2003) has suggested that an increment of about 20% in the turbulence level can increase sediment transport by six times.

In the present study, cross-sectional shape of the channel was stable during the incipient motion condition of the no seepage run (see Figure 3.3). However, after the application of downward seepage to the channel, increase in the time-mean velocities and Reynolds stresses are observed (see Figures 3.4 and 3.5). The larger Reynolds stresses are associated with the increased strength of the flow and therefore, increased sediment movement was seen over the periphery of the channel. Additionally, third-order analysis (skewness and TKE fluxes) indicate higher fluctuations around the mean velocity with the application of downward seepage. Bed features were observed in the previous studies, when the tractive stress was increased from its critical value because of increase in the inflow discharge (Williams and Kemp, 1971; van Rijn, 1982; Kapdasli and Dyer, 1986; Best, 1992; Nelson et al., 1995; Coleman and Melville, 1996; Venditti et al., 2005). Furthermore, analysis of the bursting events (see Figures 3.25 and 3.28) shows that the contributions of sweep events towards the production of Reynolds shear stresses are increased in the near-bed region under the influence of downward seepage. These sweep events are attributed to higher momentum transfer towards the channel bed, suggesting sediment transport in the channel under the action of downward seepage. Several researchers (Williams and Kemp, 1971; Raudkivi and Witte, 1990; Best, 1992; Nelson et al., 1995; Raudkivi, 1997) have also reported that the sweep events govern the sediment movement leading to the development of different bed features in a sand bed channels. Therefore, it can be concluded that the downward seepage plays a critical role on sediment movement and the development of bedforms in a fined grained sand bed channel.

Results from the instantaneous flow measurements and Shields diagram show that the downward seepage affects the hydrodynamics of flow. Two phenomena mutually occurr in the natural or man-made alluvial channels: (1) variation in the tractive stress, which influences the bed dynamics and leads to the development of bed features, and (2) these bed features in turn influence the flow characteristics. In the present experimental study, it has been observed that the tractive stresses (Reynolds stresses) were increased after the application of seepage, which initiated the movement of sediment particles from the bank zone. It can be seen from Figures 3.32, 3.33, and 3.34 that the cross-sectional shape of the channel deformed because of movement of material from banks to channel bed. This

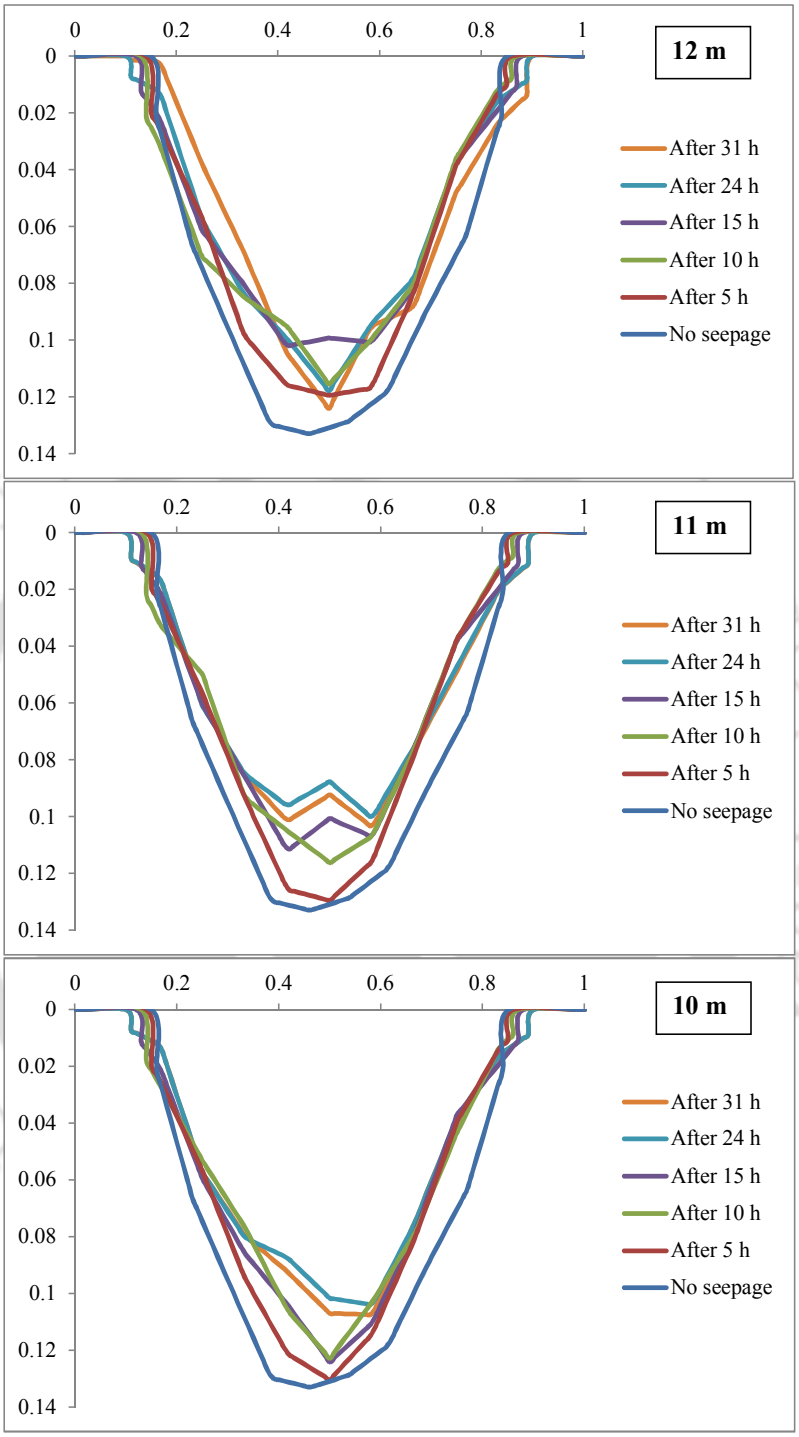

Figure 3.32: Cross-sectional profiles in the test section 12 m, 11 m, and 10 m for no seepage experiment, after 5 h, after 10 h, after 15 h, after 24 h, and after 31 h with seepage experiment

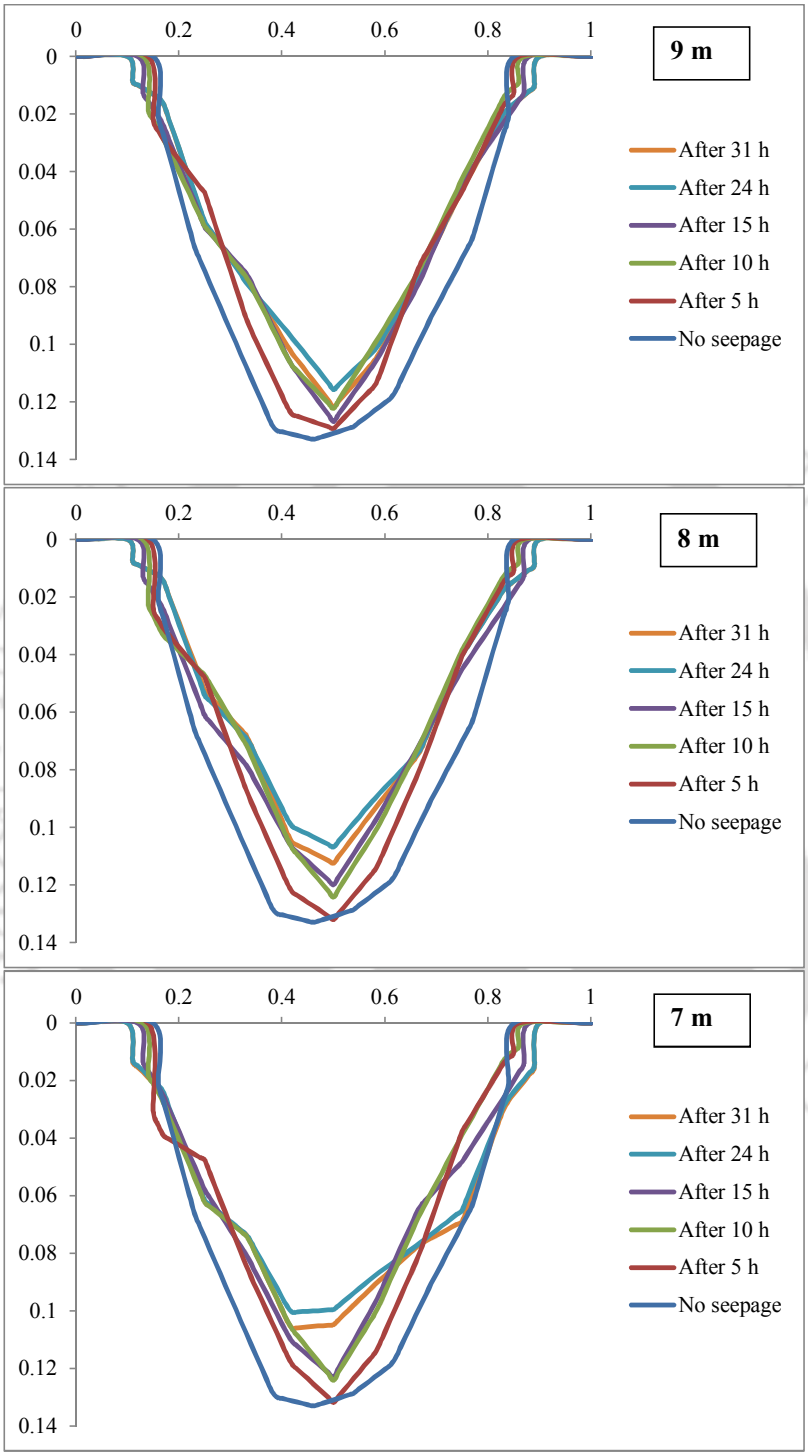

Figure 3.33: Cross-sectional profiles in the test section 9 m, 8 m, and 7 m for no seepage experiment, after 5 h, after 10 h, after 15 h, after 24 h, and after 31 h with seepage experimen

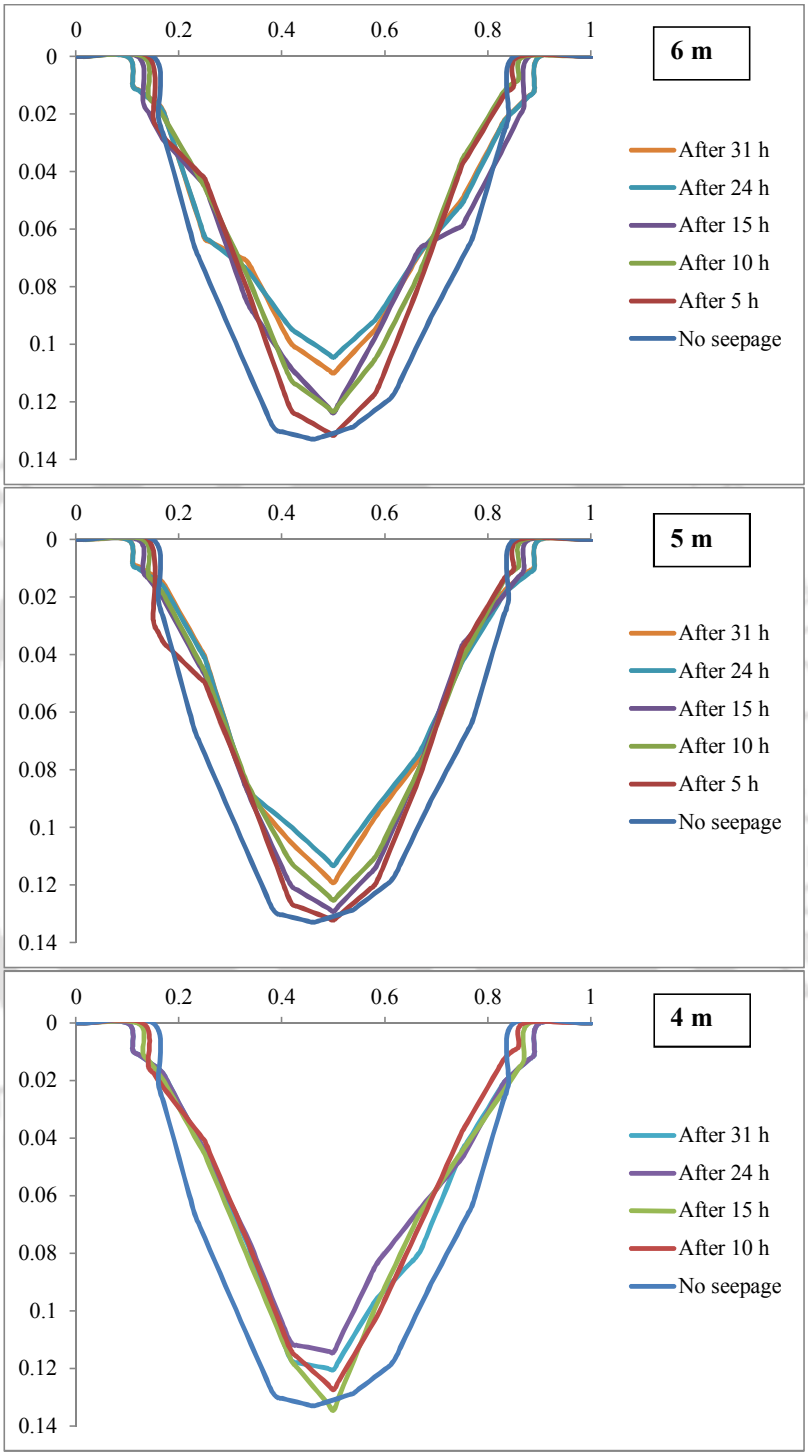

Figure 3.34: Cross-sectional profiles in the test section 6 m, 5 m, and 4 m for no seepage experiment, after 5 h, after 10 h, after 15 h, after 24 h, and after 31 h with seepage experimen

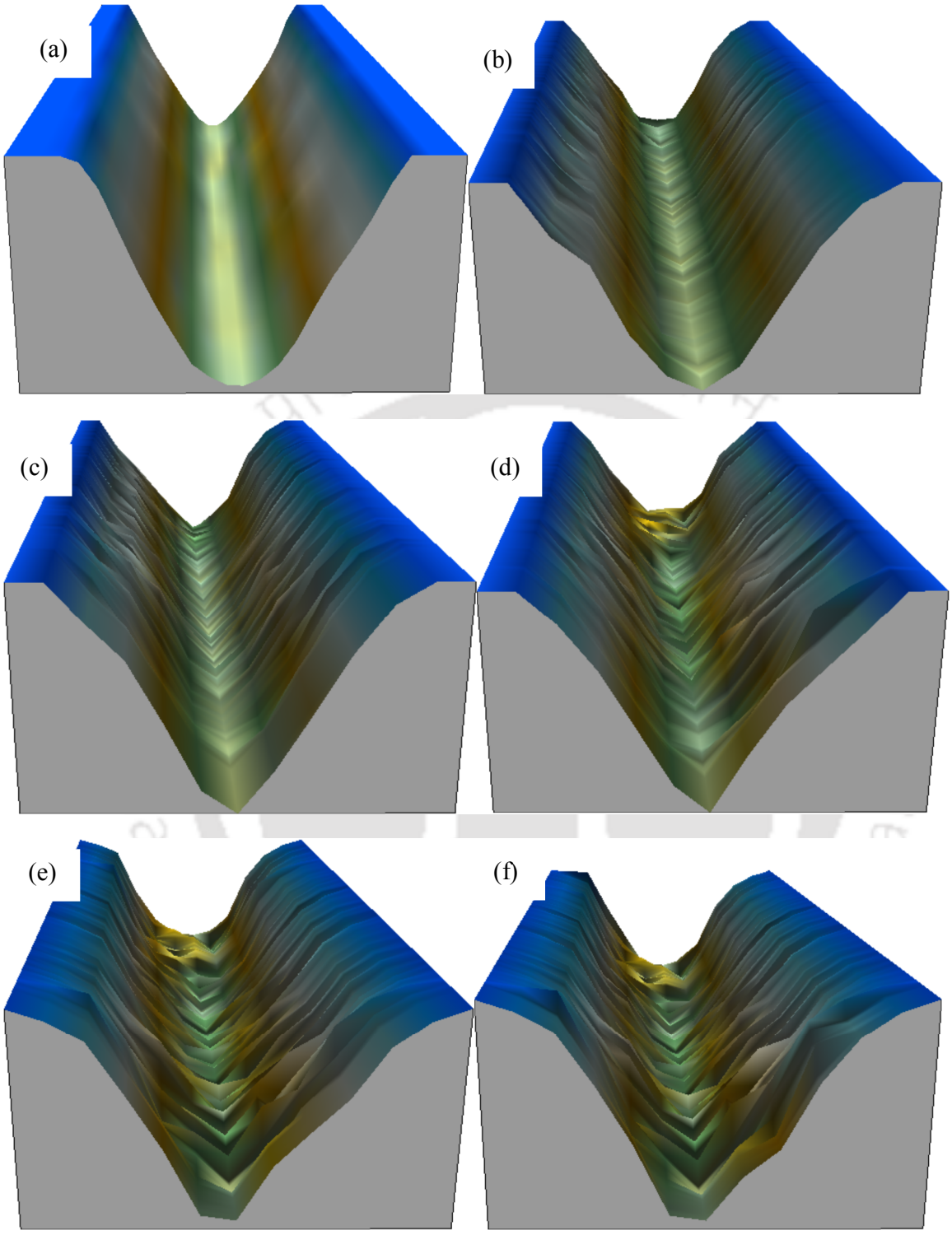

Figure 3.35: Processed 3-Dimensional plot of channel cross-sectional shape variation at different time intervals (a) no seepage experiment, (b) after 5 h, (c) after 10 h, (d) after 15 h, (e) after 24 h, and (f) after 31 h with seepage experiment

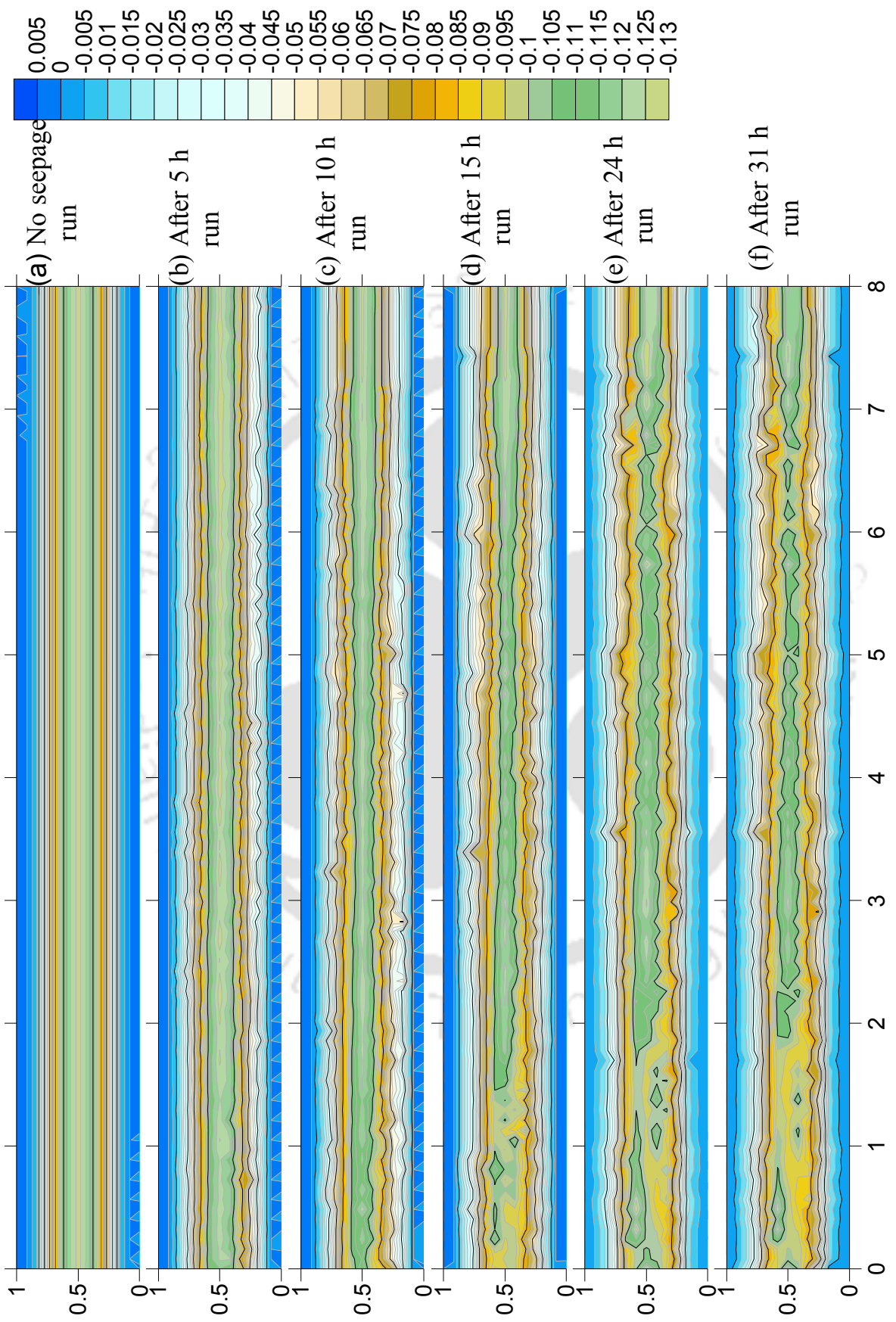

Figure 3.36: Contour map of migrating bedforms at different time intervals (a) no seepage experiment, (b) after 5 h, (c) after 10 h, (d) after 15 h, (e) after 24 h, and (f) after 31 h with seepage experiment (flow direction is left to right)

movement led to the development of a series of small bedforms over the periphery of a parabolic cross-sectional shape to counter the increased tractive stresses. Interestingly, with the period of time these current ripples were continuously fed by the eroded material from bank and these small ripples transformed into linguoid ripples. As the tractive stresses were increased, consequently, the dimensions of bedforms were also increased. These bedforms were prograded from the upstream to the downstream direction because of the flow separation process. These processes were continued till the entire cross section was deformed and channel attained an equilibrium condition. This process can be understood through Figure 3.35 that provides the information regarding temporal variation of the cross-sectional shape and migrating bedforms. Figure 3.36 shows the contour map of the temporal changes in bed morphology and dynamics in the presence of seepage. It can be seen that at the beginning the process of developing bedforms is higher, where bedforms dimensions increase rapidly and with the passage of time these bedforms reached in an equilibrium state. Thus, it is needed to quantify and classify these developing fluvial bedforms in seepage environments, which are discussed in next paragraph.

3.6 Temporal Quantification of Bedform geometry and Discussion

Bedforms play an important role in the channel morphology (Gilbert and Murphy, 1914). Several experimental studies (Simons, 1961; van Rijn, 1982; Robert and Uhlman, 2001) have been carried out to quantify and characterize the bedforms. Although inherently stochastic in nature, the bedform geometry can be characterized using simple generic relationships such as linear relations that exist between standard deviation and mean value for height, length, crest elevation, and trough elevation of bedform (Van der Mark et al., 2008). In the present study, a set of bed elevation profiles (BEPs) in the longitudinal direction was recorded for the entire cross section after 5 h, 10 h, 15 h, 24 h, and 31 h of the commencement of seepage run in the test section. Figure 3.37 shows the raw profile of measured bed elevation collected by using the ultrasonic ranging system. BEPs have been analyzed by using bedform tracking tool (BTT) developed by Van der Mark and Blom (2007). BTT is used to identify and locate the position of bedforms. It also provides the information regarding the characteristics of bedforms from a measured BEP (e.g., Figure 3.37).

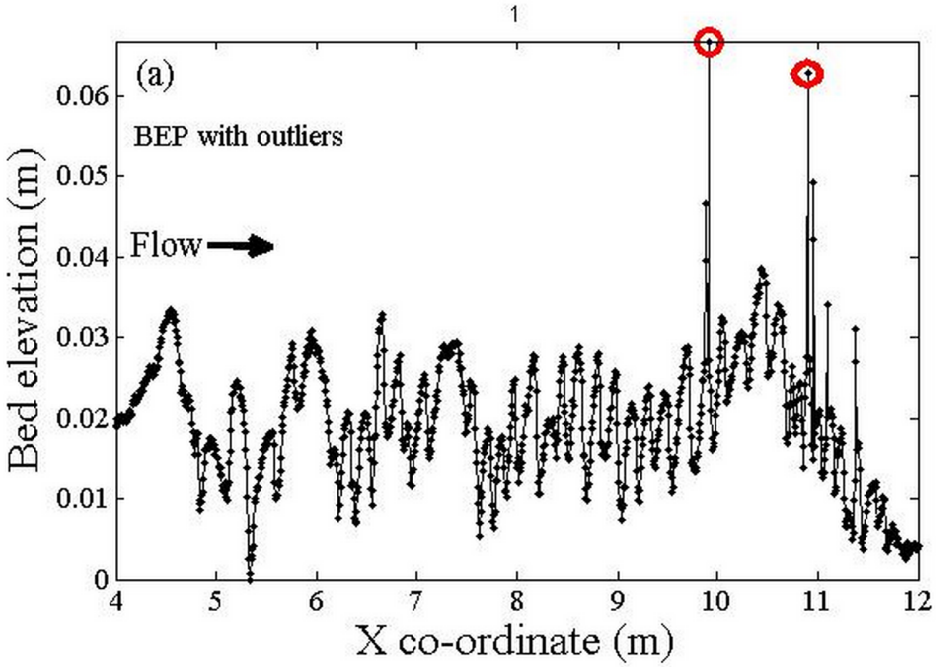

Figure 3.37: Measured profile obtained using ultrasonic ranging system, where dark red circles show the outliers i.e. measuring errors

3.6.1 Post Processing of the Geometry Data

The raw BEPs contain outliers (i.e., measuring errors), that have been removed by linear interpolation between adjacent points (see Figure 3.38). Here, it has been considered that the BEPs do not have any spatial variations because they were collected in the laboratory flume, therefore the linear trend line can fit on the BEPs (Van der Mark and Blom, 2007). A trend line is fitted on a filtered BEP to determine the zero crossings (see Figure 3.39). Zero up-crossings and zero down-crossings were determined to locate the positions of the crests and troughs. BEP has been detrended (see Figure 3.40), where points above the line show the locations of crests (denoted by dark squares) and points below the line show the locations of troughs (denoted by dark circles).

In the present study, the geometrical parameters of individual bedform i.e. length (Λ), height (Δ), crest elevation (T_c), trough elevation (T_t), and lee face slope (S_l) are evaluated from the detrended BEPs. Figure 3.41 shows the description of geometrical variables of a bedform extracted from the BEP. Where bedform length is the longitudinal distance between two consecutive crests (squares). Bedform height is the vertical distance between

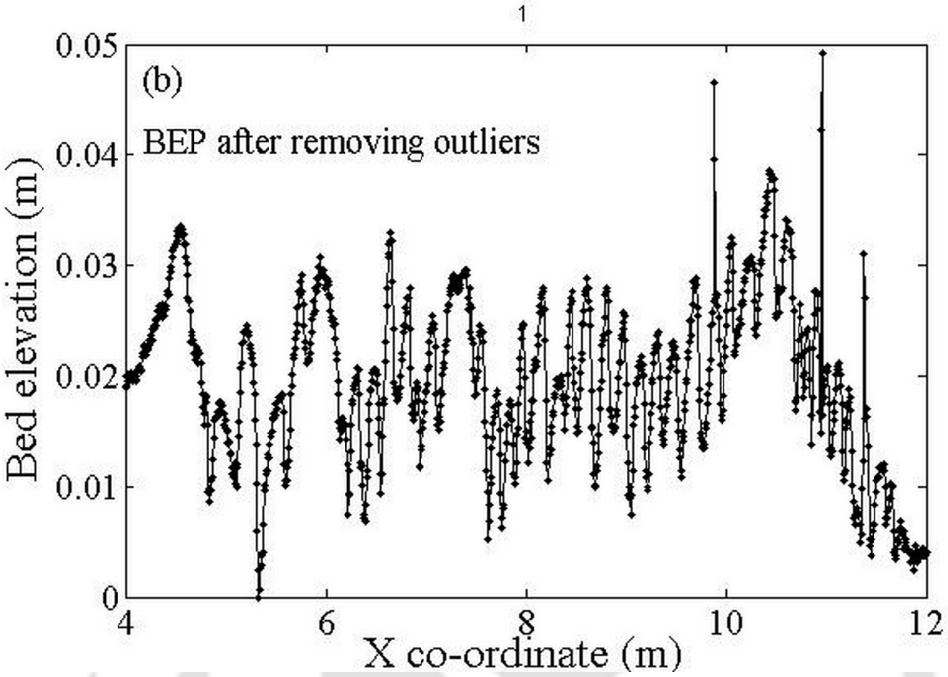

Figure 3.38: Profile of BEP after removing the outliers (c) detrended profile of BEP after fitting a linear trend line

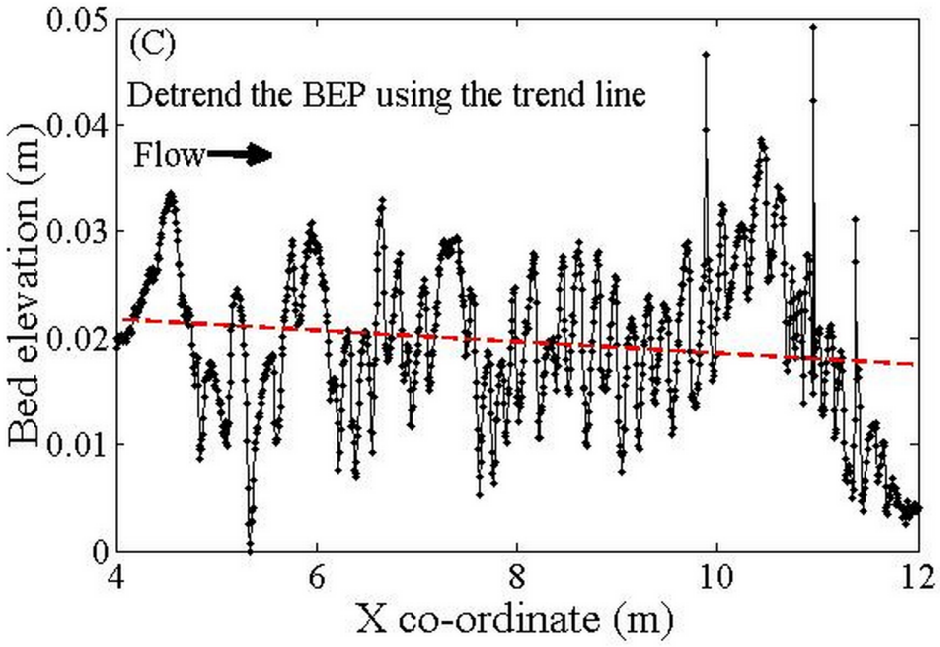

Figure 3.39: Detrended profile of BEP after fitting a linear trend line

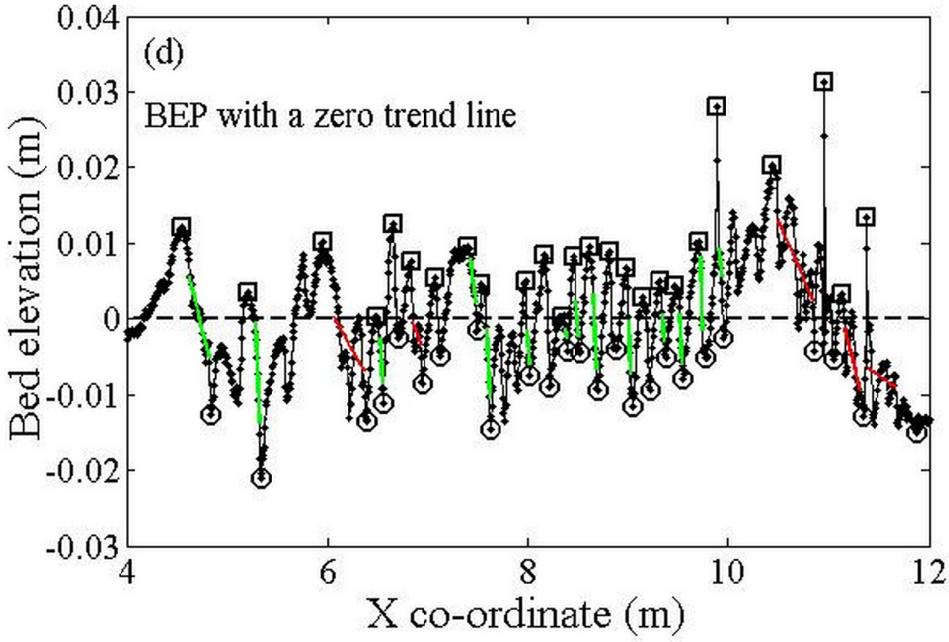

Figure 3.40: Profile of BEP with a variation about zero trend line. The flow direction is from left to right

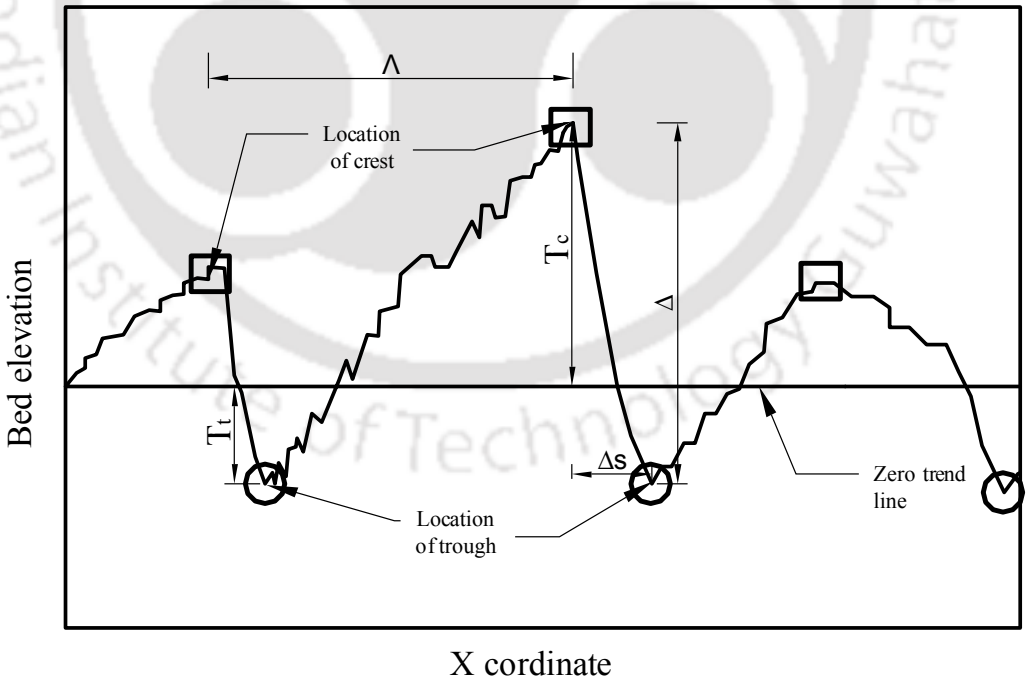

Figure 3.41: Description of geometrical variables of bedforms extracted from detrended BEPs. Where squares above the line show the locations of crest (local maxima) and circles below the line show the locations of trough (local minima)

the crest and downstream trough (circles). Crest elevation is the vertical distance from the crest to zero trend line. Trough elevation is the vertical distance from the trough to zero trend line. Lee face slope is obtained by the ratio of the vertical distance between crest and trough (i.e., bedform height, Δ) to the horizontal distance between crest and downstream trough (Δs).

3.6.2 Coefficient of Variation

In this study, mean values and standard deviations of all the geometric stochastic variables are evaluated for the data set. In order to determine the variability, coefficient of variation (C_v) for all the geometrical parameters have been caclulated. Here, C_v is the ratio of standard deviation (σ_v) to mean value (μ_v) (i.e., $C_v = \sigma_v/\mu_v$), where v is defined as the geometric stochastic variable such as bedform height (Δ) and so forth. Figures 3.42, 3.43, 3.44, 3.45, and 3.46 show a linear relation between standard deviations and mean values for some geometric variables (i.e., for bedform height, length, crest elevation, trough elevation, and lee face slope). However, linear relation for lee face slopes does not exist because of scattered data points (Figure 3.46). Standard deviations of lee face slopes vary from 0.08 to 0.26. It shows the presence of many steeper lee face bedforms, which is in accordance with the study carried out by Best and Kostaschuk (2002).

From the field study, Gabel (1993) suggested values C_Δ for the large data set varying from 0.41 to 0.53, with mean value 0.44. From the experimental studies, values of C_Δ were evaluated in the range of 0.41 to 0.51 by Wang and Shen (1980) and 0.39 to 0.48 by Leclair et al. (1997). Van der Mark et al. (2008) obtained the value of C_Δ (0.47) from a combined study of field and laboratory experiments. In the present study, the obtained value of C_Δ of about 0.44 for the bedforms height is in good agreement with the previously proposed values. In addition to this, Van der Mark et al. (2008) proposed a set of values of C_v which were 0.55, 0.57, 0.63, and 0.66 for bedform length, crest elevation, trough elevation, and lee face slope, respectively. In the present study, similar set of values of C_v for these variables (i.e., C_v for bedforms length = 0.67, for crest elevation = 0.63, for trough elevation = 0.62, and for lee face slope = 0.64) have been calculated. The coefficients of variation from present study are in good agreement for all the variables in terms of their mean values and standard deviations.

Additionally, Ostfeld (2011) have observed that the C_v of crest and trough elevations was less than 0.5 for stable natural river over fine grained sand bed, suggesting nominal

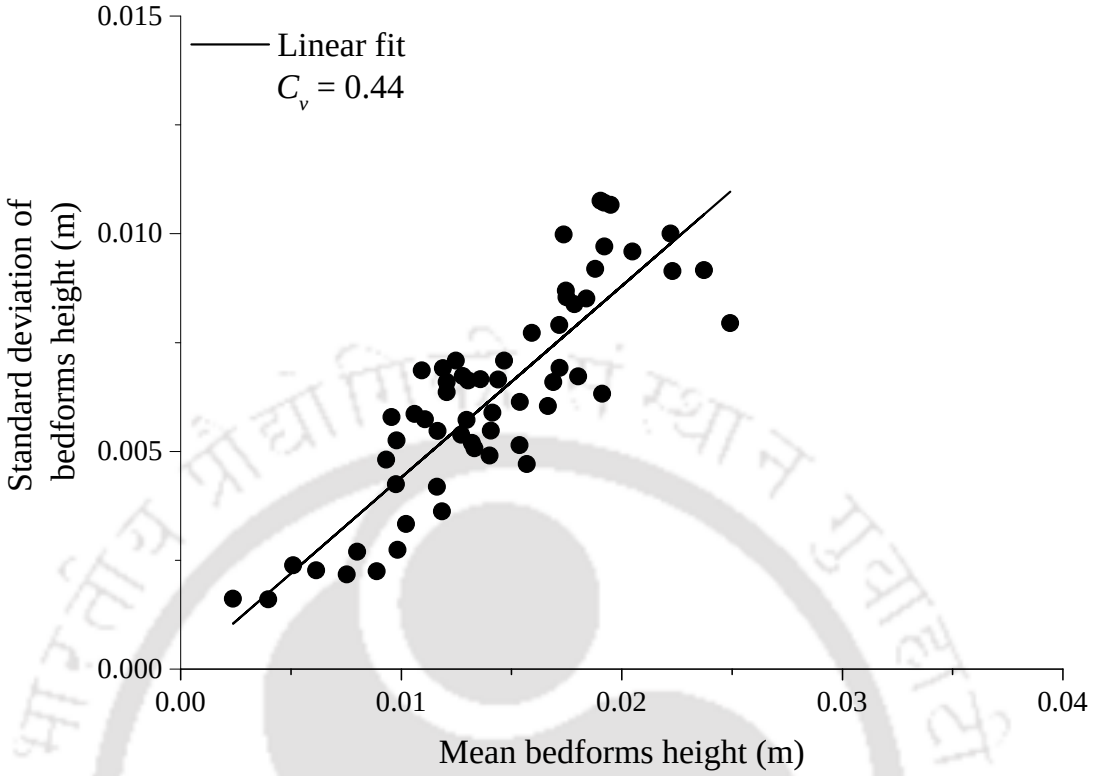

Figure 3.42: Coefficient of variation for bedform height

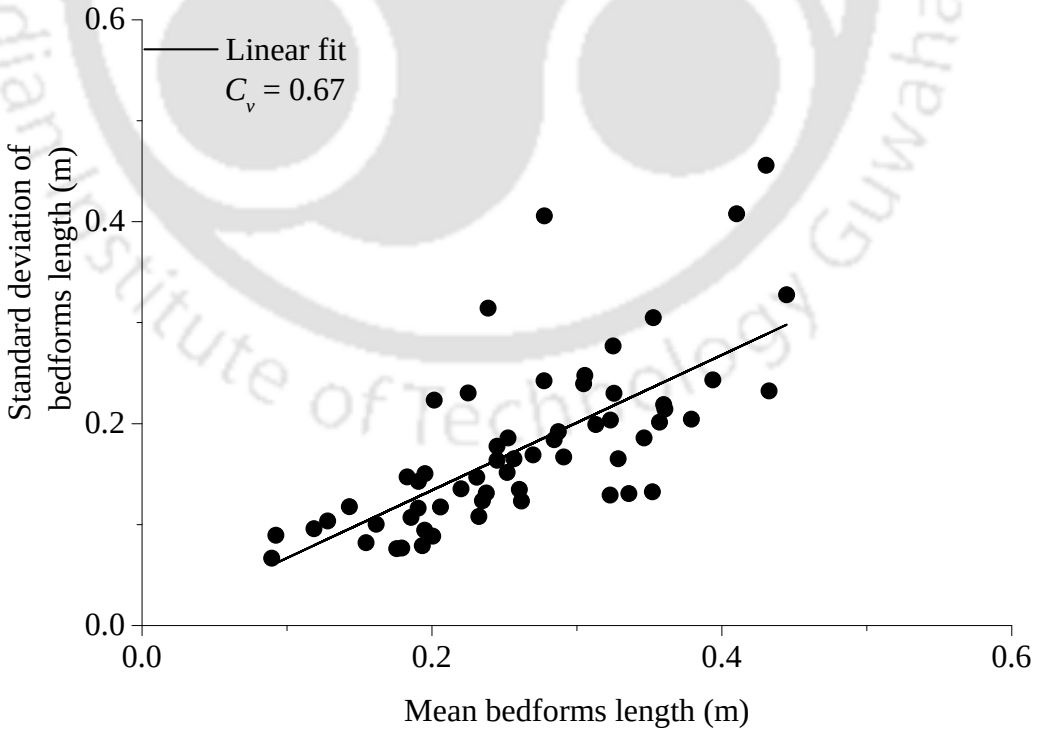

Figure 3.43: Coefficient of variation for bedform length

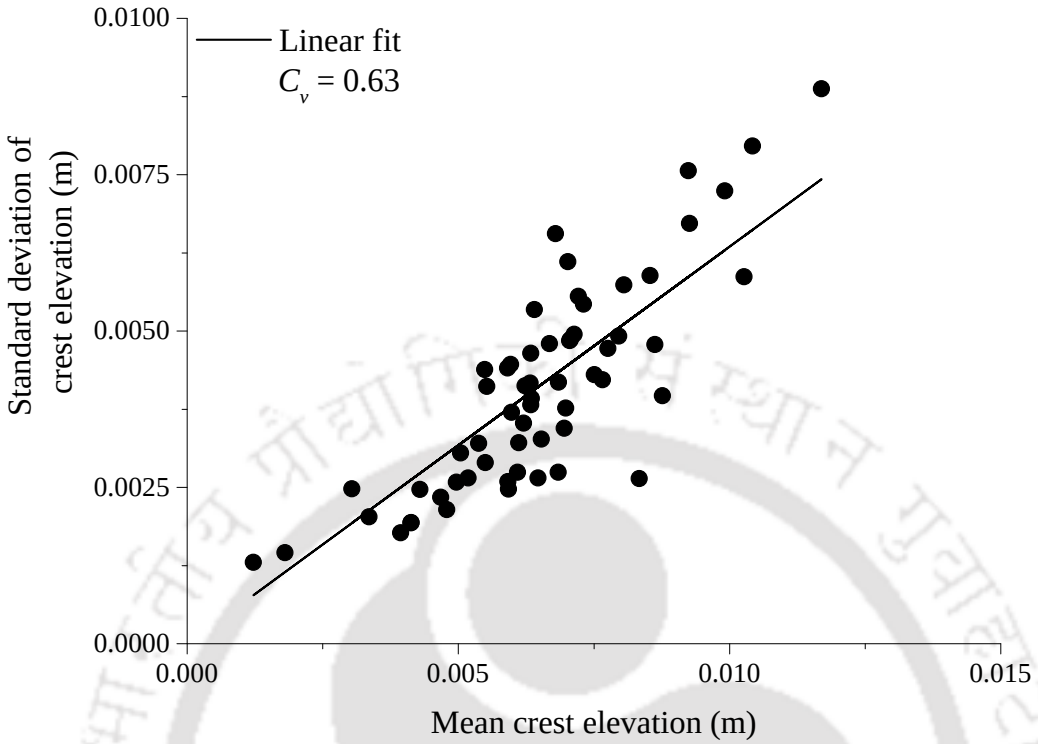

Figure 3.44: Coefficient of variation for crest elevation

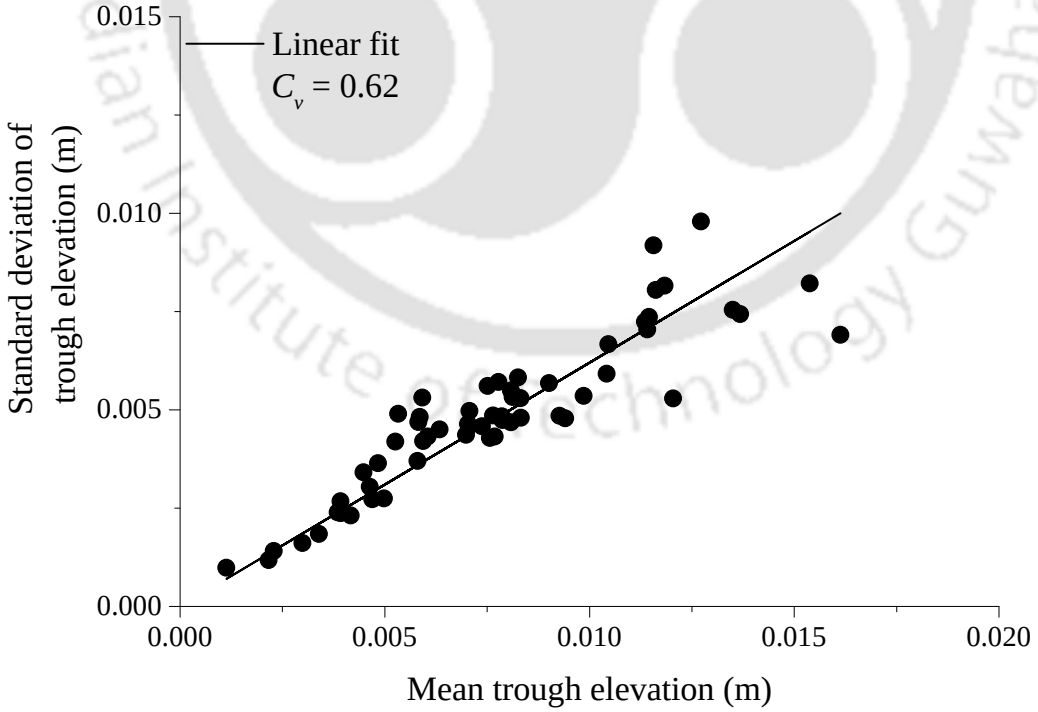

Figure 3.45: Coefficient of variation for trough elevation

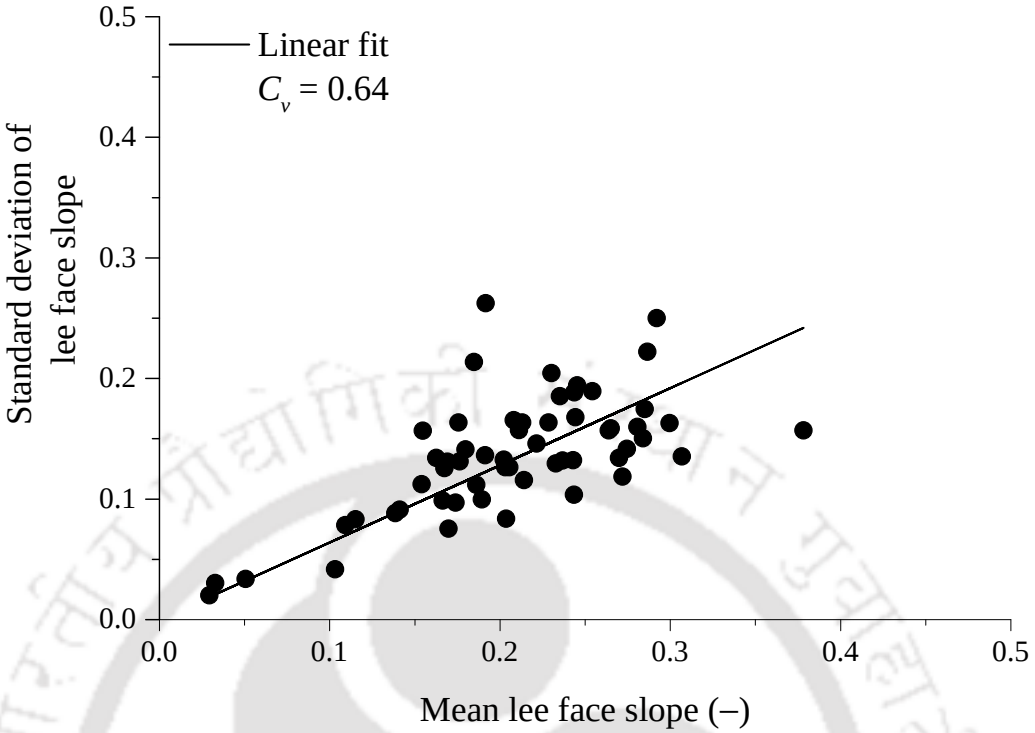

Figure 3.46: Coefficient of variation for lee face slope

dispersion of bedforms. Also, the variability of bedforms differs in accordance with the tractive stresses of flows in the longitudinal and transverse directions, which is independent from grain size (Ostfeld, 2011). In the present work, bedforms were developed because of the downward seepage and their development process was dynamic in nature, which may have different or similar variability in longitudinal and transverse directions. It reveals that the dispersion in the stochastics of bedform geometry can also vary under the influence of seepage.

Prediction of the form drag resulting because of the presence of bedforms and total resistance to flow is essential for the design and management of an alluvial channel. Estimation of the bed roughness depends on the geometry of the bedforms (i.e., size, shape, and spacing) in alluvial channels (Nelson et al., 1993; Allen, 2009). In addition to this, investigation of the variability in the bedform geometry in natural channels is of significant importance because it is essential for the modeling of the thickness of cross-strata, vertical sorting, dredging, and bed roughness (Van der Mark et al., 2008). Hence, the present work can be useful for the study of form drag, vertical sorting, dredging, and so forth.

3.6.3 Characteristics of Bedforms and Analysis

Previous researchers discussed largely about the characteristics and classification of the bedforms, which were developed in plane bed channels. Best (1992) observed ripples that were developed in the study on the sand size less than 0.7 mm, when the flow condition was hydraulically smooth throughout the experimental run (i.e., $R_* < 10$, where R_* is shear Reynolds number). In an experimental study on fine and very fine grained sands, current ripples and non-equilibrium linguoid ripples were observed by Baas (1994, 1999) Baas (1994, 1999). Current ripples have small dimensions from the geometrical point of view (i.e., average height and length are generally less than 10 mm and 0.6 m, respectively) and their development can be characterized by sediment size and shear Reynolds number (Yalin, 1976; Baas, 1994; Carling, 1999). Robert and Uhlman (2001) estimated average height of 12 mm and length of 0.13 m for current ripples and average height of 25 mm and length of 0.25 m for linguoid ripples. Present measurements of bedform dimensions (as discussed in Section 3.6.1) are compared with existing predictors. Table 3 shows the observed values of bedform dimensions (height and length) at different time intervals in the presence of seepage.

Yalin (1964) gave an equation, which is widely used to predict the current ripple (Λ) length in terms of sediment size as follows:

$$\Lambda = 1000 D_{50} \tag{3.19}$$

Later, Yalin (1985) modified the equation to predict the current ripple length as:

$$600 D_{50} \leq \Lambda \leq 2000 D_{50} \tag{3.20}$$

Recently, Soulsby et al. (2012) also proposed relations to predict the dimensions (height and length) of current ripple using dimensionless grain size (D_*) i.e. Maximum height of current ripple,

$$\Delta_{\max} = 202 d_{50} D_*^{-0.554} \tag{3.21}$$

Maximum Length of current ripple,

$$\Lambda_{\max} = \left(500 + 1881 D_*^{-3/2}\right) D_{50} \tag{3.22}$$

Where D_* can be calculated as:

$$D_* = \left[\frac{g\,(G-1)}{\nu^2}\right]^{1/3} D_{50} \tag{3.23}$$

It has been used these equations to predict the ripple length and height on the data set of present study (see Table 3.1). Ripple length is calculated as 0.410 m, 0.246-0.820 m, 0.227 m by using Equations 3.19, 3.20, and 3.21, respectively. Similarly, maximum current ripple height is calculated as 23 mm from Equation 3.21. These predicted values are in good agreement with the observed values in terms of current ripple length and height.

With the available data of temporal variation in the geometry of bedforms from the flume experiments of present study, the variation in the mean values of morphological parameters with respect to time along the center line of the test section (see Figure 3.47) has been evaluated. Figure 3.47 shows the temporal variation of Shields stress and morphological parameters of bedforms (i.e., height, length, crest elevation, and trough elevation). It can be observed from Figure 3.47 that with the increase in Shields stress under the action of downward seepage, magnitudes of other morphological parameters also increase. However, with the passage of time (from 24 h to 31 h), increase in the magnitude of Shields stress is very less (∼2% only) and accordingly the variation in corresponding morphological parameters comes to halt. This can be defined as an equilibrium state of the channel with the applied downward seepage, where no further changes were observed in the physical characteristics of the bedforms.

Table 3.1: Geometrical characteristics of bedforms at different time intervals

Time	5 (h)	10 (h)	15 (h)	24 (h)	31 (h)
Mean length (m)	0.2	0.23	0.3	0.41	0.43
Maximum length (m)	0.31	0.48	0.62	0.67	0.83
Mean height (mm)	2.38	5.11	11.65	15.01	15.7
Maximum height (mm)	5.44	14.92	19.14	30.08	30.74

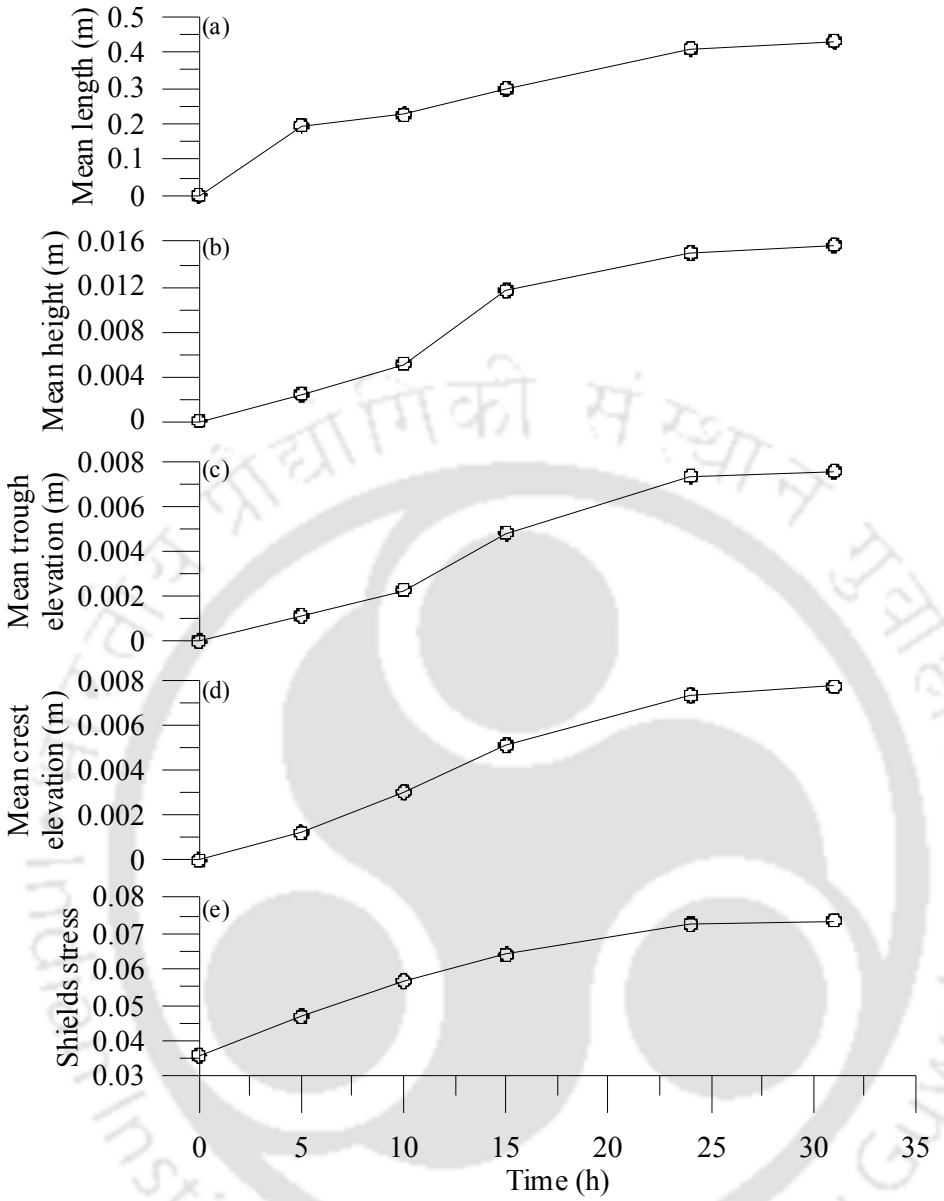

Figure 3.47: Temporal variation of Shields stress against corresponding morphological parameters at center line of the test section (a) mean bedform length (b) mean bedform height (c) trough elevation, and (d) crest elevation

3.7 Conclusions

In this work, experimental approach has been used to analyze the role of downward seepage behind the development of bedforms. In this regard, instantaneous flow velocities were measured with the help of ADV in no seepage and with seepage scenarios. Analysis of experimental observations demonstrates the changes in turbulent characteristics and geometrical features of a threshold channel under the action of downward seepage. During

experiments, it was noticed that no appreciable deformation occurred in the threshold channel at no seepage condition. Results show that with the application of downward seepage, value of Shields stress is increased from its critical value (0.037), which is responsible for the deformation of the stable shape and initiation of bedform development. In the stretch of the run from 24 to 31 h after the application of downward seepage, channel attained the stability with new cross-sectional stable shape at higher Shields stress (0.073). Following changes in turbulent flow characteristics are observed after the application of seepage:

- Velocities are increased by ∼1-4% near the bed and significant increment in RSS (∼25-40%) is observed. Increase in velocities and RSS can increase the movement of bed particle, which was in the incipient motion condition during no seepage experiment. Turbulent intensities are increased by ∼10-30%, which show the increase in the strength of turbulence and fluctuations. Such increment in near-bed velocities, RSS, and TI with downward seepage cause the increased sediment transport, consequently, development of bedforms in an otherwise threshold parabolic cross-sectional channel. The distance of the maximum value of RSS from the channel bed increases under the action of downward seepage indicating an increase in the thickness of sublayer.

- Third-order moments and TKE fluxes show that in the near-bed region, magnitudes of the positive values of moments (M_{30} and M_{30}), and streamwise TKE-Flux (F_{ku}) are increased. Also, significant increase in the magnitudes of negative values of moments (M_{12} and M_{21}), and vertical TKE-Flux (F_{kw}) are observed. These parameters support the argument of increases in sediment transport when downward seepage is applied to the threshold channel.

- Analysis of conditional RSS distributions shows that the contributions from all the events are increased, Sweep events become the largest contributor (∼89%) in the region close to the boundary, while the contribution from ejections is nearly equal to ∼70%. Consequently, the thickness of the sweep-dominated region from the wall is also increased under the action of downward seepage. Significant increase in the contribution from the sweep events corresponds to the increased sediment transport in the channel after the application of downward seepage. Further, contribution from larger event (for $H = 2$) are also increased, suggesting the development of larger eddies in the near-bed zone.

- After the application of seepage in the downward direction increase in level of turbulence in the flow has been found that is associated with higher turbulence production and decreased turbulent diffusion.
- With a longer period of seepage run (i.e., after 24 h of the application of downward seepage), change in the turbulent characteristics of the flow corresponds with the reduced sediment transport and suggests equilibrium state of the channel.

It has been observed that particles eroded from the banks were deposited at the adjacent section toward flow direction in the presence of downward seepage. This process was continued till the whole cross section was deformed and bed material migrated in the form of bedforms. In this process, it was found that the development of the current (daughter) ripples across the channel length and with the passage of time, these current ripples transformed into the linguoid ripples (larger size of bedforms).

Geometric variables of the bedforms at different time intervals, using bed elevation profiles, have been evaluated with the help of BTT. Bedforms are found to be less dispersed in terms of height but larger variability is observed for length, crest elevation, trough elevation, and lee face slope. it is compared the variability in geometric variables of bedforms, which are developed because of downward seepage, with previous study and found in good agreement. In addition, it has been observed that after a certain period of time (from 24 h to 31 h of the seepage run) variations in Shields stress and geometry of bedforms are reduced, this can be interpreted as an equilibrium state of bedform geometry in the channel with applied seepage.

"...The smaller grains remain longer in suspension, they are lifted by the inner motion of the water, while the larger grains soon settle out..."

Gotthilf Hagen
(German, 1797–1884)

4

Statistical Description of Developing Bedforms with Downward Seepage

In Chapter 3, bedforms were observed with the application of downward seepage. Further, the effect of downward seepage on the dynamic property of migrating alluvial bedforms also has a greater significance. Seepage being an integral part of alluvial flow is needed to understand the bed morphology and hydrodynamics of fluvial systems. Therefore, the influence of different percentages of seepage on the flow structure and celerity of migrating bedforms are discussed over fine sand bed in this chapter. In addition, statistical analysis is carried out to get the knowledge about bedforms develoment and their return period using probability distribution function, scale dependent statistical analysis, and power spectral density function.

4.1 Introduction

Bedforms are often developed in alluvial channels due to the complex interaction between flow turbulence, irregular sediment transport pattern, and bed material. They can vary in shape and size within a single flow system depending on the variation of bed shear stress and sediment grain size. Larger bedforms generally form under subcritical flow regime and achieve a dynamic quasi-equilibrium state under steady state flow conditions, where the change in average bedform height, length, and celerity become negligible (Coleman and Melville, 1994). However, exhaustive observations and rigorous experimental evidences in-

dicate that the equilibrium condition is characterized by uninterrupted splitting and merging of bedforms at different spatial scales (ASCE, 2002; Wilbers, 2004). This complex dynamics of bedforms is subjected to exert substantial effects on the ecological system of the river and its flow dynamics (Yarnell et al., 2006). Defina (2003) performed a numerical study on bed-features such as bars and suggested that geometry of bars and celerity are the function of each other. In addition, investigation of the morphodynamic evolution of bedforms to understand the process of splitting and merging of bedforms in different size over loose boundary channel was carried out by Jerolmack and Mohrig (2005). Recently, spectral analysis of spatial and temporal bed elevation series at multiple scales was performed to characterize the bedforms statistically (Nordin and Algert, 1966; Nikora et al., 1997; Nikora and Goring, 2001). Further, bedforms statistics was extensively carried out by Singh et al. (2011). They demonstrated that the bedform celerity decreased as a result of the increment of flow discharge and bedform dimensions. These studies have shown the presence of multi-scale dynamic properties in migrating alluvial bedforms.

4.2 Analysis of Bedforms Dynamic Characteristics

In alluvial channels, celerity shows the progradation of developing bedforms along the flow. Here, dynamic characteristics of bedforms are signified by their celerity. Alluvial bedforms show a substantial variability in propagation velocity over the range of different spatial and temporal scales. To understand the effect of downward seepage on this phenomenon, wavelet analysis has been carried out on the bed elevation series at different length scales and scale dependent celerity of bedforms has been evaluated under diverse seepage scenarios. Here, results have been presented for the for 15% and 20% seepage experiments on a bed slope 0.00116 to avoid duplicity and redundancy in the findings. Here, bed elevation series were recorded at different time intervals after 9 h, 16 h, and 21 h of seepage run using Ultrasonic Ranging System.

4.2.1 Pre-processing of Bed Elevation Series (BES)

Before performing the wavelet analysis, all the original BES (e.g., Figure 4.1a) were first de-spiked by using Fourier transformation as a filter for removing outliers (measuring errors). In this process, the spatial BES was transformed into wavenumber domain. Then the values of wavenumber, which were greater than one-eighth of the sampling resolution,

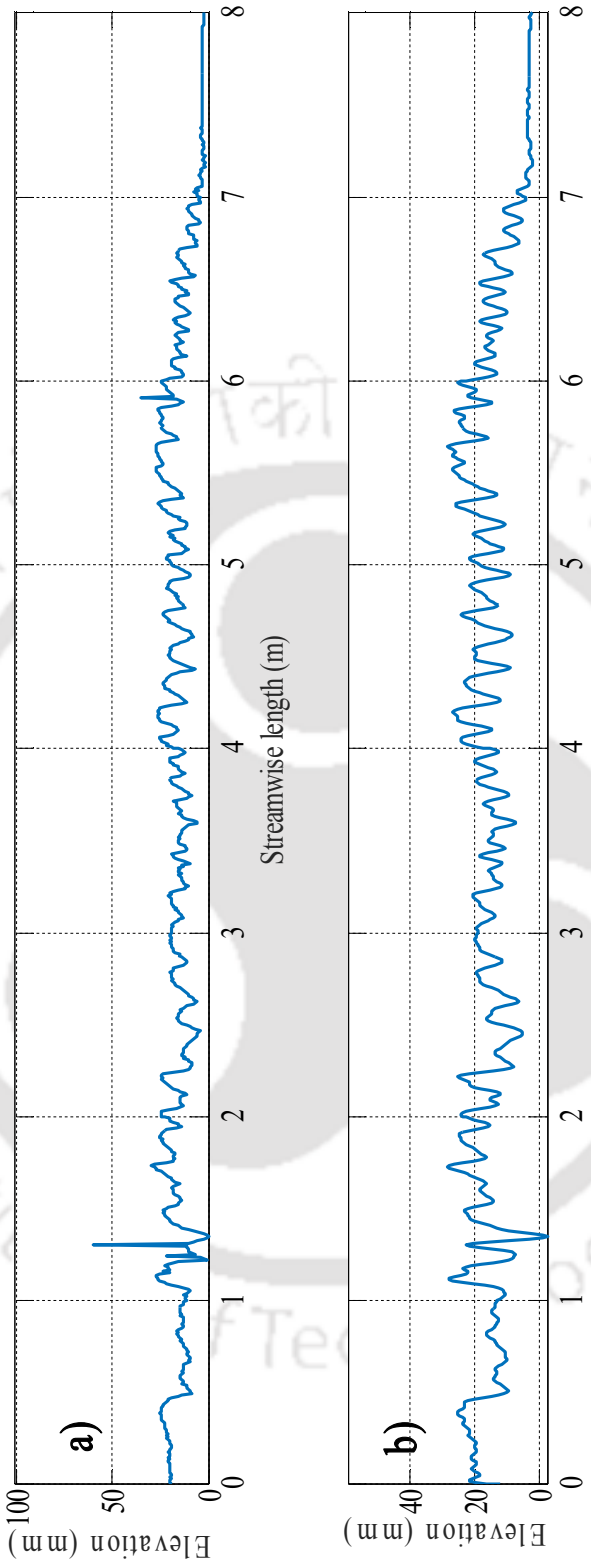

Figure 4.1: Post-processing of the bed elevation series (a) original profile and (b) reconstructed smoothened BES recorded during 15% seepage experiment. Flow direction is left to right

were removed. These removed points were then interpolated with the adjacent values. Further, after filtration, these BES were again converted into spatial domain by using inverse Fourier transformation (Figure 4.1b).

4.2.2 Wavelet Cross-Correlation

Wavelets is a proficient method in order to analyze the scale to scale correlation of bed elevation series (Kumar and Foufoula-Georgiou, 1997; Venugopal et al., 2006). It decomposes a signal into multiple signals and each signal represents the variability (energy) at a particular scale. In this method, Mexican hat wavelet was used, which is known to have optimal localization in both time and frequency domain (Singh et al., 2009). At a particular scale, wavelet coefficients signify the fluctuations in the bed elevation series. Bed elevation series at two different times is decomposed to the same length scale using wavelet transform and cross-correlation analysis is performed on the obtained sets of wavelet coefficients to obtain celerity of bedforms. Wavelet analysis has also been discussed in detail by Singh et al. (2011). In their study, time scale dependent celerity of bedforms was computed from two time series data of BES recorded simultaneously by two echo sounders, placed at a certain distance apart. These echo sounders, in their experiments, were placed at a large distance (compared to bedform dimension) from each other, which stood out as a problem in the efficient computation of celerity. However, in the present study, the data recorded was spatially varied with 7.8 mm resolution at different time spans of the experimental run. Therefore, it could be able to compute the length scale dependent celerity of the bedforms. By following this approach, it can be proposed to eliminate the error owing to the incapability of the cross-correlation method based on time series data.

In this method, wavelet coefficients of bed elevation profiles at a particular scale were considered as bed elevation fluctuations. Fluctuations (wavelet coefficients) of bed elevations at different length scales were computed using the Mexican hat wavelet as the mother wavelet, which was the second order derivative of the Gaussian function. Coefficients, at the location b and scale a, were obtained as:

$$WC_f(a,b) = \frac{1}{\sqrt{a}} \int_R \psi\left(\frac{x-b}{a}\right) f(x)\, dx \tag{4.1}$$

Where $f(x)$ is the spatially varying BES, a is defined as the scaling parameter, b is defined as the location parameter, and R is the set of real number. The factor $1/\sqrt{a}$ is scaling factor of

mother wave as discussed in earlier studies (Mallat, 1998; Kumar and Foufoula-Georgiou, 1997). Mexican hat wavelet was chosen because of the resemblance of wavelet coefficients with the original bed elevation fluctuations. Figure 4.2 shows the wavelet coefficients computed at 100 mm and 500 mm length scale for anonymous bed elevation profile after 21 h run of 15% seepage experiment. However, higher order (order 3 and 4) wavelets have also been tried to test the robustness of our choice and found no significant changes in the results.

Length scales from 100 mm to 500 mm were chosen and the elevation series were transformed with a Mexican hat wavelet at those particular scales. The reason behind choosing 100 mm as the smallest characteristic length scale and this was the limitation of our sampled dataset to capture bedforms below a characteristic length scale of 7.8 mm. This length scale was ensured to maintain reasonable accuracy for calculating the bedform celerity.

Wavelet coefficients represent bed elevation fluctuations at different characteristic length

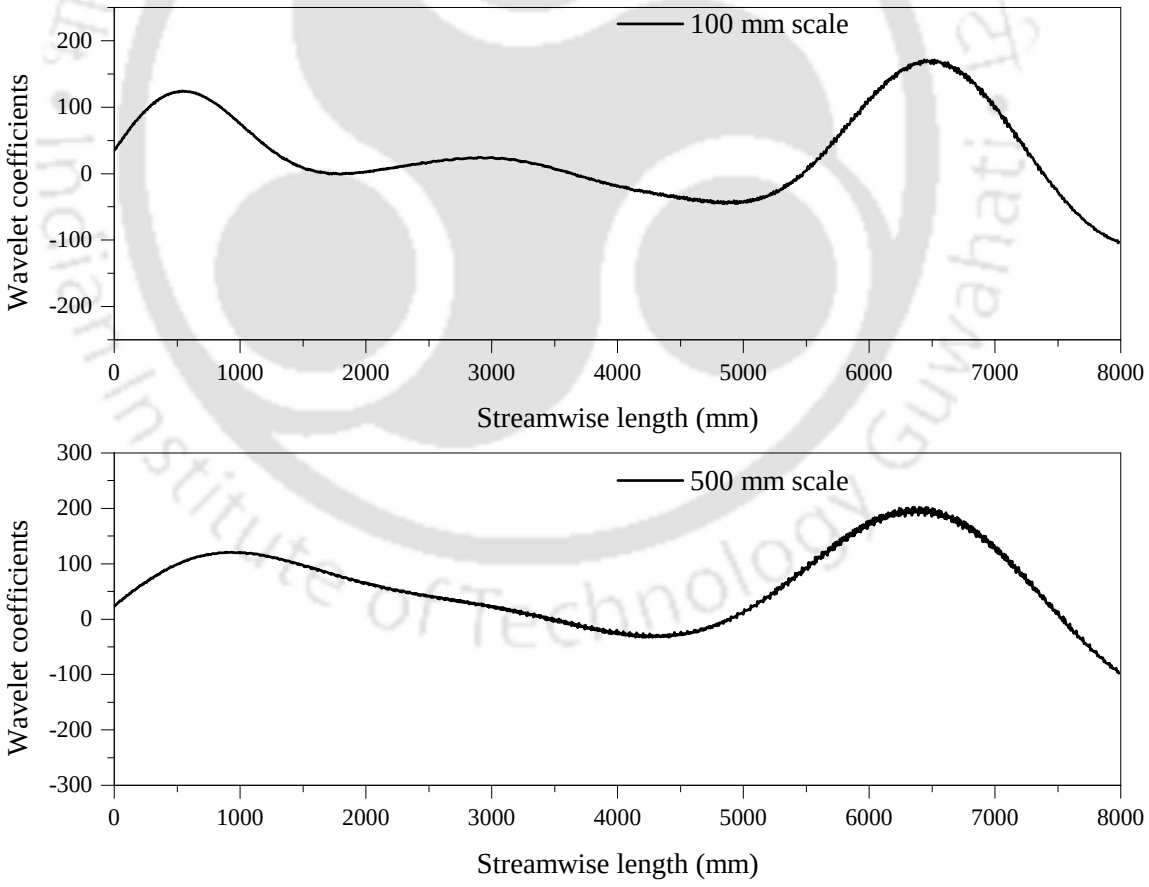

Figure 4.2: Wavelet coefficients computed at 100 mm and 500 mm length scales from the bed elevation profile after 21 h run for 15% seepage

scales. Therefore, signal has been discretized into a range of length scales instead of time scales. The wavelet cross covariance between two signals $f_1(x)$ and $f_2(x)$ can be calculated as:

$$WCC_{f_1 f_2}(a, \Delta x) = \int_{-\infty}^{+\infty} W_{f_1}(a, b)\, W_{f_2}(a, b + \Delta x)\, db \tag{4.2}$$

Where $W_{f1}(a, b)$ and $W_{f2}(a, b+\Delta x)$ are the wavelet coefficients of two BES $f_1(x)$ and $f_2(x)$, respectively, at scale a and two adjacent locations b and $b + \Delta x$, respectively. The wavelet cross -orrelation was calculated by normalizing it with the variance of the signals. For a particular scale a, the lag corresponding to the maximum cross-correlation coefficient of two series of wavelet coefficients, was obtained from the wavelet transformation of two consecutive BES. Here, one lag is equal to 7.8 mm as our datasets were sampled at a resolution of 7.8 mm. Thus, the migration velocity of bedforms (bedform celerity at particular scale) was computed by dividing the lag by the time interval between the two consecutive datasets. Celerity of the bedforms, ranging from a length scale of 100 mm to 500 mm, was calculated using wavelet cross-correlation as shown in Figure 4.3. Results show an interesting observation regarding the celerity of bedforms of the same size. Celerity of bedforms having the same length scale was observed to be lesser in the case of 20% seepage than 15% seepage experiment. It has been clearly shown that celerity of the bedforms decreases after increasing the percentage of seepage. Figure 4.3 also shows that the constancy achieved to the celerity of the larger length scales of bedforms. In this regard, bedforms size and shape govern the resistance to flow, which inhibits the further sediment transport

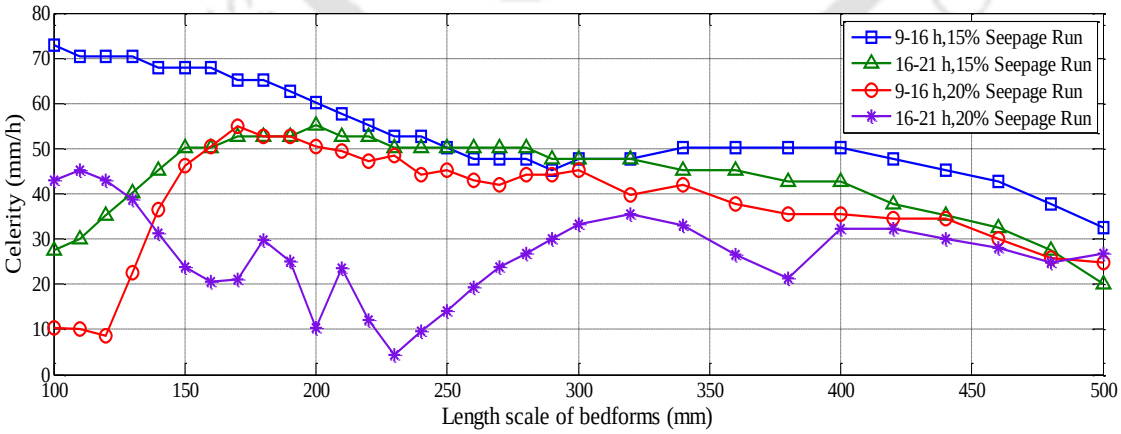

Figure 4.3: Change in the celerity of bedforms at different time intervals and percentage of seepages

Table 4.1: The statistics of the bedform celerity at different time intervals and seepages

Length scale (mm)	Celerity (mm/h)											
	15 % Seepage run						20% Seepage run					
	9-16 h	mean	std. dev.	16-21 h	mean	std. dev.	9-16 h	mean	std. dev.	16-21 h	mean	std. dev.
100	72.8			27.62			10.22			43.05		
110	70.3			30.13			10.2			45.2		
120	70.3			35.15			8.61			43.05		
130	70.3			40.18			22.6			38.74		
140	67.8			45.2			36.59			31.21		
150	67.8			50.22			46.27			23.68		
160	67.8			50.22			50.58			20.64		
170	65.3			52.73			54.88			21.02		
180	65.3			52.73			52.73			29.87		
190	62.8			52.73			52.73			25.11		
200	60.3			55.24			50.58			10.32		
210	57.8			52.73			49.5			23.67		
220	55.2			52.73			47.35			12.01		
230	52.7			50.22			48.43			4.3		
240	52.7			50.22			44.12			9.69		
250	50.2	54.2	10.7	50.22	44.2	9.1	45.2	39.3	12.6	13.99	26.4	9.9
260	47.7			50.22			43.05			19.37		
270	47.7			50.22			41.97			23.68		
280	47.7			50.22			44.12			26.9		
290	45.2			47.71			44.12			30.13		
300	47.7			47.71			45.2			33.36		
320	47.7			47.71			39.82			35.51		
340	50.2			45.2			41.97			33.11		
360	50.2			45.2			37.66			26.59		
380	50.2			42.69			35.51			21.32		
400	50.2			42.69			35.51			32.28		
420	47.7			37.66			34.44			32.28		
440	45.2			35.15			34.44			30.13		
460	42.7			32.64			30.13			27.98		
480	37.7			27.62			25.83			24.75		
500	32.6			20.09			24.75			26.9		

at large scale (Bennett, 1995). Observation suggests that the channel may have attained equilibrium in terms of sediment transport and length scale of bedforms irrespective of the seepage percentages. The statistics of the bedform celerity is given in Table 4.1.

4.2.3 Probability Distribution of Bedform Celerity

The analysis has been carried out to know, whether distributions of bedform celerity follow a particular probability density function (PDF). For each dataset, We have determined Exponential, Gamma, Normal, Log-normal, Rayleigh, and Weibull distributions of bedform celerity. In this process, mean and standard deviation values of bedform celerity have been used to obtain these distributions for the corresponding dataset.

Figure 4.4 shows the imposed probability density functions for normalized bedform celerity values at different time intervals and seepages, where, computed celerity values at different length scales were normalized by their mean values. For each distribution, we have evaluated the best approximation of the fit using relative error analysis. Relative error is defined as the absolute value of the difference between measured and imposed PDF, divided by the corresponding value of the imposed PDF i.e.

$$Relative\ Error = [PDF\ (measured)\ -\ PDF\ (imposed)]/[\ PDF\ (imposed)]$$

Relative errors for all the imposed PDFs have been determined by averaging over whole data and these values are tabulated in the Table 4.2. Here, a smallest relative error shows the best approximation of imposed PDF with the dataset. From the imposed PDFs and the relative error values, we can suggest that Rayleigh distribution provides the best approxi-

Table 4.2: Average values of relative error for best approximation of imposed PDFs for normalized bedform celerity at different time intervals and seepages.

Celerity	15% seepage		20% seepage	
Distributions	9-16 h	16-21 h	9-16 h	16-21 h
Exponential	0.63	0.19	0.40	0.74
Gamma	0.23	0.18	0.37	0.42
Lognormal	0.37	0.34	0.27	0.29
Normal	0.22	0.22	0.34	0.31
Rayleigh	**0.18**	**0.12**	**0.23**	**0.22**
Weibull	0.27	0.16	0.25	0.23

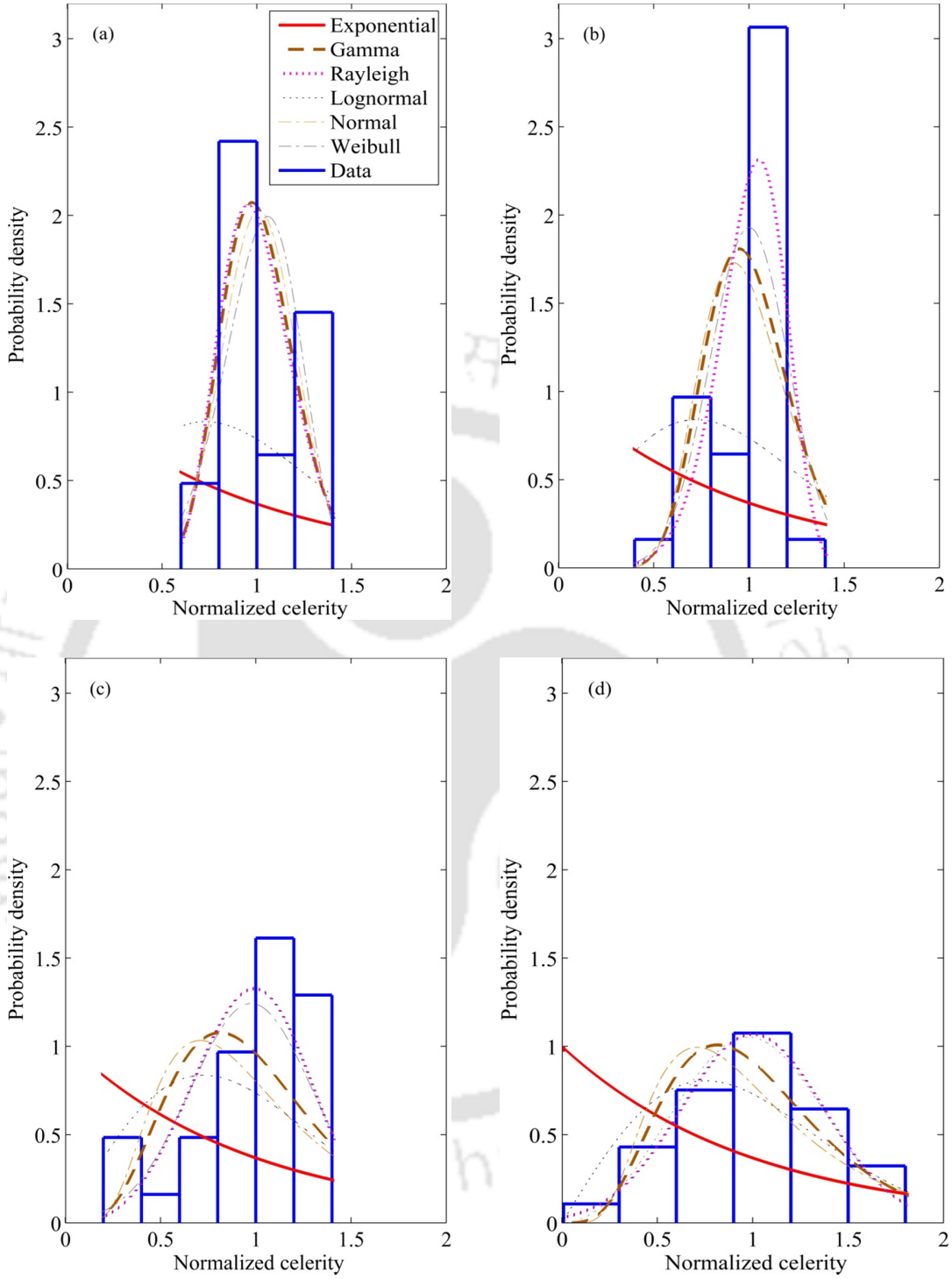

Figure 4.4: Imposed probability density functions of normalized bedform celerity for (a) 15% seepage, 9-16 h run (b) 15% seepage, 16-21 h run (c) 20% seepage, 9-16 h run (d) 20% seepage, 16-21 h run, respectively. Where normalized celerity is defined as the celerity values divided by their mean values of the dataset

mation of the probabilistic behavior of celerity of bedforms for both the seepage cases.

4.2.4 Tail Behaviour of Bedform Celerity

In the previous section, this is obvious from the visual inspection of the graphs that the body of the dataset of bedform celerity can be fitted with different distributions, while the tails of the PDFs deviate significantly. Therefore, analysis has been performed to gather an adequate knowledge about the variation of tails of the PDF. Besides, tails of the PDF signify the asymmetry between the PDFs of bedform celerity at different seepage percentages. The fit of distribution of the tails with truncated Pareto distribution can be used to obtain the asymmetry amongst different size of bedforms. This fit is a commonly used distribution for quantities showing exponentially decaying tails and a physically imposed upper bound that differentiates the tail from the rest of the PDF.

The distribution is given as:

$$f(x) = \frac{\alpha \gamma^{\alpha} x^{-\alpha-1}}{1-(\gamma/\nu)^{\alpha}}; \tag{4.3}$$

Probability of exceedance for this distribution is obtained by:

$$P(X > x) = \frac{\gamma^{\alpha}\left(x^{-\alpha} - \nu^{-\alpha}\right)}{1-(\gamma/\nu)^{\alpha}}; \tag{4.4}$$

Here, α is the tail index, γ is the lower bound, and ν is the truncation parameter or the upper bound of the random variable X. Aban et al. (2006) proposed the method to estimate the parameters of the truncated Pareto distribution. In this method, conditional Maximum Likelihood Estimation was used to determine the parameters. Here, it has been assumed for a random sample $X(X_1, X_2, .., X_N), X_{(1)} > X_{(2)} > .. > X_{(N)}$. Also, this method is based on the $(r+1)^{th}$ largest order statistics, which is given as:

$$\hat{\nu} = X_{(1)}, \hat{\gamma} = r^{\frac{1}{\hat{\alpha}}}(X_{(r+1)})[n-(n-r)(X_{(r+1)}/X_{(1)})^{\hat{\alpha}}]^{-1/\hat{\alpha}} \tag{4.5}$$

and $\hat{\alpha}$ is obtained by solving the following equation:

$$\frac{r}{\hat{\alpha}} + \frac{r(X_{(r+1)}/X_{(1)})^{\hat{\alpha}} \ln(X_{(r+1)}/X_{(1)})}{1-(X_{(r+1)}/X_{(1)})^{\hat{\alpha}}} = \sum_{i=1}^{r}\left[\ln X_{(i)} - \ln X_{(r+1)}\right] \tag{4.6}$$

In this case, the upper and lower bounds are the largest and smallest bedform celerity,

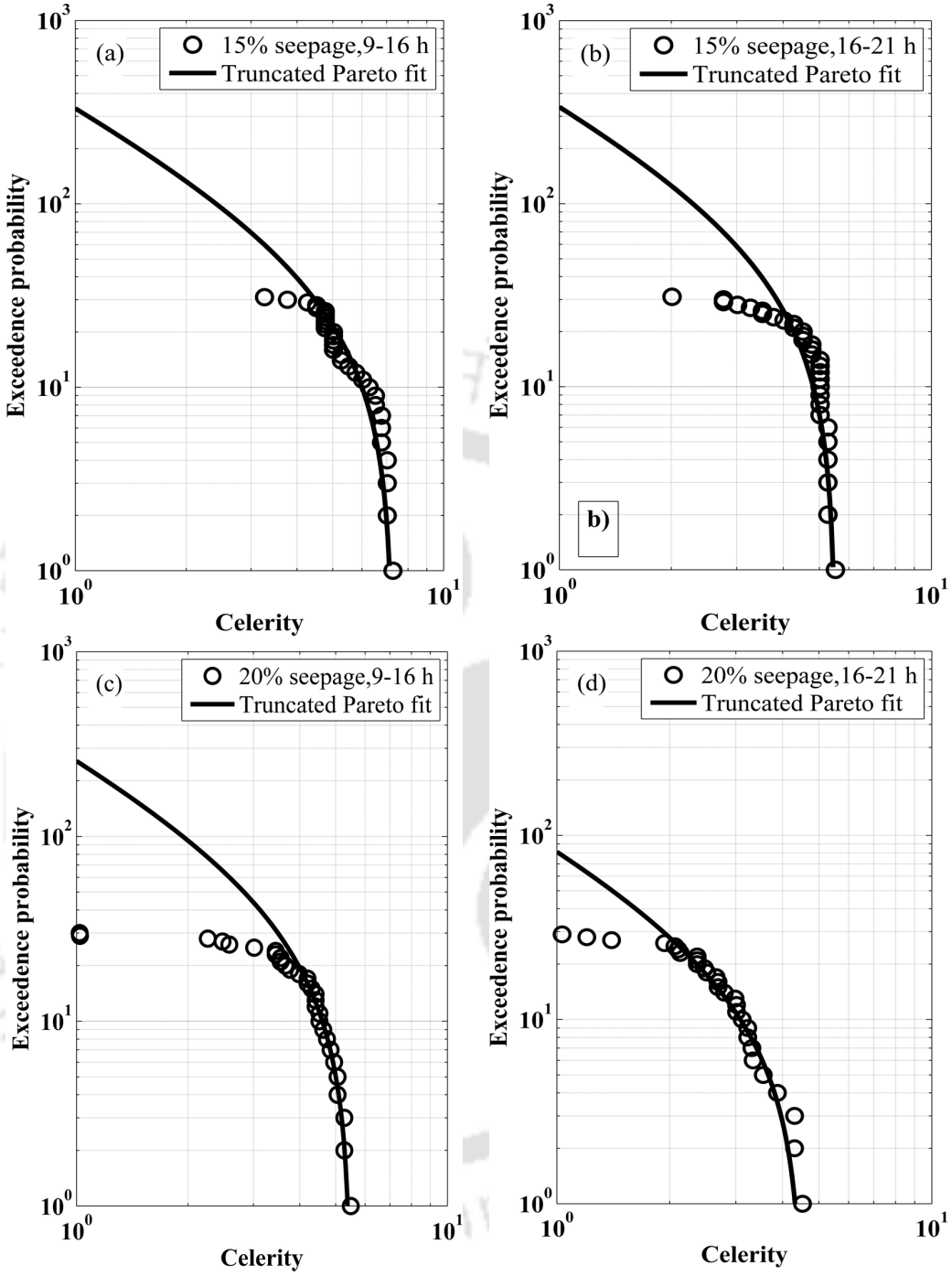

Figure 4.5: Truncated Pareto distribution fitted to celerity data obtained at different time interval and different percentage of seepage (a) and (b) correspond to the data obtained between 9-16 h and 16-21 h with 15% seepage, and (c) and (d) correspond to the data obtained between the same time frame with 20% seepage

respectively. The highest computed celerity signifies the movement of the smallest bedforms. Whereas, the smallest celerity indicates the propagation of the largest bedform that

Table 4.3: Parameters of truncated Pareto distribution

Seepage %	Time (h)	Lower bound (γ)	Upper bound (ν)	Tail index (α)
15	9-16	0.17	7.28	1.12
	16-21	0.08	5.52	1.09
20	9-16	0.07	5.49	1.08
	16-21	0.18	4.52	1.07

gradually arises because of merging of smaller bedforms.

As there is no other method to examine the truncated Pareto distribution then the visual observation of the fitted PDF has been made that shows truncated Pareto distribution is the best fit for the dataset of both seepage experiments (Figure 4.5). It can also be differentiated the tail characteristics of the PDFs by comparing the tail indexes (α) of the fitted Truncated Pareto distributions as given in Table 4.3. A lower value of tail index signifies a heavier tail. From the Table 4.3, it can be observed that the values of tail index decrease in accordance with the increase in seepage percentage. This suggests that the higher seepage discharge leads to a heavier tail of the bedform celerity PDF. Heavier tail distribution indicates a high probability to find one or more large values in the dataset. Interestingly, in the present study, the celerity of bedforms decreases and tail of PDF of celerity tends to get heavier by increasing percentage of downward seepage, where heavier tail quantifies the large asymmetry between the PDFs of bedform celerity. This may occur from the alteration of the fluvial mechanisms such as grain sorting, erosion, and transportation or deposition of sediment particles because of increased percentage of seepage. Consequently, this can cause an increase in the variability of bed geometry, which may lead to unpredictable migration patterns of bedforms.

4.3 Quantification of Bedforms

In this study, bedforms were observed after applying downward seepage and bed elevation profiles were recorded in the longitudinal (along the flow) direction with the help of transducers at different time intervals. To evaluate the physical characteristics of bedforms, longitudinal bed elevation profiles were detrended with the help of bedform tracking tool (BTT). A BTT, as proposed by Van der Mark et al. (2008), was used to extract the physical characteristics of bedforms such as length and height. Table 4.4 shows the calculated average values of length and height of bedforms at different time intervals for 15% seepage and

Table 4.4: A summary of physical characteristics of bedforms

Time (h)	Average bedform height (m)		Average bedform length(m)	
	15 % seepage	20 % seepage	15 % seepage	20 % seepage
9	0.0121	0.0162	0.281	0.267
16	0.0105	0.0238	0.331	0.323
21	0.0111	0.0261	0.330	0.392

20% seepage experiments. Where, bedform length (height) is the longitudinal (vertical) distance between two consecutive crests (trough). From Table 4.4, it can be observed that after the commencement of downward seepage, the height of bedforms is greater for 20% seepage run as compared to 15% seepage experiment. In the beginning of experiments (9-16 h), the lengths of bedforms are comparatively similar for both the seepage experiments. However, with the passage of time (after 21 h) dimensions of bedforms are increased for the higher percentage of seepage (20%). Interestingly, the size of the bedforms is increased according to eddy length and eddy turnover time as seepage percentage increases from 15% to 20%. These observations suggest that physical characteristics of bedforms varied by increasing an amount of seepage.

In general, two (three) dimensional bedforms show a similar (dissimilar) pattern in alluvial channels. In the present work, visual observations of bedforms indicate dissimilar pattern in the beginning of seepage runs (after 9 h run) and similar pattern at the end of seepage run (after $21 - 31$ h run). Bedforms dimensions and their statistics are evaluated after 9 h and 21 h run for 15% and 20% of seepage with the help of BTT as given in Table 4.5 and Table 4.6, respectively. Where the prefixes 'avg' and 'std' define the average value and standard deviation of bedform dimension, respectively.

Further, it has been observed that in all the cases, largest bedforms showed a length scale of order 500 mm. To analyze the effect of seepage on the bedform dimensions, average length and height of bedforms were calculated at different time intervals for 15% and 20% seepage experiments, which are presented in Table 4.5 and Table 4.6. After 9 h of the commencement of seepage, size of bedforms was lesser for 20% seepage experiment as compared to 15% seepage experiment. However, after 21 h, size of bedforms was significantly increased for higher percentage of seepage (20%). The observations suggest that the higher seepage discharge affects the characteristics of bedforms.

Figure 4.6 shows the cumulative distribution function of bedforms geometry after 9 h

Table 4.5: A summary of physical characteristics of bedforms after 9 h with seepage run

Seepage%	15% seepage						20% seepage					
Time (h)	Length (cm)	Height (cm)	Avg. (length)	Std. (length)	Avg. (height)	Std. (height)	Length (cm)	Height (cm)	Avg. (length)	Std. (length)	Avg. (height)	Std. (height)
	33.52	1.67					15.82	1.27				
	16.71	2.72					14.96	1.22				
	5.72	0.91					18.76	1.25				
	31.73	0.41					35.47	3.6				
	19.17	1.57					16.54	0.91				
	48.01	1.36					6.35	0.38				
	17.37	2.01					18.53	5.6				
	22.88	0.87					26.39	2.19				
	28.3	0.65					15.73	1.38				
	27.53	1.05					28.5	1.28				
	11.13	1.27					25.23	1.94				
	9.82	0.81					12.03	1.06				
	10.75	0.78					12.02	1.39				
	29.23	0.82					41.21	1.82				
	17.99	1.51					27.63	1.7				
9	19.48	1.68	28.10	24.4	1.21	0.49	13.74	1.19	26.70	12.8	1.62	0.96
	13.33	1.3					14.37	1.72				
	18.18	1.11					32.29	1.56				
	13.35	1.24					12.58	1				
	13.22	1.15					38.64	1.97				
	15.78	0.95					21.74	2.15				
	9.63	1.75					14.57	0.91				
	13.27	0.77					32.04	1.58				
	22.58	1.29					33.74	1.85				
	–	1.45					9.77	1.14				
	–	1.45					12.65	1.04				
	–	–					11.58	0.73				
	–	–					32.52	1.43				
	–	–					16.54	1.05				
	–	–					–	2.16				

Table 4.6: A summary of physical characteristics of bedforms after 21 h of seepage run

seepage %	15% seepage						20% seepage					
time (h)	Length (cm)	Height (cm)	Avg. (length)	Std. (length)	Avg. (height)	Std. (height)	Length (cm)	Height (cm)	Avg. (length)	Std. (length)	Avg. (height)	Std. (height)
	59.07	2.19					75.77	6.34				
	51.82	2.35					28.68	6.91				
	91.4	2.17					47.64	3.49				
	15.37	1.28					29.98	3.93				
	27.08	1.37					17.29	2.37	39.20	39.22	2.61	1.95
	15.61	0.91					25.6	1.94				
	33.52	1.01					9.35	2.48				
	43.57	1.73					54.96	1.23				
	13.56	1.05					28.46	4.13				
	22.97	1.57					24.81	3.77				
	9.94	0.46					72.81	2.48				
21	13.62	1.08	33.00	32.41	1.11	0.53	68.3	3.31				
	20.37	1.59					–	7.49				
	17.48	1.12					–	–				
	18.39	1.58					–	–				
	15.79	1.16					–	–				
	15.55	1.03					–	–				
	17.48	1.1					–	–				
	22.23	1.33					–	–				
	67.77	2.44					–	–				
	28.04	1.48					–	–				
	–	2.18					–	–				

and 21 h of seepage run. Average bedform's heights and lengths were normalized by subtracting their average values and dividing them by their standard deviations ($H' = \left[h_b - \overline{avg(h_b)}\right]/\overline{std(h_b)}$ and $L' = \left[l_b - \overline{avg(l_b)}\right]/\overline{std(l_b)}$). Where, $\overline{avg}$ of h_b or l_b (height or length) is obtained by the average values of bedform heights or lengths for 15% and 20% seepage runs at any particular time. It can be observed from Figure 4.6 that after 9 h of seepage run, both the cumulative distribution of bedform heights and lengths followed the Gaussian distribution closely, whereas, after 21 h of seepage run, they seem to deviate from the Gaussian distribution. Additionally, it was found that the cumulative distribution of bedforms height changes in shape for 15% and 20% seepage run. Positive tails for 20% seepage are larger than that observed for 15% seepage.

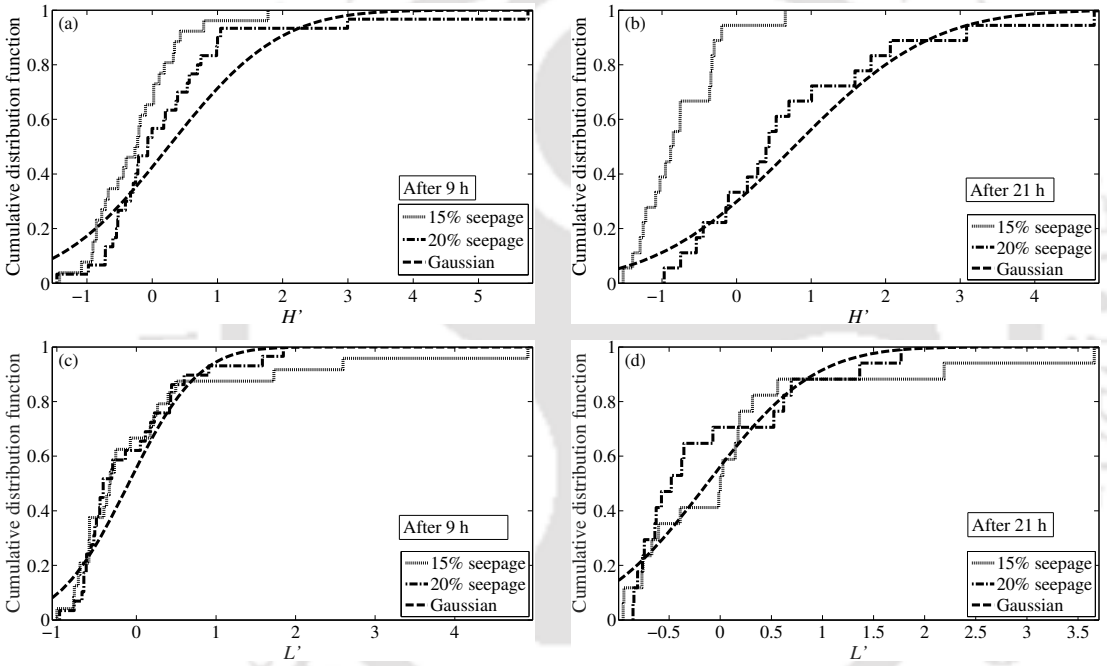

Figure 4.6: Curve of cumulative distribution functions (CDF) (a) and (b) denote the CDF of bedform heights for 9 h and 21 h runs for both the seepage experiments and (c) and (d) denote the CDF of bedform lengths for 9 h and 21 h runs for both the seepage experiments, respectively. Average height, average length and their standard deviations have been averaged for 15% and 20% seepage experiments.

Figures 4.7 and 4.8 show the probability density function (PDF) of bedforms characteristics in terms of height and length after 9 h and 21 h for both the seepage runs. Bedform's height and length were normalized by their average values to plot the PDF. It can be observed from Figures 4.7 and 4.8 that the PDF follows Gamma distribution rather than Gaussian and Weibull distribution for different percentages of seepage run. Van der Mark et

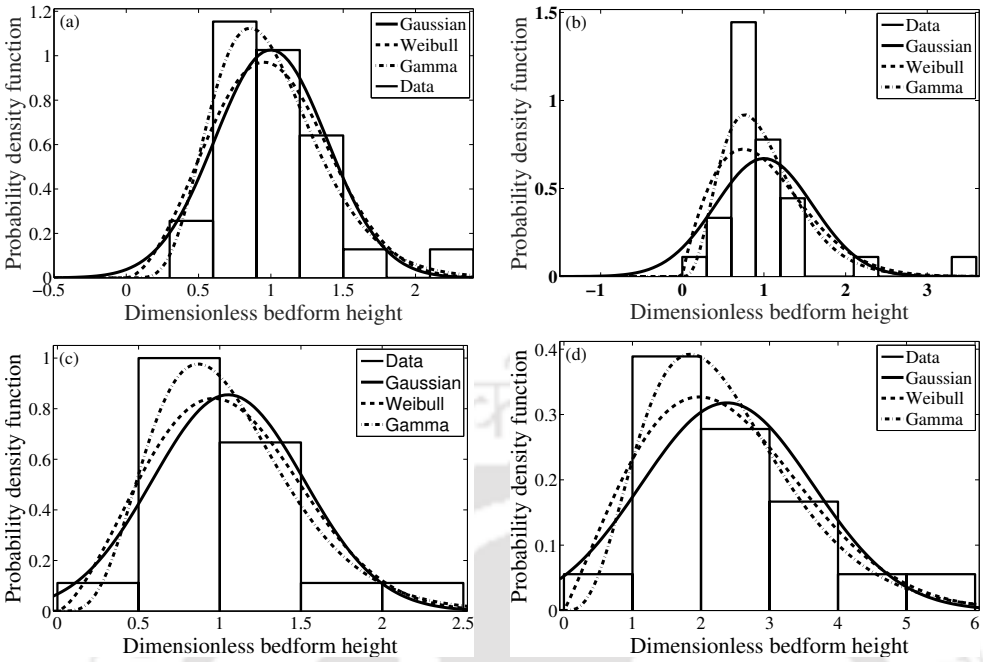

Figure 4.7: Probability density functions of dimensionless bedform heights (a) and (c) after 9 h and 21 h runs for 15% seepage (b) and (d) after 9 h and 21 h runs for 20% seepage, respectively.

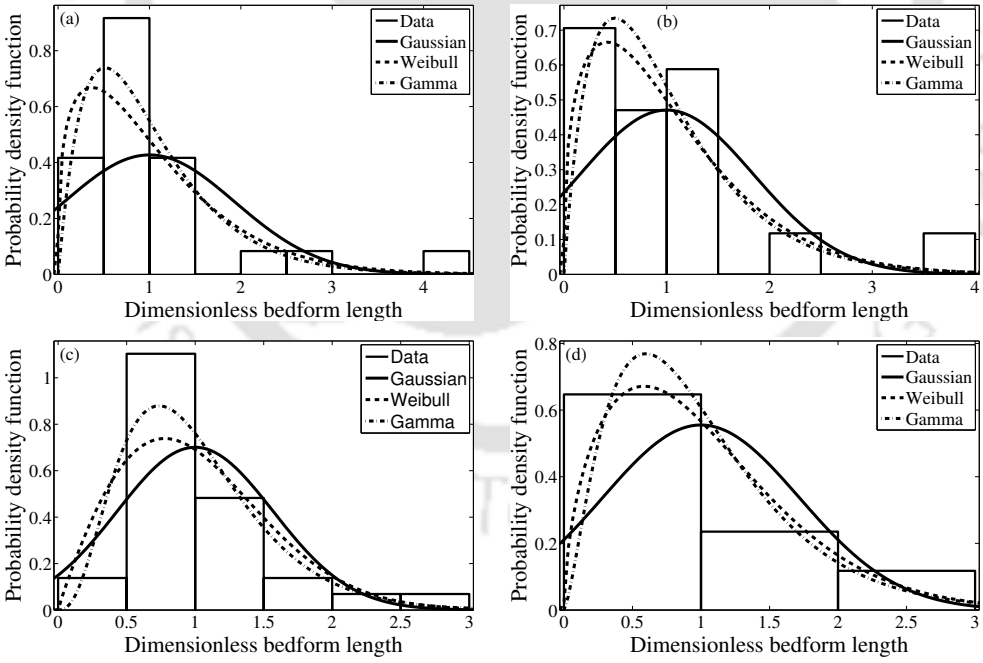

Figure 4.8: Probability density functions of dimensionless bedform lengths (a) and (c) after 9 h and 21 h run for 15% seepage (b) and (d) after 9 h and 21 h run for 20% seepage, respectively.

al. Van der Mark et al. (2008) also observed that Gamma, Gaussian, and Weibull distribution give adequate approximation in analysis of bedforms geometry for field and laboratory data. Therefore, it can be recommended Gamma distribution for developing and stable bedforms geometries in the presence of seepage.

4.4 Scale Dependent Statistical Analysis of Bed Elevation Increments

For quantifying the effect of seepage on the bed elevation profiles as well as local fluctuations, multi scale statistical analysis has been carried out. In this analysis, wavelet coefficients, derived from Mexican hat wavelet as mother wavelet, at different length scales are used. Where, the wavelet coefficients at a particular length scale show the fluctuations of bed elevation. At length scale a, q^{th} order statistical moments of the absolute values of the increments can be obtained as:

$$M(q,a) = \frac{1}{N} \times \sum_{i=1}^{N} |dh(x,a)|^q \tag{4.7}$$

where N is the number of data points of the bed elevation series at scale a. The term $M(q, a)$ is defined as the structure function or statistical moments. The statistical moments for all q values completely depict the shape of the probability density function of the bed elevation increments at scale a. Scale invariance ensured that it varies with the following power law with scale a

$$M\,(q,a) \sim\ a^{\tau(q)} \tag{4.8}$$

where $\tau(q)$ represent the scaling exponent function. In general, $\tau(q)$ follows a nonlinear relationship with q. Therefore, the following quadratic equation is used to evaluate the $\tau(q)$

$$\tau(q) = c_1 \times q - \left(\frac{c_2}{2}\right) \times q^2 \tag{4.9}$$

where c_1 and c_2 are defined as average roughness of the wave series and intermittency parameter, respectively. The parameters (c_1 and c_2) signify the variations in probability distribution function of bed elevation increment over a range of length scales. From following geometrical interpretation of the statistical scaling (Frisch, 1995; Venugopal et al., 2006), the parameter c_2 is related to the local roughness or degree of differentiability of the bed elevation signal. A non-zero value of c_2 symbolizes a temporally non-stationary or spatially

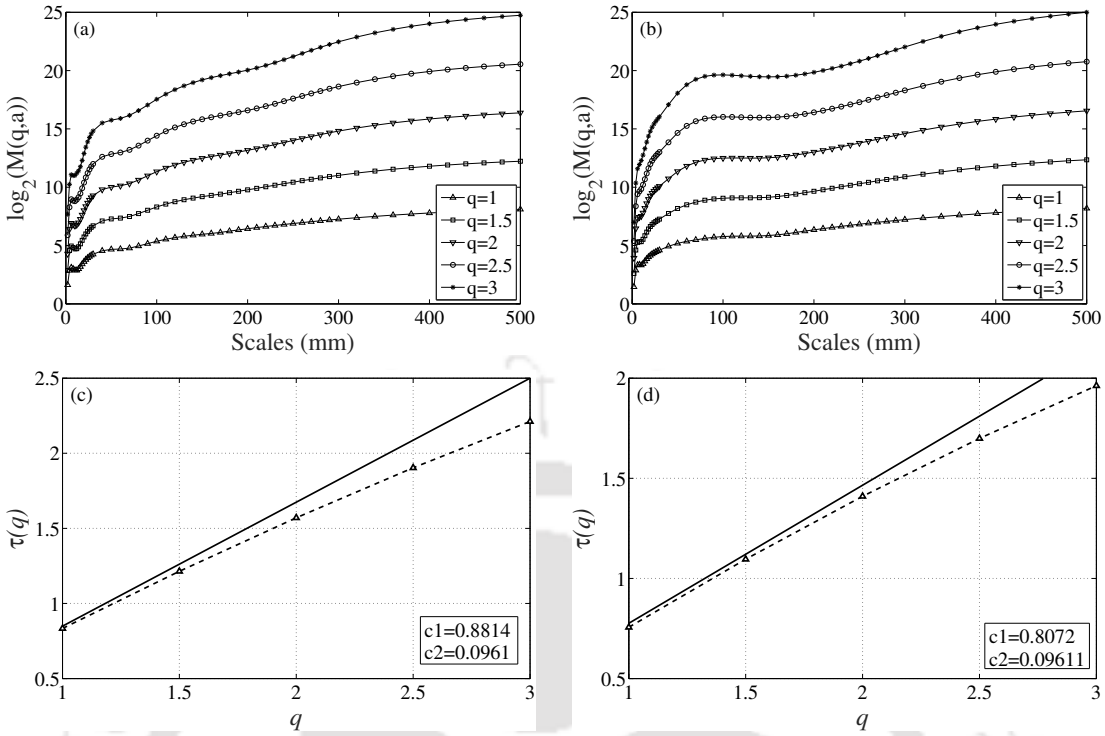

Figure 4.9: Variation of statistical moments of the bed elevation increments as a function of length scale (a) after 9 h run for 15% seepage and (b) after 21 h run for 15% seepage. Changes in scaling exponent $\tau(q)$ obtained from the log-log linear regression within the scaling regime (c) after 9 h run for 15% seepage and (d) after 21 h run for 15% seepage.

inhomogeneous arrangement of spikes or abrupt changes along the channel. In this study, structure function has been analyzed on the bed elevation spatial series after 9 h and 21 h run for both the seepage amounts (15% and 20%). Figures 4.9(a) and 4.9(b) show the scaling of the statistical moments of the bed elevation variations $dh(x,a)$ as a function of scale a after 9 h run and 21 h run, respectively for 15% seepage. These moments are plotted offset vertically (along the y-axis) to get better visualization. Figures 4.9(c) and 4.9(d) show the $\tau(q)$ curves obtained from the slopes of the statistical moments within the scaling range for 15% seepage. Similar explanations hold true for Figures 4.10(a-d) for 20% seepage. From Figures 4.9 and 4.10, it can be observed that the structure function follows power law in the scaling range from approximately 50 mm to 400 mm for both the seepage experiments. Additionally, the $\tau(q)$ curves have exhibit a nonlinear relationship with q, indicating the presence of multifractality in both of the seepage experiments. The value of the intermittency parameter c_2 is higher for 20% seepage experiment than the value obtained for 15% seepage experiment after the 9 h run. This suggests that after increasing the seepage discharge more inhomogeneous arrangement of abrupt bed elevation fluctuations was found

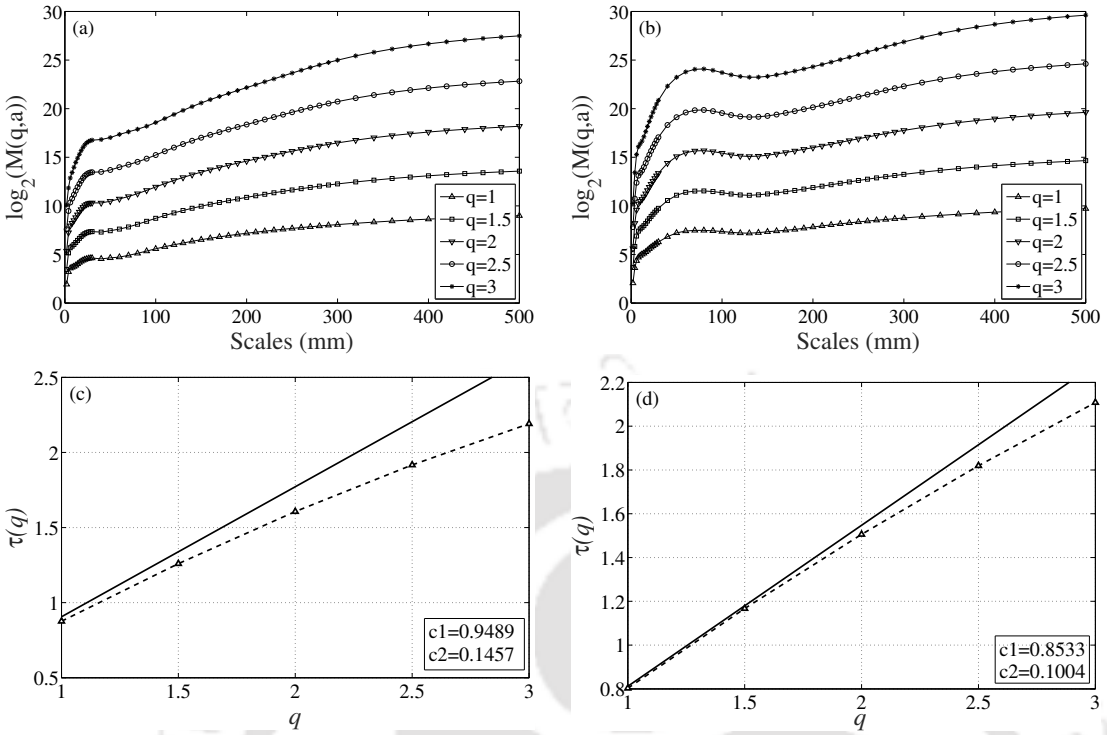

Figure 4.10: Variation of statistical moments of the bed elevation increments as a function of length scale (a) after 9 h run for 20% seepage and (b) after 21 h run for 20% seepage. Changes in scaling exponent $\tau(q)$ obtained from the log-log linear regression within the scaling regime (c) after 9 h run for 20% seepage and (d) after 21 h run for 20% seepage.

during developing bedforms (after 9 h run). While, the value of c_2 is nearby equal after 21 h run for both the seepage discharges, indicating bedforms arrangements achieve an equilibrium state after longer period of the seepage runs. In addition, the parameter c_1 defines the characteristics of the bed elevation fluctuation, in which greater value corresponds to smoother bed elevation. From the present study, it can be observed that the value of c_1 is higher after 9 h as compared with 21 h run for both the seepage discharges. This suggests that the bed elevation fluctuation is smooth in the beginning (after 9 h run) of seepage run. However, value of c_1 increases with the passage of time (after 21 h run), implying an increase of bed elevation fluctuation because of greater variability in bedforms dimensions. Therefore, the results show larger bed roughness on the channel bed at the end of seepage experiments.

4.5 Probability Distribution Function (pdf) of Dimensionalized Bed Elevation Increments as a Function of Scale

In the previous study, Wong et al. (2007) suggested that mean-removed bed elevations in plain bed channel shows nearly Gaussian distribution. For understating the patterns of bed elevation series in the case of different percentage of seepage, pdf of bed elevation fluctuations is analyzed. Figure 4.11 shows the semi-log pdfs of the bed elevation increments for 15% and 20% seepage experiments after 9 h run and 21 h run, respectively. Careful observations of Figure 4.11 reveal that the pdfs at different scales are asymmetric to each other. As the scale is increased, the width of the pdfs increases and they become more skewed to the right signifying a higher probability of occurrence of higher positive bed elevation fluctuations or increments. The pdfs also show a significant increase in width with an increase in seepage amount, suggesting larger elevation fluctuations or larger bedforms under the influence of increased seepage amount. It is very important to note that earlier in the structure function analysis; it has been seen that the value of the roughness parameter increases with the increment in seepage discharge. Further, pdf of bed elevation increments is normalized to understand the variations adequately for both the seepage discharges as

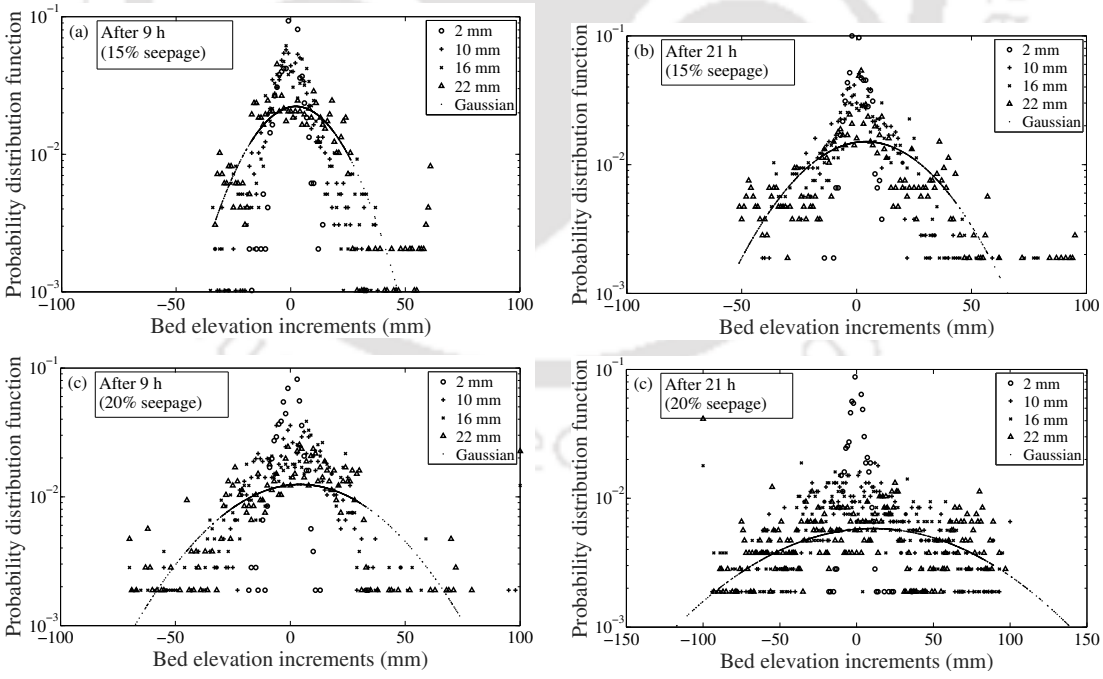

Figure 4.11: Scale dependent probability distribution function of dimensionalized bed elevation increments (a) and (b) after 9 h and 21 h runs for 15% seepage (c) and (d) after 9 h and 21 h runs for 20% seepage.

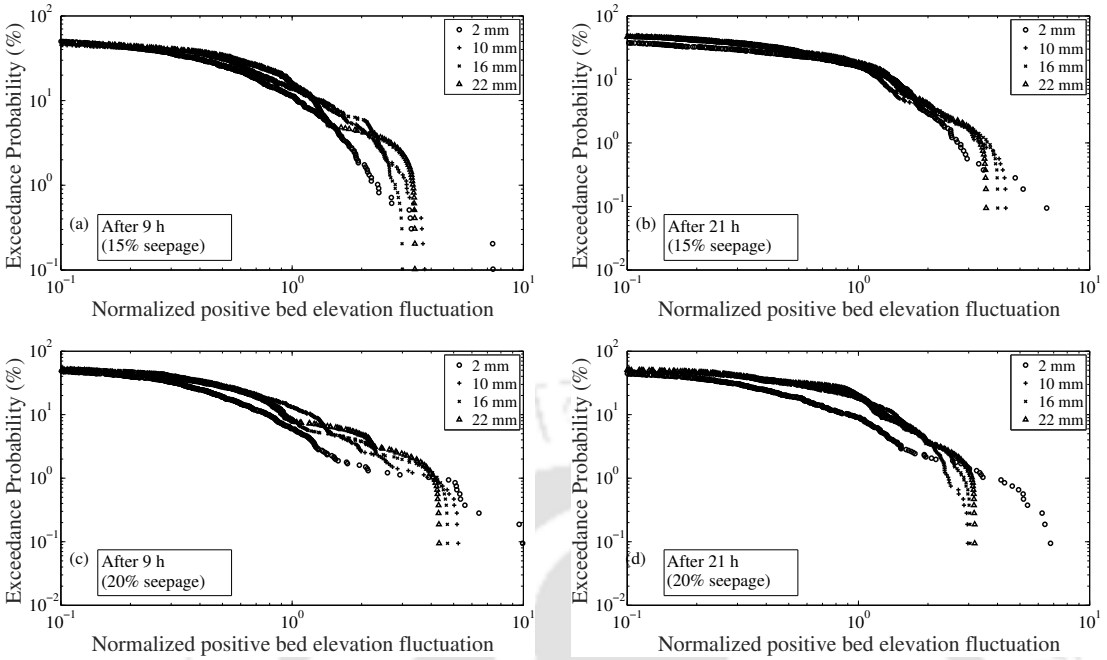

Figure 4.12: Log-log exceedance probabilities of the normalized positive bed elevation increments (a) and (b) after 9 h and 21 h for 15% seepage, (c) and (d) after 9 h and 21 h for 20% seepage.

shown in Figure 4.12. It can be observed that pdfs are getting thinner tailed at larger length scale, which can be seen from the log-log plots of the scale dependent probability of exceedance of the positive bed elevation increments. Results show that the exceedance probability curves more upwards in the case of 20% seepage experiment as compared with 15% seepage experiment. This suggests that the existence of larger bedforms is more likely for the case of higher seepage discharge.

4.6 Spectral Analysis

Power spectral density function (PSD) represents the strength of the energy as a function of frequencies (or scales). In other words, it shows whether the energy is strong or weak at any particular frequency. The PSD is the average of the Fourier transform magnitude, squared over a large time interval. The PSD, $S_x(f)$ of a random time signal $x(t)$ in the interval $(-T, T)$ can be expressed as

$$S_x(f) = \lim_{T\to\infty} E\left\{\frac{1}{2T}\left|\int_{-T}^{T} x(t)\, e^{-j2\pi ft} dt\right|^2\right\} \tag{4.10}$$

Similarly, the $S_x(f)$ can also be defined as the Fourier transform of the auto-correlation function

$$S_x(f) = \int_{-T}^{T} R_x(\tau)\, e^{-j2\pi ft} dt \tag{4.11}$$

Where τ is the time lag and the auto-correlation function $R_x(\tau)$ is defined as:

$$R_x(\tau) = \frac{\mathrm{E}[(x_t - \mu)(x_{t+\tau} - \mu)]}{\sigma^2} \tag{4.12}$$

Where μ is the mean and σ is the standard deviation of the data series. For time series signals, the unit of the frequency response is in Hertz (cycles/sec). In the present experiments, spatial data after 9 h and 21 h of seepage runs have been collected. Therefore, the representative unit of frequency is defined in terms of wave number (number of waves per unit length). Wavenumber ω is defined as the inverse of the spatial resolution (=$2\pi/\triangle x$, where $\triangle x$ = 7.8 mm). It is important to note that the length scales are proportional to inversely of the wavenumbers, obtained from the PSD plots. In the spectral density plots

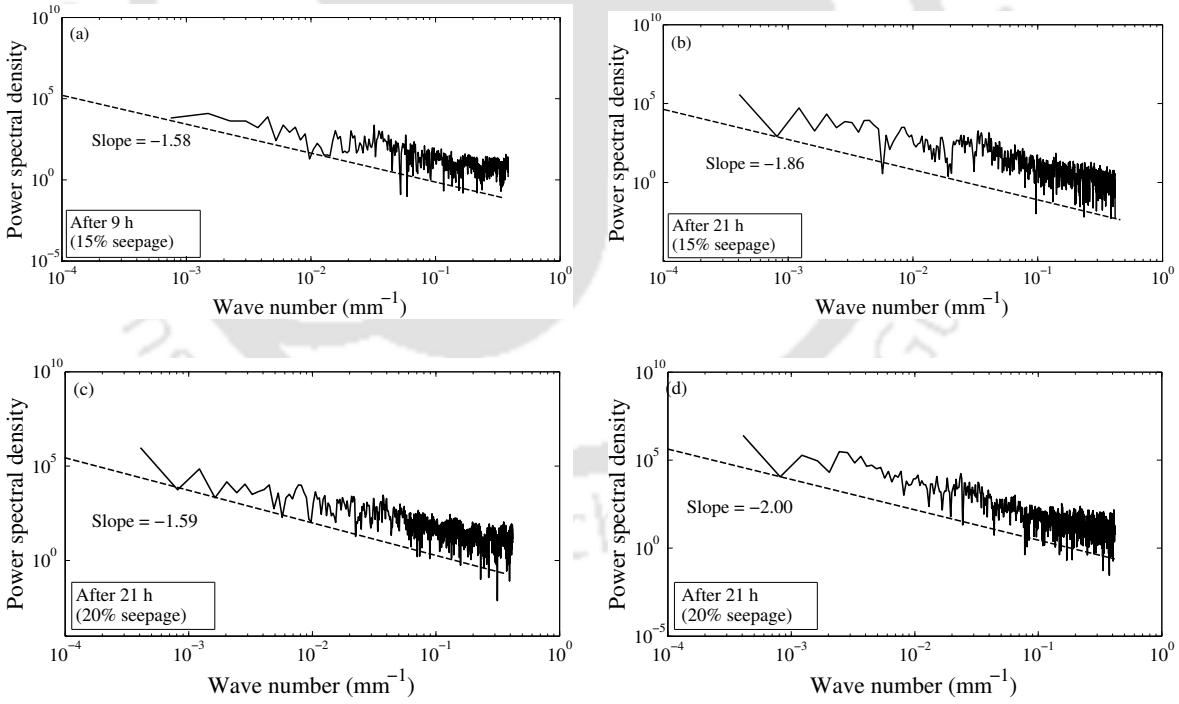

Figure 4.13: Power spectral density versus wavenumber plots of bed elevations fluctuations (a) and (b) after 9 h and 21 h runs for 15% seepage (c) and (d) after 9 h and 21 h for 20% seepage experiment. x-axis denotes wave number (mm-1) and y-axis denotes power spectral density.

the power spectra saturates near 500 mm for both the seepage experiments. This suggests that the largest amount of variance is associated with this particular length scale.

Figure 4.13 shows to the PSD versus wavenumber plots obtained from bed elevations series after 9 h and 21 h of run for 15% and 20% seepage. It can be observed that the slopes of the PSD plots are nearly equal after 9 h run for both the seepage percentages. While after 21 h, slope of the PSD for 20% seepage experiment is increased to -2.0 from -1.86 of the 15% seepage experiment. In the study of Singh et al. Singh et al. (2010) on gravel bed channel, they observed that slope of the power spectra versus wavenumber plot increased from -1.87 to -2.06 after increasing the inflow discharge from 2 to 2.8 m^3/s. In the present study, increment in the PSD slopes suggests the development of larger bedforms and more inhomogeneous arrangement of bed elevation series with the increase in seepage discharge after 21 h run.

4.7 Linkage Between Flow and Bedform Developments

In order to investigate the linkage between flow processes and bedforms development, turbulent flow parameters such as time-average velocity, Reynolds shear stress, and integral scales of flow are evaluated for no seepage run (Phase-I measurement), 15% seepage run, and 20% seepage run immediately after applying the downward seepage (Phase-II measurement).

4.7.1 Streamwise Time-mean Velocity and Reynolds Shear Stress

Figure 4.14 shows the vertical distributions of streamwise time-mean velocities against non-dimensional depth ($h^+ = z/h$). From Figure 4.14, we can observe that streamwise velocities are increased by 1-4% with the application of 15% of seepage. it can be also observed that in the lower flow region the velocity for 20% seepage case is slightly higher, with an average increasing value of 1-2%, than the velocity for 15% seepage case. This observation shows that the higher velocity zone shifts toward the channel bed in the presence of seepage. The increase in streamwise velocities caused sediment transport on the channel bed that can lead to the development of bedforms. Earlier, Patel et al. (2015) also observed higher streamwise velocities over coarse sand bed with the application of seepage.

Furthermore, variations in streamwise velocities near the channel bed lead to the formation of a shear mixing layer. Thus, RSS are calculated to describe the momentum transfer

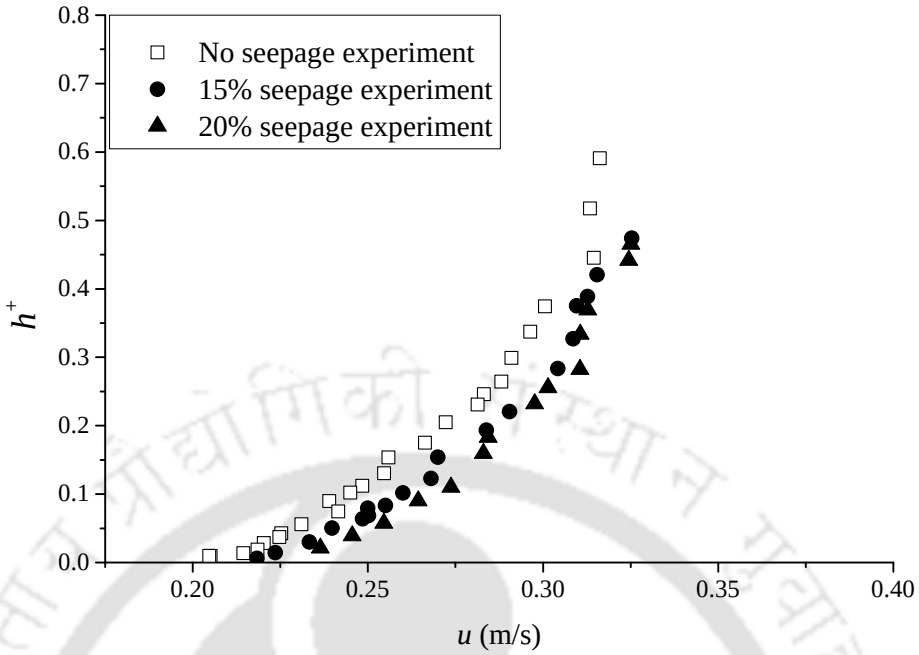

Figure 4.14: Profiles of time-mean velocities u for the no seepage (Phase-I measurement), with 15% seepage (Phase-II measurement), and with 20% seepage (Phase-II measurement) experiments

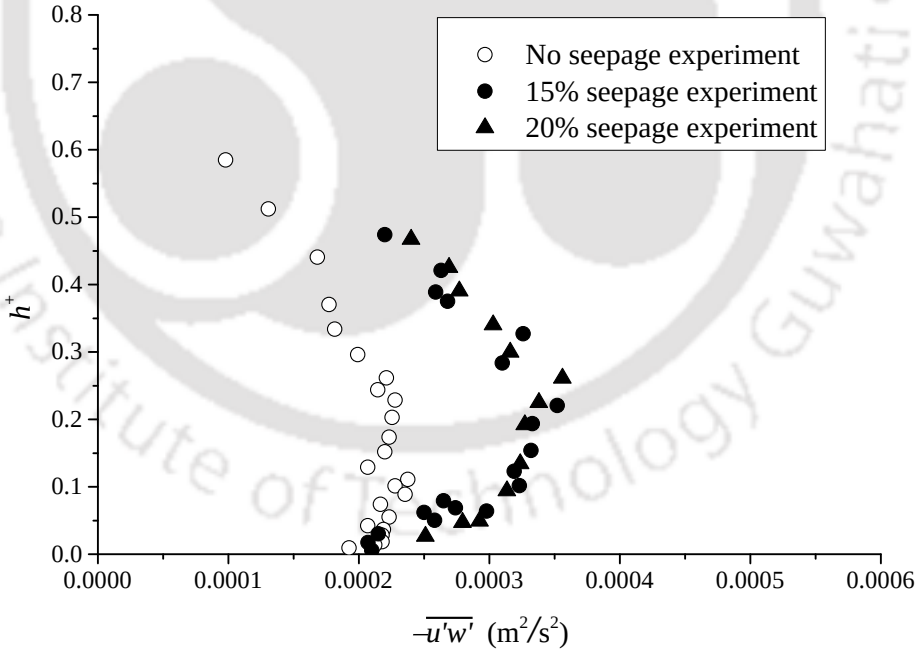

Figure 4.15: Profiles of Reynolds shear stresses $-\overline{u'w'}$ for the no seepage (Phase-I measurement), with 15% seepage (Phase-II measurement), and with 20% seepage (Phase-II measurement) experiments

mechanism in the flows. Figure 4.15 shows the vertical distribution of RSS for no seepage run, 15% seepage run, and 20% seepage run. Increased values of RSS are observed with the application of downward seepage. Careful observation from Figure 4.15 depicts that the maximum value of RSS is increased by 25% with the application of 15% seepage and it is further increased by 10% for 20% seepage than the value of 15% seepage case. This reveals that higher momentum transfers toward the channel boundary. Henceforth, the scale of fluctuating components increased, indicating increased turbulence in the flow. This suggests more mixing in the flows and larger thickness of shear mixing layer in the presence of downward seepage. In earlier studies (Gyr and Schmid, 1989; Best, 1992; Venditti et al., 2005), It was showed that the coherent structure of turbulent flow is linked with the pattern of bedforms development. In this regard, Patel et al. (2015) also observed the evolution of a sheet layer because of increased RSS in the presence of seepage. Here, increase in time-average velocities and RSS values as shown in Figure 4.15 initiate sediment transport, which may result into initiation of bedforms with the application of downward seepage.

4.7.2 Integral Time and Length Scales

Gyr and Schmid (1989) stated that the coherent structure of turbulent flow plays a significant role in the development of bed features that ascribe to initiate the variety of cross-hatched patterns on the channel boundaries. Further, Williams and Kemp (1971) and Best (1992) classified those bed pattern as flow parallel ridge. Best (1992) argued that bed defects are formed because of high-speed streak flow (hairpin vortices) in near-bed region. Venditti et al. (2005) also suggested that development of chevrons and cross-hatched pattern are linked with the integral scales of flow in near-bed region. They have observed the increased values of integral scales by increasing inflow discharge. Besides, the role of integral scales of flows behind the development of bed features with the application of seepage is needed to be studied.

In order to explore an adequate reason behind the development of different size of bedforms on a threshold channel, time and integral length scales are calculated for no seepage run, 15% seepage, and 20% seepage run at close to the channel bed. Integral time scale defines the large eddy turnover time and an integral length scale indicates the characteristics size of eddy length in the flow. These eddies are attributed to transfer the momentum and

turbulent kinetic energy in the flows. The Eulerian integral time scale E_T is defined as:

$$E_T = \int_0^k R(t)dt \tag{4.13}$$

where $R(t)$ is the autocorrelation function, dt is the lag distance, and k is the time at which $R(t)$ starts to oscillate about zero Tennekes and Lumley (1972). The value of k is determined on the basis of autocorrelation at which $R(t) \approx 0.01$ where lag time is 0.01 s. Further, the Eulerian integral length scale is calculated as:

$$E_L = E_T \,.\, u \tag{4.14}$$

where u is streamwise time-mean velocity at a particular location near the channel bed. Table 4.7 shows the calculated values of integral time and length scales of flow for no seepage run, 15% seepage run, and 20% seepage run.

Table 4.7: Integral time scales of flow for the no seepage (Phase-I measurement), with 15% seepage (Phase-II measurement), and with 20% seepage (Phase-II measurement) experiments. Where values are obtained at 10-mm vicinity of bed surface for all the experiments

Category	Time-mean velocity (u_{10}mm), m/s	(E_T), s	(E_L), m
No seepage	0.2	0.415	0.083
15% seepage	0.207	0.761	0.157
20% seepage	0.21	1.111	0.233

From Table 4.7, it can be observed that values of time and length scale are increased after application of 15% seepage. The values of integral scales are further increased after applying 20% seepage as compared with 15% seepage case. In this regard, Venditti et al. (2005) investigated the role of higher eddy size behind the initiation of larger bedforms in near-bed region by increasing the flow strength. In this study, it can be observed that the increase in eddy length and eddy turnover time with the application of seepage, suggesting a higher level of momentum and energy transfer and less destruction of turbulent motions in the flow. This suggests that the level of turbulence in the flow increases under the influence of downward seepage. Patel et al. (2015) also observed that values of integral scales are increased with the application of downward seepage, causing evolution of sheet layer over coarse sand bed channel. In the present study, results show that increase in eddy length

and eddy turnover time, leading to the development of bedforms in a fine sand bed channel when downward seepage was applied to it.

4.8 Discussion

Dynamic characteristics of bedforms are integrally related to flow variables (streamwise velocity, bed shear stress, and level of turbulence) and physical parameters (bed material, shape, and sizes). Yalin's (1976) criterion was used to obtain the threshold of sediment movement during no seepage run. In order to confirm the incipient motion conditions of bed particles over the periphery of the channel Shields curve was used (see Figure 2.21). Through experiments, it was observed that bed particles were stable on a curvilinear cross section in threshold condition and their movement was sporadic along the channel length. Also, it was observed that the cross-sectional of the channel was remained in the original cross-sectional shape (no deformation), while running several hours (10-12 h) during no seepage run at threshold condition (see Figure 4.16).

Figure 4.16: Snapshot of channel bed after no seepage experiment

However, with the application of downward seepage, forces acting on the particle were disturbed because of increased bed shear stress, leading to the detachment of bed particles from banks and bed. These detached particles were then deposited at the adjacent section toward downstream in the form of bedforms, consequently, shape of channel was distorted as shown in Figures 4.17 and 4.18. In this regard, Lu et al. (2008) also suggested that downward seepage disturbs the stability of bed particle and influences the flow characteristics on the plane bed channels. In addition, the previous literature shows that bed shear stress increases while application of downward seepage (Watters and Rao, 1971; Maclean, 1991b; Rao et al., 2011; Cao and Chiew, 2014; Patel et al., 2015) observed bedforms over plane bed channels, while increasing the strength of flow (providing excess shear stress). Moreover, in the present study, bedforms were observed over the periphery of the channel bed when water was extracted from the channel bed in downward direction in the form of downward seepage (see Figures 4.17 and 4.18).

Further, turbulent flow parameters are evaluated for no seepage and seepage experiments to understand the mechanism behind the development of bedforms. Results show that time-mean velocities and RSS are increased in seepage run as compared to no seepage run. These

Figure 4.17: Snapshot of channel bed at the end of 15% seepage experiment

Figure 4.18: Snapshot of channel bed at the end of 20% seepage experiment

increased values of streamwise time-average velocities and RSS, led to sediment transport and development of bedforms over the periphery of the channel bed. Further, it has been obtained that the scales of eddy length and eddy turn over time are higher for 20% seepage than 15% seepage case, indicating greater turbulence in the flows. In the previous study of Sumer et al. (2003) showed that the increase in turbulence by 20% may cause increase in sediment movement by six times. In this regard, Venditti et al. (2005) observed larger bedforms because of increased eddy length and turn over time by increasing strength of flow.

Earlier, various researchers documented that the migration speed of bedforms depends on bedform dimensions, for example, larger size of bedforms had lesser migration speed (Coleman and Melville, 1994; Jerolmack and Mohrig, 2005). Numerical study of Giri and Shimizu (2006) also showed that celerity of bedforms deceases with an increase in bedforms dimensions. In the aforementioned studies, the influence of downward seepage has not been considered for analysing the celerity of bedforms. Therefore, cross-correlation analyses at several scales were performed using wavelet in order to get greater insight into the dependence bedform celerity for 15% and 20% seepage experiments. Here, celerity of

bedforms is calculated at 100 mm to 500 mm length scales in the presence of downward seepage as shown in Figure 4.3. Results show that the celerity of the bedforms progressively decreases with an increase in length scale and seepage percentages from 15% to 20%. This suggests that the larger size of bedforms developed during 20% seepage experiments. On the contrary, Singh et al. (2011) evaluated the celerity of developing bedforms, using time series data of two eco-sounders placed at a large distance apart, for two different inflow discharges in a large flume. They suggested that bedforms celerity decreased with an increase in bedform size as a result of increased inflow discharge, which has a detrimental effect on the celerity of bedforms.

In addition to this, the dynamics of developing bedforms with the application of 15% and 20% seepages are analyzed. In this regard, geometry of the bedforms has been extracted from a set of bed elevation series at different time intervals using BTT provided by Van der Mark et al. (2008). The effort has been made to obtain the relationship amongst flow characteristics and geometry of bedforms. It has been found that the integral scales of flow and corresponding dimensions of the bedforms are increased by increasing the amount of downward seepage (refer Table 4.7 and Table 4.4). Thus, it can be concluded that the celerity of bedforms reduced because of increased bedforms dimension by extracting more water from the channel in the form of downward seepage. Further, it may be justified by analysis of tail of PDF of bedform celerity, in which celerity of bedforms decreased and tail of PDF of celerity tended to get heavier in the case of 20% seepage experiment. Therefore, it can be suggested that the asymmetry of the bedforms increases due to transportation or deposition of sediment particles with increase in seepage percentage. Apart from this, it has been found that the best approximation fit for the probability density functions of bedform celerity is Rayleigh distribution for both the seepage discharges and this holds true irrespective of the seepage amounts.

4.9 Conclusions

The present study investigates the effect of different percentages of downward seepage on bedforms dynamics and turbulent flow characteristics in a curvilinear cross section alluvial channel. In experiments, two downward seepage percentages, 15% and 20% of the main channel discharge, were applied on a threshold channel to understand the influence of downward seepage on flow hydrodynamics and bed morphology.

Celerity of bedforms has been obtained by using wavelet cross-correlation analysis at

different scales in order to evaluate the statistics of bedforms on different percentages of seepage. Stochastics of bedform celerity has also been evaluated for different seepage percentages and it has been found that Rayleigh distribution performs well in terms of best approximation and minimum relative error. The tail characteristics of the PDFs of bedform celerity by tail indexes of the fitted truncated Pareto distributions have also been defined. It has been observed that higher seepage discharge leads to a heavier tail of the PDF of bedform celerity, indicating larger variability in bedform distributions. Results of this study have revealed that the average celerity of bedforms is decreased. This has happened because of the dominance of larger bedforms in the case of higher seepage discharge. Interestingly, bedforms of same length scales have also shown attenuation in their celerity. It has been inferred from the results that bedforms of all length scales moved at a slower speed for the higher percentage of seepage.

Cumulative distribution of bedform's height and length deviates from the Gaussian distribution after running the seepage experiments for several hours (21 h). Probability distribution function of bedform's dimensions was analyzed for both the seepage discharges. It can be recommended Gamma distribution for developing and stable bedforms geometries in the presence of seepage. Statistical analysis has been performed on the wavelet coefficients, which represents the bed elevation fluctuation at different scales. Further, higher order statistical analysis shows greater fluctuations in the elevation of bedform, as well as the presence of multi-fractal properties, which have been described in terms of local roughness and intermittency parameters. Additionally, it is observed that channel bed became more inhomogeneous and rough after increasing the seepage discharge.

These results show that with the passage of time roughness on the channel bed increases in the presence of seepage. The dimensionalized probability distribution functions of the bed elevation fluctuations tend to become wider after increasing the amount of seepage, indicating higher probability of larger fluctuation if the amount of seepage is increased. Logarithmic exceedance probability plots of the normalized positive bed elevation fluctuations shift upwards after increasing the seepage amount, signifying a higher probability of occurrence of larger bed elevation fluctuations. Spectral analysis has been performed on same elevation series and found that slopes of power spectra increases from -1.86 to -2, showing inhomogeneous and rapid variation of bedforms in the case of increased seepage discharge.

In order to understand the flow process, turbulent flow characteristics such as time-mean

velocities, Reynolds shear stresses, and integral scales are analyzed for both the seepage experiments. The increase in streamwise time-average velocities and Reynolds shear stresses are observed with the application of downward seepage. These parameters are increased slightly with an increase in the amount of seepage discharge. In addition to this, integral length and time scales of flows at near the bed have shown a clear distinction between two seepage discharges. Eddy length and eddy turnover time were increased after applying downward seepage. It can be concluded that the downward seepage causes higher momentum and energy transfer toward the channel bed, leading to sediment transport and development of bedforms over the fine sand bed.

Hence, this can be hypothesized as the result of increased Reynolds shear stresses, streamwise time-average velocities, and integral scales of flow under the higher amount of seepage, which destabilized the bed particles hindering them to follow any continuous and unidirectional movement pattern. At this condition, size and variability of bedforms have been increased with the increase in seepage amount. These larger bedforms have been caused in the depletion of migration speed or celerity of bedforms along the flow direction.

"Turning the shingle, returning the shingle,
Changing the set of the sand..."

From *The Dyke* by Rudyard Kipling

5

Turbulent Characteristics and Evolution of Sheet Flow with downward seepage

In Chapters 3 and 4, experimental results were shown on a finer sand bed threshold channel in the presence of downward seepage. Bedforms were developed on a stable channel when water was extracted from the channel bed in the downward direction. Therefore, for signifying the effect of downward seepage on higher particle size, coarse sand was used in this study. In this chapter, influence of downward seepage on a coarse sand (median diamter = 1.1 mm) bed threshold channel with curvilinear cross-sectional shape is discussed. Downward seepage causes the greater Shields stress from its critical value, which is responsible for initiation of the sheet flow layer. The hydraulics of sheet flow and its propagation over time and space by doing experiments with downward seepage are presented. Integral scales and turbulent flow parameters are also analyzed in the near-bed region to understand the linkage between flow and evolution of the sheet layer.

5.1 Evolution of Sheet Flow

The mode of sediment transport is not always in the form of bedforms, it was also observed in sheet flow according to hydraulic conditions, shape, and size of sediment in alluvial channels. Sheet flow contributes significantly to sediment transport. Sheet flow occurs when tractive force is greater than resistive force and when the large amount of sediment is transported under sheet flow (Gotoh and Sakai, 1997). Sheet flow is a thin layer of high

sediment concentration that occurs above plane, noncohesive, sediment beds. Available literature on laboratory and field observations of the sheet flow of bed material suggests that under sheet flow conditions the bed remains fairly plane where ripples and other bed topography features are absent and the bed material movement is restricted to a layer a few centimeters in thickness and comprised of moving sediment particles Dingler and Inman (1976); Wilson (1987); King Jr (1991); Conley and Inman (1992); Ribberink and Al-Salem (1994); Sumer et al. (1996). The flow in an alluvial channel is significantly affected by the presence of the sheet flow layer as a large amount of sediment is transported, which affects the morphological processes such as erosion and disposition in canals or alluvial river systems. Existing knowledge on sediment transport in the form of sheet flow in alluvial channels involves the high bed shear stress, which could be achieved by increasing the flow discharge greater than some thresholds. However, downward seepage can also increase the bed shear stress if applied to the threshold channel with stable cross-sectional shape. Our goal is to describe how the downward seepage affects stable alluvial channels.

5.2 Results

Experiments were carried out in no seepage and with seepage conditions. Measurements of flow parameters were taken in both conditions to asses the hydraulic parameters. Here, Shields stress and stream power are analyzed for no seepage and with seepage condition at different time intervals for understanding the behavior of the channel.

5.2.1 Changes in Shields Stress, Stream Power, and Channel Geometry with Time

Threshold condition of the experimental channel during the no seepage experiment has been validated by plotting the results on a Shields curve (Rao and Sreenivasulu, 2009) that gives a relationship between Shields stress (θ_c) and shear Reynolds number (R_*) (Figure 5.1). The band on the Shields curve shows $\pm$10% variation from the mean curve. The average values of the shear velocity can be calculated as:

$$u_{*b} = \sqrt{gR_hS_f} \tag{5.1}$$

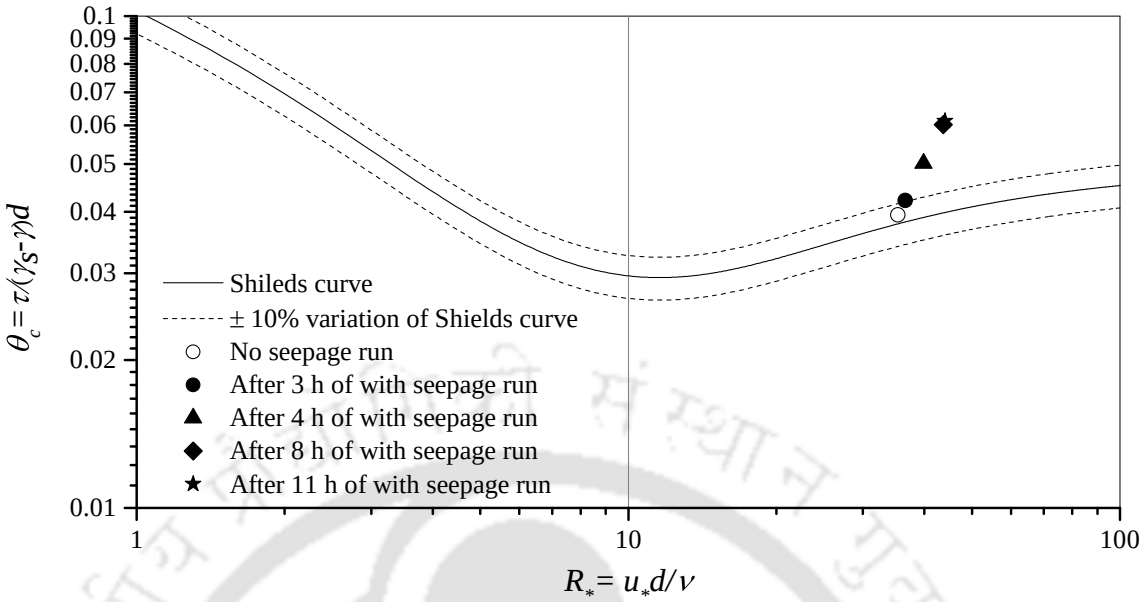

Figure 5.1: Temporal evolution of Shields stress (θ_c) and shear Reynolds number (R_*) during the no seepage run and with seepage run (where $\theta_c = 0.0399$ is the threshold value of Shields stress)

where g is gravitational acceleration, R_h is hydraulic radius, and S_f is energy slope of the spatially varied flow and can be given as (Rao et al., 2011)

$$S_f = S_w(1 - F^2) + SF^2 + 2\rho u_s V_s/(h\gamma_s) \tag{5.2}$$

where F is Froude number, S_w is water surface slope, and S is bed slope. Subscript '0' represents the parameter for no seepage experiments and subscript 's' represents the same parameter for with seepage experiments. Seepage velocity is V_s, u_s is average velocity in with seepage experiment, h is depth of flow, ρ_w is density of water. Average velocity of the flow (U) can be calculated as:

$$U = Q/A \tag{5.3}$$

where A is the cross-sectional area, Q is the main channel discharge:

$$Q_s = Q_0 - q_s\left(1 - {}^{X}/_{L}\right) \tag{5.4}$$

where Q_s is the discharge for the with seepage experiment, Q_0 is the discharge for the no seepage experiment, q_s is the seepage discharge over the reach length L of the channel, and

X is the distance from the tail gate. Seepage velocity (V_s) through the sand bed of length L can be calculated as:

$$V_s = q_s/(PL) \tag{5.5}$$

where P is the perimeter. Shields stress and shear Reynolds number can be calculated as:

$$\theta_c = \frac{\tau_s}{(\gamma_s - \gamma)\, D_{50}} \tag{5.6}$$

$$R_* = \frac{u_* D_{50}}{\nu} \tag{5.7}$$

where τ_s is bed shear stress, D_{50} is median diameter of sand particles, ν is kinematic viscosity, and γ_s and γ are specific weights of sediment particles and water, respectively.

Figure 5.1 illustrates that when the channel was at threshold condition during the no seepage run, the Shields stress and shear Reynolds number were within the limit of the band on Shields curve. After the application of downward seepage, value of the Shields stress was increased ∼30% after 3 h, ∼50% after 4 h, ∼75% after 8 h, and ∼77% after 11 h from its critical value at 8 m in the middle of the test section. Figure 5.2 shows the variation in Shields stress along the channel length in the test section. Results from previous sand-bed channels suggest sediment movement at shear stress ∼20% higher than the threshold value (Ikeda et al., 1988; Diplas, 1990). The increment in shear stress in the present experiments is caused by the application of downward seepage contrary to experiments of Ikeda et al. (1988) and Diplas (1990) on sand-bed channels. During the no seepage run, Lane's (1953) parabolic profile was stable and there was no deformation of the cross-sectional shape in the entire test length of the channel. Measurements of geometry are taken by using an ultrasonic ranging system and have been processed by using Surfer®. Processed geometrical features of the channel as a three-dimensional image after running several hours of the no seepage run is shown in Figure 5.4 (a). During the with seepage experiment, the increase of Shields stress caused distortion of the cross-sectional shape of the channel (Figure 5.4b). It was observed in the with seepage experiment that detachment of the sediment particles from channel banks and its deposition on the channel bed and that further movement of the bed material in the form of sheet flow layer toward downstream follow a regular pattern. The material from the banks at a section was deposited on the channel bed at the adjacent section in the downstream direction and carried forward by the water along the length of

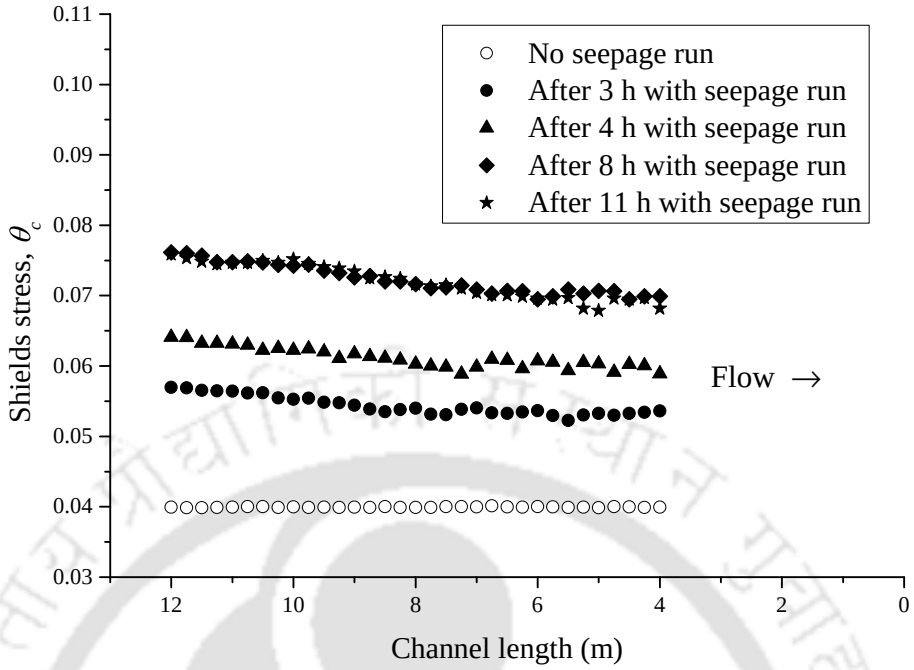

Figure 5.2: Variation in Shields stress along the channel length during no seepage and with seepage runs

the channel in the form of a sheet flow layer as shown in Figure 5.4 (b). The large amount of eroded sediment from the banks is transported in the form of sheet flow over the bed, and sediment particles move in such a way that the particles roll over one another. The snapshot of the channel obtained after the no seepage run is given in Figure 5.4 (c), whereas that obtained after the with seepage experiment is shown in Figure 5.4 (d) in which the sheet flow layer of sediment particles is clearly visible on the channel bed. Asano (1992), Gotoh and Sakai (1997), and Dong et al. (2013) observed sheet layers after the washout of bed features on higher Shields stress (up to 10). Revil-Baudard and Chauchat (2013) proposed a model to predict the sheet flow regime over a large range of Shields stress (0.5 to 2.6). In the present experimental study, higher values of Shields stress have been found during the with seepage experiment than its threshold value of the no seepage experiment. This increase in the value of Shields stress and the consequent sediment transport in the form of a sheet layer suggest that seepage in the downward direction plays a significant role in sediment transport and the formation of a sheet flow layer in alluvial channels. Cross-sectional profiles during the no seepage run and changes after 3 h, 4 h, 8 h, and 11 h during the with seepage experiment are shown in Figure 5.3 at the location 8-m from the downstream end of the channel.

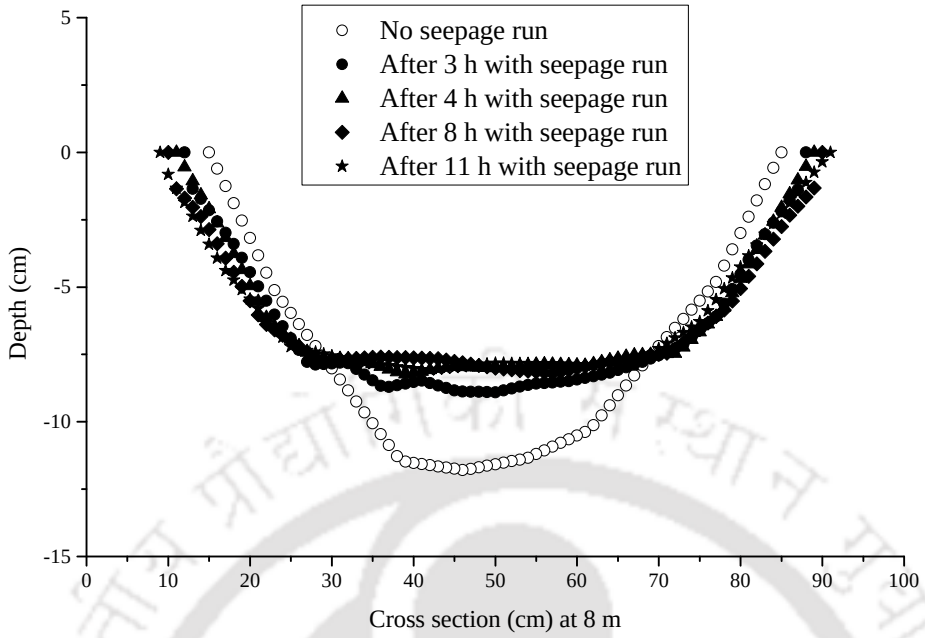

Figure 5.3: Temporal changes in the cross-sectional profile of the channel at location 8 m from the downstream end for no seepage and with seepage at 3, 4, 8, and 11 h interval

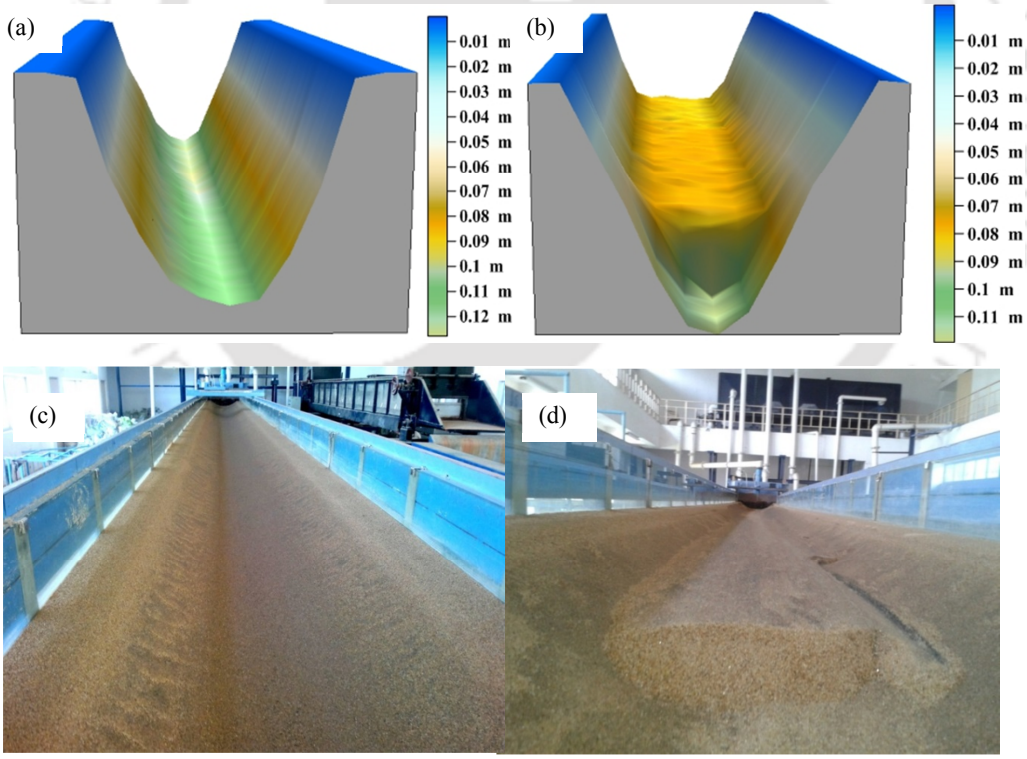

Figure 5.4: Profiles of the channel: (a) processed curvilinear three-dimensional profile of channel cross section after several hours of no seepage run, (b) processed three-dimensional trapezoidal profile of channel cross section after 11 h of seepage run, (c) snapshot of the channel after successful completion of no seepage run, and (d) snapshot of the channel after 11 h of seepage run

Fluvial processes such as channel bank erosion can also be described by using stream power associated with the flow as a governing parameter (Jha et al., 2003). Stream power is the energy of the stream to transport bed particles (Bagnold, 1966, 1977) and has been determined as:

$$\Omega = \gamma Q S_f \tag{5.8}$$

where Ω is stream power per unit length, Q is main channel discharge, and Sf is energy slope. The discharge during the with seepage experiment is calculated from Equation 5.4, where it is evident that the stream power decreases gradually toward the downstream end of the channel. This results in the corresponding decrease of stream power in the same manner. Figure 5.5 indicates the variation of stream power at different time intervals. After the application of downward seepage, the value of stream power increased ∼20% after 3 h, ∼50% after 4 h, ∼70% after 8 h, and ∼73% after 11 h in the with seepage experiment as compared with the no seepage run. More erosion of banks took place at the upstream end of the study reach because of the higher stream power associated with the flow. Figures 5.7, 5.8, and 5.9 show the variation in the cross section in the longitudinal

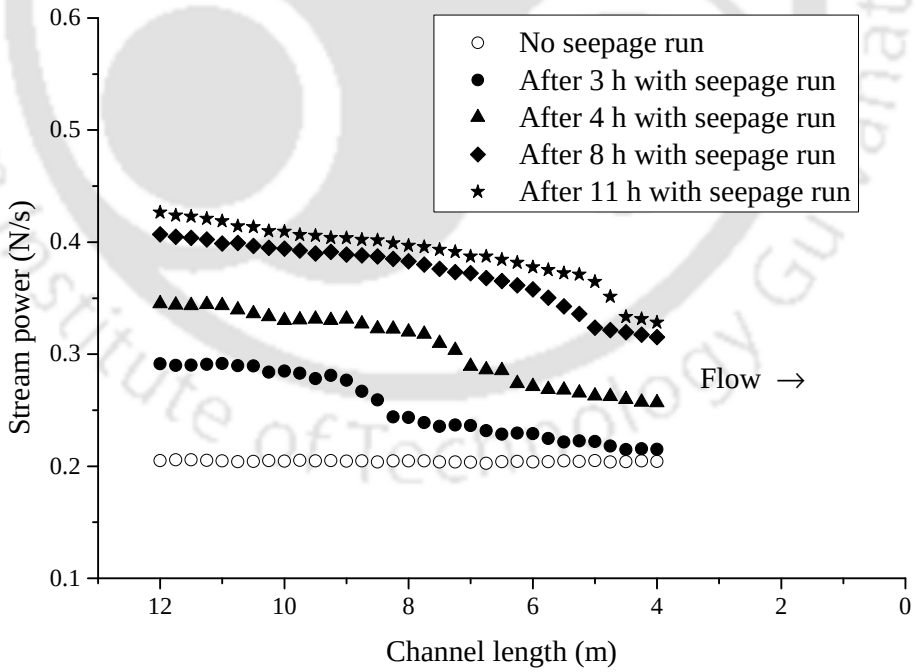

Figure 5.5: Variation of stream power in the longitudinal direction from upstream to downstream test reach (12-4 m) at the no seepage run and 3 h, 4 h, 8 h, and 11 h time intervals of the with seepage run run, where sudden steps in the with seepage run indicate the prograding front of the sheet layer

direction, where material eroded from banks and bed and transported along the flow due to higher stream power. Toward the downstream as the stream power reduced gradually, the erosion of banks also decreased (see Figure 5.9). It reveals that when the channel was in the threshold condition during the no seepage experiment, stream power was more or less constant along the length of the channel, while after the application of the downward seepage stream power increased significantly at the upstream side of the test section and decreased gradually toward the downstream direction. There are sudden steps in stream power at each time of the with seepage experiment, which represents the prograding front of the sheet layer.

After the application of downward seepage (with seepage experiment), with the passage of time thickness of the sheet flow layer changes along the length of the channel. Initially, the sheet layer moves faster, but after some period of time the rate of movement is reduced. It can be observed from the center line profile of sheet layer movement that is shown in Figure 5.6.

It can be observed from Figure 5.6 that it took only 3 and 4 h for the sheet layer to reach the sections at 8.2 and 7 m, respectively, after the application of downward seepage. The rate of the sheet layer movement reduced with time, and it took 11 h to reach the section at 4.7 m from the downstream end of the channel. There was very minimum change observed in the thickness of the sheet layer, and its further movement was reduced after 11 h.

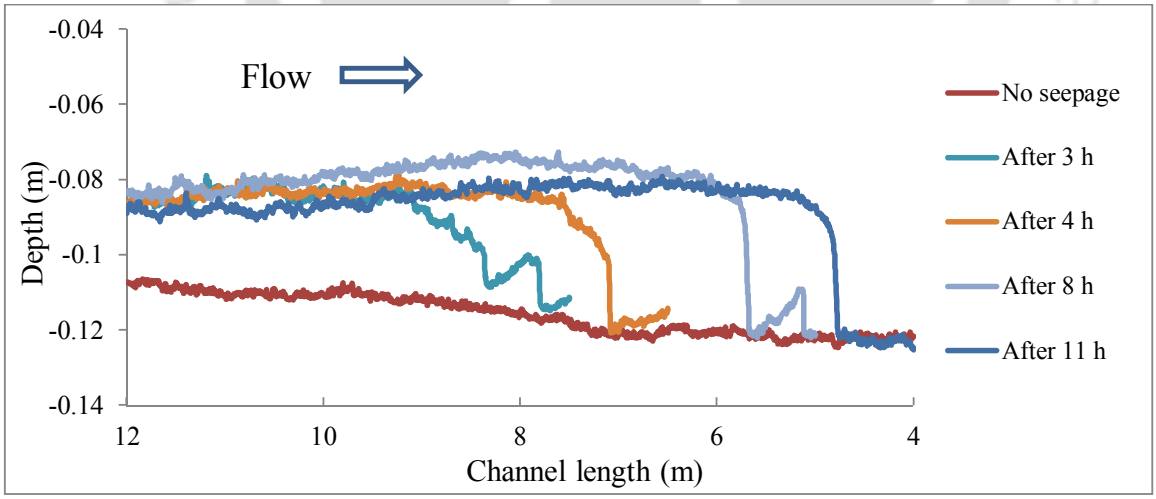

Figure 5.6: Centre line profile of sheet flow movement in the test section (4-12 m from the downstream end) at different time intervals under the conditions of no seepage and with seepage, where different colors distinguish the position of the prograding front of the sheet layer

It can be observed from Figure 5.6 that after the long duration of the experiment, such as between 8 h and 11 h in the with seepage run, a very minimal increment in Shields stress (∼2%) was found in the channel. Figure 5.5 indicates that the increment in stream power was also reduced considerably (∼3%) during this interval. With the reduced increment in Shields stress, stream power, and sheet layer movement, it can be said that the channel was about to attain the equilibrium condition with a different cross-sectional shape (see Figures 5.7, 5.8, and 5.9). The morphological changes in the channel can be visualized from the contour map as shown in Figure 5.10, which shows temporal variation in channel cross section along the channel length.

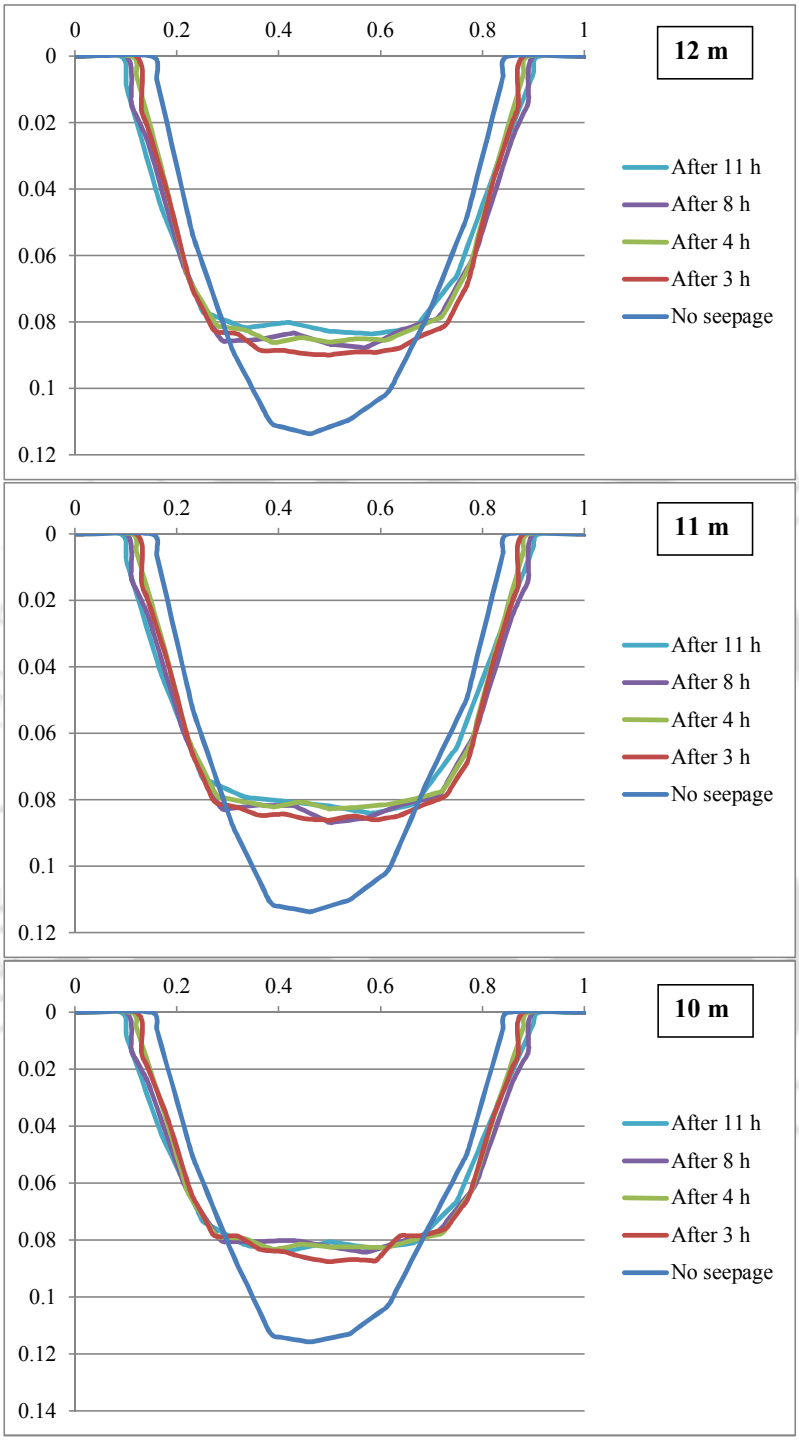

Figure 5.7: Variations in the cross-sectional shape of the channel along the flow in the test section (12 m, 11 m, 10 m) for no seepage and with seepage run at 3 h, 4 h, 8 h, and 11 h interval

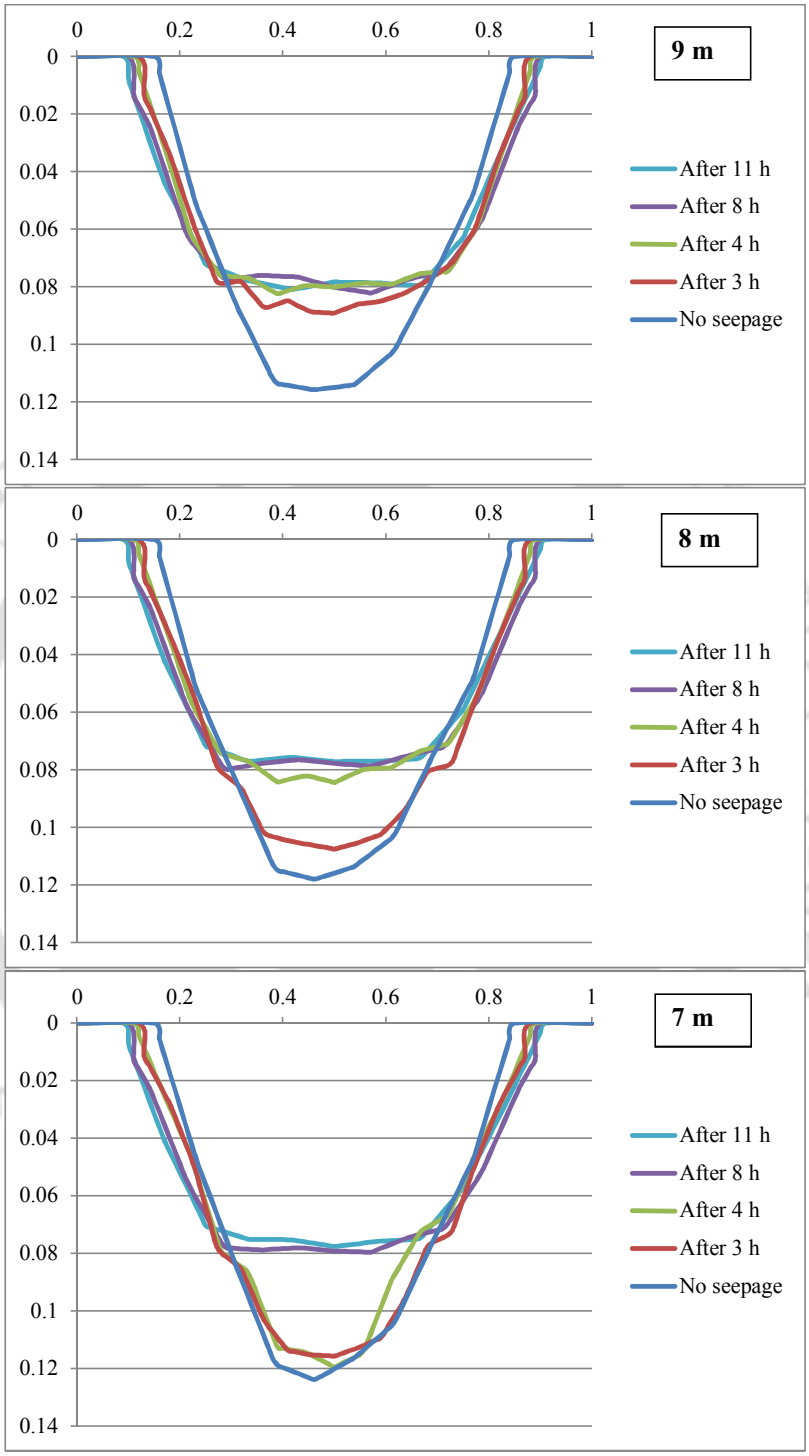

Figure 5.8: Variations in the cross-sectional shape of the channel along the flow in the test section (9 m, 8 m, 7 m) for no seepage and with seepage run at 3 h, 4 h, 8 h, and 11 h interval

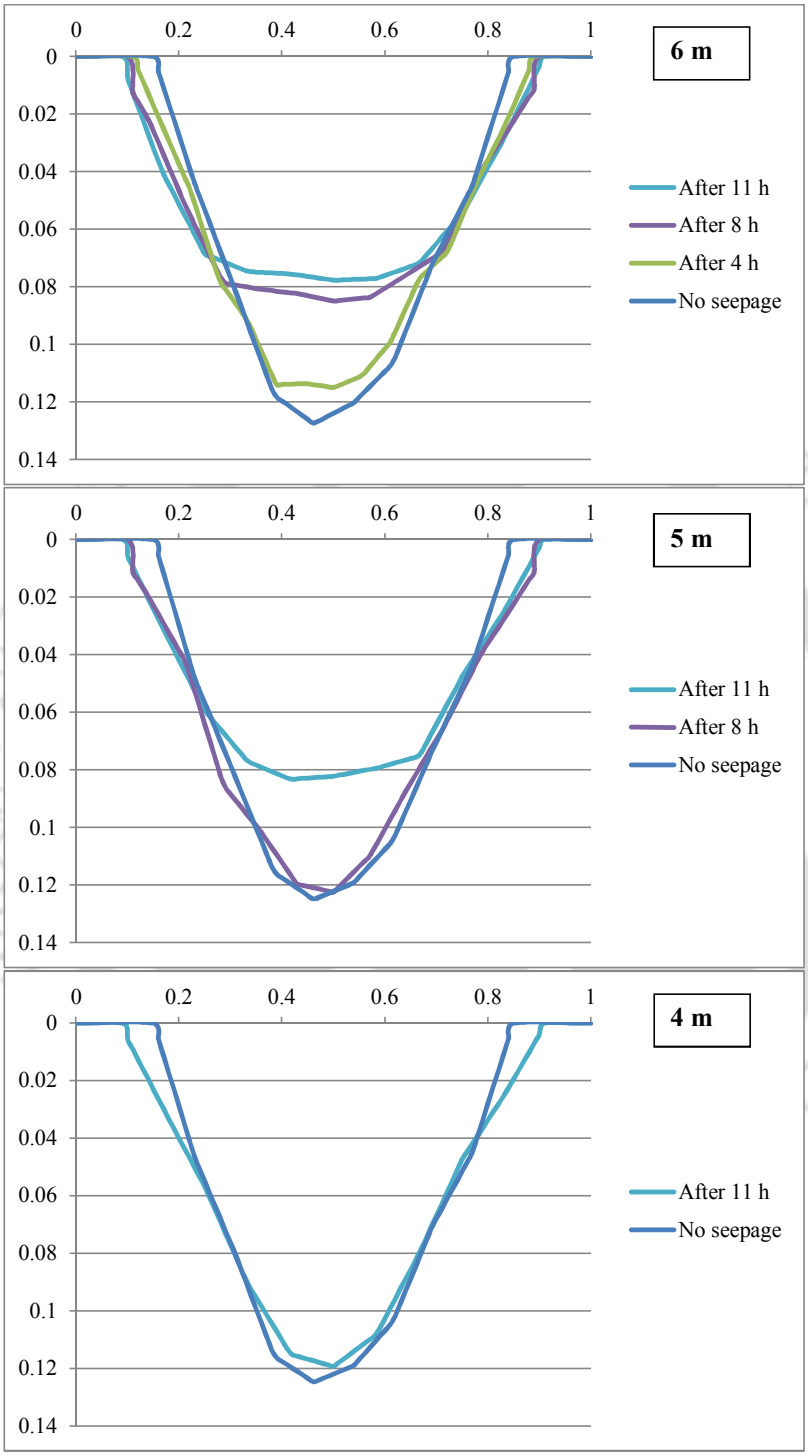

Figure 5.9: Variations in the cross-sectional shape of the channel along the flow in the test section (6 m, 5 m, 4 m) for no seepage and with seepage run at 3 h, 4 h, 8 h, and 11 h interval

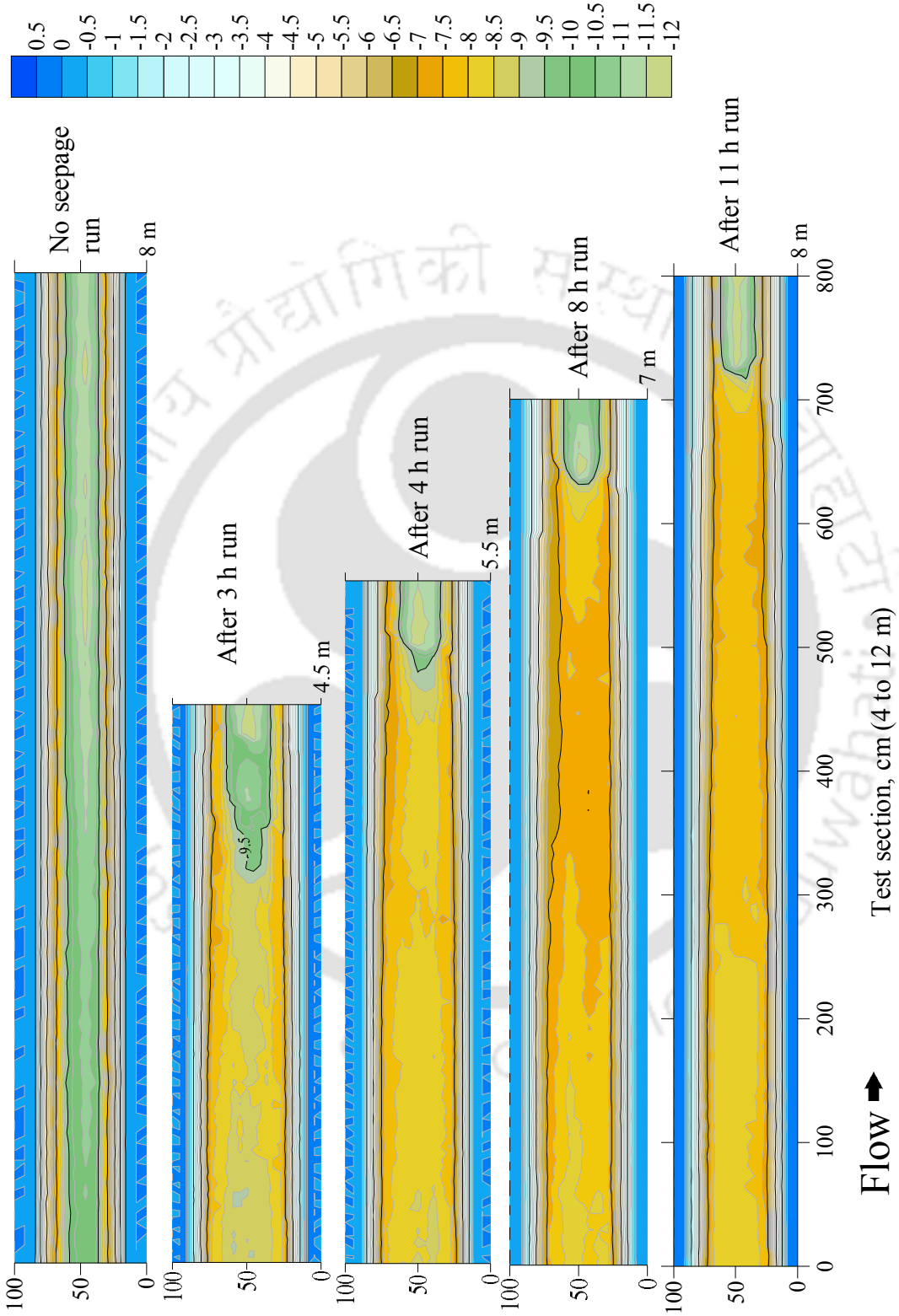

Figure 5.10: Contours map of sheet flow movement in the test section (4-12 m from the downstream end) at different time intervals under the conditions of no seepage and with seepage, where different colors distinguish the position of the prograding front of the sheet layer

5.2.2 Time-evolution of Morphological Parameters

Wilson (1987) and Asano (1992) have discussed that the increment in Shields stress from its threshold value is directly proportional to sheet thickness. In the present data set, Shields stress is plotted with sheet thickness and channel perimeter to define the morphological changes at different time intervals. Figure 5.11 shows changes in the geometrical characteristics and corresponding Shields stress during different measurement periods. Three measurement sections from the test zone (9, 8, and 7 m) were considered for comparing the results. Shields stress, at 3 h after application of seepage, increases ∼30% from the threshold value at each section (Figure 5.11a). The corresponding change in sheet thickness is ∼10% at 3 h after the application of seepage (Figure 5.11b). Figure 5.11 (a) also gives the attainment of constancy in Shields stress after 8 h. The erosion of parabolic shape and the channel attaining a different stable shape with application of seepage can be seen with widening of the channel perimeter (∼6% at 3 h and ∼0.6% during 8 to 11 h) at each section in Figure 5.11 (c).

5.3 Linkage Between Flow and Initiation of Sheet Flow Development

In order to understand the reason associated with the sheet layer development through the flow process, instantaneous flow needs to be measured in the near-bed region. The coherent structure of the turbulent flow is linked with sediment transport, and the real time measurements show changes in the characteristics of flow that are responsible for sheet layer development after the application of downward seepage. Time-mean velocities, Reynolds shear stresses, and integral scale of flow are calculated for the no seepage run (Phase-I measurement), with downward seepage (Phase-II measurement) and over the sheet layer (Phase-IV measurement) to investigate the initiation of sheet layer and flow over the sheet.

5.3.1 Time-mean Velocity

Time-mean velocities were calculated from decomposition of instantaneous velocity samples into the time-mean and fluctuating components of velocity (Tennekes and Lumley, 1972). Figure 5.12 shows the near-bed distribution of the time-mean velocities during the no seepage (Phase-I measurement), the with seepage (Phase-II measurement), and over the

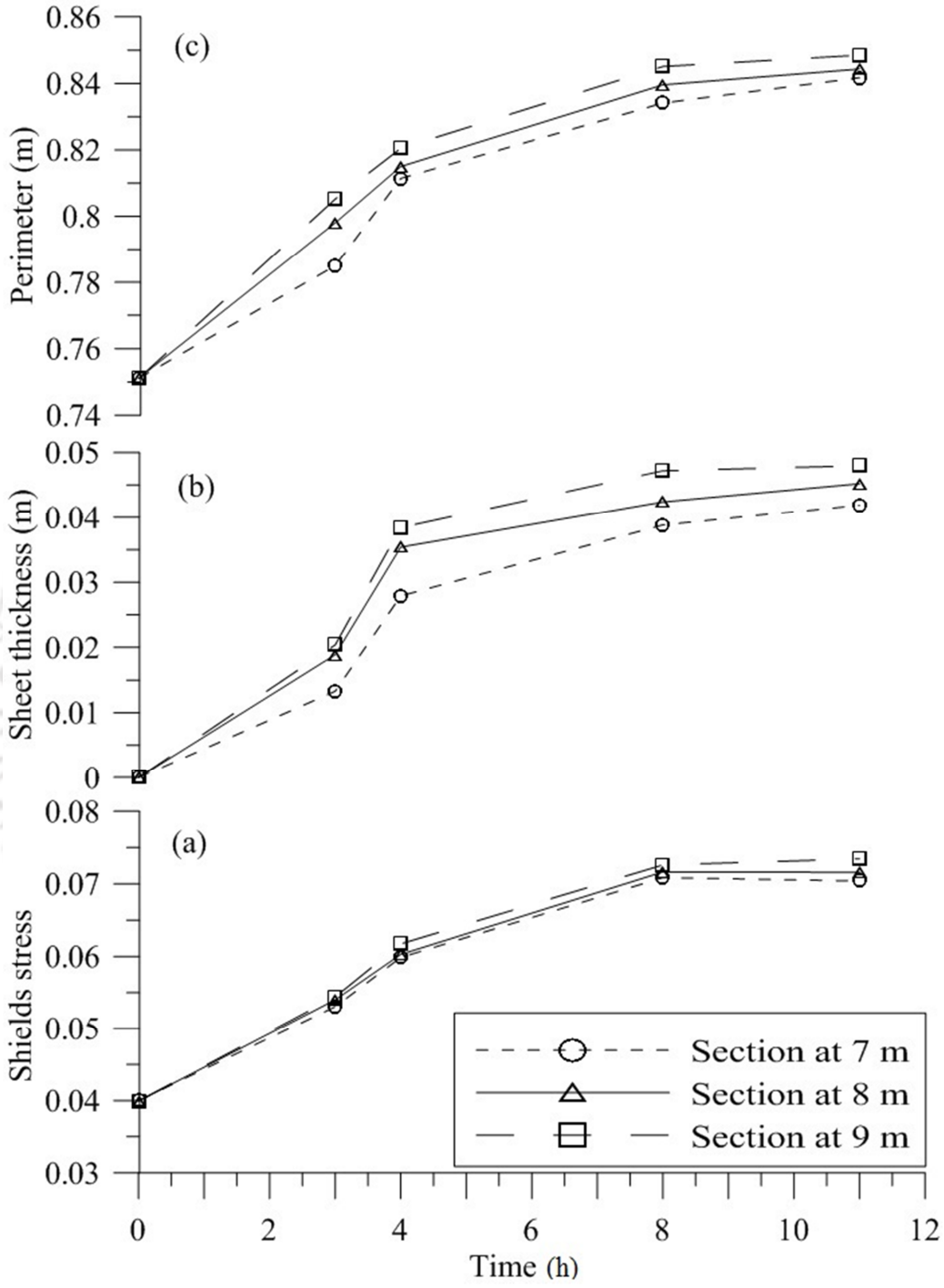

Figure 5.11: Variation of (a) Shields stress, (b) sheet thickness, and (c) perimeter with time. Three sections 9, 8, and 7 m are considered to present the morphological changes with time, where t = 0 indicates the no seepage run and 3 h, 4 h, 8 h, and 11 h indicate the time interval in with seepage run

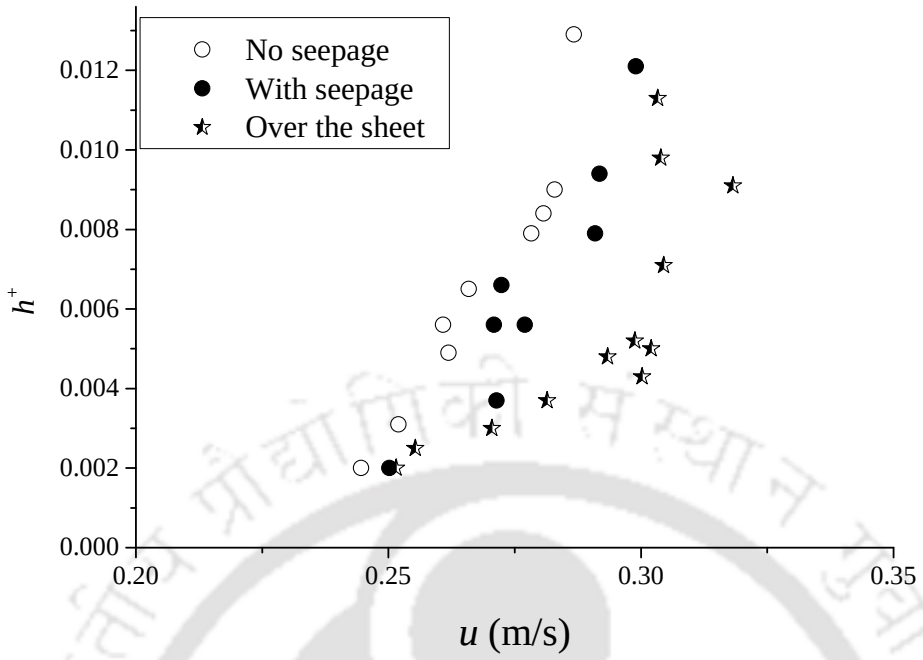

Figure 5.12: Distribution of the time-mean velocities measured in the middle of the test section (8 m from downstream) during the no seepage (Phase-I measurement), the with seepage (Phase-II measurement), and over the sheet layer (Phase-IV measurement) at time between 8 and 11 h during the with seepage run

sheet layer (Phase-IV measurement) plotted against the normalized depth of flow.

Velocities in the with seepage run were measured right after the application of downward seepage, and It can be seen from Figure 5.12 that the velocities increased (∼3 to 6%) in the near-bed region. This increase in velocities caused bed-material transport in the form of a sheet layer in the channel. When the cross-sectional shape of the channel is about to attain an equilibrium condition at the time between 8 h and 11 h after applying seepage, instantaneous velocities were measured over sheet flow. As flow depth in the channel was reduced because of formation of the sheet layer, velocities increased even more over the sheet layer, which can be seen in Figure 5.12.

5.3.2 Reynolds Shear Stress

Reynolds shear stress provides the strength of flows without seepage and after the application of seepage. Vertical distributions of RSS for the no seepage run, just after application of seepage in the with seepage and over the sheet layer, have been depicted in Figure 5.13. Upon close observation of Figure 5.13 reveals that in the region close to the channel bed, the magnitude of RSS increased approximately by 20-25% just after applying seepage from

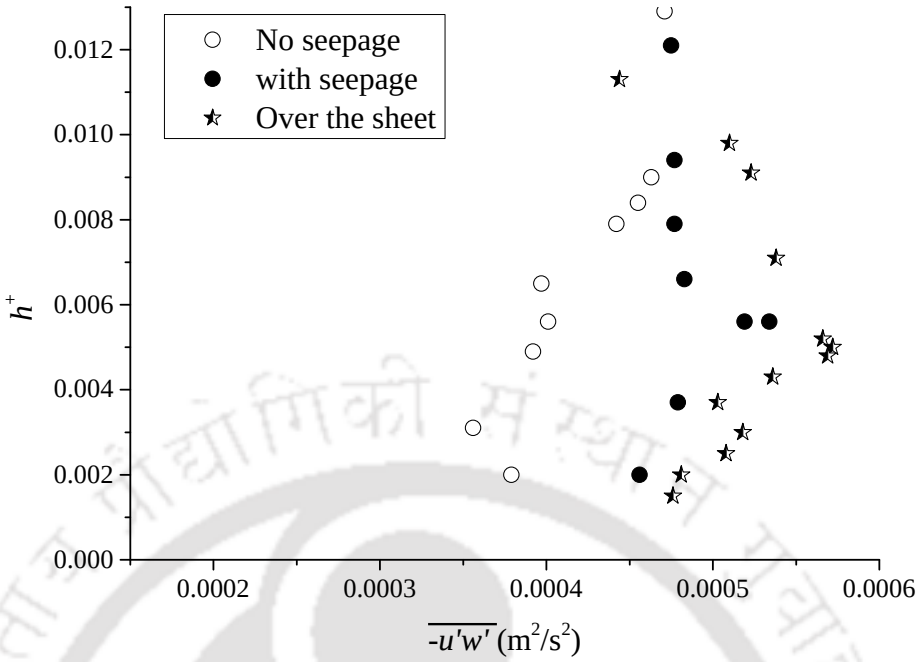

Figure 5.13: Distribution of Reynolds shear stress measured measured in the middle of the test section (8 m from downstream) during the no seepage (Phase-I measurement), the with seepage (Phase-II measurement), and over the sheet layer (Phase-IV measurement) at time between 8 h and 11 h during the with seepage run

that of the no seepage condition. This increase in the RSS suggests the higher momentum transfer occurring near the bed, immediately after the application of seepage in the downward direction. The increase in RSS resulted in increased sediment transport during the with seepage experiment. A significant increase in the RSS has also been observed in the flow over the sheet layer (Figure 5.13).

5.3.3 Integral Scales of Flow

Coherent structures of the turbulent flow are related to the initiation of bed features, which form because of the dominance of turbulent sweep events in the near-bed region (Gyr and Schmid, 1989). Williams and Kemp (1971) and Best (1992) observed the flow parallel ridge on the flat sand bed. Best (1992) claimed that these bed features were developed by coherent turbulent structure and multiple sweeps that keep the bed in mobile bed condition. In the present experiments, a thin layer of dense sediment is observed that start from the upstream side of the test reach and move along the channel. This is not in the pattern of cross-hatch and chevrons as discussed by Best (1992) and Venditti et al. (2005). Venditti et al. (2005) argued that the origin of the cross-hatch pattern and subsequent chevrons are

linked with the integral scales of flow in the near-bed region. They observed that with the consequence of the enhanced flow strength, integral scales of the flow are also increased and that is responsible for the organization of bed deformation. The mechanism behind the initiation of sheet flow in the threshold channel can be accessed through changes in time and integral length scales after the application of downward seepage. In order to describe linkage between the initiation of sheet layer after the application of seepage, time scale and integral length scale were calculated for the near-bed velocity of the no seepage experiment and the with seepage experiment. Integral time scale and length scale are determined in the near-bed region using the 300 s time series collected at ∼5 mm above the bed. An integral time scale indicates the large eddy turnover time at a given point, and an integral length scale suggests the characteristic eddy size in the flow. These eddies are associated with the transfer of momentum and turbulent kinetic energy in the flow. The Eulerian integral time scale E_T is defined as

$$E_T = \int_0^k R(t)dt \tag{5.9}$$

where $R(t)$ is the auto-correlation function, dt is the lag distance, and k is the time at which $R(t)$ started to oscillate about zero (Tennekes and Lumley, 1972). Autocorrelation was calculated using linear interpolation to convert the time series into regularly spaced events. Around $30,000$ samples of instantaneous velocities were collected in 300 s to minimize the error in the calculation of integral scales of flow. Value of k was determined on the basis of autocorrelation at which $R(t) \approx 0.01$ where lag time is 0.01 s. Eulerian integral length scale is calculated using Taylor's (1935) approximation, with the following equation:

$$E_L = E_T \,.\, u \tag{5.10}$$

where u is time mean velocity at a particular point. Integral time scale and length scale are calculated and are represented in Table 5.1. Values of E_T and E_L are increased in the with seepage run compared to the no seepage experiment. Where E_T is varied between 0.179 and 0.521 s, E_L is varied between 0.0469 and 0.145 m. Thus, eddy length and large eddy turnover time are increased significantly in the vicinity of the bed surface. Venditti et al. (2005) emphasized that initiation of the bed features is caused by the larger size of eddies in the vicinity of the bed. Contrary to the experiments of Venditti et al. (2005), which were carried out with increased discharge, the present increment in eddy size can be attributed

Table 5.1: Integral time scales of flow for the no seepage and the with seepage case

Case	Time-mean velocity (u_{5mm}), m/s	Eulerian time scale (E_T), s	Eulerian integral length scale (E_L), m
No seepage (Phase-I measurement)	0.262	0.179	0.0469
With seepage (Phase-II measurement)	0.27	0.295	0.0796
Over the sheet (Phase-IV measurement)	0.28	0.521	0.145

to the effect of downward seepage. Increased eddy size in the near-bed region corresponds to higher momentum and energy transfer and less destruction of turbulent motions. Thus higher levels of turbulence prevail near the bed with an increased eddy size, which results in evolution of the sheet layer in channel with downward seepage.

5.4 Empirical Prediction of Sediment Flow Rate in the Form of Sheet Flow Layer

Prediction of sheet flows is important because a relatively large amount of sediment can be transported within them. Wilson (1987) proposed a linear relationship between sheet thickness and the Shields parameter. Asano (1992) assumed that the thickness of the sheet flow layer might be governed by the dynamic Coulomb yield criterion, which states the proportion between shear stress and normal stress acting on a plane. He also developed a linear law correlating the thickness of sheet flow to the Shields parameter. Sumer et al. (1996) showed that the thickness of the sheet flow increases monotonously with increasing Shields parameters. Pugh and Wilson (1999) stated that the sheet flow sediment concentration profile had a linear shape in the lower section of the layer and a power law tail in the upper section. O'Donoghue and Wright (2004) also fitted a power law curve to the sheet flow sediment concentration profile, which can be used to deduce sheet flow thickness. Experimental results by Capart and Fraccarollo (2011) display a similar division of the sheet flow layer into two sublayers. The sheet flow layer thickness was defined for each individual profile as the vertical distance between the top and bottom boundary of the sheet flow layer. Lanckriet et al. (2014) compared the linear fit to predict sheet thickness and concluded that the linear models generally underpredict the measured sheet thickness. The absence of threshold values, which initiate the sheet flow, limits the predictability of the linear models. Lanckriet et al. (2014) proposed that a prediction based on the mobility number alone reproduces the trend of increasing sheet thickness with increasing shear stress. The mobility

number does not reflect bed shear stress, which is responsible for sediment movement.

The condition simulated in the present experimentation is entirely different from the existing literature. Here, sheet flow has been observed by the increased bed shear stress from its threshold value caused by downward seepage. Because the instantaneous transport rate differs between accelerating and decelerating phases of sheet layer motion, present experimentation goals are to establish a formula for the net transport rate. Horikawa et al. (1982) stated that vertical distributions of advection speed of sediment particles are quite similar to those of water particle velocity: the sand advection speed in the upper layer is almost always equal to the main flow velocity, whereas it decreases in amplitude and advances in phase with a decrease in elevation. Advection speed is governed by the level of turbulence (de Lozar and Hof, 2010), which is in turn defined by the Reynolds number. Thus, it has been attempted to obtain an empirical fit for the rate of sheet layer movement by making two different Reynolds numbers (flow Reynolds number (R_e) and seepage flow Reynolds number (R_{es}) as independent parameters:

$$q_b = f\left(\frac{u_s h}{\nu}, \frac{V_s d_{50}}{\nu}\right) = f(R_e, R_{es}) = a R_e^b e^{-R_{es}^c} \tag{5.11}$$

where q_b is the sheet flow rate. The exponential form given to seepage Reynolds number is to satisfy the boundary conditions of an impermeable channel (zero seepage rate). These

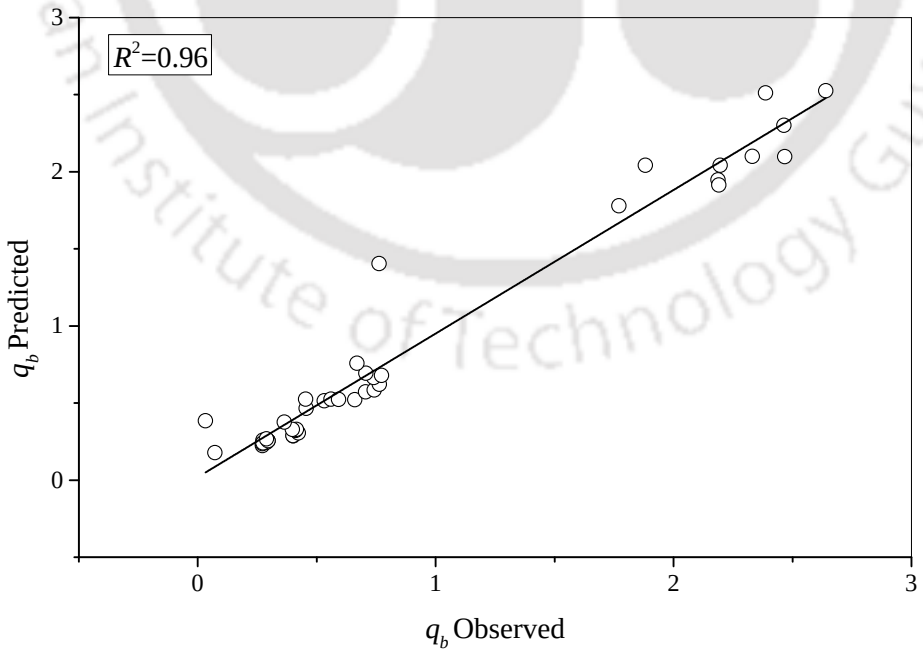

Figure 5.14: Predicted sheet flow rate by Equation 5.12

coefficients ($a, b,$ and, c) were obtained using a least square fitting procedure using all data points. For every two adjacent data points, the error function has been calculated. Then the average of the errors of all the points has been calculated and minimized with respect to these coefficients. Final form of the equation is as follows:

$$q_b = 7.4 R_e^{0.73} e^{R_{es}^{-4.9}} \tag{5.12}$$

Figure 5.14 shows the prediction of sheet flow rate by Equation 5.12 with the corresponding experimental values. Prediction by Equation 5.12 was satisfactory with the experimental data, as the value of the coefficient of regression (R^2) was 0.96 and the Nash-Sutcliffe efficiency index was 0.94.

5.5 Discussion

The results of the threshold sand-bed channel at no seepage and downward seepage conditions are evaluated with temporal variation. They describe how the stable parabolic cross-sectional shape deformed after the application of downward seepage. Downward seepage causes high Shields stress and stream power that lead to distortion of cross-sectional shape and sheet flow initiation. However, with the passage of time Shields stress and stream power become constant (still higher than the threshold value) as the channel is about to attain geometrical stability (as shown in Figures 5.3 and 5.11) with downward seepage. Interestingly, the time required to achieve stability matches the results of Pitlick et al. (2013) on sheet movement caused by high flow discharges. Pitlick et al. (2013) showed that high flow causes the bank distortion because of high Shields stress and with a longer period run (8-10 h). The bank obtained the equilibrium shape, and the corresponding Shields stress was decreased. With time, the parabolic threshold channel under the action of downward seepage evolves into another cross-sectional shape having wider width and reduced flow depth. Widening of the channel happened because of the sediment entrainment from the banks. Sediment is deposited at the center of the channel cross section in the adjacent section and moves as a sheet layer toward the downstream in the channel.

The presence of a sheet layer reduces flow depth in the channel. Thus, formulations were needed to quantify the rate of sheet layer in order to assess the channel downstream flow carrying capacity if it is subjected to downward seepage. Various researchers, as discussed earlier, have put forward empirical formulation to predict the stable sheet thickness. The

present work has made a departure from the existing formulation and developed an empirical formulation to predict the time evolution of a sheet in a stable alluvial channel under the action of downward seepage. Our aims were different from existing knowledge; the same was the case for independent parameters for the formulation. Observing statistical indicators such as R^2 and the Nash-Sutcliffe index, present empirical formulation predicts well with experimental data.

However, this aspect can be further explored with more experimentation and in correlation with field study. The results presented here can be linked to the prevalent sediment depositions in the downstream side and frequent altering of morphological parameters of the alluvial channel with time. With downward seepage, the threshold cross-sectional shape of the channel was forced to alter its perimeter and flow depth as Shields stress increased from 0.0399 (threshold value) to 0.0704 (with seepage).

Turbulence plays a key role in sediment transport mechanisms, which are largely governed by the structure of the turbulent flow in the near-bed region. Downward seepage does initiate sediment movement, which can be inferred from the increased time mean velocities and Reynolds stresses after applying the seepage. The results of integral time scale and length scale define flow characteristics that were measured before onset of the sheet layer. The integral time scale and integral length scale are increased, which suggests higher momentum and energy transfer in the near-bed region. These results provide insight into the coherent structure of turbulent flows that indicates an increase in sediment transport.

5.6 Conclusions

Experimental study on the flow characteristics and sediment transport rate under the condition of downward seepage has been carried out. Impending sediment transport has been observed, causing distortion of the curvilinear cross-sectional profile after the application of downward seepage. Increase in the values of Shields stress and stream power of the flow after the application of downward seepage is responsible for shape distortion and bed material transport. Sediment particles were collected on the bed and transport in the form of a sheet flow layer with the absence of any notable bed features. The center line profile of the sheet flow movement suggests that initally, after the application of downward seepage, the sheet moves faster, but with the period of time its movement slows down. The net effect of sheet development is to increase the cross-sectional area until the developing shape is about to attain equilibrium where Shields stress, thickness of sheet flow, and perimeter of

channel have very minimal variation. The time taken to reach this stage is around 11 h, where the values of Shields stress for no seepage and with seepage were 0.0399 and 0.0704, respectively.

An empirical equation for sheet flow rate has been formulated by considering downward seepage as a parameter. The proposed equation for the sheet flow rate through the experimental study is empirical in nature, where the uniform sand has been considered as bed material. Studies that were carried out in the field show that river sediments are seldom uniform and are generally composed of a mixture of different grain sizes. Hence, the proposed equation can further be modified using the data from actual field observations.

Instantaneous flow measurements show that downward seepage influences the flow process, resulting formation of the sheet layer of sediment particles. Time-mean velocities and Reynolds shear stresses are increased in the near-bed region when downward seepage was applied to the channel. Further, integral time scale and length scales are increased significantly with downward seepage, suggesting increased momentum and energy transfer caused by the larger size of eddies in the near-bed region. Changes in turbulent flow characteristics are showing that sediment transport increases with the application of downward seepage.

"Study how water flows in a valley stream, smoothly and freely between the rocks. Also learn from holy books and wise people. Everything - even mountains, rivers, plants and trees - should be your teacher."

Morihei Ueshiba

6

Conclusions and Recommendations for Future Work

Experimental investigation was carried out to examine the influence of downward seepage on a threshold alluvial channel on two sand beds of median diameter 0.41 mm (fine sand) and 1.1 mm (coarse bed). The experiment framework was designed in two categories: no seepage and with seepage experiments. In this study, role of downward seepage on the development of bed-features in a stable curvilinear cross-sectional shape alluvial was studied. In order to get an insight into the physics behind the initiation of bed-features, turbulent flow parameters were investigated when downward seepage was applied to the channel. With the application of downward seepage, two different types of bed-features such as bedforms and sheet layer were observed on fine and coarse sand beds, respectively. Further, temporal and spatial variations of developing bed-features are analyzed in the presence of downward seepage. Important conclusions from the present study are documented below.

6.1 Role of Downward Seepage on Development of Bedforms and Corresponding Turbulent Flow Structure

The study has been performed to understand the role of turbulent flow characteristics behind the development of bedforms when downward seepage is applied to a threshold fine grained sand (median diameter = 0.41 mm) bed channel. Analysis of experimental

observations demonstrates the changes in turbulent characteristics and geometrical features of a threshold channel under the action of downward seepage. With the application of downward seepage, value of Shields stress increases from its critical value (0.037). This increased Shields stress value is responsible for the deformation of the stable cross-sectional shape of the channel which leads to the development of bedform. In the stretch of the run from 24 h to 31 h after the application of downward seepage, channel achieves another stable cross-sectional shape at higher Shields stress value (0.073).

In the near bed region, streamwise velocities increase with the application of downward seepage. This increase in streamwise velocities is sufficient to increase the movement of particles, which were in the verge of motion earlier. Additional increase in velocities is found because of reduction in depth in the presence of bedforrms. Significant increment in Reynolds shear stress is observed when downward seepage is applied to the channel. Turbulent intensities are increased, which show the increase in the strength of turbulence. Such increment in near-bed velocities, RSS, and TI with downward seepage is an indication of increase in sediment transport and it can cause the the development of bedforms in an otherwise threshold parabolic cross-sectional channel. The distance of the maximum value of RSS from the channel bed increases under the action of downward seepage, indicating an increase in the thickness of sublayer.

Higher order analysis shows that the magnitude of positive values of moments and streamwise TKE fluxes increases in the near-bed region with the application of downward seepage, indicating sediment transport. Significant increase in the magnitude of negative values of moments and vertical TKE-flux supports the argument about increase in sediment transport after the application of the downward seepage. Analysis of conditional RSS distributions show that the contributions from all the events are increased, consequently, the thickness of the sweep-dominated region from the wall is also increased under the action of downward seepage. With the longer period of seepage run (i.e., after 24 h of the application of downward seepage), turbulent characteristics of the flow show reduction of sediment transport and suggests equilibrium state of the channel.

During experiments, it was observed that current ripples across the channel length were developed initially after the application of downward seepage and with the passage of time, these current ripples were transformed into the linguoid ripples. A MATLAB program in terms of bedform tracking tool (BTT) has been applied on the measured bed elevation profiles to evaluate the geometric variables of the bedforms at different time intervals.

Bedforms are observed to be less dispersed in terms of height but larger variability is found for length, crest elevation, trough elevation, and lee face slope in the presence of seepage. In addition, it has been observed that after a certain period of time (from 24 h to 31 h of the seepage run) variation in Shields stress and geometry of bedforms is reduced, this can be interpreted as an equilibrium state of bedform geometry in the channel with applied seepage.

6.2 Statistical Description of Developing Bedforms with Downward Seepage

It has been observed that bedforms are developed on a fine sand bed after the application of downward seepage. Therefore, this work is oriented to quantify the effect of different percentages (15% and 20%) of downward seepage on flow hydrodynamics and bed morphology using statistical analysis. Generation and propagation of bedforms are complex phenomena because of their continuous splitting and amalgamation with different length scales. Small bedforms continuously merge with larger bedforms and larger bedforms continuously split into smaller ripples. Celerity of bedforms has been obtained in order to get knowledge about the statistical behaviour of developing bedforms and has observed that stochastics of bedform celerity follows Rayleigh distribution for both the seepage cases. Tail characteristics of the PDFs of bedform celerity is signified thorough tail indexes of the fitted truncated Pareto distributions and observe that higher percentages of seepage leads to a heavier tail of the PDF of bedform celerity, indicating larger variability in bedform distributions. Celerity of bedforms is found to be decreased because of the dominance of larger bedforms, indicating bedforms of all length scales move at a slower speed in the case of higher percentage of seepage.

Effect of seepage over different spatial scales on bedform characteristics has been analyzed in which bed elevation series are discretized into multiple scales ranging from 2 mm to 500 mm by using Mexican hat wavelet. Cumulative distribution of bedform's height and length deviates from the Gaussian distribution after running the seepage experiments for several hours. Probability distribution function of bedform's dimensions is analyzed for both the seepage discharges and Gamma distribution can be recommended for developing and stable bedforms geometries in the presence of seepage. Statistical analysis is performed and observe that channel bed becomes more inhomogeneous and rough after increasing the seepage discharge. This suggests roughness on the bed increases with the passage of time in the presence of seepage. Analysis of dimensionalized probability distribution functions and

logarithmic exceedance probability show occurrence of larger bed elevation fluctuations. In addition, it has been found that slope of the power spectra increases, signifying the argument of inhomogeneous and rapid variation of bedforms in the case of increased seepage discharge.

For explaining the flow process, turbulent flow parameters such as time-mean velocities, Reynolds shear stresses, and integral scales are analyzed for both the seepage experiments. The increase in streamwise time-mean velocities and Reynolds shear stresses are observed with the application of downward seepage. Magnitude of these parameters increases slightly with an increase in the amount of seepage discharge. In addition to this, eddy length and eddy turnover time get increased after application of downward seepage. It can be concluded that the downward seepage causes higher momentum and energy transfer toward the channel bed, leading to sediment transport and development of bedforms over the fine sand bed. Hence, this can be hypothesized as the result of increased Reynolds shear stresses, streamwise time-average velocities, integral scales of flow under the higher amount of seepage, size and variability of bedforms are increased with the increase in seepage amount.

6.3 Evolution of Sheet Flow over Coarse Sand Bed Channel with Downward Seepage

Flow characteristics and sediment transport rate under the condition of downward seepage have been carried out on a coarse sand bed (median diameter = 1.1 mm) curvilinear cross-sectional shape channel. In all experiments, when seepage in the downward direction was applied, impending sediment transport was observed, which distorted the curvilinear cross-sectional profile. Sediment transport occurred in the form of a sheet flow layer with the absence of any notable bed features such as current ripples and linguoid ripples as observed on fine sand bed. Results show that the values of Shields stress and stream power of the flow are increased after the application of downward seepage, which are responsible for shape distortion and bed material transport in the form of sheet flow. Temporal movement of the sheet flow suggests that initally sheet moves faster but with the period of time (After 8 h) its movement slows down. The net effect of sheet development is to increase the cross-sectional area until the developing shape is about to attain equilibrium in terms of Shields stress and geometrical parameters. The time taken to reach this stage is around 11 h, indicating larger particle settled soon as compared to finer particles. Stable curvilinear cross-sectional shape during no seepage run transformed into trapezoidal shape in the

presence of seepage at higher Shields stress (0.0704). An empirical equation for sheet flow rate has been formulated by considering downward seepage as a dependent parameter.

Reasons behind formation of the sheet layer of sediment particles after the application of downward seepage is linked to instantaneous flow measurements. It is observed that the time-mean velocities and Reynolds shear stresses are increased in the near-bed region when downward seepage was applied to the channel. Also, the integral time scale and length scales are increased significantly with downward seepage, which defines the increased momentum and energy transfer caused by the larger size of eddies in the near-bed region. This suggest sediment transport when water was extracted from channel in the form of downward seepage.

6.4 Limitation and assumption of the study

In this study, it has been considered that the downward seepage is uniform along the channel length. Therefore, the study is limited to understand the effect of uniform seepage only. Steady state condition was maintained within the test section during each measurement. Nature of both types of experiments (no seepage and with seepage) was assumed as non-uniform flow, whereas no seepage conditions referred to the gradually varied flow and seepage conditions were considered as spatially varied flow. These all assumptions were taken to carry out the study.

6.5 Motivations

Results show that downward seepage influences the flow hydrodynamics, sediment transport, and bed morphodynamics in a threshold alluvial channel. These results provide the distinctive morphology of the fine and coarse grained bed-features and turbulent flow structure in a parabolic cross-sectional shape channel. The transition of plane bed condition to development of bed-features in the presence of seepage would have effect on resistance characteristics of natural channel. The results of such transition report in the present work will help in deciphering the different sediment modes and mechanism of seepage affected natural channel. This study can also be implemented in order to investigate the flow resistance, grain sorting, and sediment erosion, in seepage affected natural channels. Besides, these analysis techniques can be easily applied to any real dataset of natural streams bed profile as these are purely statistical analyses of bedform geometry.

Regarding effect of seepage in real life situation, the present work needs to be verified or independently conducted in the field condition to quantify the changes in water flow and sediment flow. Apart from this, seepage is a perennial problem as for as alluvial channels are concerned. As discussed in the introduction, volumetric losses of water are evident by several researchers. It does have effect on sediment transport because it modifies the turbulent characteristics acting over the bed particles.

6.6 Future Work and Recommendations

The present study, understanding of bedforms dynamics and flow process on the laboratory flume in the presence of seepage, opens the door for further detailed investigation regarding bed morphology in natural channels. In this experimental work, only two types of bed sediments were used i.e., fine bed (median diameter = 0.41 mm) and coarse (median diameter = 1.1 mm) bed materials. Therefore, more investigation is needed on different types of grain sizes for getting overall understanding of bed-features dynamics with downward seepage. The present study can be further extended to quantify and signify the bed resistance because of developing bed-features in the presence of seepage for improving the understanding and behavior of alluvial channels. Also, numerical simulation and theoretical analysis can be performed in order to understand the bedform dynamics by considering a downward seepage as an influencing parameter. Results of these studies can be compared with the experimental observations of the present study.

More experiments in the laboratory by using different grain sizes and seepage percentages can be performed to get more clarity about sheet flow dynamics and progradation on a curvilinear cross-sectional shape channel. In this study, the proposed equation for the sheet flow rate through the experimental study is empirical in nature, where the uniform sand has been considered as bed material. Studies that were carried out in the field show that river sediments are seldom uniform and are generally composed of a mixture of different grain sizes. Hence, the proposed equation can further be modified using the data from actual field observations. Similar experimental study can be carried out on cohesive sand bed to get the over all understanding of the natural channels.

Bed structure and grain sorting can be studied in the presence of seepage. Further, present study has been carried out on a mild slope and inflow discharge was provided in accordance to incipient motion condition of bed particles without feeding the sediment externally. However, rivers are complex physical and biological systems. Alluvial systems contain an irregu-

lar granular bed acted upon by temporally and spatially variable fluid forces. Steep mountain streams are especially complex; stones form structures that dominate the mobility of the bed sediment and strongly influence the nature of the flow. In addition, these streams episodically receive large inputs of sediment from adjacent hillslopes that may dominate channel morphology and thus the dynamics of the system. Bed surface arrangements and texture influence the stability of steep channels (Church and Zimmermann, 2007; Hassan et al., 2007). Although many studies have investigated the dynamics of lowland rivers with less variable sediment and flow regimes, little research has focused on steep mountain streams. Understanding of the processes active in the relatively well-studied larger rivers is not easily transferable to steeper channels. Research can be oriented to establish a better understanding of the channel stability and morphology of steep mountain streams, and the effect on ecological communities. A model can be proposed that will incorporate the physical descriptions of entrainment and transport under a wide range of geomorphic and flow conditions. This study can be conducted on flume experiments with episodic sediment inputs and highly unsteady flow to understand the channel stability and the evolution of bed surface structures.

Figure 6.1: Snapshot of Bhagirathi River at Gangotri, origin river of the Ganges (Source: https://goo.gl/i8ZN40)

The future work would have a greater significance in Indian sub-continent because studies

have not been carried out to explore mountain streams in the context of gravel bed and highly unsteady flow. Geographical literature shows that India is known to have various mountainous rivers that contribute significantly in the irrigation, hydropower, navigation, and so forth. For example, in the Himalayan regions, numerous mountain river networks exist and they have a perennial water supply throughout the year in all over the India. The largest river basin of India is the Ganga basin, receiving water from an area bounded by the Himalayas in the north. In addition to this, several rivers (e.g. Indus, Jhelum, Yamuna, Mandakini, Kosi, and Tista) start from high peaks of Himalaya and they contain high energy of flow and bed material as shown in snapshot of the Bhagirathi River (Figure 6.1).

Appendix A

Hydrodynamics of Plane Bed Channels under the Influence of Downward Seepage

Introduction

In alluvial channels, bed-features can vary in shape and size in accordance with channel cross-section. Also, they can turn in different type of forms such as bedforms and sheet layers depending upon the increase in bed shear stress from its critical value provided by the imposed flow. several studies have performed to define the bed-features over sand bed channels. In this regard, sheet flow contributes extensively to bed load transport over mobile bed channels. In the sheet flow, a large amount of sediment is transported in the form of layers of bed material (Gotoh and Sakai, 1997). Characteristics of sheet flow layer are the function of hydraulics of flow and sediment size, for example, many researchers (Wilson, 1989; Asano, 1992; Sumer et al., 1996) observed an approximately linear relation between the nondimensional sheet flow layer thickness and the Shields parameter. However, few researchers (Liu, 1957; Bogardi, 1959; Southard and Dingler, 1971) reported stable beds with little sediment transport and no signatures of bedforms were seen. In addition to this, Venditti et al. (2005) observed that the flat sand bed (median diameter < 0.7 mm) appear to be stable, for the condition of incipient motion for a longer period of run. Also, they found that a little increase in inflow discharge, sediment movement was sporadic in nature and absence of notable bed-features along the channel length up to 2 to 3 hours run.

In spite of the highlighted studies and progress regarding bed-features dynamics till date are not significant to give assured answer to the general questions such as the cause of initiation of bed-features, including variation in physical characteristics, variability, and statistical natures ASCE (2002). In our recent studies (Patel et al., 2015; Deshpande and Kumar, 2016b) observed sheet flow on a curvilinear cross section threshold alluvial channel with coarse grained (median diameter = 1.1 mm) after the application downward seepage. Aforementioned studies are carried out to observe the bed-features on curvilinear shape

cross section sand bed channel, however, influence of seepage has been neglected on their development and flow characteristics on plane bed channel with mobile bed conditions. Therefore, this study is oriented to incorporate the effect of seepage on bed morphology and turbulent flow structure over mobile plane bed channels. In this study, we have observed the sheet layers over mobile bed under the seepage environment and have examined the corresponding turbulent flow characteristics.

Experimental Methodology

In this preliminary study, similar experimental set-up was used as discussed in Chapter 2. Experiments were performed in two categories: (1) when inflow discharge was increased in such a way that no signature of bed features was observed after running the experiment for several hours at no seepage condition (2) when water was extracted in the downward direction through the channel boundary (with seepage experiment) without increasing the inflow discharge. In the no seepage run, discharge was slowly introduced to the channel so that the average value of the shear stress increased gradually until the hydrodynamic forces of the flow were slightly higher with the resistive forces of the bed particles (on the bed surface). This run was continued till 3 to 4 hours and sediment movement was sporadic in nature along the channel length. The increment of inflow discharge was maintained in a way that the bed particles were in mobile condition and no significant bed features were seen in the test section of the channel. At this condition, measurements of geometry, water surface slope, inflow discharge, and flow depth were taken.

Figure A.1 shows the Shields curve amongst Shields for no seepage experiments. It has been observed that values of Shields stress (θ_c) and shear Reynolds number (R_*) are lied on the higher side of variation ($\pm$20%) of Shields curve, indicating slight increase in bed shear stress. This indicates particles in the mobile bed condition and may turn into bedforms if further strength of flow was increased by increasing the inflow discharge. For achieving this condition, several experiments were performed in the manner of no significant presence of bed-features during no seepage run. Further, for investigating the influence of downward seepage on a mobile bed channel, water was extracted through the channel bed in the form of downward seepage without increasing the inflow discharge. During seepage run, seepage discharge, depth of flow, and water surface slope were measured at different time intervals.

A Vectrino$^+$ ADV was used to measure instantaneous flow velocities the centre line of the

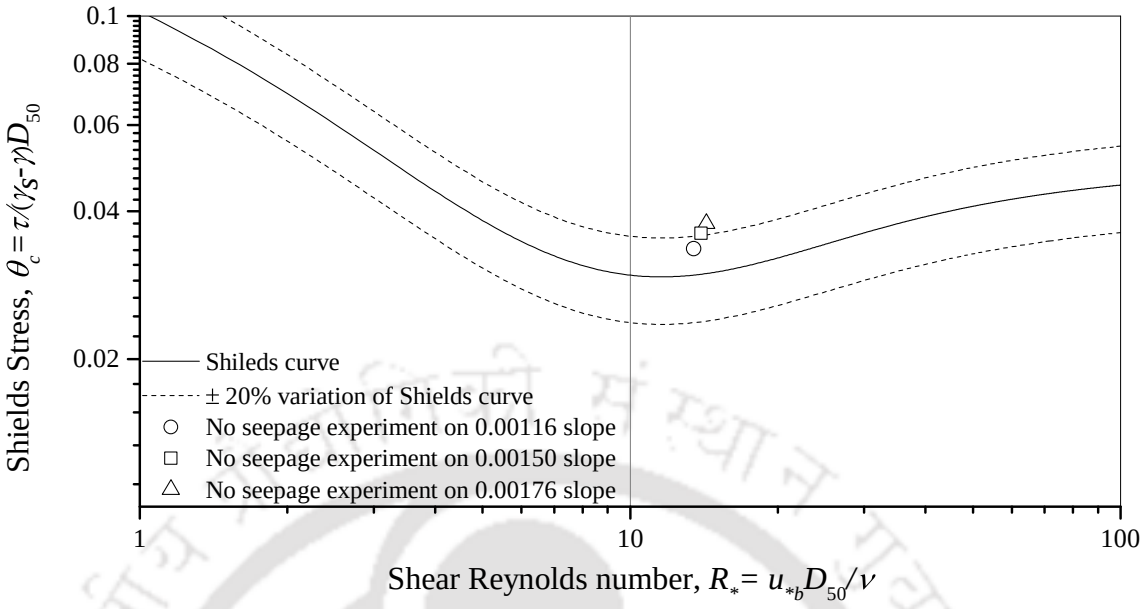

Figure A.1: Shields curve for all the no seepage experiments, where band is indicating the ±20% variation with mean values of Shields curve

channel for all the experimental runs. Samples were collected for five minutes duration at a sampling rate of 100 Hz. Around 20 to 25 velocity samples were recorded in the vertical profile at the middle of the test section (8 m from downstream reach end) during both the experimental runs. The geometric observations of sheet layers in the channel were recorded with the help of a Ultrasonic Ranging System that contains eight transducers. Main channel discharge and depth of flow were given as 0.044 m^3/s and 0.11 m, respectively for the no seepage condition. Similar experiment was performed on three channel bed slopes such as 0.00116, 0.00150, and 0.00176. In these seepage experiments, 10% of the main channel discharge was extracted through the channel bed in the form of downward seepage.

Results and Discussions

In order to understand the turbulent flow structure, time-mean velocities and RSS are obtained for the no seepage and with seepage experiments. Figure A.2 shows the vertical distribution of streamwise time-mean velocities and Reynolds shear stresses against the normalized depth for the no seepage run, seepage run and over the sheet. Careful observation from Figure A.2 ascertains that with the application of seepage, velocities are increased in the near bed region and decreased towards the water surface. This suggests that the higher velocity zone shifts towards the channel boundary under the action of downward seep-

age. Variation in the velocity profile near the channel bed leads to the formation of sheet layers of flowing sediment particles. Time-mean velocities over the sheet layer further increased because of the reduction in the depth of flow because of development of sheet layers. The distribution of RSS provides important information regarding the momentum transfer mechanism in the flows.

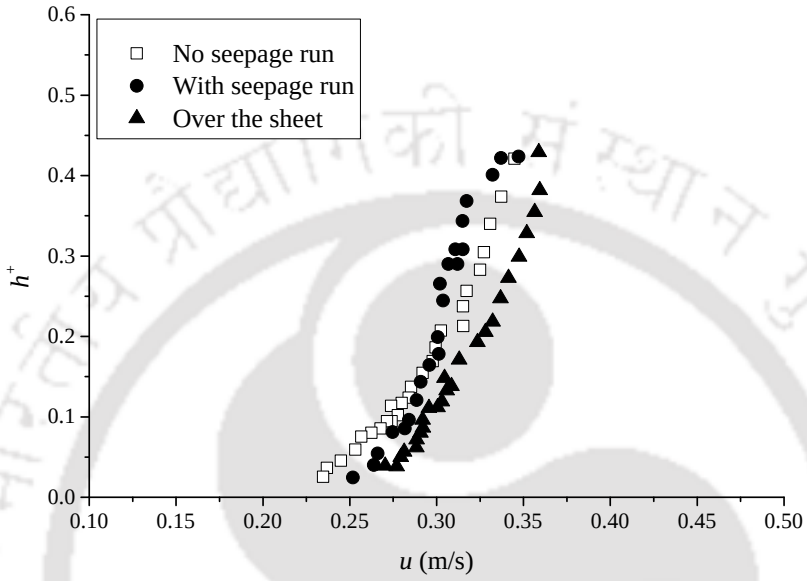

Figure A.2: Profile of the streamwise time-mean velocities for the no seepage run, seepage run, and over the sheet

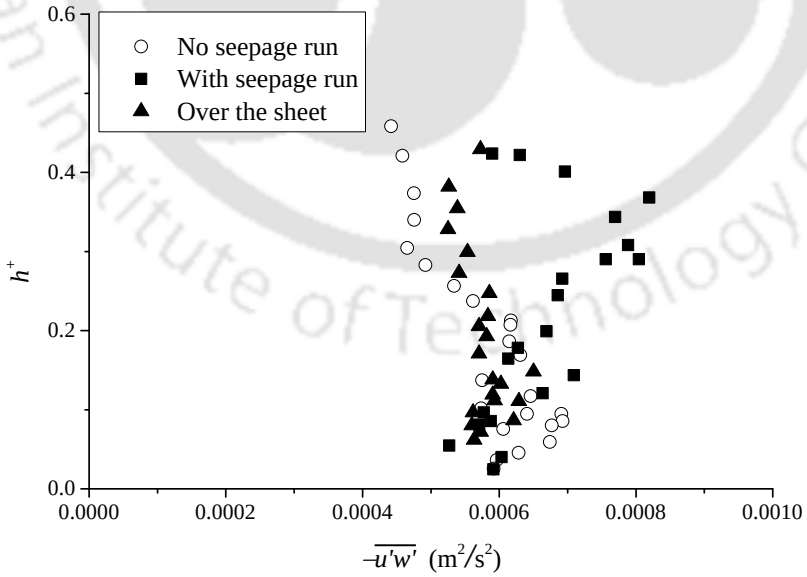

Figure A.3: Profile of the Reynolds shear stresses for the no seepage run, with seepage run, and over the sheet

Figure A.3 shows the vertical distribution of RSS for the no seepage run, seepage run, and over the sheet layer. It can be observed that the RSS are increased significantly after the application of seepage. This suggests higher momentum transfer towards the channel bed, leading to sediment transport and development of sheet layers in the channel. RSS over sheet shows the reduction of bed shear stress it may reduce because of sediment transport in sheet layers and flow required less tractive force to transport the bed particles.

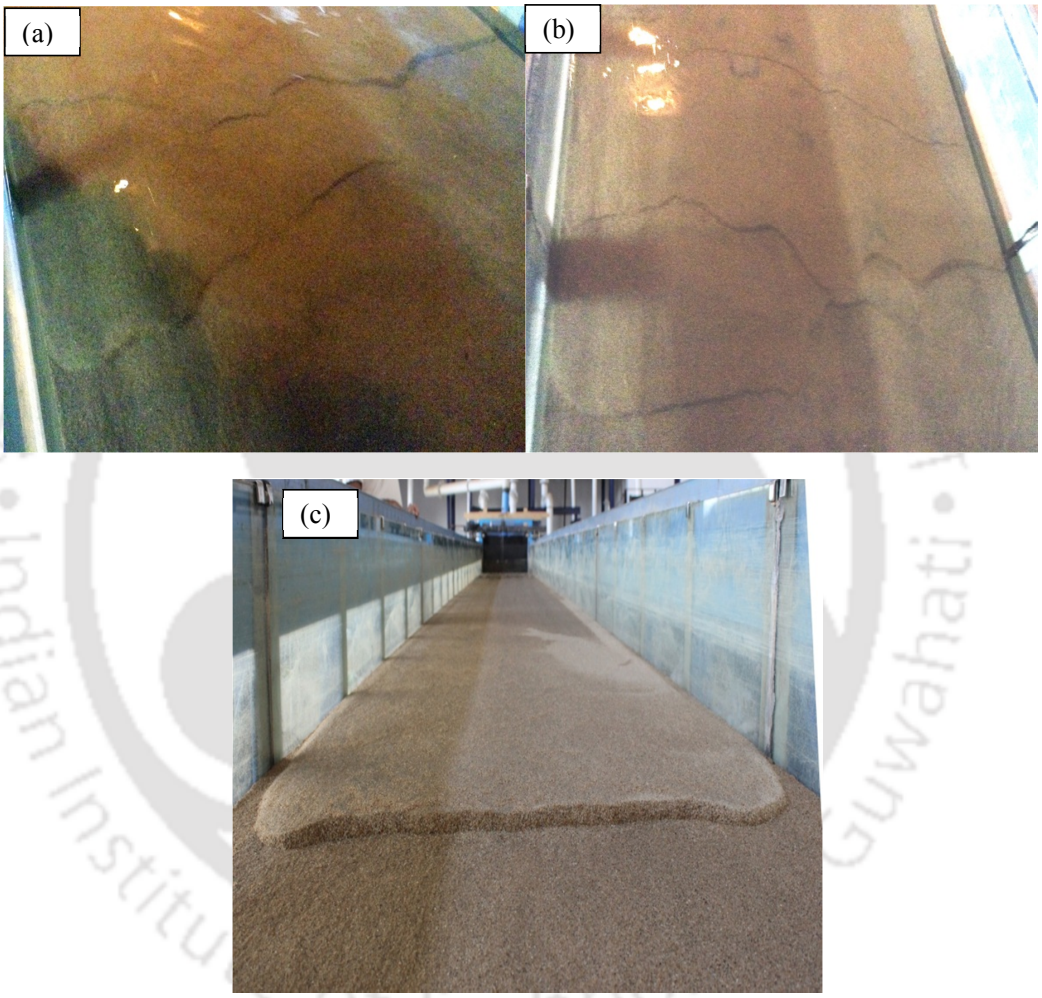

Figure A.4: Snapshot of the channel (a) beginning of seepage experiment (b) during experiment (b) at the end of experiment in the seepage condition

Figure A.4 shows the snapshots of the channel affected by the presence of seepage. It was observed that during the no seepage condition, particles were in the motion condition but no signature of bed-features was seen even after several hours (3 h to 4 h) of the run. However, after the application of seepage, small size of sheet layers developed at upstream section (Figure A.4a) and prograded along the flow. These sheet layers then increased in

their length and thickness by continuously supplied of sediment from upstream side (see Figure A.4b). Also, these sheet layers were combined and formed a thick sheet layer after 24 h of the seepage run (Figure A.4c).

Bibliography

Aban, I. B., Meerschaert, M. M., and Panorska, A. K. (2006). "Parameter estimation for the truncated Pareto distribution." *Journal of the American Statistical Association*, 101(473), 270–277.

Ahmed, A. S. M. and Sato, S. (2003). "A sheetflow transport model for asymmetric oscillatory flows: part ii: mixed grain size sediments." *Coastal Engineering Journal*, 45(03), 339–361.

Allen, J. (2009). "River bedforms: progress and problems." *Modern and Ancient Fluvial Systems/Eds. JD Collinson, J. Lewin. Oxford: Blackwell Publishing Ltd*, 19–33.

Asano, T. (1992). "Observations of granular-fluid mixture under an oscillatory sheet flow." *Coastal Engineering Proceedings*, 1(23).

ASCE (2002). "Flow and transport over dunes." *Journal of Hydraulic Engineering*, 128(8), 726–728.

Ashley, G. M. et al. (1990). "Classification of large-scale subaqueous bedforms: a new look at an old problem-SEPM bedforms and bedding structures." *Journal of Sedimentary Research*, 60(1).

Baas, J. H. (1994). "A flume study on the development and equilibrium morphology of current ripples in very fine sand." *Sedimentology*, 41(2), 185–209.

Baas, J. H. (1999). "An empirical model for the development and equilibrium morphology of current ripples in fine sand." *Sedimentology*, 46(1), 123–138.

Bagnold, R. (1977). "Bed load transport by natural rivers." *Water Resources Research*, 13(2), 303–312.

Bagnold, R. A. (1966). *An approach to the sediment transport problem from general physics*. US government printing office.

Bakker, W., Van Kesteren, W., and Yu, Z. (1989). "Grain-grain interaction in oscillating sheetflow." *Coastal Engineering 1988*, 718–731.

Bayazit, M. (1976). "Free surface flow in a channel of large relative roughness." *Journal of Hydraulic Research*, 14(2), 115–126.

Bennett, J. P. (1995). "Algorithm for resistance to flow and transport in sand-bed channels." *Journal of Hydraulic Engineering*, 121(8), 578–590.

Berenbrock, C. (1999). "Streamflow gains and losses in the Lower Boise River Basin, Idaho, 1996-97." *Report No. 99-4105*.

Best, J. (1992). "On the entrainment of sediment and initiation of bed defects: insights from recent developments within turbulent boundary layer research." *Sedimentology*, 39(5), 797–811.

Best, J. and Kostaschuk, R. (2002). "An experimental study of turbulent flow over a low-angle dune." *Journal of Geophysical Research: Oceans*, 107(C9).

Bogardi, J. (1959). "Hydraulic similarity of river models with movable bed." *Acta Technol. Acad. Sci. Hung*, 24, 417–445.

Brumley, B. H., Cabrera, R. G., Deines, K. L., and Terray, E. A. (1991). "Performance of a broad-band acoustic doppler current profiler." *IEEE Journal of Oceanic Engineering*, 16(4), 402–407.

Brunke, M. and Gonser, T. (1997). "The ecological significance of exchange processes between rivers and groundwater." *Freshwater Biology*, 37(1), 1–33.

Bucher, W. H. (1919). "On ripples and related sedimentary surface forms and their paleogeographic interpretation." *American Journal of Science*, (279), 149–210.

Cao, D. and Chiew, Y. M. (2014). "Suction effects on sediment transport in closed-conduit flows." *Journal of Hydraulic Engineering*, 140(5).

Capart, H. and Fraccarollo, L. (2011). "Transport layer structure in intense bed-load." *Geophysical Research Letters*, 38(20).

Carling, P. A. (1999). "Subaqueous gravel dunes." *Journal of Sedimentary Research*, 69(3).

Carlson, R. and Petrich, C. (1999). "New York Canal geologic cross-section, seepage gain/loss data, and ground water hydrographs: compilation and interim findings." *Report No. IWRRI-2002-09*.

Carr, J. E., Chase, E. B., Paulson, R. W., and Moody, D. W. (1990). "National water summary 1987: hydrologic events and water supply and use." *Report No. 2350*, United States Geological Survey.

Chen, X. and Chiew, Y. M. (2004). "Velocity distribution of turbulent open-channel flow with bed suction." *Journal of Hydraulic Engineering*, 130(2), 140–148.

Cheng, N. S. and Chiew, Y. M. (1998). "Turbulent open-channel flow with upward seepage." *Journal of Hydraulic Research*, 36(3), 415–431.

Cheng, N. S. and Chiew, Y. M. (1999). "Incipient sediment motion with upward seepage." *Journal of Hydraulic Research*, 37(5), 665–681.

Church, M. and Zimmermann, A. (2007). "Form and stability of step-pool channels: Research progress." *Water Resources Research*, 43(3).

Coleman, S. E. and Melville, B. W. (1994). "Bed-form development." *Journal of Hydraulic Engineering*, 120(5), 544–560.

Coleman, S. E. and Melville, B. W. (1996). "Initiation of bed forms on a flat sand bed." *Journal of Hydraulic Engineering*, 122(6), 301–310.

Conley, D. C. and Inman, D. L. (1992). "Field observations of the fluid-granular boundary layer under near-breaking waves." *Journal of Geophysical Research: Oceans*, 97(C6), 9631–9643.

Cornish, V. (1901). "On sand-waves in tidal currents." *The Geographical Journal*, 18(2), 170–200.

De La Beche, H. T. (1851). *The geological observer*. Blanchard and Lea.

de Lozar, A. and Hof, B. (2010). "Universality at the onset of turbulence in shear flows." *arXiv preprint arXiv:1001.2481*.

Deacon, G. (1894). "Discussion of paper on estuaries by hl partiot." *Proceedings of the Institution of Civil Engineers*, 118, 47–189.

Defina, A. (2003). "Numerical experiments on bar growth." *Water Resources Research*, 39(4).

Deshpande, V. and Kumar, B. (2016a). "Advent of sheet flow in suction affected alluvial channels." *Environmental Fluid Mechanics*, 16(1), 25–44.

Deshpande, V. and Kumar, B. (2016b). "Turbulent flow structures in alluvial channels with curved cross-sections under conditions of downward seepage." *Earth Surface Processes and Landforms*, 41(8), 1073–1087 ESP-15-0129.R2.

Dey, S., Das, R., Gaudio, R., and Bose, S. K. (2012). "Turbulence in mobile-bed streams." *Acta Geophysica*, 60(6), 1547–1588.

Dey, S. and Nath, T. K. (2010). "Turbulence characteristics in flows subjected to boundary injection and suction." *Journal of Engineering Mechanics*, 136(7), 877–888.

Dey, S., Sarkar, S., and Ballio, F. (2011). "Double-averaging turbulence characteristics in seeping rough-bed streams." *Journal of Geophysical Research: Earth Surface*, 116(F3).

Dingler, J. R. and Inman, D. L. (1976). "Wave-formed ripples in nearshore sands." *Coastal Engineering Proceedings*, 1(15).

Diplas, P. (1990). "Characteristics of self-formed straight channels." *Journal of Hydraulic Engineering*, 116(5), 707–728.

Dohmen-Janssen, C. M., Hassan, W. N., and Ribberink, J. S. (2001). "Mobile-bed effects in oscillatory sheet flow." *Journal of Geophysical Research: Oceans (1978–2012)*, 106(C11), 27103–27115.

Dohmen-Janssen, C. M., Kroekenstoel, D. F., Hassan, W. N., and Ribberink, J. S. (2002). "Phase lags in oscillatory sheet flow: experiments and bed load modelling." *Coastal Engineering*, 46(1), 61–87.

Dong, L. and Sato, S. (2011). "Sheetflow sediment transport under asymmetric waves and strong currents." *Coastal Engineering Proceedings*, 1(32), sediment–17.

Dong, L. P., Sato, S., and Liu, H. (2013). "A sheetflow sediment transport model for skewed-asymmetric waves combined with strong opposite currents." *Coastal Engineering*, 71, 87–101.

DuBuat, P. L. G. (1779). *Principes d'hydraulique*. Paris: L'imprimérie de monsieur, Il Giardino di Archimede.

Dukker, P. (1994). *Seepage Losses from the Lower Gugera Branch Canal, Punjab, Pakistan*, Vol. 134. IWASRI.

Faruque, M. A. A. and Balachandar, R. (2011). "Seepage effects on turbulence characteristics in an open channel flow." *Canadian Journal of Civil Engineering*, 38(7), 785–799.

Fipps, G. (2005). "Potential water savings in irrigated agriculture for the Rio Grande planning region (region m)." *Texas Cooperative Extension, Texas A&M University System*.

Flores, N. Z. and Sleath, J. F. (1998). "Mobile layer in oscillatory sheet flow." *Journal of Geophysical Research: Oceans (1978–2012)*, 103(C6), 12783–12793.

Frias, C. E. and Abad, J. D. (2013). "Mean and turbulent flow structure during the amalgamation process in fluvial bed forms." *Water Resources Research*, 49(10), 6548–6560.

Frisch, U. (1995). *Turbulence: the legacy of AN Kolmogorov*. Cambridge university press.

Gabel, S. L. (1993). "Geometry and kinematics of dunes during steady and unsteady flows in the Calamus River, Nebraska, USA." *Sedimentology*, 40(2), 237–269.

Garde, R. (1995). *History of fluvial hydraulics*. New Age International.

Gilbert, G. K. and Murphy, E. C. (1914). *The transportation of debris by running water*. Number 86. US Government Printing Office.

Giri, S. and Shimizu, Y. (2006). "Numerical computation of sand dune migration with free surface flow." *Water Resources Research*, 42(10).

Goring, D. G. and Nikora, V. I. (2002). "Despiking acoustic Doppler velocimeter data." *Journal of Hydraulic Engineering*, 128(1), 117–126.

Gotoh, H. and Sakai, T. (1997). "Numerical simulation of sheetflow as granular material." *Journal of Waterway, Port, Coastal, and Ocean Engineering*, 123(6), 329–336.

Graf, W. H. (1984). *Hydraulics of sediment transport*. Water Resources Publication.

Grass, A. (1971). "Structural features of turbulent flow over smooth and rough boundaries." *Journal of Fluid Mechanics*, 50(02), 233–255.

Grinvald, D. and Nikora, V. (1988). "River turbulence." *Hydrometeoizdat, Leningrad, Russia*.

Guglielmini (Gulieminus), D. (1665–1710). "Italian hydraulician." *Professor of mathematics in Bologna, member of the Paris and Berlin Academics of Sciences, Fellow of the Royal Society of London*, (199).

Gyr, A. and Kinzelbach, W. (2004). "Bed forms in turbulent channel flow." *Applied Mechanics Reviews*, 57(1), 77–93.

Gyr, A. and Schmid, A. (1989). "The different ripple formation mechanism." *Journal of Hydraulic Research*, 27(1), 61–74.

Harrison, S. (1968). "The effects of groundwater seepage on stream regime—a lab study." *A thesis presented to University of North Dakota, in partial fulfillment of the requirements for the degree of Doctor of Philosophy*.

Hassan, M. A., Smith, B. J., Hogan, D. L., Luzi, D. S., Zimmermann, A. E., and Eaton, B. C. (2007). "18 sediment storage and transport in coarse bed streams: scale considerations." *Developments in Earth Surface Processes*, 11, 473–496.

Hey, R. D. and Thorne, C. R. (1986). "Stable channels with mobile gravel beds." *Journal of Hydraulic Engineering*, 112(8), 671–689.

Horikawa, K., Watanabe, A., and Katori, S. (1982). "Sediment transport under sheet flow condition." *Coastal Engineering Proceedings*, 1(18).

Ikeda, S., Parker, G., and Kimura, Y. (1988). "Stable width and depth of straight gravel rivers with heterogeneous bed materials." *Water Resources Research*, 24(5), 713–722.

Inglis, C. C. (1949). *The behaviour and control of rivers and canals (with the aid of models)*. Number 13. Yeravda Prison Press.

Inman, D., Jenkins, S., Hicks, D., and Kim, H. (1986). "Oscillatory bursting over beds of fine sand." *Ref. Ser. 86*, 13, 16.

Jackson, R. G. (1976). "Sedimentological and fluid-dynamic implications of the turbulent bursting phenomenon in geophysical flows." *Journal of Fluid Mechanics*, 77(03), 531–560.

Jerolmack, D. J. and Mohrig, D. (2005). "A unified model for subaqueous bed form dynamics." *Water Resources Research*, 41(12).

Jha, S., Grayson, R., and Rutherfurd, I. (2003). "Estimating catchment-scale sediment yield from bank erosion using simple distributed variables: an example from Victoria, Australia." *Modelling and Simulation Society of Australia and New Zealand, Modsim*.

Jones, J. and Mulholland, P. (2000). *Streams and Groundwaters*. Academic Press, San Diego.

Kapdasli, M. and Dyer, K. (1986). "Threshold conditions for sand movement on a rippled bed." *Geo-marine Letters*, 6(3), 161–164.

Karambas, T. V. (2003). "Modelling of infiltration-exfiltration effects of cross-shore sediment transport in the swash zone." *Coastal Engineering Journal*, 45(1), 63–82.

Kavcar, P. C. and Wright, S. J. (2009). "Experimental results on the stability of non-cohesive sediment beds subject to vertical pore water flux." *American Society of Civil Engineers*, Vol. 342, 3562–3571.

King Jr, D. B. (1991). "Studies in oscillatory flow bedload sediment transport." Ph.D. thesis, Ph.D. thesis.

Kinzli, K.-D., Martinez, M., Oad, R., Prior, A., and Gensler, D. (2010). "Using an ADCP to determine canal seepage loss in an irrigation district." *Agricultural Water Management*, 97(6), 801–810.

Kondrat'ev, N., Lyapin, A., Popov, I., Pin'kovskii, S., Fedorov, N., and Yakunin, I. (1959). "Channel processes." *Leningrad: Gidrometeoizdat*.

Krishnamurthy, K. and Rao, S. (1969). "Theory and experiment in canal seepage estimation using radioisotopes." *Journal of Hydrology*, 9(3), 277–293.

Krogstad, P.-Å. and Kourakine, A. (2000). "Some effects of localized injection on the turbulence structure in a boundary layer." *Physics of Fluids (1994-present)*, 12(11), 2990–2999.

Krogstadt, P.-Å. and Antonia, R. (1999). "Surface roughness effects in turbulent boundary layers." *Experiments in Fluids*, 27(5), 450–460.

Kumar, P. and Foufoula-Georgiou, E. (1997). "Wavelet analysis for geophysical applications." *Reviews of Geophysics*, 35(4), 385–412.

Lanckriet, T., Puleo, J. A., Masselink, G., Turner, I. L., Conley, D., Blenkinsopp, C., and Russell, P. (2014). "Comprehensive field study of swash-zone processes. II: Sheet flow sediment concentrations during quasi-steady backwash." *Journal of Waterway, Port, Coastal, and Ocean Engineering*, 140(1), 29–42.

Lane, E. W. (1953). "Progress report on studies on the design of stable channels by the Bureau of Reclamation." Vol. 79, Separate 280, American Society of Civil Engineers, 1–31.

Langlois, V. and Valance, A. (2007). "Initiation and evolution of current ripples on a flat sand bed under turbulent water flow." *The European Physical Journal E*, 22(3), 201–208.

Leclair, S. F., Bridge, J. S., and Wang, F. (1997). "Preservation of cross-strata due to migration of subaqueous dunes over aggrading and non-aggrading beds: comparison of experimental data with theory." *Geoscience Canada*, 24(1).

Li, L. and Sawamoto, M. (1995). "Experiments on sediment transport in sheet-flow regime under oscillatory flow." *Coastal Engineering in Japan*, 38(2), 143–156.

Liu, H. K. (1957). "Mechanics of sediment-ripple formation." *Journal of the Hydraulics Division*, 83(2), 1–23.

Liu, X. and Chiew, Y. M. (2012). "Effect of seepage on initiation of cohesionless sediment transport." *Acta Geophysica*, 60(6), 1778–1796.

Liu, X.-x. and Chiew, Y. m. (2014). "Effect of upward seepage on bedload transport rate." *Water Science and Engineering*, 7(2), 208–217.

Lu, S. and Willmarth, W. (1973). "Measurements of the structure of the Reynolds stress in a turbulent boundary layer." *Journal of Fluid Mechanics*, 60(3), 481–511.

Lu, Y. (2006). "Seepage effects on dune geometry and turbulence flow characteristics." Ph.D. thesis, Ph.D. thesis.

Lu, Y. and Chiew, Y. M. (2004). "Using seepage as an auxiliary method for pier-scour countermeasure." *Second International Conference on Scour and Erosion (ICSE-2)*, 14–17.

Lu, Y. and Chiew, Y. M. (2007a). "Seepage effects on dune dimensions." *Journal of Hydraulic Engineering*, 133(5), 560–563.

Lu, Y. and Chiew, Y. M. (2007b). "Suction effects on turbulence flows over a dune bed." *Journal of Hydraulic Research*, 45(5), 691–700.

Lu, Y., Chiew, Y. M., and Cheng, N.-S. (2008). "Review of seepage effects on turbulent open-channel flow and sediment entrainment." *Journal of Hydraulic Research*, 46(4), 476–488.

Maclean, A. (1991a). "Open channel velocity profiles over a zone of rapid infiltration." *Journal of Hydraulic Research*, 29(1), 15–27.

Maclean, A. and Willetts, B. (1986). "Measurement of boundary shear stress in non-uniform open channel flow." *Journal of Hydraulic Research*, 24(1), 39–51.

Maclean, A. G. (1991b). "Bed shear stress and scour over bed-type river intake." *Journal of Hydraulic Engineering*, 117(4), 436–451.

Mahmood, K., Haque, M., and Choudri, A. (1988). *Mechanics of Alluvial Channels*. Water Resources Publications, Littleton, Colorado.

Mallat, S. (1998). *A wavelet tour of signal processing*. Academic press.

Marsh, N. A., Western, A. W., and Grayson, R. B. (2004). "Comparison of methods for predicting incipient motion for sand beds." *Journal of Hydraulic Engineering*, 130(7), 616–621.

Martin, C. A. and Gates, T. K. (2014). "Uncertainty of canal seepage losses estimated using flowing water balance with acoustic Doppler devices." *Journal of Hydrology*, 517, 746–761.

Millar, R. G. and Quick, M. C. (1993). "Effect of bank stability on geometry of gravel rivers." *Journal of Hydraulic Engineering*, 119(12), 1343–1363.

Myrhaug, D. and Holmedal, L. E. (2007). "Mobile layer thickness in sheet flow beneath random waves." *Coastal engineering*, 54(8), 577–585.

Nelson, J. M., McLean, S. R., and Wolfe, S. R. (1993). "Mean flow and turbulence fields over two-dimensional bed forms." *Water Resources Research*, 29(12), 3935–3953.

Nelson, J. M., Shreve, R. L., McLean, S. R., and Drake, T. G. (1995). "Role of near-bed turbulence structure in bed load transport and bed form mechanics." *Water Resources Research*, 31(8), 2071–2086.

Nelson, T. R., Voulgaris, G., and Traykovski, P. (2013). "Predicting wave-induced ripple equilibrium geometry." *Journal of Geophysical Research: Oceans*, 118(6), 3202–3220.

Nezu, I. (1977). "Turbulent structure in open-channel flows." Ph.D. thesis, Kyoto University, Kyoto University.

Nezu, I. and Nakagawa, H. (1993). *Turbulence in Open Channel Flows*. Balkema, Rotterdam, The Netherlands.

Nikora, V. and Smart, G. (1997). "Turbulence characteristics of New Zealand gravel-bed rivers." *Journal of Hydraulic Engineering*, 123(9), 764–773.

Nikora, V. I. and Goring, D. G. (2001). "Extended self-similarity in geophysical and geological applications." *Mathematical Geology*, 33(3), 251–271.

Nikora, V. I., Sukhodolov, A. N., and Rowinski, P. M. (1997). "Statistical sand wave dynamics in one-directional water flows." *Journal of Fluid Mechanics*, 351, 17–39.

Nordin, C. F. and Algert, J. H. (1966). "Spectral analysis of sand waves." *Journal of the Hydraulics Division*, 92(5), 95–114.

Nowell, A. R. and Jumars, P. A. (1987). "Flumes: theoretical and experimental considerations for simulation of benthic environments." *Oceanogr Mar Biol*, 25, 91–112.

O'Donoghue, T. and Wright, S. (2004). "Concentrations in oscillatory sheet flow for well sorted and graded sands." *Coastal Engineering*, 50(3), 117–138.

Oldenziel, D. M. and Brink, W. E. (1974). "Influence of suction and blowing on entrainment of sand particles." *Journal of the Hydraulics Division*, 100(7), 935–949.

Ostfeld, R. (2011). "Bedform formation in the glastonbury meanders of the connecticut river." Ph.D. thesis, Wesleyan University, Wesleyan University.

Partiot, H. (1871). "Mémoire sur les sables de la loire." *Ann Ponts Chaussees*, 5(1), 233–292.

Patel, M., Deshpande, V., and Kumar, B. (2015). "Turbulent characteristics and evolution of sheet flow in an alluvial channel with downward seepage." *Geomorphology*, 248, 161–171.

Pitlick, J., Marr, J., and Pizzuto, J. (2013). "Width adjustment in experimental gravel-bed channels in response to overbank flows." *Journal of Geophysical Research: Earth Surface*, 118(2), 553–570.

Prinos, P. (1995). "Bed-suction effects on structure of turbulent open-channel flow." *Journal of Hydraulic Engineering*, 121(5), 404–412.

Pugh, F. J. and Wilson, K. C. (1999). "Velocity and concentration distributions in sheet flow above plane beds." *Journal of Hydraulic Engineering*, 125(2), 117–125.

Raja, R., Kumar, A., and Chhabra, S. (1983). "Estimation of seepage losses from an unlined channel–a field study by nuclear techniques." *Proceedings*, Vol. II, Hydraulics, CBIP, Fiftieth annual research and development session, Simla, Himachala Pradesh, India.

Rao, A. R. (2005). "A digital micro-manometer for very low pressure measurement." *J. Instrum. Soc. India*, 35(1), 54–64.

Rao, A. R. and Sitaram, N. (1999). "Stability and mobility of sand-bed channels affected by seepage." *Journal of Irrigation and Drainage Engineering*, 125(6), 370–379.

Rao, A. R. and Sreenivasulu, G. (2009). "Design of plane sand-bed channels affected by seepage." *Periodica Polytechnica. Civil Engineering*, 53(2), 81.

Rao, A. R., Sreenivasulu, G., and Kumar, B. (2011). "Geometry of sand-bed channels with seepage." *Geomorphology*, 128(3), 171–177.

Raudkivi, A. J. (1997). "Ripples on stream bed." *Journal of Hydraulic Engineering*, 123(1), 58–64.

Raudkivi, A. J. and Witte, H.-H. (1990). "Development of bed features." *Journal of Hydraulic Engineering*, 116(9), 1063–1079.

Raupach, M. (1981). "Conditional statistics of Reynolds stress in rough-wall and smooth-wall turbulent boundary layers." *Journal of Fluid Mechanics*, 108, 363–382.

Revil-Baudard, T. and Chauchat, J. (2013). "A two-phase model for sheet flow regime based on dense granular flow rheology." *Journal of Geophysical Research: Oceans*, 118(2), 619–634.

Ribberink, J. S. and Al-Salem, A. A. (1994). "Sediment transport in oscillatory boundary layers in cases of rippled beds and sheet flow." *Journal of Geophysical Research: Oceans*, 99(C6), 12707–12727.

Richardson, J., Abt, S., and Richardson, E. (1985). "Inflow seepage influence on straight alluvial channels." *Journal of Hydraulic Engineering*, 111(8), 1133–1147.

Robert, A. and Uhlman, W. (2001). "An experimental study on the ripple-dune transition." *Earth Surface Processes and Landforms*, 26, 615–629.

Rosgen, D. L. (2006). "The natural channel design method for river restoration." *World Environmental and Water Resource Congress*.

Schindler, R. J. and Robert, A. (2005). "Flow and turbulence structure across the ripple–dune transition: an experiment under mobile bed conditions." *Sedimentology*, 52(3), 627–649.

Sharma, H. and Chawla, A. (1975). "Manual of canal lining." *Report No. 14*, Central Board of Irrigation and Power, New Delhi.

Simons, D. B. (1961). "Forms of bed roughness in alluvial channels." *Journal of the Hydraulics Division, Proc. ASCE*, 87(3), 87–105.

Simons, D. B., Richardson, E. V., and Nordin, C. F. (1965). *Bedload equation for ripples and dunes*. US Government Printing Office.

Singh, A., Fienberg, K., Jerolmack, D. J., Marr, J., and Foufoula-Georgiou, E. (2009). "Experimental evidence for statistical scaling and intermittency in sediment transport rates." *Journal of Geophysical Research: Earth Surface*, 114(F1).

Singh, A., Lanzoni, S., Wilcock, P. R., and Foufoula-Georgiou, E. (2011). "Multiscale statistical characterization of migrating bed forms in gravel and sand bed rivers." *Water Resources Research*, 47(12).

Singh, A., Porté-Agel, F., and Foufoula-Georgiou, E. (2010). "On the influence of gravel bed dynamics on velocity power spectra." *Water Resources Research*, 46(4).

Sorby, H. C. (1859). "On the structures produced by the currents present during the deposition of stratified rocks." *The geologist*, 2(4), 137–147.

Soulsby, R., Whitehouse, R., and Marten, K. (2012). "Prediction of time-evolving sand ripples in shelf seas." *Continental Shelf Research*, 38, 47–62.

Southard, J. B. and Dingler, J. R. (1971). "Flume study of ripple propagation behind mounds on flat sand beds." *Sedimentology*, 16(3-4), 251–263.

Sreenivasulu, G., Kumar, B., and Ramakrishna Rao, A. (2011). "Variation of stream power with seepage in sand-bed channels." *Water SA*, 37(1), 115–119.

Sreenivasulu, G., Rao, A. R., Kumar, B., and Tripathi, S. (2010). "Analysis of gradually and spatially varied flow in sand-bed channels." *Journal of Hydraulic Research*, 48(2), 274–279.

Sukhodolov, A., Thiele, M., and Bungartz, H. (1998). "Turbulence structure in a river reach with sand bed." *Water Resources Research*, 34(5), 1317–1334.

Sumer, B. M., Chua, L. H., Cheng, N.-S., and Fredsøe, J. (2003). "Influence of turbulence on bed load sediment transport." *Journal of Hydraulic Engineering*, 129(8), 585–596.

Sumer, B. M., Kozakiewicz, A., Fredsøe, J., and Deigaard, R. (1996). "Velocity and concentration profiles in sheet-flow layer of movable bed." *Journal of Hydraulic Engineering*, 122(10), 549–558.

Tanji, K. K. and Kielen, N. C. (2002). "Agricultural drainage water management in arid and semi-arid areas." *FAO irrigation and drainage paper*.

Tennekes, H. and Lumley, J. L. (1972). *A first course in turbulence*. MIT press.

Thorne, C. (1998). "River width adjustment. I: Processes and mechanisms." *Journal of Hydraulic Engineering*, 124(9), 881–902.

Turner, I. L. (1995). "Simulating the influence of groundwater seepage on sediment transported by the sweep of the swash zone across macro-tidal beaches." *Marine Geology*, 125(1), 153–174.

Van der Mark, C. and Blom, A. (2007). "A new and widely applicable tool for determining the geometric properties of bedforms." *University of Twente, Enschede*.

Van der Mark, C., Blom, A., and Hulscher, S. (2008). "Quantification of variability in bedform geometry." *Journal of Geophysical Research: Earth Surface*, 113(F3).

van Rijn, L. C. (1982). "Equivalent roughness of alluvial bed." *Journal of Hydraulic Engineering*, 108(10), 1215–1218.

Velikanov, M. (1955). *Dynamics of alluvial streams*, Vol. II. Sediment and bed flow.

Venditti, J. G., Church, M. A., and Bennett, S. J. (2005). "Bed form initiation from a flat sand bed." *Journal of Geophysical Research: Earth Surface (2003–2012)*, 110(F1).

Venugopal, V., Roux, S. G., Foufoula-Georgiou, E., and Arneodo, A. (2006). "Revisiting multifractality of high-resolution temporal rainfall using a wavelet-based formalism." *Water Resources Research*, 42(6).

Wang, W. and Shen, H. (1980). "Statistical properties of alluvial bed forms." *Proc. 3rd Int. Symposium on Stochastic Hydraulics*, 371–389.

Watters, G. Z. and Rao, M. V. (1971). "Hydrodynamic effects of seepage on bed particles." *Journal of the Hydraulics Division*, 97(3), 421–439.

Wilbers, A. (2004). *The development and hydraulic roughness of subaqueous dunes*. Utrecht.

Willetts, B. B. and Drossos, M. E. (1975). "Local erosion caused by rapid forced infiltration." *Journal of the Hydraulics Division*, 101(ASCE# 11796 Proceeding).

Williams, P. B. and Kemp, P. H. (1971). "Initiation of ripples on flat sediment beds." *Journal of Hydraulic Engineering*, 97(4), 502–522.

Wilson, K. (1989). "Friction of wave-induced sheet flow." *Coastal Engineering*, 12(4), 371–379.

Wilson, K. C. (1987). "Analysis of bed-load motion at high shear stress." *Journal of Hydraulic Engineering*, 113(1), 97–103.

Wobus, C. W., Kean, J. W., Tucker, G. E., and Anderson, R. S. (2008). "Modeling the evolution of channel shape: Balancing computational efficiency with hydraulic fidelity." *Journal of Geophysical Research: Earth Surface (2003–2012)*, 113(F2).

Wolfert, H., Koomen, A., and Maas, G. (2006). "Channel and bedform response to meander rehabilitation in lowland sand-bed streams." *Geomorphological Change and River Rehabilitation*, 4, 59–83.

Wong, M., Parker, G., DeVries, P., Brown, T. M., and Burges, S. J. (2007). "Experiments on dispersion of tracer stones under lower-regime plane-bed equilibrium bed load transport." *Water Resources Research*, 43(3) W03440.

Yalin, M. (1992). "River mechanics, 219 pp.

Yalin, M. S. (1964). "Geometrical properties of sand wave." *Journal of the Hydraulics Division*, 90(5), 105–119.

Yalin, M. S. (1976). *Mechanics of sediment transport*. Pergamon press.

Yalin, M. S. (1985). "On the determination of ripple geometry." *Journal of Hydraulic Engineering*, 111(8), 1148–1155.

Yang, C. T. (1976). "Minimum unit stream power and fluvial hydraulics." *Journal of the Hydraulics Division*, 102(7), 919–934.

Yarnell, S. M., Mount, J. F., and Larsen, E. W. (2006). "The influence of relative sediment supply on riverine habitat heterogeneity." *Geomorphology*, 80(3), 310–324.

Yu, Z., Niemeyer, H., and Bakker, W. (1991). "Site investigation on sand concentration in the sheet-flow layer." *Coastal Engineering 1990*, 2360–2371.

Yussuff, S., Chauhan, H., Kumar, M., and Srivastava, V. (1994). "Transient canal seepage to sloping aquifer." *Journal of Irrigation and Drainage Engineering*, 120(1), 97–109.

Vitae

Mahesh Patel was born in the Village - Gudaval, Dist.- Vidisha, Madhya Pradesh, India on 03^{th} May, 1988. He completed his schooling from Saraswati Shishu Mandir Higher Secondary School, Ganj Basoda in the year 2005. He did his Bachelor of Engineering (B.E.) degree from the Department of Civil Engineering, Samrat Ashok Technological Institute Vidisha, RGPV Bhopal, India in the year 2010. He completed his Master of Technology in the stream of Water Resources Engineering and Management, Department of Civil Engieering, Indian Institute Technology Guwahati in the year 2012. Following that, he joined the Ph.D program at the same Department in July 2012. Dr. Bimlesh Kumar was his M Tech and PhD Thesis supervisor. He has received GATE Scholarship for his Masters and MHRD Govt of India Fellowship for pursuing his PhD programme. His research interests include turbulent flow statistics, hyporheic flow over fixed bedforms, hydrodynamics, flow resistance, sediment transport, bed morphology, seepage in alluvial channels.

Contact Information

Email	:	p.mahesh@iitg.ernet.in, mahesh.patelsati@gmail.com
Web	:	https://www.researchgate.net/profile/Mahesh_Patel7
Permanent Address	:	Mahesh Patel, S/o Mr. Suresh Singh, Village- Gudaval, Post- Mainwada, Dist.- Vidisha, Pin Code-464331. Madhya Pradesh, India